

Advanced modeling using large eddy simulations applied to particle-laden turbulent flows

Dissertation

zur Erlangung des akademischen Grades

**Doktoringenieur
(Dr.-Ing.)**

von Dipl.-Ing. Max Hausmann
geb. am 09.04.1998 in Halle (Saale)

genehmigt durch die Fakultät für Verfahrens- und Systemtechnik der Otto-von-Guericke-Universität Magdeburg

Gutachter:

Prof. Dr. Berend van Wachem

Prof. Dr. habil. Dominique Thévenin

Prof. Dr. habil. Jochen Fröhlich

Promotionskolloquium am 09.10.2024

Abstract

Many natural phenomena and industrial applications involve turbulent flows, but the modeling of turbulence remains challenging, especially in complex configurations such as particle-laden turbulence. A popular alternative to resolving the turbulence from its largest scales down to the smallest flow structures in numerical simulations is large eddy simulations (LES), which only solve for the low-pass filtered fluid velocity and pressure and, therefore, significantly reduce the computational costs. The present cumulative thesis is dedicated to adapt the LES methodology to particle-laden turbulent flows in order to achieve accurate particle and flow statistics while maintaining the computational efficiency of a single-phase LES.

In this thesis, modeling framework is proposed that consists of two steps. The first step is the reconstruction of the subfilter fluid velocity, i.e., the velocity that is not resolved in an LES. The reconstructed subfilter fluid velocity is added to the fluid velocity field that is resolved in the LES and the resulting turbulent velocity field is used to transport the particles. An accurate reconstruction of the subfilter velocity is achieved by approximately solving the governing equations for the subfilter fluid velocity with two different bases: a Fourier basis discretized in space by means of statistically homogeneous sub-domains, and a wavelet basis. Both bases allow for a statistically inhomogeneous and anisotropic subfilter fluid velocity field and predict the particle clustering and particle pair dispersion accurately over a wide range of Stokes numbers.

Once a realistic particle motion in the scope of an LES is achieved, the remaining second step of the proposed modeling framework is to model the turbulence modulation by the particles. In LES, the effect of the unresolved turbulence on the resolved scales is accounted for by the subgrid-scale stress tensor. In particle-laden turbulence, the subgrid-scale stress tensor has to account for the turbulence modulation by the particles at the subfilter level. In the proposed modeling framework,

this is achieved by solving a transport equation for the subgrid-scale kinetic energy, which includes a particle source term. The subgrid-scale kinetic energy is used to model the subgrid-scale stress tensor and serves as a target kinetic energy for the reconstructed subfilter fluid velocity field, the first step of the proposed modeling framework.

With the proposed modeling framework, we can now successfully predict the expected reduction of subgrid-scale kinetic energy compared to the corresponding single-phase flow configuration in two-way coupled particle-laden turbulence. This yields a good agreement of the kinetic energy of the fluid velocity that is resolved in the LES with the kinetic energy of the explicitly filtered fluid velocity containing all turbulent length scales.

Kurzfassung

Viele der relevanten natürlichen Phänomene und industriellen Anwendungen beinhalten turbulente Strömungen, aber die Modellierung von Turbulenz bleibt eine Herausforderung, insbesondere in komplexen Konfigurationen wie turbulente Partikelströmungen. In numerischen Simulationen sind sogenannte Grobstruktursimulationen (LES) eine beliebte Alternative zur Auflösung der Turbulenz von den größten bis zu den kleinsten Strömungsstrukturen, welche lediglich die tiefpassgefilterte Strömungsgeschwindigkeit und den tiefpassgefilterten Druck auflösen und somit die Rechenkosten erheblich reduzieren. Die vorliegende kumulative Dissertation widmet sich der Anpassung der LES-Methodik an turbulente Partikelströmungen um damit genaue Partikel- und Strömungsstatistiken unter Beibehaltung geringer Rechenkosten zu erzielen.

Es wird ein Modell vorgeschlagen, welches aus zwei Schritten besteht. Der erste Schritt ist die Rekonstruktion der Feinstruktur-Fluidgeschwindigkeit, der Geschwindigkeit, die in einer LES nicht aufgelöst wird. Die rekonstruierte Feinstruktur-Fluidgeschwindigkeit wird zum aufgelösten Fluidgeschwindigkeitsfeld addiert. Das resultierende turbulente Geschwindigkeitsfeld wird zum Transport der Partikel verwendet. Eine genaue Rekonstruktion der Feinstruktur-Fluidgeschwindigkeit wird durch die angenäherte Lösung der Erhaltungsgleichungen für die Feinstruktur-Fluidgeschwindigkeit erzielt. Dafür wird die Feinstruktur-Fluidgeschwindigkeit durch eine Fourier-Basis mit räumlich getrennten statistisch homogenen Teilbereichen oder einer Wavelet-Basis repräsentiert. Beide Basen ermöglichen ein statistisch inhomogenes und anisotropes Feinstruktur-Fluidgeschwindigkeitsfeld und eine genaue Vorhersage über die Clusterbildung der Partikel und die Dispersion von Partikelpaaren über einen weiten Bereich von Stokes-Zahlen.

Nachdem eine realistische Partikelbewegung im Rahmen einer LES erreicht ist, besteht der verbleibende zweite Schritt des vorgeschlagenen Modells darin, die Tur-

bulenzveränderung durch die Partikel zu modellieren. In LES wird der Effekt der nicht aufgelösten Turbulenz auf die aufgelösten Skalen durch den Feinstrukturspannungstensor berücksichtigt. In turbulenten Partikelströmungen muss der Feinstrukturspannungstensor jedoch die Turbulenzveränderung durch die Partikel im Bereich der nicht aufgelösten Skalen berücksichtigen. Im entwickelten Modell wird dies durch die Lösung einer Transportgleichung für die kinetische Energie der Feinstruktur erreicht, die einen Partikelquellterm enthält. Die kinetische Energie der Feinstruktur wird verwendet um den Feinstrukturspannungstensor zu modellieren und dient als angestrebte kinetische Energie für das rekonstruierte Feinstrukturfluidgeschwindigkeitfeld, welches aus dem ersten Modellierungsschritt hervorgeht.

In turbulenten Partikelströmungen mit Zweiwege-Kopplung sagt das Modell erfolgreich die erwartete Reduktion der kinetischen Energie der Feinstruktur im Vergleich zur entsprechenden partikelfreien Strömungskonfiguration voraus. Dies führt zu einer guten Übereinstimmung der kinetischen Energie der in der LES aufgelösten Fluidgeschwindigkeit mit der kinetischen Energie der explizit gefilterten Fluidgeschwindigkeit der vollständig aufgelösten Turbulenz.

Table of contents

Table of contents	7
List of figures	9
List of abbreviations	11
I Introduction	13
I.1 Background	13
I.2 Objectives	16
I.3 Outline of the thesis	17
II Fundamentals of particle-laden turbulence	19
II.1 Characterization of single-phase turbulence	19
II.2 Characterization of particle-laden turbulence	29
II.2.1 Influence of the turbulence on the particles	29
II.2.2 Influence of the particles on the turbulence	35
III Modeling of particle-laden turbulence	39
III.1 Modeling the flow using LES	39
III.2 Coupling between flow and particles	46
III.3 Optimal basis functions for different physical quantities	49
III.4 LES of particle-laden turbulence	51
III.4.1 Interactions that require modeling	51
III.4.2 Modeling the effect of the unresolved turbulence on the particles	53
III.4.3 Modeling the effect of the particles and the interscale fluid interactions	58
IV Summaries of publications	61
IV.1 An efficient model for subgrid-scale velocity enrichment for large eddy simulations of turbulent flows	61
IV.1.1 Summary of the publication	61
IV.1.2 Individual contributions of the candidate	62

IV.2	Large eddy simulation model for two-way coupled particle-laden turbulent flows	63
IV.2.1	Summary of the publication	63
IV.2.2	Individual contributions of the candidate	65
IV.3	Wavelet-based modeling of subgrid scales in large eddy simulation of particle-laden turbulent flows	65
IV.3.1	Summary of the publication	65
IV.3.2	Individual contributions of the candidate	66
V	Conclusions and outlook	67
V.1	Conclusions	67
V.2	Outlook	69
	List of Publications	71
	Bibliography	75
	References	75
	Appendices	87
A.1	Paper I	89
A.2	Paper II	109
A.3	Paper III	139

List of figures

I.1	Fluid velocity magnitude and particles of a DNS of a particle-laden turbulent channel flow (a) and particle-laden HIT (b)	15
II.1	Kinetic energy spectrum of HIT at $Re_\lambda = 75$	25
II.2	PDF of the longitudinal (a) and transverse (b) velocity gradients in HIT at $Re_\lambda = 75$ normalized by their standard deviation. The dashed lines correspond to Gaussian functions for comparison.	26
II.3	Illustration of the dispersion of a particle pair.	31
II.4	Clustering of particles of three different Stokes numbers in HIT at $Re_\lambda = 75$. The particle positions are projected from a slice of thickness η	34
II.5	Kinetic energy spectrum of HIT at $Re_\lambda = 75$ without particles and with particles of three different Stokes numbers. The particle mass fraction is $\phi = 1.0$ for all of the three Stokes numbers and the simulations are conducted using the point-particle assumption.	37
III.1	PDF of the normalized energy exchange term of the explicitly filtered velocity field of HIT. The fluid velocity field is filtered with a spectrally sharp filter of three different cut-off wave numbers k_{cut} . The vertical dotted lines indicate the mean values.	42
III.2	Kinetic energy spectrum (a) and second invariant of the velocity gradient tensor (b) obtained from the DNS and an LES with the LDKM of HIT at $Re_\lambda = 75$	46

III.3	Visualization of the support in wave number space and real space of different bases. The lengths of the rectangles in the respective coordinate directions, δk and δx , illustrate the size of the support of the basis functions. The figure is inspired by a figure from Brunton and Kutz [15].	50
III.4	Sketch of the interactions between filtered and subgrid scales and particles.	52
III.5	Comparison of the particle pair dispersion between the DNS and an LES with the LDKM of particles with $St = 1$ in HIT at $Re_\lambda = 75$	54
III.6	Fluid velocity magnitude of HIT at $Re_\lambda = 75$ (top left) and the corresponding filtered velocity field (top right). Below, the positions of particles of $St = 2$ that are transported with the respective velocity field are shown.	55
IV.1	Enrichment strategy consisting of (I) averaging large scale quantities of the LES within statistically homogeneous sub-domains that are coarser than the LES grid, (II) solution of the modeled SFNSE in Fourier space in every sub-domain, and (III) approximating the turbulent fluid velocity field as the sum of LES velocity and modeled subgrid-scale velocity.	62
IV.2	Subgrid-scale kinetic energy of decaying HIT predicted by the classical LES without the proposed modeling framework and by the modeled LES with the proposed modeling framework. The results are compared to the explicitly filtered DNS using a spectrally sharp filter and volume averaging in the LES grid cells. The results are shown for three different Stokes numbers.	64
IV.3	Piecewise linear ϕ_0, ψ_0 (a) and piecewise quadratic ϕ_1, ψ_1 (b) spline scaling and wavelet functions that represent the modeled subgrid-scale velocity.	66

List of abbreviations

DNS	Direct Numerical Simulation
FNSE	Filtered Navier-Stokes Equations
HIT	Homogeneous Isotropic Turbulence
LDKM	Localized Dynamic Kinetic Energy Model
LES	Large Eddy Simulation
mLDKM	Modified Localized Dynamic Kinetic Energy Model
NSE	Navier-Stokes Equations
PDF	Probability Density Function
PSIC	Particle-Source-In-Cell
RANS	Reynolds Averaged Navier-Stokes
RDT	Rapid Distortion Theory
SFNSE	Subfilter Navier-Stokes Equations

Introduction

I.1 Background

The complexity of swirling flows appears to have fascinated, but also puzzled, researchers for centuries. Already 500 years ago, Leonardo da Vinci described the chaotic behavior of what was later termed turbulence in his drawings of water mixing in a tank. Despite decades of intense turbulence research, its understanding is still relatively superficial compared to more recent and, seemingly, more intricate problems of physics. Direct conclusions from the governing equations are very rare and the majority of knowledge is empirical. The problem is summarized by Feynman *et al.* [37] as follows:

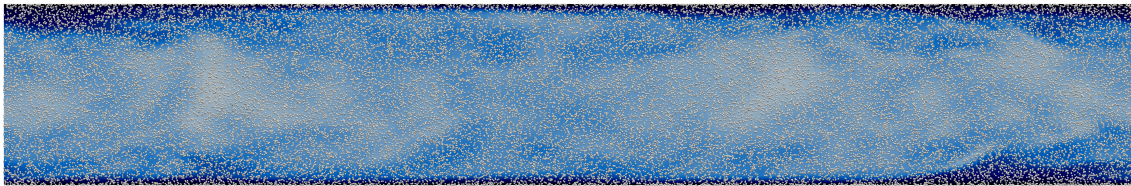
“There is a physical problem that is common to many fields, that is very old, and that has not been solved. It is not the problem of finding new fundamental particles, but something left over from a long time ago—over a hundred years. Nobody in physics has really been able to analyze it mathematically satisfactorily in spite of its importance to the sister sciences. It is the analysis of circulating or turbulent fluids.”

Another degree of complexity is added by the fact that the turbulent flows of interest, ranging from natural phenomena such as weather predictions to complex industrial application such as fluidized beds, often contain at least a second phase that interacts with the turbulence. In many applications this second phase consists of rigid, or weakly deforming particles that are affected by the turbulent flow and, vice versa, modulate the turbulence.

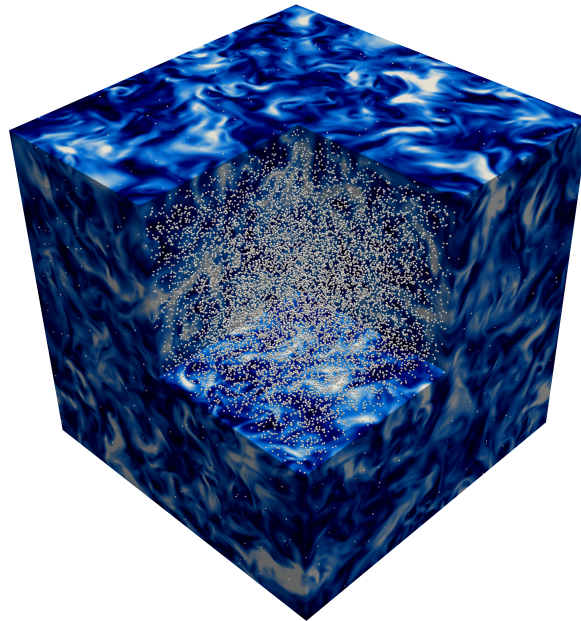
With increasing computational resources, the importance of numerical simulations of turbulence and particle-laden turbulence is continuously growing, enabling re-

liable predictions of increasingly complex physics. However, full resolution of the turbulence from the largest down to the smallest scales, which is referred to as direct numerical simulation (DNS), is only affordable for relatively small problems of mostly academic relevance. A common academic example is the particle-laden turbulent channel-flow, i.e., a turbulent flow between two flat plates, which is depicted in figure I.1a. There exists a great variety of experimental and computational studies of the turbulent channel flow with and without particles, e.g., Marchioli *et al.* [79], Moin and Kim [89], Ptasinski *et al.* [99], which makes it a popular test case of novel models before they are applied to more complex industrial applications that cannot be simulated with DNS. Due to the mere existence of walls, however, the main body of theoretical knowledge of turbulence, which is often required for model development, does not strictly apply to channel flows. Therefore, testing the models in a turbulent channel flow is typically the second step after the models are developed with the much simpler and theoretically better accessible configuration of homogeneous isotropic turbulence (HIT). An example of particle-laden HIT is given in figure I.1b, which is simulated in a cube that is periodic in every direction.

The modeling of turbulence can generally be divided into two branches, the Reynolds averaged Navier-Stokes (RANS) simulations, which solve for the ensemble averaged fluid field and the LES, that solve for the spatially low-pass filtered flow field. While RANS simulations typically lead to a stronger reduction of computational costs, LES preserve more essential features, especially temporal features, of the turbulent flow. RANS simulations and LES of turbulent single-phase flows require closures that are often tailored to the specific flow configurations. Although satisfactory results can be achieved for single-phase flows, the industrially highly relevant particle-laden turbulent flows are typically predicted with poor accuracy. The unresolved flow quantities that seem to be less essential for the flow, the fluctuating quantities in RANS simulations and the subfilter quantities in LES, turn out to be crucial for predicting the right particle behavior. Furthermore, the particles can alter the flow in an unknown way. It may happen that a RANS simulation or LES of a particle-laden turbulent flow, which gives sufficiently accurate results for the corresponding single-phase flow configuration, predicts the flow and particle behavior quantitatively or even qualitatively wrong. Therefore, models are required that improve the flow and particle predictions in RANS simulations and LES of particle-laden turbulent flows. Due to their early stage of development, the models are still evaluated based on the HIT configuration [7, 94, 131].



(a)



(b)

Figure I.1: Fluid velocity magnitude and particles of a DNS of a particle-laden turbulent channel flow **(a)** and particle-laden HIT **(b)**.

I.2 Objectives

The overall objective of the present thesis is the development of a modeling framework that can be applied to LES of particle-laden turbulent flows and that predicts similar particle behavior as particles transported in a DNS and similar flow behavior as the filtered flow field of the corresponding DNS. Considering the high degree of modeling in an LES, expecting to perfectly reproduce the particle and flow movement would be too ambitious. Therefore, the aim is to reproduce key statistics, such as the formation of particle clusters and the dispersion of particle pairs, and the kinetic energy of the filtered fluid velocity.

Since to the best of the author's knowledge no framework exists that predicts the essential statistics of an LES of a particle-laden turbulent flow satisfactorily and with reasonable computational costs, restrictions regarding the complexity of the considered flow configuration are imposed. The first major restriction concerns the boundary conditions of the flow, which are assumed to be periodic throughout the thesis. The presence of walls, i.e., a Dirichlet boundary condition for the fluid velocity, already constitutes a difficulty in single-phase LES as the spatial low-pass filtering is not precisely defined in the near-wall region. Therefore, the presence of walls is excluded in the scope of this thesis for the significantly more complex case of LES of particle-laden turbulence. However, it should be emphasized that the aspired modeling framework should be capable of handling inhomogeneous and anisotropic flow configurations, albeit without walls. The second major restriction limits the density ratio between particles and fluid. In the present thesis, density ratios typical for gas-solid flows are considered, i.e., high ratios of particle to fluid density, as the fluid dynamical force on the particle reduces to the drag force (see, e.g., Kuerten [67]). Furthermore, as the third major restriction, it is assumed that the particles are spherical and smaller than the smallest turbulent length scale.

The objective of an LES modeling framework for particle-turbulence interactions is divided into two parts. For the first part, the turbulence modulation by the particles is ignored and the focus lies exclusively on modeling the right particle behavior based on information that is available in an LES. The path followed in the present thesis is to reconstruct the subfilter velocity, i.e., the difference between the complete turbulent fluid velocity field and the filtered fluid velocity field, such that turbulence characteristics that are crucial to predict the right particle behavior are reproduced. The reconstructed subfilter velocity field is added to the approximation of the filtered velocity field, which is available in an LES, and the resulting velocity field is used to transport the particles. If the sum of the LES velocity and the reconstructed

subfilter velocity is similar to the fluid velocity field of the corresponding DNS, the particles moves as in a DNS.

The second part of the modeling framework requires a realistic particle behavior and aims to predict the turbulence modulation by the particles. The single-phase LES modeling, commonly referred to as subgrid-scale modeling, has to take into account the turbulence modification of the subfilter scales by the particles.

The resulting modeling framework is to be tested in HIT and compared with DNS of the same configuration, and the resulting computational costs should be of the order of an LES without particular modeling of the particle-turbulence interactions.

I.3 Outline of the thesis

The main body of research conducted in the scope of the present cumulative thesis is published in three different journal articles. To put this research into a unified context, a broader background is provided in the following chapters that connect and motivate the research that is published in the three articles. The remainder of this thesis is structured the following way:

In Chapter II the fundamental physics of turbulence and particle-laden turbulence are reviewed. Particular emphasize is given to characteristics that make turbulence unique and that are crucial for particle transport, and mathematical manipulations that enable LES modeling.

Chapter III introduces fundamental modeling strategies of single-phase LES, particle-laden flows, and particle-laden turbulence that serve as basis for the proposed modeling framework. Strengths and weaknesses of existing methodologies are reviewed and the pathways followed in the articles belonging to the present thesis are motivated.

Individual parts of the proposed modeling framework are published in three independent journal articles that are briefly summarized in Chapter IV.

Conclusions and pathways for future extensions and improvements are drawn in Chapter V.

The journal articles containing the research conducted in the present thesis can be found in appendix A.1-A.3.

Fundamentals of particle-laden turbulence

II.1 Characterization of single-phase turbulence

Although the term turbulence is widely used, a rigorous definition of turbulence does not exist. To differentiate turbulence from swirling, but not yet turbulent flows and from other vector fields, properties need to be formulated that characterize a turbulent flow. Based on the criteria proposed by Tennekes and Lumley [125], the following criteria may be formulated to identify turbulence:

- **Irregularity:** Turbulent fluid motion appears random, as precise long term predictions of turbulence fail. Chaos theory provides an explanation for this observation by claiming that the flow is not random but infinitely sensitive to initial conditions. Therefore, even the tiniest error in measuring the current state eventually causes very large errors in the prediction of future states [58].
- **Diffusivity:** Turbulence enhances diffusion, or mixing, of objects or properties that are transported by the fluid velocity field [92]. Increased mixing can, for instance, be observed for particles, concentrations of chemicals, temperature, or even the velocity itself. In wall-bounded flows, a turbulent boundary layer is significantly different to a laminar boundary layer since the turbulent eddies mix faster velocity structures away from the wall with the slow near-wall velocity [96].
- **Large Reynolds number:** The Reynolds number, Re , is defined as the proportion of inertial effects relative to the effect of viscosity and defined as $Re = \rho_f \mathcal{U} \mathcal{L} / \mu_f$, where ρ_f is the density of the fluid, \mathcal{U} is a characteristic fluid

velocity, \mathcal{L} is a characteristic length scale, and μ_f is the dynamic viscosity of the fluid. For large Reynolds numbers, the non-linear components of the governing fluid equations become predominant and the chaotic nature of the resulting flow field increases, whereas the viscosity has a stabilizing effect as it increases the importance of the diffusive character of the governing equations. The Reynolds number can also be interpreted as the proportion of the largest length scales to the smallest length scales of the flow, implying that turbulence is multiscale in nature.

- **Three-dimensional:** Swirling fluid flow behaves very different in two and three spatial dimensions. Since three spatial dimensions is the by far most relevant case in industrial and natural phenomena, turbulence refers to three-dimensional fluid flow. Three-dimensional mechanisms govern the energy transfer of turbulence, such as vortex stretching and strain self-amplification [18, 56, 124, 126].
- **Dissipative:** Turbulence exhibits an energy cascade, wherein kinetic energy is transferred from the large scales to small scales until it is dissipated to heat as a result of large spatial gradients that mostly occur at the smallest scales. Although this energy cascade can be locally inverse, the so-called forward energy cascade is dominant and eventually yields dissipation of the kinetic energy. Therefore, to maintain statistically steady turbulence, the flow has to be permanently supplied with energy [96].
- **Continuum:** Turbulence is a phenomenon that can be described under the assumptions of continuum mechanics if the smallest flow structures are much larger than the mean free path of the fluid molecules.
- **A feature of the flow, not the fluid:** Turbulence exhibits similar features even if the fluids are fundamentally different, e.g., liquids and gases. At equivalent Reynolds number, it is impossible to distinguish the turbulent velocity field of a liquid from the turbulent velocity field of a gas.

These qualitative criteria provide a general characterization of turbulence, but in order to pursue turbulence modeling, turbulent flows have to be analyzed quantitatively. In the scope of this thesis, the discussions are limited to HIT. In HIT, the statistics of the flow quantities, the fluid velocity, \mathbf{u} , the pressure, p , and derived quantities, are invariant with respect to the position or direction of evaluation. HIT allows several simplifications that are beneficial for the development and evaluation

of new models. However, HIT is an idealized case that can differ fundamentally from the turbulence observed in practical applications, which can limit the applicability of models developed in HIT.

A turbulent flow satisfies conservation of mass and momentum. For an incompressible fluid of density ρ_f , constant dynamic viscosity μ_f , and without external forces, the governing equations are the following Navier-Stokes equations (NSE)

$$\frac{\partial u_i}{\partial x_i} = 0, \quad (\text{II.1})$$

$$\rho_f \frac{\partial u_i}{\partial t} + \rho_f \frac{\partial u_i u_j}{\partial x_j} = -\frac{\partial p}{\partial x_i} + \mu_f \frac{\partial}{\partial x_j} \left[\left(\frac{\partial u_i}{\partial x_j} + \frac{\partial u_j}{\partial x_i} \right) \right], \quad (\text{II.2})$$

where x_i and t indicate spatial coordinates and time, respectively. Note that summation is assumed in terms where indices occur twice. Since no closed-form solution to the NSE exists for HIT, quantitative knowledge of HIT mainly stems from statistical analysis and evaluation of experimental data.

Early studies address the quantitative characterization of turbulence using spatial velocity correlations, which are relatively easily accessible in experimental measurements, the only way of accessing high Re turbulence data at the time of early breakthroughs [62, 105, 123, 128]. The spatial fluid velocity autocorrelation tensor (for HIT) is defined as [41, 96]

$$B_{ij}(\mathbf{r}) = \frac{\langle u_i(\mathbf{x}) u_j(\mathbf{x}') \rangle}{\langle u_i(\mathbf{x}) u_j(\mathbf{x}) \rangle}, \quad (\text{II.3})$$

with

$$\mathbf{r} = \mathbf{x}' - \mathbf{x}, \quad (\text{II.4})$$

where $\langle \cdot \rangle$ indicates ensemble averaging. Note that the time dependency of the fluid velocity is omitted for conciseness and that no summation is carried out over the indices in equation (II.3). The autocorrelation function identifies how strongly the fluid velocities of two points separated by the vector \mathbf{r} correlate. For large distances $r = |\mathbf{r}|$, fluid velocities of a turbulent flow are fully uncorrelated, hence B_{ij} tends towards zero. In HIT, two scalar functions are sufficient to describe the whole autocorrelation tensor B_{ij} , the longitudinal and transverse autocorrelation functions,

$f(r)$ and $g(r)$. With

$$f(r) = B_{11}(r\mathbf{e}_1), \quad (\text{II.5})$$

$$g(r) = B_{22}(r\mathbf{e}_1), \quad (\text{II.6})$$

the autocorrelation tensor is given as [96]

$$B_{ij} = g(r)\delta_{ij} + (f(r) - g(r))\frac{r_i r_j}{r^2}, \quad (\text{II.7})$$

where \mathbf{e}_1 is a unit vector and δ_{ij} is the Kronecker delta. The autocorrelation functions contain information about the turbulent length scales present in the flow, since small length scales lead to rapidly decaying autocorrelations while large length scales maintain high correlations of the velocities, even for large distances, r . A characteristic measures of the turbulent length scales are given with the longitudinal and transverse integral length scales

$$L_{11}^{(1)} = \int_0^\infty f(r)dr, \quad (\text{II.8})$$

$$L_{22}^{(1)} = \int_0^\infty g(r)dr \quad (\text{II.9})$$

and the longitudinal and transverse Taylor microscales

$$\lambda_f^2 = \frac{2\langle u_1^2 \rangle}{\langle (\partial u_1 / \partial x_1)^2 \rangle} = -\frac{2}{\left. \frac{d^2 f}{dr^2} \right|_{r=0}}, \quad (\text{II.10})$$

$$\lambda_g^2 = \frac{2\langle u_2^2 \rangle}{\langle (\partial u_2 / \partial x_1)^2 \rangle} = -\frac{2}{\left. \frac{d^2 g}{dr^2} \right|_{r=0}}. \quad (\text{II.11})$$

Both definitions, the integral length scales and the Taylor microscales, are commonly used as characteristic fluid length scales in the definition of the Reynolds number of HIT.

Further information can be extracted from the velocity autocorrelation in spectral space. Applying the Fourier transform to the velocity autocorrelation tensor (without normalization) gives the velocity spectrum tensor

$$F_{ij}(\mathbf{k}) = \frac{1}{(2\pi)^3} \int \langle u_i(\mathbf{x})u_j(\mathbf{x}') \rangle e^{-i\mathbf{k}\cdot\mathbf{r}} d\mathbf{r}, \quad (\text{II.12})$$

where \mathbf{k} is the wave vector. Averaging over spherical shells in wave number space, i.e., wave vectors with the same magnitude, leads to the kinetic energy spectrum

$$E(k) = \frac{1}{2} \int_{k=|\mathbf{k}|} F_{ii}(\mathbf{k}) dS(k). \quad (\text{II.13})$$

The kinetic energy spectrum is a scalar function that depends on a scalar variable, the magnitude of the wave vector $k = |\mathbf{k}|$, and contains information on how much kinetic energy flow structures of a particular wave number possess.

Richardson [105] formulated that kinetic energy does not remain static at flow structures of specific size l , but rather is transferred to flow structures of a smaller size. The flow structures are termed eddies or whorls, and lack a precise definition. The inertial effects of the large eddies outweigh the effect of viscosity, while the small eddies are dominated by viscous effects. In between, Richardson [105] reports a successive break up of larger eddies into smaller eddies, until the smallest eddies are, eventually, dissipated by the viscosity. This process is referred to as the energy cascade. Tsinober [126] criticizes Richardson's description of the energy cascade mainly because of the ambiguous definition of eddies. Mathematically, the energy transfer is between Fourier modes or wave numbers and caused by the non-linear and non-local (in spectral space) interactions of the advective term in the NSE. In contradiction to the energy cascade of Richardson, the energy transfer is bidirectional and non-local, i.e., energy can also be transferred from large wave numbers to small wave numbers and the energy transfer does not exclusively occur among neighboring wave numbers but potentially across the whole range of wave numbers. The ideas of Richardson are formalized by Kolmogorov [62] under the assumption that for turbulent flows of sufficiently high Re , the small scales, i.e., the scales that are much smaller than largest length scales of the flow, l_0 , are isotropic in a statistical sense, i.e., ensemble averages are independent of the direction. There is evidence, however, that the statistical isotropy of the small scales is violated at least for anisotropic large scale turbulent motion [126]. In addition to the hypothesis of local isotropy, Kolmogorov postulates the following first similarity hypothesis:

The locally isotropic small scale turbulent motion ($l \ll l_0$) possesses probability distributions that are uniquely determined by the kinematic fluid viscosity ν_f and the ensemble averaged fluid dissipation $\langle \epsilon \rangle$.

From the kinematic fluid viscosity, ν_f , and the ensemble averaged fluid dissipation, $\langle \epsilon \rangle$, a length, time, and velocity scale can be defined that characterize the smallest

flow structures, the Kolmogorov scales

$$\eta = \left(\frac{\nu_f^3}{\langle \epsilon \rangle} \right)^{1/4}, \tau_\eta = \left(\frac{\nu_f}{\langle \epsilon \rangle} \right)^{1/2}, u_\eta = (\nu_f \langle \epsilon \rangle)^{1/4}. \quad (\text{II.14})$$

A second similarity hypothesis is formulated by Kolmogorov concerning the scales that are small enough to be assumed isotropic but much larger than the Kolmogorov length scale:

The turbulent motion of scales $\eta \ll l \ll l_0$ possesses probability distributions that are uniquely determined by the ensemble averaged fluid dissipation $\langle \epsilon \rangle$.

Based on the second similarity hypothesis, Kolmogorov derives relations for the longitudinal fluid velocity structure functions of the order p

$$S_p(r) = \langle (u_1(\mathbf{x} + r\mathbf{e}_1) - u_1(\mathbf{x}))^p \rangle. \quad (\text{II.15})$$

By dimensional analysis, it can be concluded for the second order structure function that

$$S_2(r) \propto \langle \epsilon \rangle^{2/3} r^{2/3}. \quad (\text{II.16})$$

Likewise by dimensional arguments, the kinetic energy spectrum can be derived to have the following functional form for the wave number range $2\pi/l_0 \ll k \ll 2\pi/\eta$ [96]

$$E(k) \propto \langle \epsilon \rangle^{2/3} k^{-5/3}. \quad (\text{II.17})$$

Figure II.1 shows the kinetic energy spectrum for HIT at $\text{Re}_\lambda = 75$. The Taylor-Reynolds number is defined as

$$\text{Re}_\lambda = \frac{\lambda_g \sqrt{\langle K \rangle}^{2/3}}{\nu_f}, \quad (\text{II.18})$$

where $\langle K \rangle = u_i u_i / 2$ is the kinetic energy of the fluid per unit mass, typically just referred to as kinetic energy of the fluid. For intermediate wave numbers, $k = |\mathbf{k}|$, i.e., $2\pi/l_0 \ll k \ll 2\pi/\eta$, there is indeed an almost constant slope of the kinetic energy spectrum proportional to $k^{-5/3}$, the so-called inertial range. For higher wave numbers, the kinetic energy spectrum decreases rapidly, which is referred to as dissipation range. The second similarity hypothesis does not hold in the dissipation

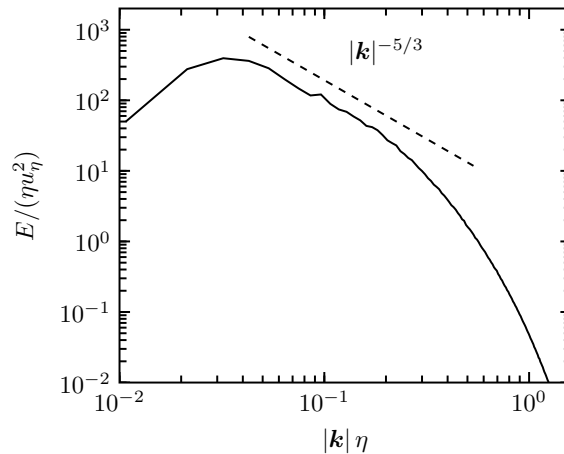


Figure II.1: Kinetic energy spectrum of HIT at $\text{Re}_\lambda = 75$.

range and the flow is substantially affected by the viscosity. The dimensional analysis can be extended to structure functions of arbitrary order, such that the structure function of order p is given as

$$S_p(r) \propto \langle \epsilon \rangle^{p/3} r^{p/3}. \quad (\text{II.19})$$

The third order structure function, $S_3(r)$, is an exception as an exact relation can be analytically obtained from the NSE. Kolmogorov [61] expresses the Karman-Howarth equation, an equation for the velocity autocorrelation directly derived from the NSE [128], in terms of second and third order longitudinal structure functions. In the statistically steady state, the Kolmogorov equation is

$$S_3(r) = 6\nu_f \frac{\partial S_2(r)}{\partial r} - \frac{4}{5} \langle \epsilon \rangle r. \quad (\text{II.20})$$

According to the second similarity hypothesis, the structure functions are independent of the viscosity in the inertial range. Therefore, the exact relation for the third order structure function is obtained for the inertial range

$$S_3(r) = -\frac{4}{5} \langle \epsilon \rangle r. \quad (\text{II.21})$$

Contrary to Kolmogorov's predictions, however, experimental measurements do not confirm the predictions of equation (II.19) for $p \geq 4$, which is commonly known as anomalous scaling. These deviations are a consequence of the non-Gaussian statistics of turbulence, which is commonly referred to as intermittency [96]. Although the dimensions match, the ensemble averaging of the fluid dissipation is a somewhat

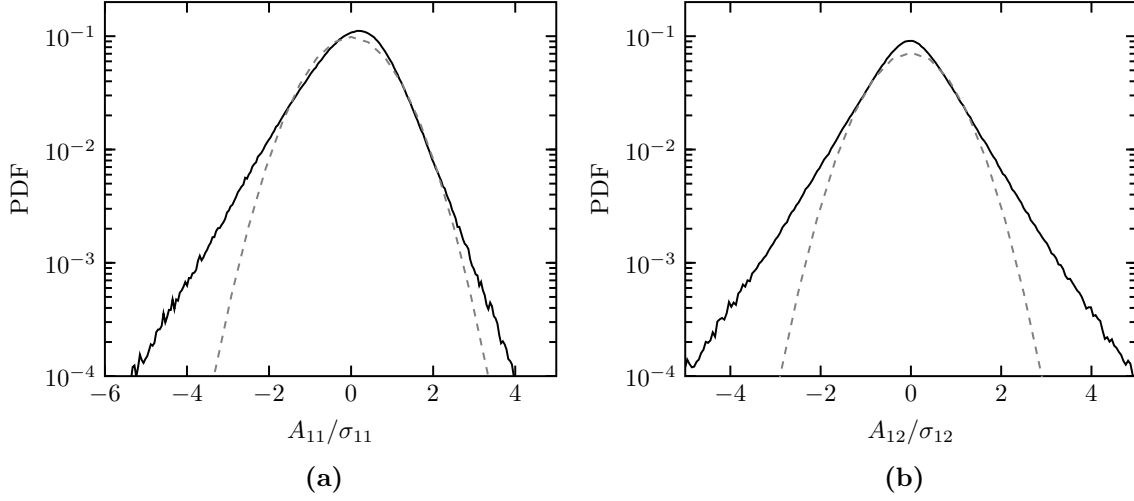


Figure II.2: PDF of the longitudinal (a) and transverse (b) velocity gradients in HIT at $\text{Re}_\lambda = 75$ normalized by their standard deviation. The dashed lines correspond to Gaussian functions for comparison.

arbitrary choice. Kolmogorov [63] proposed a refined theory to account for intermittency. The non-Gaussian behavior of the dissipation becomes evident in figure II.2, where the probability density function (PDF) of the longitudinal and transverse velocity gradients, $A_{11} = \partial u_1 / \partial x_1$ and $A_{12} = \partial u_1 / \partial x_2$, are shown normalized by their respective standard deviations, σ_{11} and σ_{12} . In HIT, the dissipation can be expressed as [41]

$$\langle \epsilon \rangle = \nu_f \left\langle \frac{\partial u_i}{\partial x_j} \frac{\partial u_i}{\partial x_j} \right\rangle = 15 \nu_f \left\langle \left(\frac{\partial u_1}{\partial x_1} \right)^2 \right\rangle = \frac{15}{2} \nu_f \left\langle \left(\frac{\partial u_1}{\partial x_2} \right)^2 \right\rangle. \quad (\text{II.22})$$

The tails of the PDFs of the velocity gradients are significantly wider than the tails of a Gaussian, a phenomenon which becomes increasingly dominant for higher moments. The power of the ensemble averaged dissipation, $\langle \epsilon \rangle^p$, and the ensemble average of the power of the dissipation, $\langle \epsilon^p \rangle$, increasingly deviate from each other for increasing p . The non-Gaussian PDFs are an important quantitative measure to identify turbulence and not straightforward to reproduce in artificial turbulence.

The kinetic energy of the fluid, K , is governed by the kinetic energy transport equation, which is obtained by contracting the momentum equation (II.2) with the fluid velocity [96]

$$\rho_f \frac{\partial K}{\partial t} + \rho_f \frac{\partial u_j K}{\partial x_j} = - \frac{\partial u_i p}{\partial x_i} + \mu_f \frac{\partial^2 K}{\partial x_j \partial x_j} - \mu_f \frac{\partial u_i}{\partial x_j} \frac{\partial u_i}{\partial x_j}. \quad (\text{II.23})$$

The kinetic energy of the fluid is advected by the local fluid velocity (second term on the left-hand side), redistributed by the pressure (first term on the right-hand side), diffused (second term on the right-hand side), and dissipated (last term on the right-hand side). After ensemble averaging, terms of the form $\partial(\dots)/\partial x_j$ can be shown to vanish in HIT (see, e.g., George [41]), such that the ensemble averaged kinetic energy evolves according to

$$\rho_f \frac{\partial \langle K \rangle}{\partial t} = -\mu_f \left\langle \frac{\partial u_i}{\partial x_j} \frac{\partial u_i}{\partial x_j} \right\rangle = -\rho_f \langle \epsilon \rangle. \quad (\text{II.24})$$

Since the right-hand side is never positive, the fluid dissipation only removes kinetic energy from the flow. The fluid dissipation is the only term that alters the ensemble averaged kinetic energy of the flow, the remaining terms of equation (II.23) solely redistribute kinetic energy in space and in spectral space.

The energy cascade as described by Richardson [105] suggests that flow structures of different scales interact with each other. The interscale momentum and kinetic energy exchange is typically studied by decomposing the flow quantities into large scale and small scale contributions [12, 44, 56, 68], which has practical relevance in LES. This is achieved by filtering the flow quantity, Φ , with a filter kernel, G , by convolution

$$\tilde{\Phi}(\mathbf{x}, t) = \int_{\Omega} G(|\mathbf{x} - \mathbf{y}|) \Phi(\mathbf{y}, t) dV_{\mathbf{y}}, \quad (\text{II.25})$$

where Ω is the flow domain and $\tilde{\Phi}$ is the filtered flow quantity. The filter kernel, which is assumed to be homogeneous and isotropic, must satisfy

$$\int_{\Omega} G(|\mathbf{x}|) dV_{\mathbf{x}} = 1. \quad (\text{II.26})$$

Therefore, flow quantities can be additively decomposed into a large scale contribution, $\tilde{\Phi}$, and a small scale contribution, $\Phi' = \Phi - \tilde{\Phi}$, or, more precisely, a filtered and a subfilter contribution. Applying the filtering operation to the NSE leads to the governing equations for the large flow scales, the filtered Navier-Stokes equations (FNSE),

$$\frac{\partial \tilde{u}_i}{\partial x_i} = 0, \quad (\text{II.27})$$

$$\rho_f \frac{\partial \tilde{u}_i}{\partial t} + \rho_f \frac{\partial \tilde{u}_i \tilde{u}_j}{\partial x_j} = -\frac{\partial \tilde{p}}{\partial x_i} + \frac{\partial}{\partial x_j} \left[\mu_f \left(\frac{\partial \tilde{u}_i}{\partial x_j} + \frac{\partial \tilde{u}_j}{\partial x_i} \right) \right] - \rho_f \frac{\partial \tau_{ij}}{\partial x_j}, \quad (\text{II.28})$$

where τ_{ij} is the subfilter stress tensor, often also referred to as subgrid-scale stress tensor, and given as

$$\tau_{ij} = \widetilde{u_i u_j} - \tilde{u}_i \tilde{u}_j. \quad (\text{II.29})$$

The subfilter stress tensor arises from filtering the non-linear advective term in the NSE and represents exchange of momentum between filtered and subfilter scales. The subfilter stress tensor also influences the kinetic energy of the filtered scales, which becomes evident by considering the evolution of the ensemble averaged kinetic energy of the filtered scales, $K_F = \tilde{u}_i \tilde{u}_i / 2$,

$$\rho_f \frac{\partial \langle K_F \rangle}{\partial t} = -\mu_f \langle 2\tilde{S}_{ij} \tilde{S}_{ij} \rangle + \tilde{S}_{ij} \tau_{ij} \quad (\text{II.30})$$

which is obtained by contracting equation (II.28) with \tilde{u}_i and subsequently ensemble averaging, where \tilde{S}_{ij} is the filtered strain-rate tensor and defined as

$$\tilde{S}_{ij} = \frac{1}{2} \left(\frac{\partial \tilde{u}_i}{\partial x_j} + \frac{\partial \tilde{u}_j}{\partial x_i} \right). \quad (\text{II.31})$$

Note that the following relation can be assumed in incompressible HIT [96]

$$\langle 2\tilde{S}_{ij} \tilde{S}_{ij} \rangle = \left\langle \frac{\partial \tilde{u}_i}{\partial x_j} \frac{\partial \tilde{u}_i}{\partial x_j} \right\rangle, \quad (\text{II.32})$$

since the terms of the form $\partial(\dots)/\partial x_j$ vanish in HIT. The subfilter stress term causes non-linear energy transfer by scale local and scale non-local vortex stretching and strain self-amplification and the interactions of large scale strain with small scale strain vorticity covariance [57]. Overall, the subfilter stress term removes energy from large scales but can be locally negative, which is commonly known as energy backscatter or the backward energy cascade.

By subtracting the FNSE from the NSE, the governing equations for the small flow scales are obtained, the subfilter Navier-Stokes equations (SFNSE)

$$\frac{\partial u'_i}{\partial x_i} = 0, \quad (\text{II.33})$$

$$\rho_f \frac{\partial u'_i}{\partial t} + \rho_f \frac{\partial}{\partial x_j} (\tilde{u}_i u'_j + u'_i \tilde{u}_j + u'_i u'_j) = -\frac{\partial p'}{\partial x_i} + \frac{\partial}{\partial x_j} \left[\mu_f \left(\frac{\partial u'_i}{\partial x_j} + \frac{\partial u'_j}{\partial x_i} \right) \right] + \rho_f \frac{\partial \tau_{ij}}{\partial x_j} \quad (\text{II.34})$$

The advection in the SFNSE consists of three contributions, namely (from left to right) the straining term, the sweeping term and the non-linear relaxation term. It can be argued that if $|\langle \tilde{u}_i \rangle| \gg |\langle u'_i \rangle|$, the magnitude of the non-linear relaxation term is negligible compared to the other terms. This turns out to be valid in flows of strong large scale strain and is the fundamental assumption of the rapid distortion theory (RDT), i.e., the linearization of the SFNSE (see, e.g., [54, 96]). Laval *et al.* [68] solve the linearized SFNSE together with the FNSE in HIT and observe an overestimation of the kinetic energy spectrum in the dissipation range and the degree of intermittency. They conclude that the non-linear relaxation term attenuates the intermittency and propose to replace it with either a constant additional viscosity or the following expression, which is obtained using renormalization groups [16]

$$\nu'_t(k) = \left(\nu_f^2 + \frac{2}{5} \int_k^\infty q^{-2} E(q) dq \right)^{1/2} - \nu_f, \quad (\text{II.35})$$

where ν'_t is the additional turbulent viscosity.

II.2 Characterization of particle-laden turbulence

II.2.1 Influence of the turbulence on the particles

The complexity of a turbulent flow is further increased if the fluid is suspended with particles. The momentum balance for each individual particles is given by Newton's second law, neglecting body forces such as gravity,

$$\frac{d\mathbf{v}}{dt} = \frac{1}{\rho_p V_p} \mathbf{F}_f, \quad (\text{II.36})$$

where \mathbf{v} is the velocity of the particle, ρ_p is the density of the particle, and V_p is the particle volume. The particle position, \mathbf{x}_p , follows as

$$\frac{d\mathbf{x}_p}{dt} = \mathbf{v}. \quad (\text{II.37})$$

The fluid dynamical force acting on the particle is obtained by integrating the pressure and viscous stresses of the fluid over the particle surface, $\partial\Omega_p$,

$$F_{f,i} = \int_{\partial\Omega_p} \left(-p\delta_{ij} + \mu_f \left(\frac{\partial u_i}{\partial x_j} + \frac{\partial u_j}{\partial x_i} \right) \right) n_j dA, \quad (\text{II.38})$$

where δ_{ij} is the Kronecker delta and n_j is the normal vector on the particle surface pointing outward from the particle surface into the fluid.

For an analytical evaluation of the fluid dynamical force acting on the particle, the fluid velocity and pressure field of the flow around the particle have to be known, which is generally not the case. Under the assumption of a particle moving slowly in viscous fluid, i.e., a very small particle Reynolds number, $\text{Re}_p = d_p |\mathbf{u}(\mathbf{x}_p) - \mathbf{v}| / \nu_f$, where d_p is the diameter of the spherical particle, the fluid dynamical force can be evaluated analytically under some circumstances by solving the unsteady Stokes equations instead of the NSE

$$\frac{\partial u_i}{\partial x_i} = 0, \quad (\text{II.39})$$

$$\rho_f \frac{\partial u_i}{\partial t} = -\frac{\partial p}{\partial x_i} + \mu_f \frac{\partial}{\partial x_j} \left[\left(\frac{\partial u_i}{\partial x_j} + \frac{\partial u_j}{\partial x_i} \right) \right]. \quad (\text{II.40})$$

A variety of physical mechanisms can be identified that contribute to the fluid dynamical force that are collectively accounted for by the Basset-Boussinesq-Oseen equation under the assumption of uniform Stokes flow [8, 13, 91]. The Maxey-Riley-Gatignol equation [40, 84] additionally accounts for curvature of the free stream flow by incorporating the Faxén correction [33]. In many flow configurations, however, some of the forces contribute only negligibly to the total fluid dynamical force. A review of the influence of the various forces in different flow regimes is provided by Kuerten [67]. In flows with a density ratio $\rho_p / \rho_f \gg 1$, such as in the presently considered particle-laden gas flows, the drag force is usually the dominant fluid dynamical force contribution. For spherical particles that are smaller than the Kolmogorov length scale in locally nearly uniform flow with negligible particle rotation, dynamical lift forces on the particle are negligible. In dilute flows with small particle volume fractions $\varepsilon_p \ll 1$, the fluid dynamical force on the particle can be approximately assumed to be independent of the flow modification due to other ambient particles. Under all the mentioned restrictions, the fluid dynamical force acting on the particle is given as

$$\mathbf{F}_f = \mathbf{F}_D, \quad (\text{II.41})$$

where \mathbf{F}_D is the drag force on an isolated spherical particle in uniform flow. The behavior of the considered particles in HIT is characterized by the Stokes number, St , a measure of the required time it takes particles to adapt to local changes of the flow. The Stokes number is defined as the ratio of the particle relaxation time

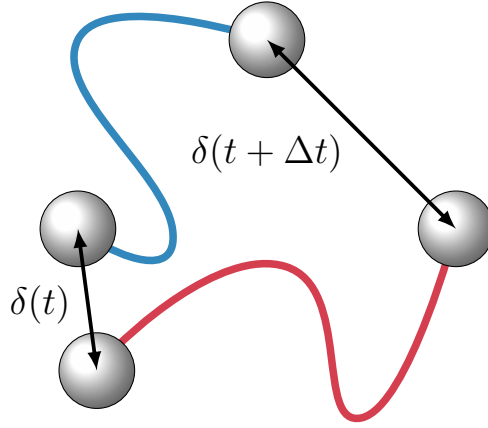


Figure II.3: Illustration of the dispersion of a particle pair.

to the characteristic fluid time scale

$$\text{St} = \frac{\tau_p}{\tau_\eta}, \quad (\text{II.42})$$

where τ_η is the Kolmogorov time scale and the particle relaxation time for particles in the Stokes regime is given as

$$\tau_p = \frac{\rho_p d_p^2}{18\mu_f}. \quad (\text{II.43})$$

Dependent on the Stokes number, particle pairs, i.e., two particles of a specific initial separation, $\delta(t = 0)$, exhibit distinct dispersion statistics in time. The distance between the two particles, $\delta(t)$, may be tracked in time and ensemble averaged, which yields the particle pair dispersion defined as

$$\langle \delta \rangle(t) = \langle |\mathbf{x}_{p0} - \mathbf{x}_{p1}| \rangle, \quad (\text{II.44})$$

where $\mathbf{x}_{p0}(t)$ and $\mathbf{x}_{p1}(t)$ are the positions of the two particles. This particle-pair dispersion is illustrated in figure II.3. For small Stokes numbers, the particles follow the spatially correlated motion of the turbulent flow before they rapidly disperse and reach their maximum separation, which is defined by the size of the periodic domain. For large Stokes numbers, particles are less affected by the local fluid velocity and possess statistically higher relative velocities even at small distances. Therefore, the particles rapidly disperse without a pronounced phase of correlated motion.

Based on the momentum balance of a particle in Stokes flow

$$\frac{d\mathbf{v}(t)}{dt} = \frac{\mathbf{u}_{@p}(t) - \mathbf{v}(t)}{\tau_p}, \quad (\text{II.45})$$

Csanady [24] analytically derives a relation for how particles respond to the temporal modes of the local fluid velocity. The fluid velocity at the particle position is abbreviated as $\mathbf{u}_{@p}(t) = \mathbf{u}(\mathbf{x}_p(t), t)$. The temporal Fourier transform of the particle momentum balance reads

$$(1 + i\omega\tau_p)\hat{\mathbf{v}}(\omega) = \hat{\mathbf{u}}_{@p}(\omega), \quad (\text{II.46})$$

where i is the imaginary unit and ω is the frequency. After taking the dot product of the equation with their respective complex conjugate, which is indicated by the superscript \star , the modal particle kinetic energy response, $E_p(\omega)$, is obtained as a function of the local modal fluid kinetic energy, $E_f(\omega)$,

$$E_p(\omega) = H^2(\omega)E_f(\omega), \quad (\text{II.47})$$

where $E_p(\omega) = \hat{\mathbf{v}}(\omega) \cdot \hat{\mathbf{v}}^*(\omega)/2$, $E_f(\omega) = \hat{\mathbf{u}}_{@p}(\omega) \cdot \hat{\mathbf{u}}_{@p}^*(\omega)/2$, and the response function is given as

$$H^2(\omega) = \frac{1}{1 + \omega^2\tau_p^2}. \quad (\text{II.48})$$

The response function shows that the particle kinetic energy increasingly lags behind the fluid kinetic energy for increasing particle relaxation times (large particles, dense particles, and small fluid viscosity) and for increasing frequency. Therefore, particles can follow the slow fluid motion well, but cannot respond to fast fluid velocity changes. In turbulent flows, small frequencies (temporal modes) mainly correspond to small wave numbers (spatial modes) and large frequencies to large wave numbers. Hence, particles follow large scale fluid motion better than small scale fluid motion. The motion of a spherical particle in turbulent flow at small particle Reynolds numbers can be further analyzed by considering the differential equation system consisting of equation (II.37) and equation (II.45). After sufficiently long times, the solution in a turbulent flow is qualitatively independent of the initial conditions. The formal solution of the differential equation system with the initial conditions $\mathbf{x}_p(t=0) = 0$ and $\mathbf{v}(t=0) = 0$ is given as

$$\mathbf{x}_p(t) = \int_0^t \mathbf{u}(\mathbf{x}_p(t'), t') \left[1 - e^{-(t-t')/\tau_p}\right] dt'. \quad (\text{II.49})$$

Integrating by parts and truncating errors of the order of $\mathcal{O}(\tau_p^2)$ gives

$$\mathbf{x}_p(t) = \int_0^t \mathbf{u}(\mathbf{x}_p(t'), t') dt' - \tau_p \mathbf{u}(\mathbf{x}_p(t), t) + \mathcal{O}(\tau_p^2), \quad (\text{II.50})$$

and after differentiating with respect to time

$$\mathbf{v}(t) = \mathbf{u}(\mathbf{x}_p(t), t) - \tau_p \frac{d\mathbf{u}(\mathbf{x}_p(t), t)}{dt} + \mathcal{O}(\tau_p^2), \quad (\text{II.51})$$

where the operator d/dt applied to the fluid velocity indicates the time derivative along a particle trajectory. The temporal derivative of the fluid velocity along a particle trajectory may be approximated as

$$\begin{aligned} \frac{d\mathbf{u}(\mathbf{x}_p(t), t)}{dt} &= \frac{\partial \mathbf{u}(\mathbf{x}_p(t), t)}{\partial t} + \mathbf{v} \cdot \nabla \mathbf{u}(\mathbf{x}_p(t), t) \\ &= \frac{\partial \mathbf{u}(\mathbf{x}_p(t), t)}{\partial t} + \mathbf{u}(\mathbf{x}_p(t), t) \cdot \nabla \mathbf{u}(\mathbf{x}_p(t), t) + \mathcal{O}(\tau_p), \end{aligned} \quad (\text{II.52})$$

which yields the following approximation for the particle velocity of particles with small particle relaxation times derived by Maxey [83]

$$\mathbf{v}(t) = \mathbf{u}(\mathbf{x}_p(t), t) - \tau_p \left(\frac{\partial \mathbf{u}(\mathbf{x}_p(t), t)}{\partial t} + \mathbf{u}(\mathbf{x}_p(t), t) \cdot \nabla \mathbf{u}(\mathbf{x}_p(t), t) \right) + \mathcal{O}(\tau_p^2). \quad (\text{II.53})$$

By taking the divergence of the approximation of the particle velocity, it becomes evident that the particle velocity possesses sources and sinks

$$\nabla \cdot \mathbf{v} = 2\tau_p Q + \mathcal{O}(\tau_p^2), \quad (\text{II.54})$$

where Q is the second invariant of the fluid velocity gradient tensor

$$Q = \frac{1}{2} (\Omega_{ij} \Omega_{ij} - S_{ij} S_{ij}), \quad (\text{II.55})$$

and the rotation-rate tensor is given as

$$\Omega_{ij} = \frac{1}{2} \left(\frac{\partial u_i}{\partial x_j} - \frac{\partial u_j}{\partial x_i} \right). \quad (\text{II.56})$$

Note that the evaluation of the divergence operator applied to the particle velocity, a Lagrangian quantity, requires an infinite number of uniformly distributed particles. A spatial derivative is not defined for a single particle.

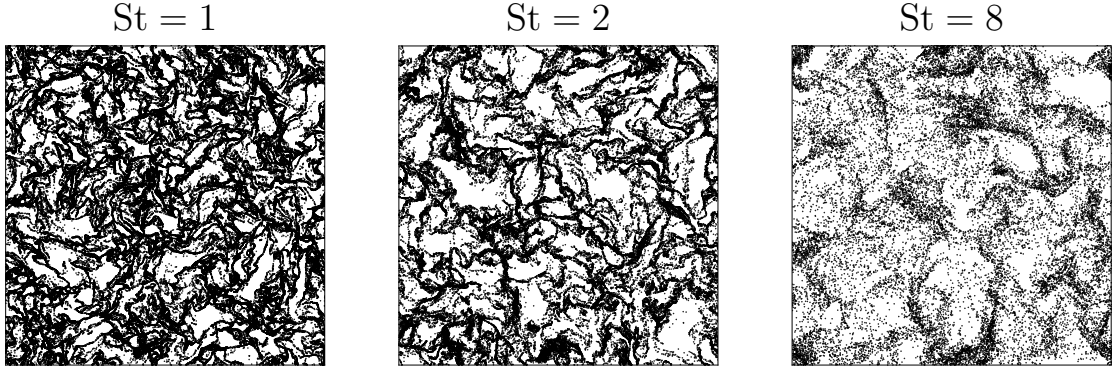


Figure II.4: Clustering of particles of three different Stokes numbers in HIT at $Re_\lambda = 75$. The particle positions are projected from a slice of thickness η .

Equation (II.54) shows that for particles of small τ_p , strain leads to negative divergence (particles are attracted) and rotation to positive divergence (particles are expelled). This clustering of particles is indeed observed in simulations and experiments and strongly depends on the Stokes number. At very small Stokes numbers, particles follow the streamlines of the divergence-free fluid velocity almost perfectly and, hence, do not exhibit significant clustering. At large Stokes numbers, particles are weakly influenced by the turbulent velocity fluctuations and experience them as pseudo random homogeneous and isotropic forcing, which yields a nearly uniform particle distribution. There are different explanations for the clustering of particles at intermediate Stokes numbers. The vortex centrifuge mechanism states that particles cannot completely follow the curved streamlines in vortical structures because of the centrifugal force and, therefore, are less likely to be found in these regions of the flow [5, 14]. The sweep-stick mechanism proposed by Chen *et al.* [20], explains particle clustering by an accumulation of particles in zero fluid acceleration regions. According to either of the mechanisms, however, the reproduction of particle clustering requires the particles to be transported with a vector field of similar spatial and temporal structure as real turbulence.

Figure II.4 shows the clustering of particles with $St = 1$, $St = 2$, and $St = 8$ in HIT. It is clearly observed that the density and the shape of the particle clusters depends on the Stokes number. Particles with $St = 1$ produce many small clusters of high density and regions that are completely particle-free. Increasing the Stokes number to $St = 2$ yields slightly coarser clusters because of the reduced tendency of particles to follow the small flow structures. Particles with $St = 8$ are much more uniformly distributed but some coarse regions of increased particle density are still observed.

II.2.2 Influence of the particles on the turbulence

With increasing mass fraction, $\phi = m_p/m_f$, where m_p is the total mass of the particles and m_f is the fluid mass, the impact of the particles on the turbulence increases. The governing equations of the fluid (II.1) and (II.2) do not change in the particle-laden case, solely additional boundary conditions for the velocity and the pressure at the particle surface are required. The additional boundary conditions may effect the turbulence severely, such that characteristic features of single-phase turbulence, e.g., the inertial range slope of the kinetic energy spectrum, do not persist. Because of the Eulerian description of the fluid flow and the Lagrangian description of the particles, drawing theoretical conclusions is intricate. A common simplification to analyze the effect of small particles on turbulence is to set the particle size to zero. The boundary conditions degenerate to zero-dimensional points and the fluid momentum balance becomes (see, e.g., Boivin *et al.* [11], Elghobashi and Truesdell [32], Ferrante and Elghobashi [36], Maxey [81], Maxey and Patel [82], Maxey *et al.* [85], Squires and Eaton [116])

$$\rho_f \frac{\partial u_i}{\partial t} + \rho_f \frac{\partial u_i u_j}{\partial x_j} = -\frac{\partial p}{\partial x_i} + \mu_f \frac{\partial}{\partial x_j} \left[\left(\frac{\partial u_i}{\partial x_j} + \frac{\partial u_j}{\partial x_i} \right) \right] - \sum_q \delta(\mathbf{x} - \mathbf{x}_{p,q}) F_{f,q,i} \quad (\text{II.57})$$

where $\delta(\mathbf{x} - \mathbf{x}_p)$ is the Dirac distribution and q the index of a particle. With the point-particle assumption, the ensemble averaged transport equation of the fluid kinetic energy (II.24) can be extended to particle-laden HIT [86, 119, 129]

$$\frac{d\langle K \rangle}{dt} = -\langle \epsilon \rangle + \phi \langle \Phi_p \rangle, \quad (\text{II.58})$$

where $\langle \Phi_p \rangle$ is the ensemble averaged particle energy exchange term in Stokes flow. Note that averaging over the fluid volume is equivalent to ensemble averaging in HIT. Approximating the particle velocity for small particle relaxation times according to equation (II.53), the ensemble averaged particle energy exchange term can be expressed as

$$\begin{aligned} \langle \Phi_p \rangle &= - \int_{\Omega} \sum_q \mathbf{u} \cdot \left(\frac{\mathbf{u} - \mathbf{v}_q}{\tau_p} \right) \delta(\mathbf{x} - \mathbf{x}_{p,q}) dV \\ &= - \int_{\Omega} \sum_q \left(\frac{\partial K}{\partial t} + u_j \frac{\partial K}{\partial x_j} \right) \delta(\mathbf{x} - \mathbf{x}_{p,q}) dV + \mathcal{O}(\tau_p) = -\frac{d\langle K \rangle}{dt} + \mathcal{O}(\tau_p), \end{aligned} \quad (\text{II.59})$$

The last equality holds for a sufficiently large number of uniformly distributed particles. Inserting the resulting expression into equation (II.58), gives [30]

$$\langle \Phi_p \rangle = \frac{1}{1 + \phi} \langle \epsilon \rangle + \mathcal{O}(\tau_p), \quad (\text{II.60})$$

and, hence

$$\frac{d\langle K \rangle}{dt} = \langle \epsilon \rangle \left(\frac{\phi}{1 + \phi} - 1 \right) + \mathcal{O}(\tau_p). \quad (\text{II.61})$$

For small particle relaxation times, the particle energy exchange term adds energy to the fluid, which is confirmed by Letournel *et al.* [71] using point-particle DNS. Point-particle DNS rely on the point-particle assumption, which conserves the total momentum but leads to an unphysical loss of energy of the fluid-particle mixture as shown by Xu and Subramaniam [129]. However, the point-particle assumption is extensively used in studies of turbulence modulation by particles [11, 32, 36, 71, 77, 116] and, at least partially, justified by Fröhlich *et al.* [38], Schneiders *et al.* [111], Subramaniam *et al.* [119], who show theoretically and with numerical simulations that the point-particle approximation predicts a realistic fluid kinetic energy, although the fluid dissipation and the particle energy exchange term differ from the actual expressions.

Although the particle energy exchange term in the limit of vanishing particle relaxation time in equation (II.61) is positive, the ensemble averaged fluid kinetic energy is not necessarily larger in the particle-laden case than in the single-phase flow. In fact, the fluid dissipation is also a function of the mass fraction [77]. The impact of particles smaller than the Kolmogorov length scale in turbulence on the kinetic energy and its spectral distribution is investigated extensively in a variety of studies [11, 32, 36, 71, 77, 116]. An important conclusion is that particles of this size can attenuate or enhance turbulence dependent on the configuration. A typically observed behavior is that the particles remove fluid kinetic energy from the large flow scales and add kinetic energy to small scales relative to the corresponding single-phase flow. To which extent the turbulence is modulated and which scales are impacted, strongly depends on the parameters of the turbulence and the particles. Typically investigated influence parameters for the turbulence modulation by the particles include, e.g., the Stokes number, the mass fraction, the volume fraction and the particle size with respect to the Kolmogorov length scale. Figure II.5 shows the kinetic energy spectrum of particles with three different Stokes numbers compared to the corresponding single-phase kinetic energy spectrum. In

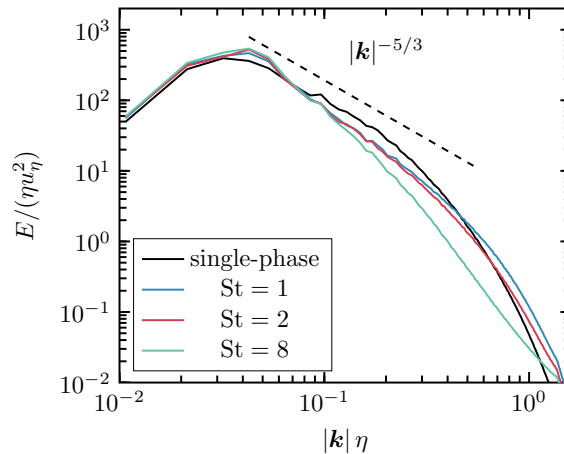


Figure II.5: Kinetic energy spectrum of HIT at $\text{Re}_\lambda = 75$ without particles and with particles of three different Stokes numbers. The particle mass fraction is $\phi = 1.0$ for all of the three Stokes numbers and the simulations are conducted using the point-particle assumption.

all of the three particle-laden cases, the particle mass fraction is $\phi = 1.0$. For all Stokes numbers, particles remove kinetic energy from the inertial range and add it to the dissipation range. The amount of transferred energy and the point where the single-phase kinetic energy spectrum is crossed differ between the Stokes numbers. Particles of larger Stokes number remove more energy from the inertial range and cross the single-phase kinetic energy spectrum at larger wave numbers. Based on similar observations, Mallouppas *et al.* [77] propose an empirical correlation for the particle energy transfer dependent on the wave number that resembles the transfer of energy from the inertial range to the dissipation range by the particles. Apart from HIT, however, the general understanding of turbulence modulation by particles is very limited.

Modeling of particle-laden turbulence

III.1 Modeling the flow using LES

From a computational point of view, the simulation of turbulence of high Reynolds numbers is demanding because of its multi-scale nature. In numerical simulations of fluid flow, the governing equations (II.1) and (II.2) are discretized using a computational grid, which results in an algebraic equation system that can be solved by a computer. In HIT, the ratio of the largest flow scale, \mathcal{L} , (minimal size of the computational domain) to the Kolmogorov length scale, η , (the order of the largest size of a computational grid cell) scales as $\mathcal{L}/\eta = \mathcal{O}(\text{Re}^{3/4})$. Therefore, the number of computational grid cells in a three-dimensional domain scales as $\mathcal{O}(\text{Re}^{9/4})$. Since the ratio of largest to smallest time scale is proportional to $\mathcal{O}(\text{Re}^{1/2})$ and, independent of the convergence order of the time integration scheme, the time step is typically reduced linearly with the grid cell size for stability and consistency reasons [22], the required computational resources are proportional to $\mathcal{O}(\text{Re}^3)$ [106].

The question may be raised if all of the detailed flow features of the turbulent flow are equally important or if there are applications where specific features of the flow can be neglected and the essential behavior of the considered system is conserved. This idea suggests to decompose the flow quantities into essential and less essential contributions. Because of the non-linearity of the governing equations (II.1) and (II.2), the less essential contributions affect the essential contributions and closures are required. The Reynolds decomposition proposed by Reynolds [103], divides the flow quantities into an ensemble averaged and a fluctuating component and forms the basis of the widely used RANS simulations. In many flow configurations, how-

ever, the ensemble averaged fluid velocity and pressure are not the essential flow features. In HIT, for instance, the ensemble averaged fluid velocity and pressure field is a constant value everywhere. In dynamic problems, such as vortex shedding of the wake of an object, the ensemble averaged fields do not contain information about the temporal dynamics of the flow. Essential features of the application, e.g., the fluid dynamical forces acting on the object, may be incorrect. More information is retained by decomposing the flow quantities into large scales and small scales using the filtering operation defined in equation (II.25), which gives the filtered (large scale) quantity, $\tilde{\Phi}$, and the subfilter (small scale) quantity, Φ' . It can be argued that the large scales are the essential scales in a turbulent flow because they possess the majority of the kinetic energy as suggested by the steep slope of the kinetic energy spectrum in the inertial range. Solving the FNSE (II.27) and (II.28) for the large scales and providing a closure for the subfilter stress tensor, $\tau_{ij} = \widetilde{u_i u_j} - \tilde{u}_i \tilde{u}_j$, is called LES [72, 106, 112, 115]. Note that in the scope of LES the subfilter stress tensor is commonly referred to as subgrid-scale stress tensor and the subfilter scales as subgrid scales. In the remainder of the thesis, the words subgrid and subfilter are used interchangeably.

The size of the smallest flow structures of the filtered flow field increases with the filter width of the filter kernel G . The size of the computational grid cells is typically increased accordingly, which leads to fewer computational grid cells and, hence, less computational effort. Increasing the filter width, however, results in a larger range of scales that require modeling and the uncertainties in the calculation of the filtered flow field increase.

In an LES of a single-phase flow, the interactions between the filtered scales and the subgrid scales are fully contained in the subgrid-scale stress tensor. To compute the subgrid-scale stress tensor, the fluid velocity, u_i , is required, which is not known in an LES. To derive models for the subgrid-scale stress tensor, it is instructive to study the phenomenology of the interactions between filtered scales and subgrid scales. The analysis is significantly simplified if the energetic interactions between the scales are investigated instead of the momentum exchange. The subgrid-scale stress tensor can either transfer energy from large to small scales or vice versa at every point in space. Contracting the filtered momentum equation (II.28) with the filtered fluid velocity \tilde{u}_i gives the transport equation for the local fluid kinetic energy of the filtered scales $K_F = \tilde{u}_i \tilde{u}_i / 2$ [12, 56]

$$\rho_f \frac{\partial K_F}{\partial t} + \frac{\partial J_j}{\partial x_j} = -2\mu_f \tilde{S}_{ij} \tilde{S}_{ij} + \rho_f \tau_{ij} \tilde{S}_{ij}, \quad (\text{III.1})$$

with the spatial fluxes

$$J_j = \rho_f \tilde{u}_j K_F + \tilde{u}_j \tilde{p} - 2\mu_f \tilde{u}_i \tilde{S}_{ij} + \rho_f \tilde{u}_i \tau_{ij}. \quad (\text{III.2})$$

The terms belonging to J_j transfer kinetic energy in space and can locally exchange kinetic energy with the subgrid scales. However, since in HIT $\langle \partial J_j / \partial x_j \rangle = 0$, the spatial fluxes, including the term with the subgrid-scale stress tensor, do not contribute to the net energy transfer. The first term on the right-hand side of equation (III.1) is the fluid dissipation, which always removes energy, especially in high strain regions. The second term on the right-hand side of equation (III.1), referred to as energy exchange term $\rho_f \Pi = -\rho_f \tau_{ij} \tilde{S}_{ij}$, includes the subgrid-scale stress tensor and can potentially have a non-zero global mean. This term occurs with opposite sign in the transport equation for the subgrid-scale kinetic energy $K_{\text{sgs}} = \tau_{ii}/2$ (see, e.g., Ghate and Lele [44], Johnson [55]) and, therefore, represents the energy exchange between the filtered and subgrid scales. Figure III.1 shows the PDF of the energy exchange term in HIT. The fluid velocity field is obtained from a DNS and is explicitly filtered using a spectrally sharp filter of three different cut-off wave numbers k_{cut} . The PDFs are skewed towards positive values and possess a positive mean, which results in a net energy transfer from the filtered scales to the subgrid scales. The larger the filter width, the more energy is removed, on average, from the filtered scales. The energy transfer from large to small scales is commonly referred to as forward energy cascade and the opposite process of energy transfer from small to large scales as backward energy cascade. It is worth noting that the energy is not necessarily transferred from the smallest filtered scales to the largest subgrid scales. Because of the spectral non-locality of the energy exchange, even the largest filtered scales and smallest subgrid scales can exchange energy [126]. The phenomenological observation that, on average, the subgrid-scale stress tensor acts as an energy sink in HIT motivates the modeling of the subgrid-scale stress tensor using an additional viscosity. According to the Boussinesq hypothesis, the modeled subgrid-scale stress tensor is expressed as [106]

$$\tau_{\text{mod},ij} - \frac{1}{3}\tau_{\text{mod},kk}\delta_{ij} = -2\nu_t \tilde{S}_{ij}, \quad (\text{III.3})$$

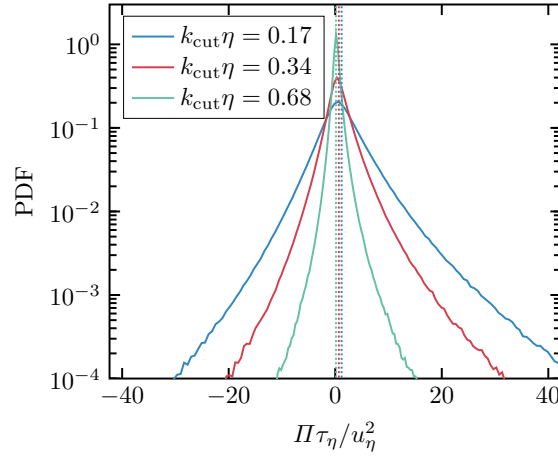


Figure III.1: PDF of the normalized energy exchange term of the explicitly filtered velocity field of HIT. The fluid velocity field is filtered with a spectrally sharp filter of three different cut-off wave numbers k_{cut} . The vertical dotted lines indicate the mean values.

where ν_t is an additional (kinematic) turbulent viscosity. Therefore, the modeled filtered momentum equation of the fluid is given as

$$\rho_f \frac{\partial \tilde{u}_i}{\partial t} + \rho_f \frac{\partial \tilde{u}_i \tilde{u}_j}{\partial x_j} = -\frac{\partial \tilde{P}}{\partial x_i} + \frac{\partial}{\partial x_j} \left[(\mu_f + \rho_f \nu_t) \left(\frac{\partial \tilde{u}_i}{\partial x_j} + \frac{\partial \tilde{u}_j}{\partial x_i} \right) \right], \quad (\text{III.4})$$

where the trace of the subgrid-scale stress tensor is absorbed by the modified pressure, \tilde{P} .

To derive expressions for the turbulent viscosity, strong assumptions are required that are, at most, valid only in very specific flow configurations. If it is assumed that the energy that is transferred to the small scales is instantaneously dissipated by the small scales such that the kinetic energy spectrum remains constant, i.e., the turbulence is in local equilibrium, the dissipation induced by the turbulent viscosity equals the viscous dissipation of the subgrid scales. Additionally, a model spectrum for HIT has to be assumed to obtain an expression for the viscous dissipation. This leads to the Smagorinsky model for the turbulent viscosity [115]

$$\nu_t = (C_S \Delta)^2 (2\tilde{S}_{ij}\tilde{S}_{ij})^{1/2}, \quad (\text{III.5})$$

where Δ is the filter width and C_S is a constant. Note that the outlined derivation is only valid for the ensemble averaged turbulent viscosity and there is no theoretical justification for evaluating the turbulent viscosity in the widely used form of equation (III.5). The constant C_S is typically chosen in the range $0.1 \leq C_S \leq 0.2$ [21, 26] or

computed dynamically [42, 73].

Unless the turbulent viscosity is locally negative, the effect of the modeled subgrid-scale stress tensor is exclusively dissipative, which is contrary to what is observed in figure III.1. An improved model for the subgrid-scale stress tensor that is capable of modeling the backward energy cascade is the localized dynamic kinetic energy model (LDKM) of Menon and coworkers [59, 88] according to which

$$\tau_{\text{mod},ij} = -2\nu_t \tilde{S}_{ij} + \frac{2}{3} K_{\text{sgs}} \delta_{ij}, \quad (\text{III.6})$$

where the turbulent viscosity is a function of the subgrid-scale kinetic energy

$$\nu_t = C_k \Delta \sqrt{K_{\text{sgs}}}. \quad (\text{III.7})$$

The subgrid-scale kinetic energy is not available in an LES but it can be estimated with the transport equation [72, 88]

$$\frac{\partial K_{\text{sgs}}}{\partial t} + \tilde{u}_i \frac{\partial K_{\text{sgs}}}{\partial x_i} = -\tau_{\text{mod},ij} \frac{\partial \tilde{u}_i}{\partial x_j} - C_\epsilon \frac{K_{\text{sgs}}^{3/2}}{\Delta} + \frac{\partial}{\partial x_i} \left(\nu_t \frac{\partial K_{\text{sgs}}}{\partial x_i} \right). \quad (\text{III.8})$$

With this procedure, severe limitations of the Smagorinsky model are mitigated. The turbulence does not necessarily have to be in local equilibrium, because energy that is transferred to the subgrid scales can accumulate, be transferred back to large scales or dissipate. Furthermore, the direction of the energy transfer is not predetermined but can be in both directions dependent on the local flow. The constants C_k and C_ϵ are computed dynamically to match the subgrid-scale stress tensor and dissipation at a larger filter level. The dynamic computation allows the constant C_k to be negative, which mimics the backward energy cascade.

A fundamental limitation of the turbulent viscosity models for the subgrid-scale stress tensor following the Boussinesq hypothesis according to equation (III.3) is that they are constructed to replicate the energetic effect of the subgrid-scale stress tensor and disregard its effect on the fluid momentum. A relatively strong correlation can be observed between the energy exchange term computed with the turbulent viscosity and computed by explicit filtering [21, 74], but poor agreement is observed for the subgrid-scale stress tensor itself. The turbulent viscosity subgrid-scale models result in a modeled subgrid-scale stress tensor that possesses Eigenvectors aligned with those of the filtered strain-rate tensor. As shown by Horiuti [53], Tao *et al.* [121, 122], however, the Eigenvectors of the subgrid-scale stress tensor obtained by explicit filtering have a preferential alignment that clearly deviates from the

Eigenvectors of the filtered strain-rate tensor. Tensor based subgrid-scale models exist that predict excellent alignment and correlation with the subgrid-scale stress tensor [12, 87] such as the scale similarity model proposed by Bardina *et al.* [6]

$$\tau_{\text{mod},ij} \propto \overline{\tilde{u}_i \tilde{u}_j} - \tilde{u}_i \tilde{u}_j, \quad (\text{III.9})$$

where $\bar{\cdot}$ indicates filtering at a larger scale, or the so-called non-linear model according to which the subfilter stress tensor is modeled as [70]

$$\tau_{\text{mod},ij} \propto \Delta^2 \frac{\partial \tilde{u}_i}{\partial x_k} \frac{\partial \tilde{u}_j}{\partial x_k}, \quad (\text{III.10})$$

which is essentially an approximation of the scale similarity model by means of a first order spatial Taylor series expansion of the filtered fluid velocity. It is shown analytically by Johnson [55] that the non-linear model exactly represents the mechanisms of filtered scale strain self-amplification and vortex stretching in the case of a Gaussian filter. However, these two models predict too few energy transfer towards the small scales and are, hence, not suitable for the most applications. The subgrid-scale stress tensor of mixed models combines the scale similarity and turbulent viscosity approach, which leads to a modeled subgrid-scale stress tensor that predicts enough dissipation and relatively strong alignment with the subgrid-scale stress tensor obtained from explicit filtering [74].

It is worth noting that there are several difficulties or even conceptual problems associated to LES that require attention when new LES methodologies are applied or developed. A detailed discussion exceeds the scope of this thesis but some of these issues are briefly outlined in the following list.

- Practical applications of LES typically involve complex geometries that require inhomogeneous and anisotropic computational grids. If the filter in these configurations is adapted to the computational grid, additional closures arise [106]. Consequently, local grid refinement in LES is not straightforward since either models for the additional closures have to be applied, or the large filter width and, therefore, a potentially large modeling error persists in the whole domain.
- The discretization of the governing equation imposes a numerical error. If the filter width in the subgrid-scale model is chosen too small, the numerical error exceeds the impact of the modeled subgrid-scale stress tensor and dominates the flow dynamics in a potentially undesired way. Subgrid-scale models exist, the so-called implicit LES models, that tailor the numerical error to match

the desired dynamics of the subgrid-scale stress tensor instead of explicitly modeling it (see, e.g., Margolin *et al.* [80]).

- It can be argued that many subgrid-scale models are actually exact expressions without any modeling error, as long as the filter kernel, G , is not specified. If a potentially anisotropic and inhomogeneous filter, G , exist, such that $\tau_{\text{mod},ij} = \widetilde{u_i u_j} - \tilde{u}_i \tilde{u}_j$, the modeled subgrid-scale stress tensor is equal to the exact subgrid-scale stress tensor. Even if no subgrid-scale model is applied at all, the numerical error imposes an unknown filter that yields a subgrid-scale stress tensor that exactly matches the discretization error. For interpretable results, however, spatially compact, homogeneous, and isotropic filters are desired. Strictly speaking, proposing subgrid-scale models without specifying the targeted filter kernel is pointless. In the LES model development a top-hat or Gaussian filter kernel is often implicitly assumed.
- LES are typically performed on a grid that is fine enough to resolve the highest wave numbers occurring in the filtered velocity \tilde{u}_i . However, the non-linear advective term $\partial \tilde{u}_i \tilde{u}_j / \partial x_j$ and the subgrid-scale stress tensor contain wave numbers that are too large to be resolved by the grid, which can lead to aliasing errors [65, 90]. Even an exact expression for the subgrid-scale stress tensor may require an additional viscosity to dampen the aliasing errors and to avoid instabilities as they are observed when applying the scale similarity model or the non-linear model.
- The question may be raised if the division of turbulence into large and small scales is a suitable decomposition of turbulence at all. There exist vortex structures in turbulence that contain wave numbers very far apart, such as elongated eddies or vortex filaments [126]. In LES, such structures are partially resolved and must be partially modeled, which does not only require statistical but fully localized knowledge of the subgrid scales. Furthermore, the energy transferred to small scales and the dissipation are only weakly correlated, i.e., the energy is not dissipated where it is transferred to the small scales [12]. Both facts suggest that it could be impossible to suitably model the subgrid-scale stress tensor from knowledge of the large scale turbulence only.
- The fundamental assumption of LES that the large flow scales are the essential flow scales is often, but not always, appropriate. It is shown in section III.4 that the small scales can significantly influence the dynamics of a particle-laden turbulent flow and the subgrid turbulence may require explicit reconstruction.

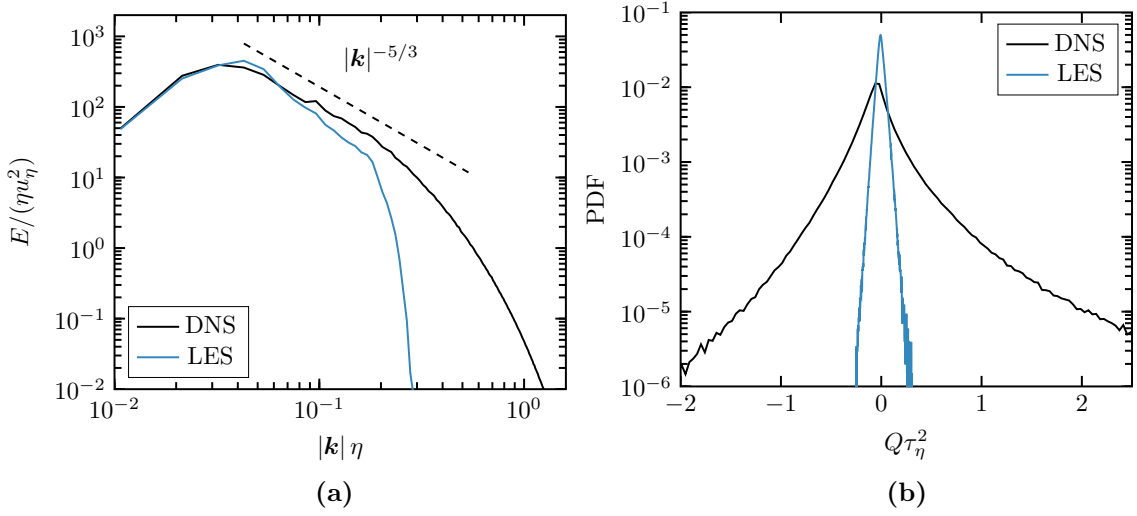


Figure III.2: Kinetic energy spectrum (a) and second invariant of the velocity gradient tensor (b) obtained from the DNS and an LES with the LDKM of HIT at $\text{Re}_\lambda = 75$.

More detailed discussions and other difficulties of LES may be found in Pope [97], Tsinober [126].

The effect that an LES has on flow quantities particularly relevant for particle-laden flows is shown in figure III.2. The kinetic energy spectrum and the second invariant of the velocity gradient tensor are compared between the DNS and an LES using the LDKM. The kinetic energy spectrum of the LES possesses the majority of the kinetic energy of the DNS but the small scales are absent. The PDF of the second invariant of the velocity gradient tensor is very narrow in the case of the LES compared to the DNS. Large strain and vorticity events predominantly occur at the small scales because of the statistically higher probability of large velocity gradients. At least for small particle relaxation times, analytical analysis suggests that the second invariant of the velocity gradient tensor substantially influences the particle clustering (see section II.2.1).

III.2 Coupling between flow and particles

The physical coupling between fluid and particles is by means of boundary conditions. At the surface of the sphere, the fluid velocity is typically assumed to be equal to the velocity of the particle, which consists in the case of a rigid particle of a superposition of particle translational and rotational motion. The particle experiences

a translational and rotational acceleration caused by the fluid dynamical stresses at the particle surface. If the computational mesh possesses a sufficient number of degrees of freedom on the particle surface, the boundary conditions can be directly applied to the fluid and the fluid dynamical stresses on the particle surface can be computed. Therefore, no additional modeling errors are introduced and solely the discretization errors remain. The described methodology is commonly referred to as particle-resolved simulation and limited to a relatively small number of particles, because the number of computational mesh cells rapidly reaches the maximum of what is possible with currently available computational resources. Hence, it is inevitable for flow configurations that include millions of particles to model the coupling between fluid and particles.

The fluid-particle coupling is divided into the effect of the flow on the particles and the modification of the flow by the particles. If only the effect of the fluid on the particle is modeled, the simulation is commonly referred to as one-way coupled and if both directions of interaction are considered it is referred to as two-way coupled. Although collisions between particles are ignored in the present work, it is worth mentioning that an additional inclusion of particle-particle interactions is called four-way coupling.

Particle rotation is not considered in the present work and, therefore, the one-way coupling problem consists of determining the fluid dynamical force acting on the particle. As discussed in section II.2.1, the dominant force in a particle-laden gas flow is the drag force, which can be estimated from empirical correlations, e.g., the correlation of Schiller and Naumann [108], that assumes the fluid velocity at the particle position to be equal to the uniform free stream velocity of the flow around an isolated sphere. Note that the correlation of Schiller and Naumann [108] is not applicable if other particles in the close vicinity disturb the flow significantly. In this case, corrections for the mean drag and drag fluctuations are required, which is still an active topic of research [1, 104].

The most common model for the two-way coupling is based on the point-particle assumption that is introduced in section II.2.2. The particle momentum source in the fluid momentum equation (II.57) contains the Dirac distribution, which is not suitable for numerical treatment. Different numerical methods differ in how the Dirac distribution is regularized. Integrating the particle momentum source over a computational mesh cell Ω_{cell} , which is consistent with the finite volume fluid discretization, gives the particle momentum source according to the particle-source-in-cell (PSIC)

method [23]

$$\int_{\Omega_{\text{cell}}} \sum_q \delta(\mathbf{x} - \mathbf{x}_{p,q}) \mathbf{F}_{f,q} dV = \sum_{q \in \Omega_{\text{cell}}} \mathbf{F}_{f,q}, \quad (\text{III.11})$$

where the latter sum indicates the sum over all particles belonging to the computational grid cell, Ω_{cell} . Another option is to replace the Dirac distribution with a Gaussian, which distributes the force from the particle across several computational grid cells [81, 82]. Note however, that for particles of a size comparable to the size of the smallest flow scales, considering the particles as points may introduce significant modeling errors. A consistent concept across all particle size to flow scale size ratios is the volume-filtering [2, 17]. Analog to the spatial filtering applied in the LES methodology, a filter is applied to the fluid-particle mixture, but the region of integration is restricted to the volume occupied by the fluid, Ω_f ,

$$\varepsilon_f \tilde{\Phi}^{\text{vf}}(\mathbf{x}, t) = \int_{\Omega_f(t)} G(|\mathbf{x} - \mathbf{y}|) \Phi(\mathbf{y}, t) dV_y, \quad (\text{III.12})$$

where the fluid volume fraction is defined as

$$\varepsilon_f(\mathbf{x}, t) = \int_{\Omega_f(t)} G(|\mathbf{x} - \mathbf{y}|) dV_y. \quad (\text{III.13})$$

A filter width may be defined as a measure of the width of the filter kernel, G , that determines the size of the smallest flow structures in the volume-filtered fluid velocity field. Similar to the FNSE, the explicitly volume-filtered NSE are not closed but contain terms that depend on flow quantities that are not volume-filtered. The implications of these closures are not very clear and because of a lack of models, the closures are typically neglected without much evidence or replaced with expression that have not been proven to be appropriate in independent studies [17, 118]. In a recent study, however, Hausmann *et al.* [52] systematically investigate the impact of the closures and provide expressions for them. Since the volume-filtering is inherently linked to LES filtering and even equal to LES filtering far away from particles, it seems to be a promising alternative to the point-particle approach for particle-turbulence coupling.

III.3 Optimal basis functions for different physical quantities

One main objective of the present thesis is the reconstruction of a turbulent fluid velocity field to predict the transport of particles in LES accurately. The reconstructed turbulent fluid velocity field has to be represented by some kind of basis functions. The choice of the basis functions plays a pivotal role for the physics that can be represented and for the required computational costs to reconstruct the turbulent fluid velocity field. In the present section, the concept of basis functions is introduced, and some possible basis functions are assessed regarding their suitability to represent a turbulent velocity field.

Given a function $f : \mathbb{R} \mapsto \mathbb{R}$ to be represented by an infinite series of orthogonal basis functions, $\varphi_i : \mathbb{R} \mapsto \mathbb{R}$, (see, e.g., Brunton and Kutz [15])

$$f(x) = \sum_{i=0}^{\infty} c_i \varphi_i(x), \quad (\text{III.14})$$

where $(\varphi_i(x), \varphi_j(x)) = 0$ if $i \neq j$, the coefficients, c_i , are given as

$$c_i = \frac{(f(x), \varphi_i(x))}{(\varphi_j(x), \varphi_j(x))}. \quad (\text{III.15})$$

The inner product of two real functions $f(x)$ and $g(x)$ is defined as

$$(f(x), g(x)) = \int f(x)g(x)dx. \quad (\text{III.16})$$

Representing the function $f(x)$ by an orthogonal basis is similar to a coordinate transformation in linear algebra. For specific physical problems, some functional bases are more suitable than others as they allow to truncate the series expansion given in equation (III.14) after few terms while preserving the essential properties of the physical system.

A common basis for turbulent flows is the Fourier basis, leading to the representation of the function $f(x)$ as a Fourier series expansion, which contains information about the size of flow structures characterized by the wave number k . In turbulence, for instance, the Fourier basis allows to compute the kinetic energy spectrum and to obtain information on how much energy is contained in flow structures of a particular size. However, the Fourier basis is limited in that it is not localized in physical space because of the infinite support of the trigonometric basis functions, i.e., there is only

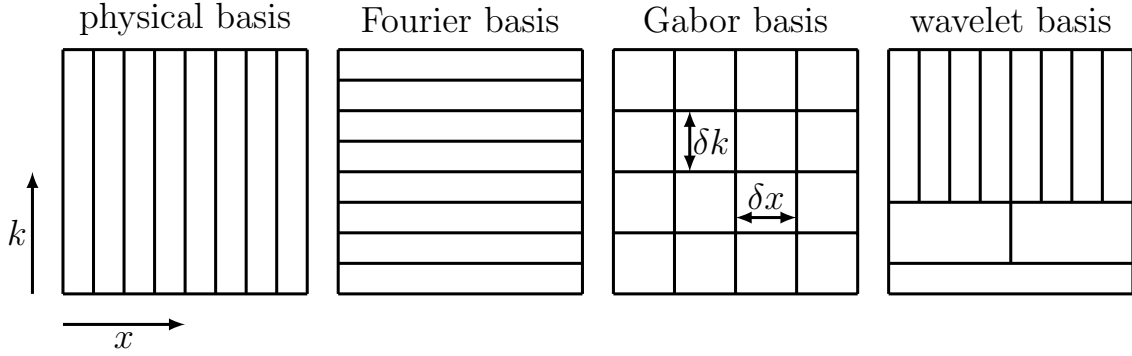


Figure III.3: Visualization of the support in wave number space and real space of different bases. The lengths of the rectangles in the respective coordinate directions, δk and δx , illustrate the size of the support of the basis functions. The figure is inspired by a figure from Brunton and Kutz [15].

information that a specific wave number exists with a specific magnitude, but not on where it is localized in space.

Figure III.3 illustrates the support of different basis functions in physical space, characterized by the position x , and in wave number space, characterized by the wave number k . The support of the basis functions in wave number space and physical space is determined by the length of the rectangles, δk and δx , respectively. A physical basis consists of Dirac distributions at every point in space corresponding to $\delta x = 0$ and, therefore, perfect localization in physical space. However, the support of the Dirac distribution in wave number space is infinite, such that a physical basis does not contain information on the wave number of turbulent structures. A Fourier basis has zero support in wave number space and infinite support in physical space and can perfectly localize wave numbers, but not where they occur in space.

In order to localize physical quantities in physical space and in wave number space, the Fourier basis can be multiplied by a function that is compact (or at least rapidly decaying) in physical and wave number space. If this function is a Gaussian, the resulting basis is referred to as Gabor basis [100]. Note that the Gabor basis is not orthogonal. According to the uncertainty principle, the support in physical and wave number space cannot be arbitrarily reduced [15]. Decreasing the support in physical space increases the support in wave number space and vice versa. The Gabor basis is characterized by a constant support for all wave numbers, which is not optimal. Small wave numbers characterize slow changes in space, which do not require a high spatial resolution. Therefore, the support in physical space can be wide for small wave numbers and a higher resolution in wave number space can be

afforded. Large wave numbers on the contrary, rapidly change in space and require a high spatial resolution to the cost of a wider support in wave number space. In this case, more essential information can be captured with the same number of coefficients as the Gabor basis. The wave number dependent support of the basis functions is realized with wavelet basis functions, which are constructed by scaling and shifting in physical space of a prototype function, the so-called mother wavelet [25, 45].

Note that the optimal basis to represent a physical problem, such as turbulence, is not always the basis with the most compression. If the turbulence is modeled, the basis must provide the option of incorporating knowledge of the turbulence. Another criterion is if the basis is able to significantly simplify the governing equations. The Fourier basis, for instance, may transform differential equations into algebraic equations, which is particularly useful to enforce that a vector field is divergence-free. Although a wavelet basis does not possess this property, wavelet bases may be constructed that are always divergence-free vector fields, independent of the choice of coefficients [27, 28, 69].

III.4 LES of particle-laden turbulence

III.4.1 Interactions that require modeling

The fundamental assumption of LES that the large flow scales are sufficient to capture the essential behavior of the flow is violated if the particles are small enough, such that their motion is substantially affected by the subgrid scales. The response function, that is discussed in section II.2.1, shows that particles with a small particle relaxation time are particularly influenced by the subgrid-scale fluid velocity (see equation (II.48)). In the same section, the analysis of particles with small particle relaxation times analytically demonstrates that the particles enhance the turbulent kinetic energy proportionally to the fluid dissipation, which is a quantity that mainly acts at the subgrid scales (see equation (II.61)). Both analyses suggest that knowledge of the filtered flow scales does not ensure an accurate prediction of the particle dynamics.

The momentum interactions between the turbulence and the particles are sketched in figure III.4. The red arrows indicate the influence of the fluid on the particles by means of the local fluid velocity field. A correct calculation of the drag force acting on the particle requires knowledge of the sum of the filtered fluid velocity and the

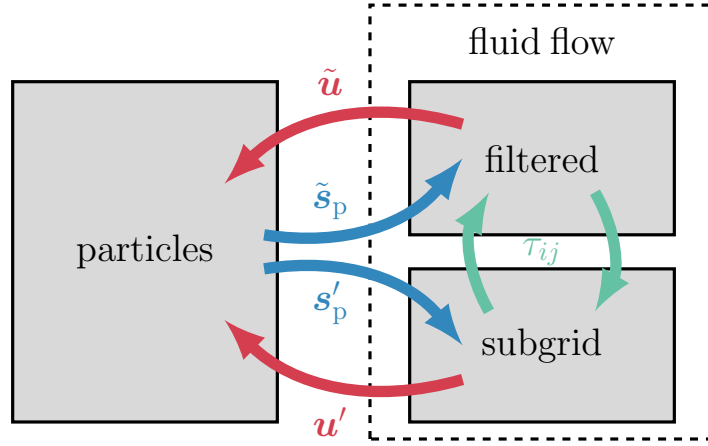


Figure III.4: Sketch of the interactions between filtered and subgrid scales and particles.

subgrid-scale fluid velocity at the particle location

$$\mathbf{u}(\mathbf{x}_{p,q}) = \tilde{\mathbf{u}}(\mathbf{x}_{p,q}) + \mathbf{u}'(\mathbf{x}_{p,q}). \quad (\text{III.17})$$

To conserve momentum, the same force that acts on the particles has to act with opposite sign on the fluid. This feedback to the fluid is represented by the blue arrows in figure III.4. Different ways of distributing the drag force over the fluid are presented in section III.2, which are collectively represented by the particle momentum source term, $\mathbf{s}_p(\mathbf{x})$, that is added to the right-hand side of the single-phase fluid momentum equation (II.2). Therefore, the particle momentum source term can represent, e.g., the average of the drag forces of all particles found in a computational cell according to the PSIC method introduced in section III.2

$$\mathbf{s}_p(\mathbf{x}) = -\frac{1}{V_{\text{cell}}} \sum_{q \in \Omega_{\text{cell}}} \mathbf{F}_{D,q}, \quad \mathbf{x} \in \Omega_{\text{cell}}, \quad (\text{III.18})$$

where V_{cell} is the volume of a computational cell, or the sum of the drag forces spread with the kernel G

$$\mathbf{s}_p(\mathbf{x}) = -\sum_q G(|\mathbf{x} - \mathbf{x}_{p,q}|) \mathbf{F}_{D,q}. \quad (\text{III.19})$$

Note that the time dependencies are omitted for conciseness. Since the fluid flow is considered to be split into filtered and subgrid-scale motion, the particle momentum source term is divided as well, such that $\tilde{\mathbf{s}}_p$ is applied to the FNSE and \mathbf{s}'_p to the

SFNSE. The total momentum conservation requires

$$\mathbf{s}_p(\mathbf{x}) = \tilde{\mathbf{s}}_p(\mathbf{x}) + \mathbf{s}'_p(\mathbf{x}). \quad (\text{III.20})$$

The interactions between the filtered and subgrid scales of the fluid are indicated by green arrows in figure III.4 and represented by the subgrid-scale stress tensor in the governing equations of the fluid. These interaction also exist in a single-phase flow, but the knowledge of interscale momentum and energy exchange in single-phase turbulence may not apply to the particle-laden case as the particles can substantially modify the filtered and subgrid scales.

III.4.2 Modeling the effect of the unresolved turbulence on the particles

The modeling of particle-turbulence interactions in the scope of an LES is discussed separately for the one-way coupling and the two-way coupled case. One-way coupling is assumed when the particles do not substantially modify the flow. Therefore, the blue interaction in figure III.4 are neglected and the subgrid-scale stress tensor is assumed to be similar to the subgrid-scale stress tensor in single-phase turbulence. To accurately compute the drag force acting on the particle, the subgrid-scale velocity at the particle position is required in addition to the filtered velocity. The former requires modeling and the latter is approximated by solving the FNSE with a modeled subgrid-scale stress tensor in an LES. A variety of studies exist that demonstrate that particle clustering and dispersion of particles with Stokes numbers $St = \mathcal{O}(1)$ is poorly predicted if the particles are only transported with the filtered fluid velocity field [3, 34, 76, 78, 98, 101].

The particle pair dispersion of particles with $St = 1$ is depicted in figure III.5 for the DNS and an LES with the LDKM of HIT at $Re_\lambda = 75$. Since the small fluid velocity scales are absent in the LES, the particle pairs disperse slower than in the DNS. The large scale velocity decorrelates much slower than the small scale velocity, which causes a small relative motion between the particles in the LES, even at significant separations.

Figure III.6 shows the fluid velocity magnitude of HIT at $Re_\lambda = 75$ and of the corresponding filtered field together with particles of $St = 2$ that are transported with the respective field. The subgrid-scale velocity, although only containing a small fraction of the total kinetic energy of the flow, has significant impact on the clustering of the particles. The fluid velocity field of the DNS yields many small

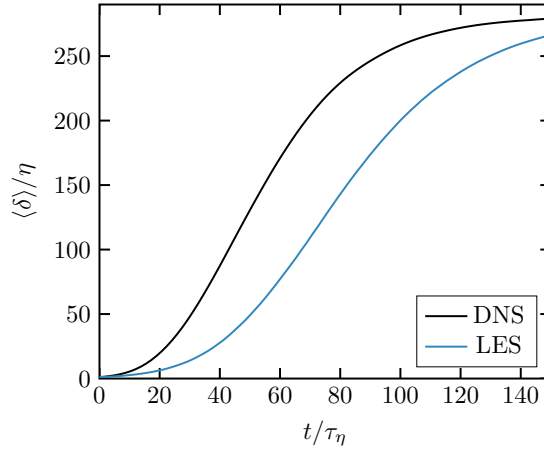


Figure III.5: Comparison of the particle pair dispersion between the DNS and an LES with the LDKM of particles with $St = 1$ in HIT at $Re_\lambda = 75$.

particle clusters while the filtered fluid velocity causes the particles to form large regions that almost contain no particles. In order to predict the correct particle clustering for particles with Stokes numbers $St = \mathcal{O}(1)$, the subgrid-scale velocity requires reconstruction in the scope of an LES.

The variety of models for the subgrid-scale velocity in LES can be generally classified into two groups, Lagrangian models that reconstruct the fluid velocity only at the particle positions and evolve this Lagrangian fluid velocity for each particle individually, and the structural models that reconstruct the continuous fluid velocity field at every point in the domain.

Lagrangian models [9, 10, 35, 60, 98, 114] aim to reconstruct the subgrid-scale fluid velocity at the position of the particle, $\mathbf{u}'_{@p,q}(t) = \mathbf{u}'(\mathbf{x}_{p,q}, t)$, using a Langevin equation of the form

$$d\mathbf{u}'_{@p,q} = \underbrace{\mathcal{A}dt}_{\text{drift term}} + \underbrace{\mathcal{B} \cdot d\mathbf{W}}_{\text{diffusion term}}, \quad (\text{III.21})$$

where $d\mathbf{u}'_{@p,q}(t) = \mathbf{u}'_{@p,q}(t + dt) - \mathbf{u}'_{@p,q}(t)$ and $d\mathbf{W}$ is an increment of an vectorial Wiener process, i.e., Gaussian white noise. The first term on the right-hand side of equation (III.21) is a deterministic term containing information about the previous subgrid-scale velocity and filtered quantities. The second term on the right-hand side of equation (III.21) is a stochastic term representing the uncertainties from missing subgrid-scale information and the diffusive characteristic of turbulence. The different Lagrangian models differ in how the drift and diffusion terms are modeled [9, 10, 35, 60, 98, 114]. Although the Lagrangian models are simple to implement,

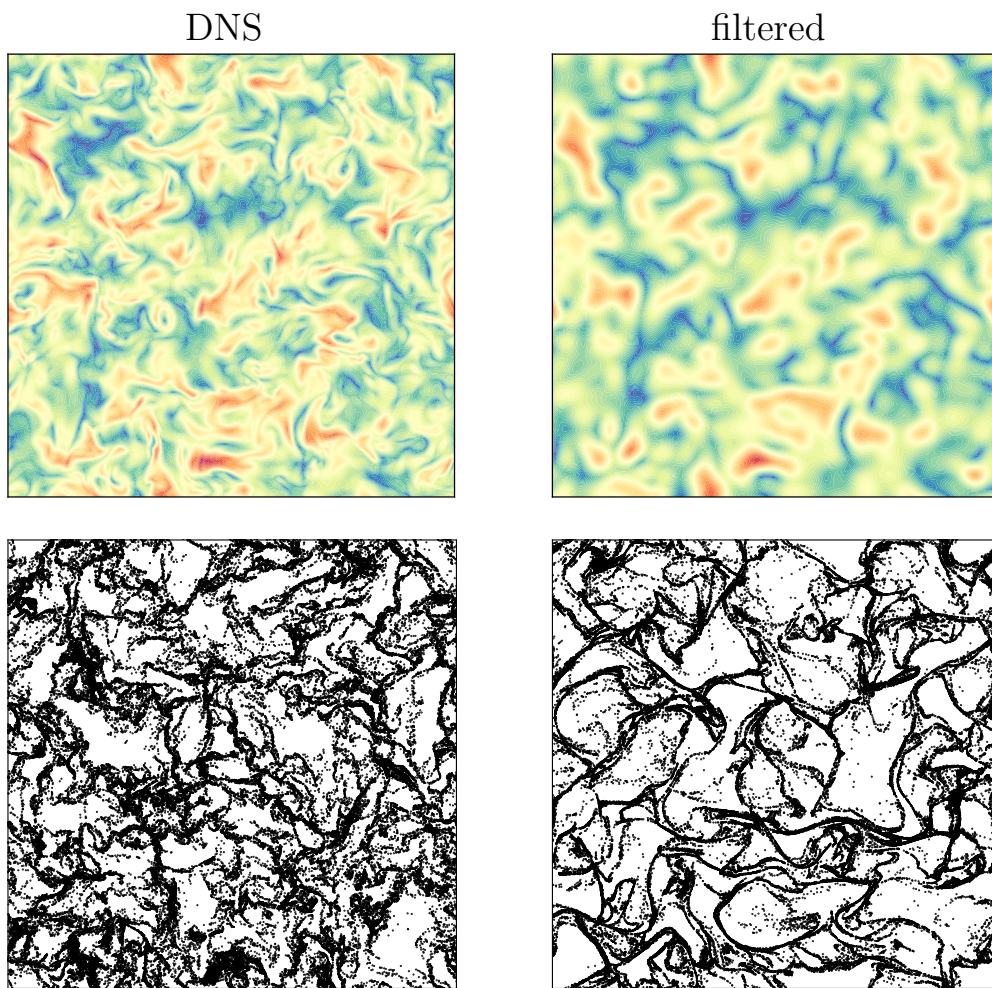


Figure III.6: Fluid velocity magnitude of HIT at $Re_\lambda = 75$ (top left) and the corresponding filtered velocity field (top right). Below, the positions of particles of $St = 2$ that are transported with the respective velocity field are shown.

computationally efficient, and can be relatively easily adapted to different boundary conditions, they cannot reproduce the right spatial velocity correlations. By construction, particles that are close together may experience different fluid velocities because of the diffusion term. Consequently, Lagrangian models fail to predict accurate particle clustering and are strongly dependent on model parameters [19, 78]. Recent advances suggest that structural models that reconstruct the entire subgrid-scale fluid velocity field are more promising to replicate the particle statistics of a DNS in an LES [7, 102, 131]. A spatially continuous field allows to incorporate knowledge about spatial correlations in turbulence. However, other difficulties arise, such as ensuring that the generated field is divergence-free and is capable of representing inhomogeneous and anisotropic fluid velocity fields.

Kinematic simulation based structural models reconstruct the subgrid-scale velocity by generating random divergence-free Fourier modes, such that the subgrid-scale velocity is approximated as [39, 64, 75]

$$\mathbf{u}'(\mathbf{x}, t) = \sum_m \mathbf{A}_m \cos(\mathbf{k}_m \cdot \mathbf{x} + \omega_m t) + \mathbf{B}_m \sin(\mathbf{k}_m \cdot \mathbf{x} + \omega_m t), \quad (\text{III.22})$$

where \mathbf{k}_m is the wave number vector of the mode m , ω_m is the frequency corresponding to the mode m , and \mathbf{A}_m and \mathbf{B}_m are the Fourier coefficient vectors. To obtain a divergence-free velocity, the coefficient vectors are chosen such that $\mathbf{A}_m \cdot \mathbf{k}_m = 0$ and $\mathbf{B}_m \cdot \mathbf{k}_m = 0$. Their magnitude is chosen, such that a desired kinetic energy spectrum is replicated. When applied to LES of particle-laden turbulence, the particle clustering is improved for $\text{St} \geq 2$ but for small Stokes numbers only minor improvements compared to the LES are observed [102, 131]. Kinematic simulations do not recover the right structure of turbulence, e.g., they cannot accurately predict the second invariant of the velocity gradient tensor, which is crucial for the clustering of particles with small Stokes numbers. Another problem of kinematic simulations is that the Gaussian distribution of the Fourier coefficient vectors is contrary to the intermittent (non-Gaussian) behavior of turbulence. Furthermore, it is problematic from a practical point of view that the kinetic energy spectrum is required, which is not known in an LES, and that the Fourier modes are homogeneous and isotropic, which limits the application of kinematic simulations to HIT.

The approximate deconvolution method is a simple approximation of the unfiltered velocity using the successively filtered velocity [66, 113, 117, 127]. The fluid velocity field may be obtained by truncating the following series expansion after sufficiently

many terms

$$\mathbf{u} = \sum_{p=0}^{\infty} (1 - G^*)^p \tilde{\mathbf{u}}, \quad (\text{III.23})$$

where $*$ indicates the convolution operation. The approximate deconvolution procedure does not introduce wave numbers that are larger than the wave numbers of the LES. A related method is the dynamic differential filter method proposed by Park *et al.* [94]. Since the deficiency of small scale velocity features remains, the improvements in predicting the particle clustering compared to an LES are relatively small. Domaradzki and Loh [29] propose to compute the subgrid-scale velocity on a refined grid by extrapolation of the non-linear term, which gives a subgrid-scale velocity that is not divergence-free without further interventions. Bassenne *et al.* [7] combine the extrapolation of Domaradzki and Loh [29] with the dynamic differential filtering of Park *et al.* [94]. Although accurate particle clustering is predicted, the model requires a projection operation on a very fine computational grid diminishing the advantage of the small computational costs of the LES.

Another class of models reconstructs the subgrid-scale fluid velocity by solving the SFNSE linearized according to the RDT [31, 43, 44]. A fundamental advantage is that subgrid-scale velocity field possesses directional dependencies based on the filtered fluid velocity field. In the case of a turbulent shear flow, for instance, the subgrid-scale velocity adapts accordingly following RDT. Ghate and Lele [43] use Gabor modes to represent the subgrid-scale fluid velocity and achieve excellent agreement with the velocity field in the planetary boundary layer. However, the generated velocity is not perfectly divergence-free and the Gabor modes require reinitialization to prevent them from decaying.

The approximate solution of the linearized SFNSE according to the RDT shows promising reconstructions of the subgrid-scale velocity in previous studies, which is why the models proposed in the scope of the present thesis follow a similar direction [47, 51]. Particularly relevant to predict the right particle clustering is to reproduce the second invariant of the velocity gradient tensor. To predict the right particle dispersion, the spatial velocity correlations and intermittency of the subgrid-scale velocity have to be reproduced. As shown previously, RDT can theoretically provide a framework to capture these statistics [68]. It is not clear, however, what is the most suitable type of basis functions to represent the subgrid-scale velocity. At least the following properties of the basis have to be considered:

- The computational costs should be of the order of the LES and, hence, the number of degrees of freedom to represent the subgrid-scale velocity must be reduced compared to a physical basis. The functional basis has to be able to represent the essential features of the subgrid-scale velocity by a small number of degrees of freedom. Representing the subgrid-scale velocity in physical space requires sampling on a very fine computational grid and is not suitable.
- Since the subgrid-scale velocity is divergence-free, this property should be either satisfied by construction (e.g., by divergence-free basis functions), or it should be possible to easily enforce it (in spectral space the projection is an algebraic equation).
- The basis should provide a sufficient localization in spectral space to be able to distinguish between filtered and subgrid-scale velocity and to incorporate spectral space knowledge of turbulence, such as the kinetic energy spectrum.
- The basis should provide a sufficient localization in physical space to represent statistically inhomogeneous subgrid-scale velocity fields.

Every potential functional basis is typically a compromise of these properties. However, if the methodology around the chosen functional basis is designed well, some of the disadvantageous properties may be diminished. In the scope of the present thesis, a model is developed that reconstructs the subgrid-scale velocity representing it with a Fourier-basis [47] and another model that represents the subgrid-scale velocity using divergence-free wavelets [51].

III.4.3 Modeling the effect of the particles and the inter-scale fluid interactions

After modeling the effect of the subgrid-scale velocity on the particle motion (red interactions in figure III.4), the treatment of the influence that the particles have on the flow (blue interactions in figure III.4) and the interactions between the filtered and the subgrid scales (green interactions in figure III.4) remain to be specified. The literature on these interactions is very sparse. Although some models for the subgrid-scale stress tensor under the influence of particles exist [93, 107, 130], their accuracy has to be proven in standardized test cases, such as HIT. A major difficulty is that the modeling of the subgrid-scale stress tensor requires consistent coupling with the model that provides the subgrid-scale fluid velocity. The trace of the subgrid-scale

stress tensor is the subgrid-scale kinetic energy, which has to be consistent with the kinetic energy of the generated subgrid-scale velocity, \mathbf{u}' . The subgrid-scale contribution of the particle momentum source, \mathbf{s}'_p , which is influenced by \mathbf{u}' , modifies the subgrid-scale kinetic energy and, therefore, τ_{ij} . This strong physical coupling requires strongly coupled models for the subgrid-scale velocity and the subgrid-scale stress tensor. In the scope of the present thesis, a modeling framework is proposed that takes into account all the interactions between particles and turbulence shown in figure III.4 [49].

The simplest of the interactions that remains to be modeled is the impact of the particles on the filtered flow, i.e., the filtered particle momentum source $\tilde{\mathbf{s}}_p$. Assuming that the particles are small enough to accurately approximate their influence on the flow with the PSIC method, the filtered particle momentum source is given as

$$\begin{aligned}\tilde{\mathbf{s}}_p(\mathbf{x}) &= -\frac{1}{\tilde{V}_{\text{cell}}} \int_{\tilde{\Omega}_{\text{cell}}} \sum_q \delta(\mathbf{x} - \mathbf{x}_{p,q}) \mathbf{F}_{D,q} dV \\ &= -\frac{1}{\tilde{V}_{\text{cell}}} \sum_{q \in \tilde{\Omega}_{\text{cell}}} \mathbf{F}_{D,q}, \quad \mathbf{x} \in \tilde{\Omega}_{\text{cell}},\end{aligned}\quad (\text{III.24})$$

where $\tilde{\Omega}_{\text{cell}}$ is a computational grid cell used in the LES and \tilde{V}_{cell} is its volume. Note that this term can only be computed accurately, if the drag force is computed using the subgrid-scale velocity in addition to the filtered fluid velocity.

The modeling of the subgrid-scale velocity and the subgrid-scale stress tensor is linked to the subgrid-scale kinetic energy. Therefore the modeled transport equation for the subgrid-scale kinetic energy (III.8) is supplemented with a particle source term, Φ_p , that accounts for the subgrid-scale kinetic energy modification by the particles, such that

$$\frac{\partial K_{\text{sgs}}}{\partial t} + \tilde{u}_i \frac{\partial K_{\text{sgs}}}{\partial x_i} = -\tau_{\text{mod},ij} \frac{\partial \tilde{u}_i}{\partial x_j} - C_\epsilon \frac{K_{\text{sgs}}^{3/2}}{\Delta} + \frac{\partial}{\partial x_i} \left(\nu_t \frac{\partial K_{\text{sgs}}}{\partial x_i} \right) + \Phi_p. \quad (\text{III.25})$$

The particle source term can be obtained analog to the transport equation for K_{sgs} , i.e., by contracting the fluid momentum equation with the fluid velocity and subsequent filtering and subtracting the filtered fluid momentum equation contracted with the filtered fluid velocity. The resulting particle source term for the PSIC

method is given as

$$\Phi_p(\mathbf{x}) = \frac{1}{\rho_f \tilde{V}_{\text{cell}}} \left(\sum_{q \in \tilde{\Omega}_{\text{cell}}} \mathbf{F}_{D,q} \cdot \mathbf{u}(\mathbf{x}_{p,q}) - \tilde{\mathbf{u}}(\mathbf{x}) \cdot \sum_{q \in \tilde{\Omega}_{\text{cell}}} \mathbf{F}_{D,q} \right), \quad \mathbf{x} \in \tilde{\Omega}_{\text{cell}}. \quad (\text{III.26})$$

Note that the time dependencies are omitted for conciseness. The resulting subgrid-scale kinetic energy is used to compute the subgrid-scale stress tensor according to the LDKM and serves as target kinetic energy of the subgrid-scale velocity. The framework is referred to as modified localized dynamic kinetic energy model (mLDKM) and models at least the energetic impact of \mathbf{s}'_p and τ_{ij} [49].

Summaries of publications

IV.1 An efficient model for subgrid-scale velocity enrichment for large eddy simulations of turbulent flows

Published in *Physics of Fluids* 34, 115135 (2022)

IV.1.1 Summary of the publication

Predicting the subgrid-scale fluid velocity with properties similar to the subgrid-scale velocity of a turbulent flow is crucial to predict accurate particle statistics. This paper, which is found in the appendix A.1, proposes a model for the subgrid-scale fluid velocity field based on LES quantities while keeping the computational costs on the order of the computational costs of an LES without subgrid-scale velocity enrichment.

The subgrid-scale fluid velocity is governed by the SFNSE. In the presented methodology, the SFNSE are linearized according to the RDT and the term involving the subgrid-scale stress tensor, which essentially supplies the subgrid-scale velocity with kinetic energy, is modeled by a random forcing term. The resulting equations are referred to as modeled SFNSE and solved in Fourier space using the ansatz given in equation (III.22), which results in an algebraic set of equations. Since the subgrid-scale velocity is represented in Fourier space, the subgrid-scale velocity statistics are homogeneous without further interventions. In order to reproduce inhomogeneous subgrid-scale velocity statistics, statistically homogeneous sub-domains are defined each of which receives a distinct set of Fourier coefficients allowing the flow statistics to vary across the whole domain. The enrichment strategy, which is illustrated in

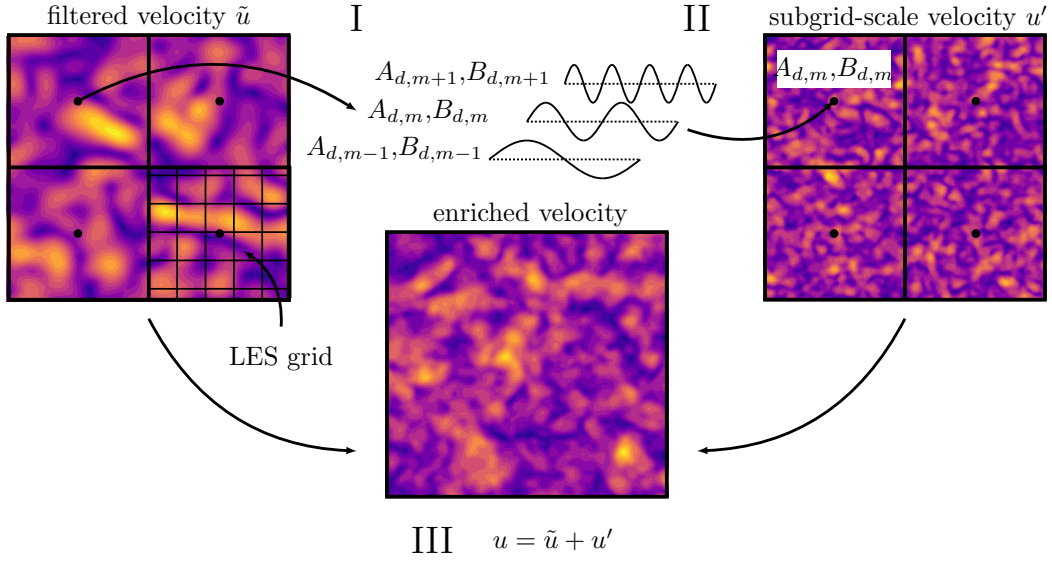


Figure IV.1: Enrichment strategy consisting of (I) averaging large scale quantities of the LES within statistically homogeneous sub-domains that are coarser than the LES grid, (II) solution of the modeled SFNSE in Fourier space in every sub-domain, and (III) approximating the turbulent fluid velocity field as the sum of LES velocity and modeled subgrid-scale velocity.

figure IV.1, consists of averaging the LES quantities in the sub-domains, solving for the Fourier coefficients in every sub-domain, and superposing the LES velocity and the modeled subgrid-scale velocity.

The generated enriched fluid velocity field, i.e., the sum of the LES velocity and the modeled subgrid-scale velocity, approximates the kinetic energy spectrum of the DNS well, significantly improves the PDF of the second invariant of the velocity gradient tensor, and predicts accurate non-Gaussian PDFs of the longitudinal and transverse velocity gradients, which indicates intermittency. Furthermore, it is shown with the configuration of a turbulent shear flow that the subgrid-scale velocity possesses inhomogeneous and anisotropic statistics.

IV.1.2 Individual contributions of the candidate

My contribution to the present article [47], which was published in the peer-reviewed journal *Physics of Fluids*, was the conceptualization and the development of the new model, its implementation in the in-house flow solver, the execution of the presented simulations, the interpretation of the results, and the writing of the manuscript.

IV.2 Large eddy simulation model for two-way coupled particle-laden turbulent flows

Published in *Physical Review Fluids* 8, 084301 (2023)

IV.2.1 Summary of the publication

Based on the previously proposed methodology for reconstructing the subgrid-scale velocity in the scope of an LES, a modeling framework is presented to predict the two-way coupled particle-turbulence interactions in LES, which is found in appendix A.2.

In the proposed modeling framework, the modeled transport equation for the subgrid-scale kinetic energy given in equation (III.25) is solved using the particle source term given in equation (III.26). Therefore, the subgrid-scale kinetic energy contains information of the turbulence modulation by the particles at the subgrid-scale level. According to the LDKM, the subgrid-scale stress tensor is computed using the subgrid-scale kinetic energy from the transport equation, which consequently also contains information of the subgrid-scale particle-turbulence interactions. The fluid velocity at the particle positions is composed of the fluid velocity from the LES and the subgrid-scale velocity approximated by the previously proposed subgrid-scale enrichment model. The subgrid-scale kinetic energy serves as target kinetic energy for the model equations solved in the enrichment model, which is enforced by the random forcing term. The resulting modeling framework is referred to as mLDKM and is fully coupled by the subgrid-scale kinetic energy, which determines the modeled subgrid-scale stress tensor and the kinetic energy of the modeled subgrid-scale velocity.

The proposed framework is tested in one-way coupled and two-way coupled simulations of HIT. The particle clustering and the particle pair dispersion is predicted accurately for a wide range of Stokes numbers. Figure IV.2 compares the predicted subgrid-scale kinetic energy with and without the proposed modeling framework with the explicitly filtered DNS using different filters for particles with $St = 1$, $St = 2$, and $St = 8$. Without the proposed modeling, the predicted subgrid-scale kinetic energy is significantly overestimated, which causes a too large turbulent viscosity and a too large kinetic energy of the reconstructed subgrid-scale kinetic energy. With the mLDKM, the expected reduction of the subgrid-scale kinetic energy by the presence of the particles is captured well.

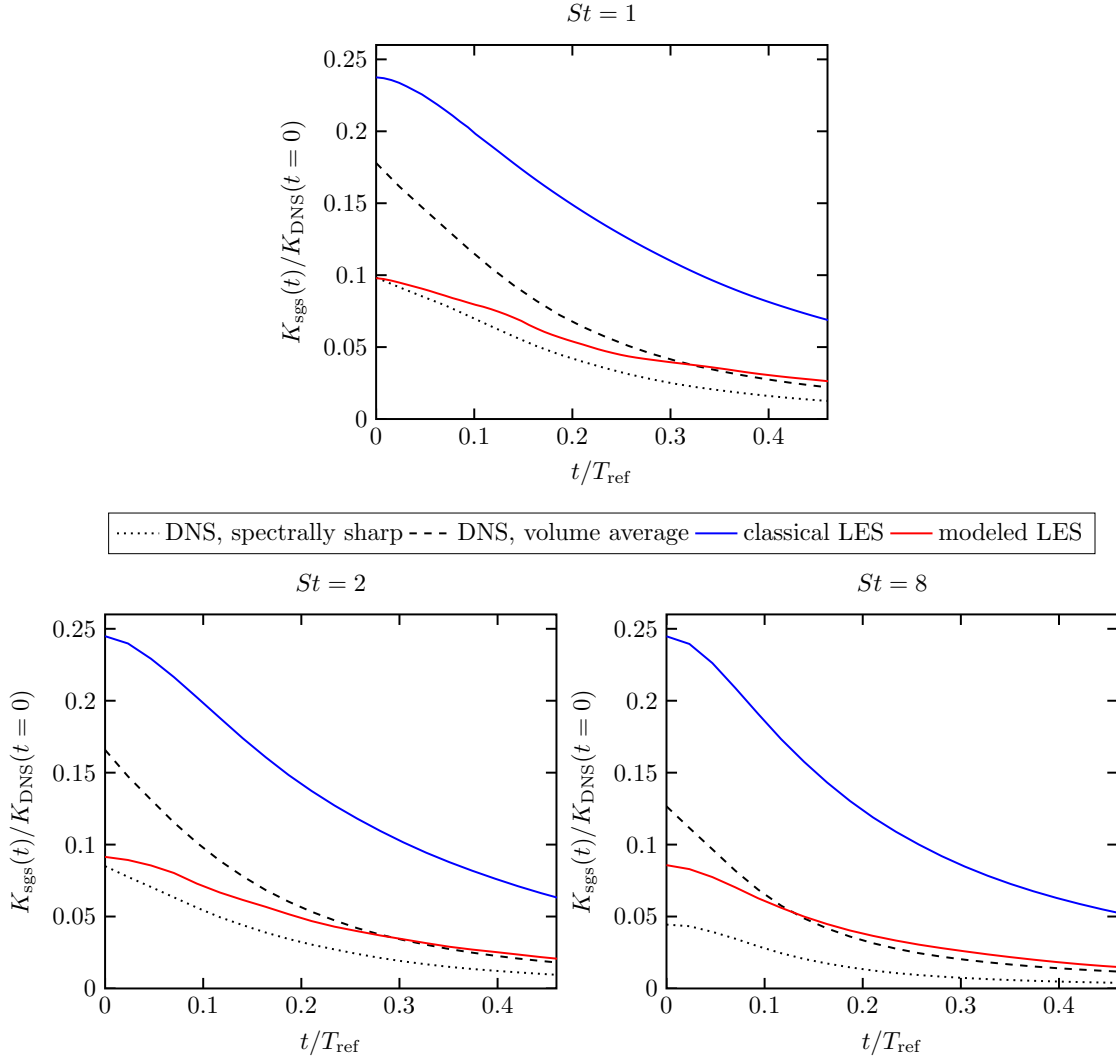


Figure IV.2: Subgrid-scale kinetic energy of decaying HIT predicted by the classical LES without the proposed modeling framework and by the modeled LES with the proposed modeling framework. The results are compared to the explicitly filtered DNS using a spectrally sharp filter and volume averaging in the LES grid cells. The results are shown for three different Stokes numbers.

IV.2.2 Individual contributions of the candidate

My contribution to the present article [49], which was published in the peer-reviewed journal *Physical Review Fluids*, was the conceptualization and the development of the new model, its implementation in the in-house flow solver, the execution of the presented simulations, the interpretation of the results, and the writing of the manuscript.

IV.3 Wavelet-based modeling of subgrid scales in large eddy simulation of particle-laden turbulent flows

Published in *Physical Review Fluids* 8, 104604 (2023)

IV.3.1 Summary of the publication

Representing the subgrid-scale velocity with a Fourier basis, as in the previously proposed modeling framework, is a highly efficient approach to approximately solve the modeled SFNSE, as the linear set of differential equations reduces to a set of algebraic equations. However, the Fourier basis entails the fundamental drawback of an infinite support in physical space and, therefore, the necessity of additional interventions to generate a statistically inhomogeneous subgrid-scale velocity field. The statistically homogeneous sub-domains proposed in Hausmann *et al.* [47] are not optimal, since divergence-free interpolation of the subgrid-scale velocity field is required between the sub-domains, an ad hoc intervention with the thickness of the interpolation region as an additional parameter.

This paper, which is found in appendix A.3, presents a methodology to represent the subgrid-scale velocity using a wavelet basis, which is conceptually superior to model statistically inhomogeneous fields. The wavelet basis functions are depicted in figure IV.3, which have finite support in physical space and infinite, but rapidly decaying support in Fourier space. More precisely, a divergence-free but non-orthogonal vector wavelet basis with piecewise linear and piecewise quadratic spline wavelets is used, which allows to solve only the curl-free part of the modeled SFNSE that is obtained after Helmholtz decomposition. However, the modeled SFNSE do not automatically turn into an algebraic set of equations such as with a Fourier basis. Instead, a Galerkin approach is used to determine the wavelet coefficients that minimize the

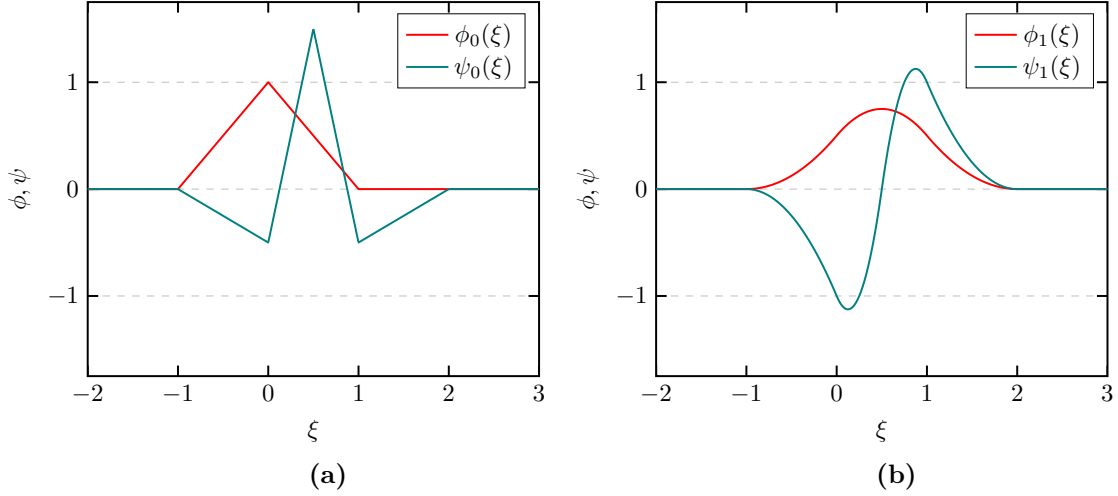


Figure IV.3: Piecewise linear ϕ_0, ψ_0 (a) and piecewise quadratic ϕ_1, ψ_1 (b) spline scaling and wavelet functions that represent the modeled subgrid-scale velocity.

violation of the modeled SFNSE. The computational costs are reduced by exploiting the linearity of the modeled SFNSE and solve for local least squares, so-called local wave packets.

The LES velocity field enriched with the modeled subgrid-scale velocity predicts several single-phase turbulence statistics accurately. The particle pair dispersion and clustering of particles transported with the wavelet enriched LES velocity field is significantly improved compared to the LES without the enrichment. The predicted subgrid-scale kinetic energy of the mLDKM shows the expected reduction relative to a single-phase flow in two-way coupled particle-laden turbulence.

IV.3.2 Individual contributions of the candidate

My contribution to the present article [51], which was published in the peer-reviewed journal *Physical Review Fluids*, was the conceptualization and the development of the new model, its implementation in the in-house flow solver, the execution of the presented simulations, the interpretation of the results, and the writing of the manuscript.

Conclusions and outlook

V.1 Conclusions

The objective of the present thesis is the design of a modeling framework in the scope of an LES that captures the essential interactions between the particles and the turbulence. Because of the substantial lack of small scale information of the flow field in LES and the ambitious aim to not only model the effect of the turbulence on the particles, but also the two-way coupled interactions between particles and turbulence, the considered test cases are limited to fully periodic problems in the present thesis. Furthermore, the presented modeling framework is designed for particle-laden gas flows with particles sizes smaller than the Kolmogorov length scale.

Considering one-way coupled simulations of particle-laden turbulent flows as a first step allows to separate the modeling of the effect of the turbulence on the particles from the turbulence modulation by the particles. Although a large variety of models exist for predicting the particle clustering and dispersion in LES, the particle statistics are either predicted unsatisfactorily or to computational costs that are not acceptable in the scope of an LES. In the literature, most promising results are obtained by structural models that reconstruct the subgrid-scale fluid velocity field. Typical difficulties of structural models are, e.g., the generation of a divergence-free subgrid-scale velocity field, the generation of a statistically inhomogeneous and anisotropic subgrid-scale velocity field, and keeping the computational costs reasonable.

The approaches proposed in the present thesis mitigate the common issues of structural models and rely on the approximate solution of the SFNSE linearized according to the RDT. The resulting modeled SFNSE are approximately solved representing

the subgrid-scale velocity with two different bases, a Fourier basis that is discretized in space using statistically homogeneous sub-domain, and a divergence-free wavelet vector basis. Both basis allow for an inhomogeneous and anisotropic subgrid-scale velocity field and take into account large scale velocity features by solving the modeled SFNSE. Both approaches accurately predict single-phase flow statistics, such as the PDF of the second invariant of the velocity gradient tensor and the non-Gaussian PDFs of velocity gradients, which indicates intermittency. Furthermore, both approaches significantly improve the prediction of particle clustering and particle pair dispersion over a wide range of Stokes numbers. Although both models predict relatively similar single-phase and particle-laden flow statistics, the wavelet basis is conceptually superior as it does not require interpolation of the subgrid-scale velocity between the sub-domains. However, the wavelet basis leads to computational costs approximately twice the computational costs of the Fourier basis.

In the two-way coupled case, the particles affect the turbulence at the filtered scales and at the subgrid scales. The effect on the subgrid-scales is not resolved but must be considered by means of the modeled subgrid-scale stress tensor, which accounts for the effect of the unresolved turbulence on the turbulence resolved in an LES. The central quantity for the proposed coupled modeling framework is the subgrid-scale kinetic energy, which serves as target kinetic energy for the reconstructed subgrid-scale velocity and can be used to design a turbulent viscosity model for the subgrid-scale stress tensor. The subgrid-scale kinetic energy is estimated by solving a transport equation with a particle source term that accounts for the subgrid-scale turbulence modulation by the particles. The occurring constants are computed dynamically according to the LDKM. The resulting coupled framework is referred to as mLDKM and successfully predicts the reduction of subgrid-scale kinetic energy relative to the corresponding single-phase flow turbulence. The kinetic energy of the fluid velocity field resolved in the LES still shows relatively small deviations from the kinetic energy of the explicitly filtered DNS velocity. It is shown in Hausmann *et al.* [49], however, that deviations of a similar magnitude also persist in an LES of single-phase turbulence. In particle-laden turbulence, it is shown that the kinetic energy of the filtered fluid velocity is fairly well predicted in an LES without the proposed modeling because two errors are compensating. (i) The subgrid-scale kinetic energy is too large because of the missing particle source term in the transport equation, which yields a too large turbulent viscosity and, therefore, a smaller kinetic energy of the resolved fluid velocity. (ii) Transporting the particles with the enriched fluid velocity instead of only the resolved fluid velocity of the LES reduces the kinetic energy of the resolved fluid velocity. Both effects contribute with opposite

sign to the kinetic energy of the resolved fluid velocity. With the proposed modeling framework, the predicted kinetic energy of the fluid in particle-laden turbulence is of similar accuracy as an LES of the corresponding single-phase flow.

The proposed modeling framework is a significant step towards accurately modeling particle-turbulence interactions with LES in complex flow configurations. Although the modeling framework is only designed and tested for periodic boundary conditions, its capabilities of predicting inhomogeneous and anisotropic turbulence opens doors for further developments enabling predictions in configurations of higher practical relevance.

V.2 Outlook

A somewhat natural extension of the presented work is the adaption of the proposed modeling framework to wall-bounded flows. However, there are various difficulties that arise even in LES of single-phase flows. LES of wall-bounded flows can be generally classified into two categories [106]: (i) The wall-normal thickness of the computational grid cells can be reduced as the wall is approached. This is referred to as wall-resolved LES, which is assumed to not require special treatment of the near-wall region as a DNS resolution is achieved in the wall-normal direction. If the filter width is reduced as the wall is approached, additional closures caused by the non-uniform filter arise. The overall reduction in computational costs compared to a DNS is relatively small. (ii) The computational grid of the LES can be kept coarse and equidistant in the wall-normal direction and the unresolved wall shear stress is modeled, which is referred to as wall-modeled LES. The large grid cells next to the wall require additional modeling but the computational costs are significantly smaller compared to a DNS. Since the LES filtering is not defined when the convolution kernel is ranging beyond the fluid domain, wall-modeled LES are conceptually problematic near walls.

A common issues observed in LES of wall-bounded flows is that the temporarily fluctuating streamwise velocity component of the LES exceeds the one of the DNS, while the spatially filtered fluid velocity field is actually expected to possess smaller temporal fluctuations (see, e.g., Bae *et al.* [4], Piomelli *et al.* [95]). An enrichment with subgrid-scale velocity using the proposed models consistently further increases the temporal fluctuations. Due to the modeling error of the resolved LES velocity, however, the enriched fluid velocity field further deviates from the actual velocity field. Before adapting the proposed modeling framework to wall-bounded flows, the

overestimation of the streamwise temporal fluid velocity fluctuations has to be fixed. The observed mismatch could be caused by the additional, and typically neglected, closures due to the non-uniform filter. Another potential reason is that the filter width used in the LES subgrid-scale model is too small. In fact, it is not sufficient if the computational grid is fine enough to resolve \tilde{u}_i . The non-linear term in the FNSE, $\tilde{u}_i\tilde{u}_j$, contains wave numbers twice as large as the filtered fluid velocity. Furthermore, the spurious alignment of the Eigenvectors of the modeled subgrid-scale stress tensor with the Eigenvectors of the strain-rate tensor imposed by the Boussinesq hypothesis could be more severe in the highly anisotropic near-wall flow than in HIT. A potential remedy could be a tensor based subgrid-scale model, such as the non-linear model.

Another promising path for future improvements of LES of particle-laden turbulence is the concept of volume-filtering as generalization of the standard filtering used in LES. The concept of volume-filtering provides a theoretical framework to consistently incorporate particles and even solid walls. However, additional closures arise with widely unknown implications. New insights from a recent study of Hausmann *et al.* [52] may guide the development of new models.

List of publications

Journal manuscripts

- [52] Hausmann, M., Chéron, V., Evrard, F., and van Wachem, B. (2024). Study and derivation of closures in the volume-filtered framework for particle-laden flows *Manuscript submitted to Journal of Fluid Mechanics*.
- [51] Hausmann, M., Evrard, F. and van Wachem, B. (2023c). Wavelet-based modeling of subgrid scales in large-eddy simulation of particle-laden turbulent flows. *Physical Review Fluids*, **8**(10), 104604.
- [49] Hausmann, M., Evrard, F. and van Wachem, B. (2023a). Large eddy simulation model for two-way coupled particle-laden turbulent flows. *Physical Review Fluids*, **8**(8), 084301.
- [110] Schiødt, M., Hodžić, A., Evrard, F., Hausmann, M., van Wachem, B., and Velte, C. M. (2023). Spectral response between particle and fluid kinetic energy in decaying homogeneous isotropic turbulence. *Physics of Fluids*, **35**(5), 053333.
- [47] Hausmann, M., Evrard, F. and van Wachem, B. (2022a). An efficient model for subgrid-scale velocity enrichment for large-eddy simulations of turbulent flows. *Physics of Fluids*, **34**(11), 115135.
- [109] Schiødt, M., Hodžić, A., Evrard, F., Hausmann, M., van Wachem, B., and Velte, C. M. (2022). Characterizing Lagrangian particle dynamics in decaying homogeneous isotropic turbulence using proper orthogonal decomposition. *Physics of Fluids*, **34**(6), 063303.
- [120] Tajfirooz, S., Meijer, J. G., Kuerten, J. G. M., Hausmann, M., Fröhlich, J., and Zeegers, J. C. H. (2021). Statistical-learning method for predicting hydrodynamic drag, lift, and pitching torque on spheroidal particles. *Physical Review E*, **103**(2), 023304.

Conference proceedings

- [46] Hausmann, M. and van Wachem, B. (2024). Predicting particle dynamics and turbulence modulation in large eddy simulations using structural models. In *DECHEMA*, Bremen, Germany
- [50] Hausmann, M., Evrard, F., and van Wachem, B. (2023b). A new model for large eddy simulations of particle-laden turbulent flows. In *11th International Conference on Multiphase Flow*, Kobe, Japan
- [48] Hausmann, M., Chéron, V., Evrard, F., and van Wachem, B. (2022b). Subgrid-scale enrichment of particle-laden turbulence by solution of a set of physically derived equations in Eulerian frame. In *EUROMECH Colloquium 625 “Advances in LES of Turbulent Multiphase Flows”*, Udine, Italy

No further content of the present thesis has been published before or is intended to be published in the future by the author.

Declaration of honor

I hereby declare that I produced this thesis without prohibited external assistance and that none other than the listed references and tools have been used.

In the case of co-authorship, especially in the context of a cumulative dissertation, the own contribution is correctly and completely stated. I did not make use of any commercial consultant concerning graduation. A third party did not receive any nonmonetary perquisites neither directly nor indirectly for activities which are connected with the contents of the presented thesis. All sources of information are clearly marked, including my own publications.

In particular I have not consciously:

- Fabricated data or rejected undesired results,
- Misused statistical methods with the aim of drawing other conclusions than those warranted by the available data,
- Plagiarized data or publications,
- Presented the results of other researchers in a distorted way.

I do know that violations of copyright may lead to injunction and damage claims of the author and also to prosecution by the law enforcement authorities.

I hereby agree that the thesis may need to be reviewed with an electronic data processing for plagiarism.

This work has not yet been submitted as a doctoral thesis in the same or a similar form in Germany or in any other country. It has not yet been published as a whole.

Magdeburg, 30.04.2024

References

- [1] Akiki, G., Jackson, T. L., and Balachandar, S. (2017). Pairwise interaction extended point-particle model for a random array of monodisperse spheres. *Journal of Fluid Mechanics*, **813**, 882–928.
- [2] Anderson, T. B. and Jackson, R. (1967). A fluid mechanical description of fluidized beds. *I and EC Fundamentals*, **6**(4), 524–539.
- [3] Armenio, V., Piomelli, U., and Fiorotto, V. (1999). Effect of the subgrid scales on particle motion. *Physics of Fluids*, **11**(10), 3030.
- [4] Bae, H. J., Lozano-Durán, A., Bose, S. T., and Moin, P. (2018). Turbulence intensities in large-eddy simulation of wall-bounded flows. *Physical Review Fluids*, **3**(1), 014610.
- [5] Balachandar, S. and Eaton, J. K. (2010). Turbulent Dispersed Multiphase Flow. *Annual Review of Fluid Mechanics*, **42**(1), 111–133.
- [6] Bardina, J., Ferziger, J., and Reynolds, W. (1980). Improved subgrid-scale models for large-eddy simulation. In *13th Fluid and Plasma Dynamics Conference*, Snowmass, CO, U.S.A. American Institute of Aeronautics and Astronautics.
- [7] Bassenne, M., Esmaily, M., Livescu, D., Moin, P., and Urzay, J. (2019). A dynamic spectrally enriched subgrid-scale model for preferential concentration in particle-laden turbulence. *International Journal of Multiphase Flow*, **116**, 270–280.
- [8] Basset, A. B. (1888). *A Treatise on Hydrodynamics, with Numerous Examples*. Bell and co., Cambridge Deighton.

- [9] Berrouk, A. S., Laurence, D., Riley, J. J., and Stock, D. E. (2007). Stochastic modelling of inertial particle dispersion by subgrid motion for LES of high Reynolds number pipe flow. *Journal of Turbulence*, **8**, N50.
- [10] Bini, M. and Jones, W. P. (2007). Particle acceleration in turbulent flows: A class of nonlinear stochastic models for intermittency. *Physics of Fluids*, **19**(3), 035104.
- [11] Boivin, M., Simonin, O., and Squires, K. D. (1998). Direct numerical simulation of turbulence modulation by particles in isotropic turbulence. *Journal of Fluid Mechanics*, **375**(1), 235–263.
- [12] Borue, V. and Orszag, S. A. (1998). Local energy flux and subgrid-scale statistics in three-dimensional turbulence. *Journal of Fluid Mechanics*, **366**, 1–31.
- [13] Boussinesq, J. V. (1885). Sur la résistance qu’oppose un fluide indéfini au repos, sans pesanteur, au mouvement varié d’une sphère solide qu’il mouille sur toute sa surface, quand les vitesses restent bien continues et assez faibles pour que leurs carrés et produits soient négligeables. *Comptes Rendus de l’Académie des Sciences*, **100**, 935–937.
- [14] Brandt, L. and Coletti, F. (2022). Particle-Laden Turbulence: Progress and Perspectives. *Annual Review of Fluid Mechanics*, **54**(1), 159–189.
- [15] Brunton, S. L. and Kutz, J. N. (2019). *Data-Driven Science and Engineering: Machine Learning, Dynamical Systems, and Control*. Cambridge University Press, 1 edition.
- [16] Canuto, V. M. and Dubovikov, M. S. (1996). A dynamical model for turbulence. I. General formalism. *Physics of Fluids*, **8**(2), 571–586.
- [17] Capecelatro, J. and Desjardins, O. (2013). An Euler–Lagrange strategy for simulating particle-laden flows. *Journal of Computational Physics*, **238**, 1–31.
- [18] Carbone, M. and Bragg, A. D. (2020). Is vortex stretching the main cause of the turbulent energy cascade? *Journal of Fluid Mechanics*, **883**, R2.
- [19] Cernick, M., Tullis, S., and Lightstone, M. (2015). Particle subgrid scale modelling in large-eddy simulations of particle-laden turbulence. *Journal of Turbulence*, **16**(2), 101–135.

- [20] Chen, L., Goto, S., and Vassilicos, J. C. (2006). Turbulent clustering of stagnation points and inertial particles. *Journal of Fluid Mechanics*, **553**(-1), 143.
- [21] Clark, R. A., Ferziger, J. H., and Reynolds, W. C. (1979). Evaluation of subgrid-scale models using an accurately simulated turbulent flow. *Journal of Fluid Mechanics*, **91**(01), 1.
- [22] Courant, R., Friedrichs, K., and Lewy, H. (1928). Über die partiellen Differenzgleichungen der mathematischen Physik. *Mathematische Annalen*, **100**, 32–74.
- [23] Crowe, C. T., Sharma, M. P., and Stock, D. E. (1977). The Particle-Source-In-Cell (PSI-CELL) Model for Gas-Droplet Flows. *Journal of Fluids Engineering*, **99**(2), 325–333.
- [24] Csanady, G. T. (1963). Turbulent diffusion of heavy particles in the atmosphere. *Journal of Atmospheric Sciences*, **20**, 201–208.
- [25] Daubechies, I. (1992). *Ten Lectures on Wavelets*. Number 61 in CBMS-NSF Regional Conference Series in Applied Mathematics. Society for Industrial and Applied Mathematics, Philadelphia, Pa.
- [26] Deardorff, J. W. (1970). A numerical study of three-dimensional turbulent channel flow at large Reynolds numbers. *Journal of Fluid Mechanics*, **41**(02), 453.
- [27] Deriaz, E. and Perrier, V. (2006). Divergence-free and curl-free wavelets in two dimensions and three dimensions: Application to turbulent flows. *Journal of Turbulence*, **7**, N3.
- [28] Deriaz, E. and Perrier, V. (2009). Direct Numerical Simulation of Turbulence Using Divergence-Free Wavelets. *Multiscale Modeling & Simulation*, **7**(3), 1101–1129.
- [29] Domaradzki, J. A. and Loh, K.-C. (1999). The subgrid-scale estimation model in the physical space representation. *Physics of Fluids*, **11**(8), 2330–2342.
- [30] Druzhinin, O. A. (2001). The influence of particle inertia on the two-way coupling and modification of isotropic turbulence by microparticles. *Physics of Fluids*, **13**(12), 3738–3755.

- [31] Dubrulle, B., Laval, J. P., Nazarenko, S., and Kevlahan, N. K.-R. (2001). A dynamic subfilter-scale model for plane parallel flows. *Physics of Fluids*, **13**(7), 2045–2064.
- [32] Elghobashi, S. and Truesdell, G. C. (1993). On the two-way interaction between homogeneous turbulence and dispersed solid particles. I: Turbulence modification. *Physics of Fluids A*, **5**(7), 1790.
- [33] Faxén, H. (1922). Der Widerstand gegen die Bewegung einer starren Kugel in einer zähen Flüssigkeit, die zwischen zwei parallelen ebenen Wänden eingeschlossen ist. *Annalen der Physik*, **373**(10), 89–119.
- [34] Fede, P. and Simonin, O. (2006). Numerical study of the subgrid fluid turbulence effects on the statistics of heavy colliding particles. *Physics of Fluids*, **18**(4), 045103.
- [35] Fede, P., Simonin, O., Villedieu, P., and Squires, K. D. (2006). Stochastic modeling of the turbulent subgrid fluid velocity along inertial particle trajectories. In *Proceedings of the Summer Program*, page 247.
- [36] Ferrante, A. and Elghobashi, S. (2003). On the physical mechanisms of two-way coupling in particle-laden isotropic turbulence. *Physics of Fluids*, **15**(2), 315.
- [37] Feynman, R. P., Leighton, R. B., Sands, M., and Hafner, E. M. (1965). The Feynman Lectures on Physics; Vol. I. *American Journal of Physics*, **33**(9), 750–752.
- [38] Fröhlich, K., Schneiders, L., Meinke, M., and Schröder, W. (2018). Validation of Lagrangian Two-Way Coupled Point-Particle Models in Large-Eddy Simulations. *Flow, Turbulence and Combustion*, **101**(2), 317–341.
- [39] Fung, J. C. H., Hunt, J. C. R., Malik, N. A., and Perkins, R. J. (1992). Kinematic simulation of homogeneous turbulence by unsteady random Fourier modes. *Journal of Fluid Mechanics*, **236**, 281–318.
- [40] Gatignol, R. (1983). The Faxén formulas for a rigid particle in an unsteady non-uniform Stokes-flow. *Journal de Mécanique théorique et appliquée*, **2**(2), 143–160.
- [41] George, W. K. (2013). Lectures in Turbulence for the 21st Century. Technical report, Department of Applied Mechanics, Chalmers University of Technology, Gothenburg, Sweden.

- [42] Germano, M., Piomelli, U., Moin, P., and Cabot, W. H. (1991). A dynamic subgrid-scale eddy viscosity model. *Physics of Fluids A*, **3**(7), 1760–1765.
- [43] Ghate, A. S. and Lele, S. K. (2017). Subfilter-scale enrichment of planetary boundary layer large eddy simulation using discrete Fourier–Gabor modes. *Journal of Fluid Mechanics*, **819**, 494–539.
- [44] Ghate, A. S. and Lele, S. K. (2020). Gabor mode enrichment in large eddy simulations of turbulent flow. *Journal of Fluid Mechanics*, **903**, A13.
- [45] Graps, A. (1995). An introduction to wavelets. *IEEE Computational Science and Engineering*, **2**(2), 50–61.
- [46] Hausmann, M. and van Wachem, B. (2024). Predicting particle dynamics and turbulence modulation in large eddy simulations using structural models. In *DECHEMA*, Bremen, Germany.
- [47] Hausmann, M., Evrard, F., and van Wachem, B. (2022a). An efficient model for subgrid-scale velocity enrichment for large-eddy simulations of turbulent flows. *Physics of Fluids*, **34**(11), 115135.
- [48] Hausmann, M., Chéron, V., Evrard, F., and van Wachem, B. (2022b). Subgrid-scale enrichment of particle-laden turbulence by solution of a set of physically derived equations in Eulerian frame. In *EUROMECH Colloquium 625 “Advances in LES of Turbulent Multiphase Flows”*, Udine, Italy.
- [49] Hausmann, M., Evrard, F., and van Wachem, B. (2023a). Large eddy simulation model for two-way coupled particle-laden turbulent flows. *Physical Review Fluids*, **8**(8), 084301.
- [50] Hausmann, M., Evrard, F., and van Wachem, B. (2023b). A new model for large eddy simulations of particle-laden turbulent flows. In *11th International Conference on Multiphase Flow*, Kobe, Japan.
- [51] Hausmann, M., Evrard, F., and van Wachem, B. (2023c). Wavelet-based modeling of subgrid scales in large-eddy simulation of particle-laden turbulent flows. *Physical Review Fluids*, **8**(10), 104604.
- [52] Hausmann, M., Chéron, V., Evrard, F., and van Wachem, B. (2024). Study and derivation of closures in the volume-filtered framework for particle-laden flows.

- [53] Horiuti, K. (2003). Roles of non-aligned eigenvectors of strain-rate and subgrid-scale stress tensors in turbulence generation. *Journal of Fluid Mechanics*, **491**, 65–100.
- [54] Hunt, J. C. R. and Carruthers, D. J. (1990). Rapid distortion theory and the ‘problems’ of turbulence. *Journal of Fluid Mechanics*, **212**(-1), 497.
- [55] Johnson, P. L. (2020). Energy Transfer from Large to Small Scales in Turbulence by Multiscale Nonlinear Strain and Vorticity Interactions. *Physical Review Letters*, **124**(10), 104501.
- [56] Johnson, P. L. (2021). On the role of vorticity stretching and strain self-amplification in the turbulence energy cascade. *Journal of Fluid Mechanics*, **922**, A3.
- [57] Johnson, P. L. (2022). A physics-inspired alternative to spatial filtering for large-eddy simulations of turbulent flows. *Journal of Fluid Mechanics*, **934**, A30.
- [58] Kellert, S. H. (1994). *In the Wake of Chaos: Unpredictable Order in Dynamical Systems*. University of Chicago Press, Chicago.
- [59] Kim, W.-W. and Menon, S. (1999). An unsteady incompressible Navier-Stokes solver for large eddy simulation of turbulent flows. *International Journal for Numerical Methods in Fluids*, **31**(6), 983–1017.
- [60] Knorps, M. and Pozorski, J. (2021). Stochastic modeling for subgrid-scale particle dispersion in large-eddy simulation of inhomogeneous turbulence. *Physics of Fluids*, **33**(4), 043323.
- [61] Kolmogorov, A. N. (1941a). Dissipation of energy in the locally isotropic turbulence. *Proceedings of the Royal Society of London. Series A: Mathematical and Physical Sciences*, **434**(1890), 15–17.
- [62] Kolmogorov, A. N. (1941b). The local structure of turbulence in incompressible viscous fluid for very large Reynolds numbers. *Doklady Akademii Nauk Sssr*, **30**(1890), 301–305.
- [63] Kolmogorov, A. N. (1962). A refinement of previous hypotheses concerning the local structure of turbulence in a viscous incompressible fluid at high Reynolds number. *Journal of Fluid Mechanics*, **13**(01), 82.

- [64] Kraichnan, R. H. (1970). Diffusion by a Random Velocity Field. *Physics of Fluids*, **13**(1), 22.
- [65] Kravchenko, A., Moin, P., and Moser, R. (1996). Zonal Embedded Grids for Numerical Simulations of Wall-Bounded Turbulent Flows. *Journal of Computational Physics*, **127**(2), 412–423.
- [66] Kuerten, J. G. M. (2006). Subgrid modeling in particle-laden channel flow. *Physics of Fluids*, **18**(2), 025108.
- [67] Kuerten, J. G. M. (2016). Point-Particle DNS and LES of Particle-Laden Turbulent flow - a state-of-the-art review. *Flow, Turbulence and Combustion*, **97**(3), 689–713.
- [68] Laval, J.-P., Dubrulle, B., and Nazarenko, S. (2001). Nonlocality and intermittency in three-dimensional turbulence. *Physics of Fluids*, **13**(7), 1995–2012.
- [69] Lemarié-Rieusset, P. G. (1992). Analyses multi-résolutions non orthogonales, commutation entre projecteurs et dérivation et ondelettes vecteurs à divergence nulle. *Revista Matemática Iberoamericana*, pages 221–237.
- [70] Leonard, A. (1975). Energy Cascade in Large-Eddy Simulations of Turbulent Fluid Flows. In *Advances in Geophysics*, volume 18, pages 237–248. Elsevier.
- [71] Letournel, R., Laurent, F., Massot, M., and Vié, A. (2020). Modulation of homogeneous and isotropic turbulence by sub-Kolmogorov particles: Impact of particle field heterogeneity. *International Journal of Multiphase Flow*, **125**, 103233.
- [72] Lilly, D. K. (1966). The representation of small scale turbulence in numerical simulation experiments. In *In: Proceedings of the IBM Scientific Computing Symposium on Environmental Sciences. Yorktown, NY, USA. National Center for Atmospheric Research (USA), NCAR Manuscript; No. 281.*, pages 195–210.
- [73] Lilly, D. K. (1992). A proposed modification of the Germano subgrid scale closure method. *Physics of Fluids A*, **4**(3), 633–635.
- [74] Liu, S., Meneveau, C., and Katz, J. (1994). On the properties of similarity subgrid-scale models as deduced from measurements in a turbulent jet. *Journal of Fluid Mechanics*, **275**, 83–119.
- [75] Malik, N. A. and Vassilicos, J. C. (1999). A Lagrangian model for turbulent dispersion with turbulent-like flow structure: Comparison with direct numerical

- simulation for two- particle statistics flow structure. *Physics of Fluids*, **11**(6), 1572.
- [76] Mallouppas, G. (2013). *Modelling of Turbulent Gas-Solid Flows from DNS to LES*. Ph.D. thesis, Imperial College London.
- [77] Mallouppas, G., George, W., and van Wachem, B. (2017). Dissipation and inter-scale transfer in fully coupled particle and fluid motions in homogeneous isotropic forced turbulence. *International Journal of Heat and Fluid Flow*, **67**, 74–85.
- [78] Marchioli, C. (2017). Large-eddy simulation of turbulent dispersed flows: A review of modelling approaches. *Acta Mechanica*, **228**(3), 741–771.
- [79] Marchioli, C., Soldati, A., Kuerten, J. G. M., Arcen, B., Taniere, A., Golden-soph, G., Squires, K. D., Cargnelutti, M. F., and Portela, L. M. (2008). Statistics of particle dispersion in direct numerical simulations of wall-bounded turbulence: Results of an international collaborative benchmark test. *International Journal of Multiphase Flow*, **34**(9), 879–893.
- [80] Margolin, L. G., Rider, W. J., and Grinstein, F. F. (2006). Modeling turbulent flow with implicit LES. *Journal of Turbulence*, **7**, N15.
- [81] Maxey, M. (2017). Simulation Methods for Particulate Flows and Concentrated Suspensions. *Annual Review of Fluid Mechanics*, **49**(1), 171–193.
- [82] Maxey, M. and Patel, B. (2001). Localized force representations for particles sedimenting in Stokes flow. *International Journal of Multiphase Flow*, **27**(9), 1603–1626.
- [83] Maxey, M. R. (1987). The gravitational settling of aerosol particles in homogeneous turbulence and random flow fields. *Journal of Fluid Mechanics*, **174**, 441.
- [84] Maxey, M. R. and Riley, J. R. J. (1983). Equation of motion for a small rigid sphere in a nonuniform flow. *Physics of Fluids*, **26**(4), 883.
- [85] Maxey, M. R., Patel, B. K., Chang, E. J., and Wang, L.-P. (1997). Simulations of dispersed turbulent multiphase flow. *Fluid Dynamics Research*, **20**(1-6), 143.
- [86] Mehrabadi, M., Horwitz, J. a. K., Subramaniam, S., and Mani, A. (2018). A direct comparison of particle-resolved and point-particle methods in decaying turbulence. *Journal of Fluid Mechanics*, **850**, 336–369.

-
- [87] Meneveau, C. and Katz, J. (2000). Scale-Invariance and Turbulence Models for Large-Eddy Simulation. *Annual Review of Fluid Mechanics*, **32**(1), 1–32.
- [88] Menon, S., Yeung, P.-K., and Kim, W.-W. (1996). Effect of subgrid models on the computed interscale energy transfer in isotropic turbulence. *Computers & Fluids*, **25**(2), 165–180.
- [89] Moin, P. and Kim, J. (1982). Numerical investigation of turbulent channel flow. *Journal of fluid mechanics*, **118**, 341–377.
- [90] Moser, R. D., Haering, S. W., and Yalla, G. R. (2021). Statistical Properties of Subgrid-Scale Turbulence Models. *Annual Review of Fluid Mechanics*, **53**(1), 255–286.
- [91] Oseen, C. W. (1910). Über die Stokes’sche formel, und über eine verwandte Aufgabe in der Hydrodynamik. *Arkiv för matematik, astronomi och fysik*, **6**(19).
- [92] Ottino, J. M. (1990). Mixing, Chaotic Advection, and Turbulence. *Annual Review of Fluid Mechanics*, **22**(1), 207–254.
- [93] Pannala, S. and Menon, S. (1999). On LEM/LES methodology for two-phase flows. In *35th Joint Propulsion Conference and Exhibit*, Los Angeles, CA, U.S.A. American Institute of Aeronautics and Astronautics.
- [94] Park, G. I., Bassenne, M., Urzay, J., and Moin, P. (2017). A simple dynamic subgrid-scale model for LES of particle-laden turbulence. *Physical Review Fluids*, **2**(4).
- [95] Piomelli, U., Moin, P., and Ferziger, J. H. (1988). Model consistency in large eddy simulation of turbulent channel flows. *The Physics of Fluids*, **31**(7), 1884–1891.
- [96] Pope, S. B. (2000). *Turbulent Flows*. Cambridge University Press, Cambridge, 6th edition.
- [97] Pope, S. B. (2004). Ten questions concerning the large-eddy simulation of turbulent flows. *New Journal of Physics*, **6**, 35–35.
- [98] Pozorski, J. and Apte, S. (2009). Filtered particle tracking in isotropic turbulence and stochastic modeling of subgrid-scale dispersion. *International Journal of Multiphase Flow*, **35**(2), 118–128.
-

- [99] Ptasiniski, P. K., Boersma, B. J., Nieuwstadt, F. T. M., Hulsen, M. A., Van Den Brule, B. H. A. A., and Hunt, J. C. R. (2003). Turbulent channel flow near maximum drag reduction: Simulations, experiments and mechanisms. *Journal of Fluid Mechanics*, **490**, 251–291.
- [100] Qian, S. and Chen, D. (1993). Discrete Gabor transform. *IEEE Transactions on Signal Processing*, **41**(7), 2429–2438.
- [101] Ray, B. and Collins, L. R. (2011). Preferential concentration and relative velocity statistics of inertial particles in Navier–Stokes turbulence with and without filtering. *Journal of Fluid Mechanics*, **680**, 488–510.
- [102] Ray, B. and Collins, L. R. (2014). A subgrid model for clustering of high-inertia particles in large-eddy simulations of turbulence. *Journal of Turbulence*, **15**(6), 366–385.
- [103] Reynolds, O. (1895). IV. On the dynamical theory of incompressible viscous fluids and the determination of the criterion. *Philosophical Transactions of the Royal Society of London. (A.)*, **186**, 123–164.
- [104] Richardson, J. F. and Zaki, W. N. (1954). The sedimentation of a suspension of uniform spheres under conditions of viscous flow. *Chemical Engineering Science*, **3**(2), 65–73.
- [105] Richardson, L. F. (1922). *Weather Prediction by Numerical Process*. Cambridge University Press, 2 edition.
- [106] Sagaut, P. (2005). *Large Eddy Simulation for Incompressible Flows*. Springer, third edition.
- [107] Sankaran, V. and Menon, S. (2002). LES of spray combustion in swirling flows. *Journal of Turbulence*, **3**, N11.
- [108] Schiller, L. and Naumann, A. (1933). Über die grundlegenden Berechnungen bei der Schwerkraftaufbereitung. *Zeitschrift des Vereines Deutscher Ingenieure*, **77**, 318–320.
- [109] Schiødt, M., Hodžić, A., Evrard, F., Hausmann, M., Van Wachem, B., and Velte, C. M. (2022). Characterizing Lagrangian particle dynamics in decaying homogeneous isotropic turbulence using proper orthogonal decomposition. *Physics of Fluids*, **34**(6), 063303.

-
- [110] Schiødt, M., Hodžić, A., Evrard, F., Hausmann, M., van Wachem, B., and Velte, C. M. (2023). Spectral response between particle and fluid kinetic energy in decaying homogeneous isotropic turbulence. *Physics of Fluids*, **35**(5), 053333.
- [111] Schneiders, L., Meinke, M., and Schröder, W. (2017). Direct particle–fluid simulation of Kolmogorov-length-scale size particles in decaying isotropic turbulence. *Journal of Fluid Mechanics*, **819**, 188–227.
- [112] Schumann, U. (1975). Subgrid scale model for finite difference simulations of turbulent flows in plane channels and annuli. *Journal of Computational Physics*, **18**(4), 376–404.
- [113] Shotorban, B. and Mashayek, F. (2005). Modeling subgrid-scale effects on particles by approximate deconvolution. *Physics of Fluids*, **17**, 081701.
- [114] Shotorban, B. and Mashayek, F. (2006). A stochastic model for particle motion in large-eddy simulation. *Journal of Turbulence*, **7**(April 2013), N18.
- [115] Smagorinsky, J. (1963). General circulation experiments with the primitive equations. I: The basic experiment. *Month. Weath. Rev.*, **91**(3), 99–165.
- [116] Squires, K. D. and Eaton, J. K. (1990). Particle response and turbulence modification in isotropic turbulence. *Physics of Fluids A: Fluid Dynamics*, **2**, 1191.
- [117] Stolz, S. and Adams, N. A. (1999). An approximate deconvolution procedure for large-eddy simulation. *Physics of Fluids*, **11**(7), 1699–1701.
- [118] Subramaniam, S. and Balachandar, S. (2022). *Modelling Approaches and Computational Methods for Particle-laden Turbulent Flows*. Academic Press, Elsevier, 1st edition.
- [119] Subramaniam, S., Mehrabadi, M., Horwitz, J. A. K., and Mani, A. (2014). Developing improved Lagrangian point particle models of gas-solid flow from particle-resolved direct numerical simulation. In *Studying Turbulence Using Numerical Simulation Databases–XV, Proceedings of the CTR 2014 Summer Program*, pages 5–14, Center for Turbulence Research, Stanford University.
- [120] Tajfirooz, S., Meijer, J. G., Kuerten, J. G. M., Hausmann, M., Fröhlich, J., and Zeegers, J. C. H. (2021). Statistical-learning method for predicting hydrodynamic drag, lift, and pitching torque on spheroidal particles. *Physical Review E*, **103**(2), 023304.
-

- [121] Tao, B., Katz, J., and Meneveau, C. (2000). Geometry and scale relationships in high Reynolds number turbulence determined from three-dimensional holographic velocimetry. *Physics of Fluids*, **12**(5), 941–944.
- [122] Tao, B., Katz, J., and Meneveau, C. (2002). Statistical geometry of subgrid-scale stresses determined from holographic particle image velocimetry measurements. *Journal of Fluid Mechanics*, **457**, 35–78.
- [123] Taylor, G. (1935). Statistical theory of turbulence. *Proceedings of the Royal Society of London. Series A*, pages 421–444.
- [124] Taylor, G. (1938). Production and dissipation of vorticity in a turbulent fluid. *Proceedings of the Royal Society of London. Series A - Mathematical and Physical Sciences*, **164**(916), 15–23.
- [125] Tennekes, H. and Lumley, J. L. (1972). *A First Course in Turbulence*. The MIT Press, 3rd edition.
- [126] Tsinober, A. (2009). Dynamics. In R. M. Madyam, editor, *An Informal Conceptual Introduction to Turbulence*, volume 92, pages 123–203. Springer Netherlands, Dordrecht.
- [127] Van Cittert, P. H. (1931). Zum Einfluß der Spaltbreite auf die Intensitätsverteilung in Spektrallinien. II. *Zeitschrift für Physik*, **69**(5-6), 298–308.
- [128] von Karman, T. and Howarth, L. (1938). On the Statistical Theory of Isotropic Turbulence. *Proceedings of the Royal Society of London. Series A - Mathematical and Physical Sciences*, **164**(917), 192–215.
- [129] Xu, Y. and Subramaniam, S. (2007). Consistent modeling of interphase turbulent kinetic energy transfer in particle-laden turbulent flows. *Physics of Fluids*, **19**(8), 085101.
- [130] Yuu, S., Ueno, T., and Umekage, T. (2001). Numerical simulation of the high Reynolds number slit nozzle gas-particle jet using subgrid-scale coupling large eddy simulation. *Chemical engineering science*, **56**, 4293–4307.
- [131] Zhou, Z., Wang, S., Yang, X., and Jin, G. (2020). A structural subgrid-scale model for the collision-related statistics of inertial particles in large-eddy simulations of isotropic turbulent flows. *Physics of Fluids*, **32**(9), 095103.

Appendices

A.1 Paper I

An efficient model for subgrid-scale velocity enrichment for large-eddy simulations of turbulent flows

M. Hausmann, F. Evrard, B. van Wachen

Published in *Physics of Fluids* 34, 115135 (2022)


An efficient model for subgrid-scale velocity enrichment for large-eddy simulations of turbulent flows

Cite as: Phys. Fluids **34**, 115135 (2022); <https://doi.org/10.1063/5.0127231>

Submitted: 20 September 2022 • Accepted: 19 October 2022 • Accepted Manuscript Online: 20 October 2022 • Published Online: 10 November 2022

 M. Hausmann,  F. Evrard and  B. van Wachem

COLLECTIONS

 This paper was selected as Featured



View Online



Export Citation



CrossMark

ARTICLES YOU MAY BE INTERESTED IN

[Stochastic modeling for subgrid-scale particle dispersion in large-eddy simulation of inhomogeneous turbulence](#)

Physics of Fluids **33**, 043323 (2021); <https://doi.org/10.1063/5.0046320>

[The effect of sub-filter scale dynamics in large eddy simulation of turbulence](#)

Physics of Fluids **34**, 095104 (2022); <https://doi.org/10.1063/5.0098925>

[Effects of thermal expansion on moderately intense turbulence in premixed flames](#)

Physics of Fluids **34**, 115127 (2022); <https://doi.org/10.1063/5.0123211>



Physics of Plasmas Physics of Fluids
Special Topic: Turbulence in Plasmas and Fluids
[Submit Today!](#)

An efficient model for subgrid-scale velocity enrichment for large-eddy simulations of turbulent flows

Cite as: Phys. Fluids **34**, 115135 (2022); doi: [10.1063/5.0127231](https://doi.org/10.1063/5.0127231)

Submitted: 20 September 2022 · Accepted: 19 October 2022 ·

Published Online: 10 November 2022



View Online



Export Citation



CrossMark

M. Hausmann,  F. Evrard, ^{a)}  and B. van Wachem ^{b)} 

AFFILIATIONS

Chair of Mechanical Process Engineering, Otto-von-Guericke-Universität Magdeburg, Universitätsplatz 2, 39106 Magdeburg, Germany

^{a)}Also at: Sibley School of Mechanical and Aerospace Engineering, Cornell University, Ithaca, New York 14853, USA

^{b)}Author to whom correspondence should be addressed: berend.vanwachem@ovgu.de

ABSTRACT

In some applications of large-eddy simulation (LES), in addition to providing a closure model for the subgrid-scale stress tensor, it is necessary to also provide means to approximate the subgrid-scale velocity field. In this work, we derive a new model for the subgrid-scale velocity that can be used in such LES applications. The model consists in solving a linearized form of the momentum equation for the subgrid-scale velocity using a truncated Fourier-series approach. Solving within a structured grid of statistically homogeneous sub-domains enables the treatment of inhomogeneous problems. It is shown that the generated subgrid-scale velocity emulates key properties of turbulent flows, such as the right kinetic energy spectrum, realistic strain–rotation relations, and intermittency. The model is also shown to predict the correct inhomogeneous and anisotropic velocity statistics in unbounded flows. The computational costs of the model are still of the same order as the costs of the LES.

© 2022 Author(s). All article content, except where otherwise noted, is licensed under a Creative Commons Attribution (CC BY) license (<http://creativecommons.org/licenses/by/4.0/>). <https://doi.org/10.1063/5.0127231>

I. INTRODUCTION

The concept of large-eddy simulation (LES) has emerged as an enormously successful tool to describe turbulent flows in their many different varieties. The property of turbulence of rapidly decreasing kinetic energy with increasing wave numbers enables capturing the majority of the kinetic energy of a flow by only resolving its largest scales. In many applications, a decent approximation of the large scales of the flow already allows a sufficient understanding of the underlying processes governing the main features of the flow. The present paper is dedicated to problems where this is not the case.

The majority of applications that suffer from missing subgrid-scale velocity content in LES can be found in multiphase flows. The LES of dispersed multiphase flows performs notoriously poorly with regard to predicting multi-particle statistics.^{1–3} Furthermore, when droplets are deformable, the lack of access to the unresolved rotation and strain of the velocity field renders the modeling of their deformation challenging.⁴ Even for simulation methods that at least partially resolve interfaces, a subgrid-scale velocity closure is needed, for example, as in the dual-scale approach of Herrmann and coworkers.^{5,6}

Apart from multiphase flows, information about the subgrid-scale velocity may for example also be used to accurately predict the aerodynamical loads on wind turbines that are immersed in the planetary boundary layer,⁷ the chemical reactions and location of the flame front in reactive flows,⁸ and combustion applications or heat transfer with significant turbulent mixing due to the subgrid-scale velocity.

A perfect model for the subgrid-scale velocity in the context of LES would satisfy the governing flow equations [i.e., the Navier–Stokes equations (NSE)], which can only be achieved with the computational cost of a direct numerical simulation (DNS). Characteristic properties indicating that a generated velocity field is similar to that of a real turbulent flow are, among others, the kinetic energy spectrum, the non-Gaussian distribution of derived flow quantities, and the relations between strain and rotation of the velocity. In addition to the physical properties of the generated subgrid-scale velocity, additional demands can be formulated so as to guarantee the practical applicability of the model: (i) the computational costs of the model have to be in the same order of magnitude as the costs of a LES; (ii) if the model contains tuning parameters, the solution should not sensitively depend

on their choice; (iii) the model should not be limited to homogeneous and isotropic flows. Homogeneous isotropic turbulence (HIT) constitutes an important case for theoretical studies of turbulent flows, but rarely occurs in realistic flow configurations; and (iv) finally, it is desirable for the model to be implemented and parallelized straightforwardly, as well as to be appendable to any LES flow solver.

A variety of different approaches for the approximate reconstruction of the subgrid-scale velocity have emerged in the past decades. Scotti and Meneveau⁹ derived a fractal interpolation technique to reconstruct the subgrid-scale velocity. This purely geometrical reconstruction does not incorporate important physical properties of turbulence. A related idea, but with a realization in spectral space, is the so-called “kinematic simulation.”^{10–14} With this approach, a divergence-free velocity field that matches a given kinetic energy spectrum is generated. Apart from the assumption of a spatially constant kinetic energy spectrum, it is difficult to define a physically realistic temporal evolution of the modes. Domaradzki *et al.*^{15,16} proposed a reconstruction of the subgrid-scale velocity by a defiltering operation that incorporates information of the non-linear term. In the work of Park *et al.*,¹⁷ a deconvolution is derived that is dynamically adjusted such that the model is either kinetic energy or dissipation consistent with the subgrid-scale model. However, the model does not introduce length scales that are smaller than the cutoff length scale of the LES grid. A combination of the models of Domaradzki *et al.* and Park *et al.* was proposed by Bassenne *et al.*¹⁸ The idea is a stepwise reconstruction of the subgrid-scale velocity based on alternating applications of spectral extrapolation and dynamical approximate deconvolution. Although key parameters, such as the second invariant of the velocity gradient tensor, can be predicted well, a severe drawback of the method is the projection operation that has to be carried out in real space on a grid comparable to the DNS grid. Thus, the computational costs are of the order of a DNS. The class of the multilevel methods relies on successive explicit filtering operations of the Navier–Stokes equations. Within that class, the variational multiscale method has emerged that uses a Galerkin method to solve the linearized residual velocity equations together with the filtered Navier–Stokes equations (FNSE). Apart from this linearization, no modeling assumptions are introduced.^{19,20} However, even the solution of a linear set of equations with a high resolution leads to a large computational overhead compared to a classical LES on a coarse grid. A second type of multilevel methods uses more than two levels of velocity scales and is based on temporarily frozen velocity of the respective subgrid scales (see, e.g., Terracol *et al.*²¹). Another approach is to derive a set of auxiliary subfilter equations from the Navier–Stokes equation using localized modes that are extracted via the Gabor transform.^{22,23} The conducted studies have been of a rather theoretical nature or have only been performed in two dimensions. More recently, Ghate and Lele^{24,25} further developed these ideas and achieved excellent agreement of the kinetic energy spectrum and velocity correlations in a boundary layer with the generated velocity and DNS results. However, for long simulation times, the quenching of the modes, which constitutes an application-specific external intervention of relatively high complexity, is required.

As it is clear from above, existing models for the subgrid-scale velocity are still limited in computational efficiency, practical applicability, and accuracy of the predictions.

In this paper, we derive a new model for the enrichment of the LES with a subgrid-scale velocity including physical assumptions and

details for practical realization in Sec. II. Subsequently, two simulation cases are introduced for evaluating the performance of the enrichment model compared to the respective DNS in Sec. III. In Sec. IV, the results of the simulation cases are presented and discussed. Finally, Sec. V concludes the present paper.

II. THEORY

Despite the main focus of this section lying in the modeling of the subgrid-scale velocity, the modeling of the filtered velocity (i.e., the LES) is also briefly summarized for the sake of completeness. The aim of the newly proposed model is to approximate the velocity field of a DNS using only information that is available in a LES.

First, the physical background is provided in Sec. II A. The remaining sections address the assumptions, the discretization, and the realization of the model in detail.

A. Scale decomposition and the assumptions of the rapid distortion theory

The foundation of LES and of the following discussions is that any physical quantity of interest, ϕ (e.g., velocity and pressure), is decomposed in a filtered (later referred to as LES part) and a subfilter part (later also referred to as subgrid part). The filtered part of a physical quantity, $\bar{\phi}$, may be defined by the following spatial low-pass filtering operation, as proposed by Leonard:²⁶

$$\bar{\phi}(x) = \int_{-\infty}^{\infty} G(x - \xi)\phi(\xi)d\xi, \quad (1)$$

where G denotes a filter kernel. This filtering kernel determines the shape of the spectrum of the resulting filtered quantity. The subfilter-scale contribution, ϕ' , is the difference between the original quantity, ϕ , and the filtered quantity, $\bar{\phi}$. Note that in a LES, the filtering operation is typically not explicitly performed but rather arises naturally from a numerical bandwidth limitation such as a (too) coarse grid. Furthermore, space and time are coupled in a flow by the velocity which implicitly introduces a filtering in time. However, the definition in Eq. (1) is commonly used for derivations in the LES context and is therefore also adapted in the present paper. Even if not fully consistent, the notations \bar{u} and u' are used for referring to the LES velocity and the modeled subgrid-scale velocity, respectively.²⁷

The incompressible Navier–Stokes equations, with a fluid density ρ_f and a kinematic viscosity ν_f are given by

$$\frac{\partial u_i}{\partial x_i} = 0, \quad (2)$$

$$\frac{\partial u_i}{\partial t} + u_j \frac{\partial u_i}{\partial x_j} = -\frac{1}{\rho_f} \frac{\partial p}{\partial x_i} + \nu_f \frac{\partial^2 u_i}{\partial x_j \partial x_j} + s_i, \quad (3)$$

where u_i is the velocity, p the pressure, and s_i an optional source term. Applying the explicit filtering operation (1) to the Navier–Stokes equations (NSE) leads to the filtered Navier–Stokes equations (FNSE) that can be written independently of the filter kernel G ,

$$\frac{\partial \bar{u}_i}{\partial x_i} = 0, \quad (4)$$

$$\frac{\partial \bar{u}_i}{\partial t} + \bar{u}_j \frac{\partial \bar{u}_i}{\partial x_j} = -\frac{1}{\rho_f} \frac{\partial \bar{p}}{\partial x_i} + \nu_f \frac{\partial^2 \bar{u}_i}{\partial x_j \partial x_j} - \frac{\partial \tau_{ij}}{\partial x_j} + \bar{s}_i. \quad (5)$$

The additional term $\partial\tau_{ij}/\partial x_j$ appears because of the application of the filter to the non-linear advection term. The subgrid-scale stress tensor τ_{ij} can be expanded using the general relation $\phi = \tilde{\phi} + \phi'$ to become

$$\tau_{ij} = \widetilde{\widetilde{u}_i u_j} + \widetilde{u'_i \widetilde{u}_j} + \widetilde{\widetilde{u}_i u'_j} + \widetilde{u'_i u'_j} - \widetilde{u}_i \widetilde{u}_j. \quad (6)$$

Subtracting the FNSE from the NSE results in a set of equations for the subgrid-scale variables

$$\frac{\partial u'_i}{\partial x_i} = 0, \quad (7)$$

$$\frac{\partial u'_i}{\partial t} + u'_j \frac{\partial u'_i}{\partial x_j} + \widetilde{u}_j \frac{\partial u'_i}{\partial x_j} + u'_i \frac{\partial \widetilde{u}_j}{\partial x_j} = -\frac{1}{\rho_f} \frac{\partial p'}{\partial x_i} + \nu_f \frac{\partial^2 u'_i}{\partial x_j \partial x_j} + \frac{\partial \tau_{ij}}{\partial x_j} + s'_i. \quad (8)$$

The subgrid-scale equations contain three advection terms, to which we refer to as: non-linear relaxation (second term on the left-hand side), sweeping (third term on the left-hand side), and straining (fourth term on the left-hand side). The coupled system consisting of Eqs. (4)–(8) can be solved equivalently to the NSE. However, from a numerical point of view solving this coupled system is much more challenging than solving the NSE.

Laval *et al.*²⁸ performed a numerical analysis of the coupled system consisting of Eqs. (4)–(8) and omitted the non-linear relaxation. Taking into account only the linear terms in Eqs. (7) and (8) resembles the governing equations for the rapid distortion theory (RDT) that makes use of this linearization to obtain insights of the small-scale turbulence modification under large-scale distortion.²⁹ Note that under very high mean strain the viscous term is often also neglected in analytical studies.^{30,31} It emanates from these studies that without the non-linear relaxation term, the turbulent kinetic energy spectrum is overestimated and the intermittency is increased (i.e., the probability distribution function of the velocity increments shows wider tails). With the addition of a turbulent viscosity term, these two effects can essentially be compensated.²⁸

Apart from the energetic and intermittency effects that have been observed as a consequence of the neglected non-linear relaxation term by Laval *et al.*,²⁸ the strain-rotation relations of the velocity may also be influenced. This can be quantified with the probability distribution function of the second invariant of the velocity gradient tensor $Q = 1/2(\Omega_{ij}\Omega_{ij} - S_{ij}S_{ij})$, or the angle between the eigenvectors of the rotation-rate tensor Ω_{ij} and the strain-rate tensor S_{ij} as for example investigated by Horiuti.³² In Sec. IV A, evidence is provided that the non-linear relaxation term contributes to the strain-rotation relations. Furthermore, the term $u'_j \partial u'_i / \partial x_j$ redistributes kinetic energy in spectral space, whereas a diffusive term $\partial^2 u'_i / (\partial x_j \partial x_j)$ exclusively removes kinetic energy if the (turbulent) viscosity is positive (see, e.g., Pope³⁰). It can be concluded that the replacement of the non-linear relaxation term with a turbulent viscosity may approximate the effects of attenuation of intermittency and high wave numbers of the kinetic energy spectrum well, but does not reproduce all physical mechanisms of the original term.

B. Modeling the filtered and subgrid-scale equations

In applications where only a coarse resolution is feasible, the FNSE can be solved instead of the NSE, using a suitable approximation for τ_{ij} . In such a case, all present flow structures can be resolved by the grid, because the high wave number content of the physical quantities

is removed. Since in a LES the equations for the small scales are not solved, the subgrid-scale stresses are unknown and require modeling. Many approaches exist that attempt to close the equations for the large scales that typically rely on the use of a turbulent viscosity to mimic at least the energetic effect of additional dissipation by small scales.^{33–36} This eddy-viscosity type of subgrid-scale models yields a modeled subgrid-scale stress tensor of the form

$$\tau_{ij,mod} = -2\nu_t \widetilde{S}_{ij} + \frac{1}{3} \tau_{kk,mod} \delta_{ij}, \quad (9)$$

where ν_t is the model-specific turbulent viscosity, δ_{ij} is the Kronecker tensor, and \widetilde{S}_{ij} is the strain-rate tensor of the large-scale velocity, given by

$$\widetilde{S}_{ij} = \frac{1}{2} \left(\frac{\partial \widetilde{u}_i}{\partial x_j} + \frac{\partial \widetilde{u}_j}{\partial x_i} \right). \quad (10)$$

Even with a subgrid-scale model that perfectly reproduces the subgrid-scale stress tensor, only one part of the coupled problem is solved, that is, only Eqs. (4) and (5) of the system of equations (4)–(8) are solved. Due to the rapid decrease in the kinetic energy spectrum of a turbulent flow for increasing wave numbers, the filtered velocity already possesses the majority of the kinetic energy, which is sufficient for many applications. However, there are applications for which knowledge of the subgrid-scale velocity field is required. In this paper, we propose a model for the subgrid-scale velocity that enables an approximate solution of the full problem consisting of Eqs. (4)–(8) (including the filtered velocity and the subgrid-scale velocity), but with a computational cost of the same order of magnitude as that of LES.

The proposed model exploits the previous findings of Laval *et al.*,²⁸ who suggest replacing the non-linear relaxation term in Eq. (8) by a turbulent viscosity ν'_t . Based on this work, the following expression for the turbulent viscosity is used, which is derived from renormalization groups to be³⁷

$$\nu'_t(k) = \left(\nu_f^2 - C_\nu \int_k^\infty q^{-2} E(q) dq \right)^{1/2} - \nu_f, \quad (11)$$

where k is the wave number, $E(k)$ is the kinetic energy spectrum, and C_ν is a constant with an analytical value of $C_\nu = 2/5$. Equation (11) is advantageous for the resulting kinetic energy spectrum compared to a constant turbulent viscosity for the following reason: The omitted non-linear relaxation is not only responsible for attenuating intermittency, but also for redistributing kinetic energy (mainly toward smaller scales). The turbulent viscosity of Eq. (11) is larger for small wave numbers and converges toward zero for high wave numbers. This means that the turbulent viscosity removes more kinetic energy from larger scales than from the smaller scales comparable to the physical mechanism of energy transfer toward small scales.

In addition to the introduction of a turbulent viscosity, a second modeling step is required for coupling the filtered scales with the subgrid scales, that is, modeling the subgrid-scale stress tensor. Assuming the forward energy cascade to be dominant, the influence of the filtered scales on the subgrid scales is mainly characterized by the subgrid scales being supplied with kinetic energy from the filtered scales. A simple way of mimicking this energy supply is by adding an additional source term to the right-hand side of the subgrid-scale momentum equations (8). This is inspired by numerical forcing of turbulence

for maintaining statistical steadiness in HIT, in particular by the forcing scheme of Mallocouppas *et al.*³⁸ It is important to understand that the forcing maintains a desired kinetic energy of the subgrid scales, which may be estimated using the model of Yoshizawa³⁹ or the dynamical model of Moin *et al.*⁴⁰ The amount of kinetic energy that is added to the subgrid scales is not necessarily equal to the kinetic energy that is removed from the filtered scales. The enrichment constitutes a more general process if it operates independently of the subgrid-scale model and its choices of constants. Furthermore, modeling errors of the subgrid-scale model weigh much more for the subgrid scales since their kinetic energy is only a small fraction of the total kinetic energy.

C. Discretization of the subgrid-scale equations

Even with the modeling described in Sec. II B, a numerical solution of Eqs. (7) and (8) (e.g. with a finite volume solver) would still require a grid that is fine enough to resolve the smallest flow structures. Since this would exceed the acceptable amount of computational time of a LES, a different discretization approach is proposed.

We assume that the subgrid-scale velocity \mathbf{u}' can be represented by the finite sum

$$\mathbf{u}' = \sum_{m=0}^{N_m-1} (\mathbf{A}_m(t) \cos(\mathbf{k}_m \cdot \mathbf{x}) + \mathbf{B}_m(t) \sin(\mathbf{k}_m \cdot \mathbf{x})), \quad (12)$$

where $\mathbf{A}_m(t)$ and $\mathbf{B}_m(t)$ are vectorial coefficients that depend on time t . Equation (12) is equivalent to a truncated Fourier series expansion with N_m modes, so the coefficients can be interpreted as contributions to the velocity at the respective wave number $k_m = |\mathbf{k}_m|$, where \mathbf{k}_m is the wave number vector. If the coefficients and the wave number vectors are known, the subgrid-scale velocity can be computed at arbitrary positions using the expansion given by Eq. (12).

The same approach is utilized in kinematic simulations.^{10–14} It consists of determining the coefficients, such that (i) the kinetic energy equals that of a given spectrum, and (ii) the random Gaussian directions of the coefficients lead to a divergence free velocity field, which yields the requirement $\mathbf{k}_m \cdot \mathbf{A}_m(t) = \mathbf{k}_m \cdot \mathbf{B}_m(t) = 0$. In kinematic simulations, a continuous velocity field that can be evaluated at every arbitrary position is obtained. The resulting velocity field can lead to decent predictions of second-order Lagrangian statistics of fluid particles.¹⁴ Since the coefficients do not change in space and the directions are chosen from a Gaussian distribution with fixed mean and standard deviation, the resulting velocity is statistically homogeneous and stationary. Furthermore, it is not clear how to maintain realistic time correlations when the kinetic energy spectrum varies in time. These issues are addressed and overcome with the present approach.

Consider the NSE for the subgrid scales with the turbulent viscosity, from Eq. (11), that replaces the non-linear relaxation term

$$\frac{\partial u'_i}{\partial x_i} = 0, \quad (13)$$

$$\frac{\partial u'_i}{\partial t} + \tilde{u}_j \frac{\partial u'_i}{\partial x_j} + u'_j \frac{\partial \tilde{u}_i}{\partial x_j} = -\frac{1}{\rho_f} \frac{\partial p'}{\partial x_i} + (\nu_f + \nu'_i) \frac{\partial^2 u'_i}{\partial x_j \partial x_j} + f_i, \quad (14)$$

where f_i is a forcing term that models the kinetic energy transfer from the filtered scales to the subgrid scales. Note that we assume the spectral turbulent viscosity constant in space, so it is treated similar to the

molecular viscosity in the viscous term. In the next step, the series expansion of the subgrid velocity in Eq. (12) is inserted into the modeled momentum equations (14) for every term of the sum separately and the pressure term is dropped. Sorting the result by sine and cosine terms the following equations for the coefficients $\mathbf{A}_m(t)$ and $\mathbf{B}_m(t)$ are obtained:

$$\begin{aligned} \frac{A_{m,i}^*(t) - A_{m,i}^n(t)}{\Delta t} + \tilde{u}_j^n k_{m,j} B_{m,i}^n(t) + A_{m,j}^n(t) \frac{\partial \tilde{u}_i^n}{\partial x_j} \\ = -(\nu_f + \nu'_i) |\mathbf{k}_m|^2 A_{m,i}^n(t) + f_{m,i}, \end{aligned} \quad (15)$$

$$\begin{aligned} \frac{B_{m,i}^*(t) - B_{m,i}^n(t)}{\Delta t} - \tilde{u}_j^n k_{m,j} A_{m,i}^n(t) + B_{m,j}^n(t) \frac{\partial \tilde{u}_i^n}{\partial x_j} \\ = -(\nu_f + \nu'_i) |\mathbf{k}_m|^2 B_{m,i}^n(t) + g_{m,i}, \end{aligned} \quad (16)$$

where Δt indicates the numerical time step. The time level of the coefficients is indicated with the index n . For this and all the following equations, no implicit summation over the index m is carried out. Without the pressure term, only a preliminary solution (indicated with an asterisk) is obtained. These coefficients do not lead to a divergence-free velocity field. However, if the pressure is formally expanded in spectral space and the divergence of the difference of Eqs. (15) and (16) and the same equations with pressure is computed, the following projection operation (details in the Appendix) is obtained to generate a set of coefficients that lead to a divergence-free velocity field:

$$\mathbf{A}_m^{n+1}(t) = \mathbf{A}_m^*(t) - \mathbf{k}_m \frac{\mathbf{k}_m \cdot \mathbf{A}_m^*(t)}{|\mathbf{k}_m|^2}, \quad (17)$$

$$\mathbf{B}_m^{n+1}(t) = \mathbf{B}_m^*(t) - \mathbf{k}_m \frac{\mathbf{k}_m \cdot \mathbf{B}_m^*(t)}{|\mathbf{k}_m|^2}. \quad (18)$$

The computational cost of the solution of one time step consisting of Eqs (15)–(18) scales linear with the number of modes N_m . In fact, the coefficients of the new time step are obtained by the explicit solution of two sets of algebraic equations, which makes their solution affordable.

Finally, determining the forcing terms $f_{m,i}$ and $g_{m,i}$ is addressed. Their modeling consists of two components: the magnitude and the direction. Ideally, the direction of the forcing terms is equal to the direction of the divergence of the subgrid-scale stress tensor, as defined in Eq. (9). However, this non-linear expression consists of contributions from the subgrid-scale velocity, the filtered velocity, their interaction, and the explicit filtering operations. In the present model, the directions are chosen from a uniform distribution over a spherical shell

$$\mathbf{V}_{m,0} = (\sin(\theta_m) \cos(\phi_m), \sin(\theta_m) \sin(\phi_m), \cos(\theta_m))^T \quad (19)$$

with

$$\phi_m \in [0, 2\pi], \quad \cos(\theta_m) \in [-1, 1]. \quad (20)$$

In order for the forcing directions to have realistic time correlation, the following algorithm is used to propagate the directions in time:

$$\mathbf{V}_m^n = \alpha_m \mathbf{V}_m^{n-1} + \beta_m \mathbf{V}_{m,0}, \quad (21)$$

where $\mathbf{V}_{m,0}$ is a random vector that is newly generated for every wave number and every time step, and \mathbf{V}_m^{n-1} is the normalized direction of

the previous time step. The vector \mathbf{V}_m^n is the direction of the forcing term at the current time step. Note that both forcing terms have directions that are propagated independently. Similar to the divergence of the subgrid-scale stress tensor, the vector field \mathbf{V}_m^n is not divergence free ($\mathbf{k}_m \cdot \mathbf{V}_m^n \neq 0$). The weights α_m and β_m determine how fast the directions change in time, and are computed as follows:

$$\alpha_m = \exp(-\Delta t T_{E,m}), \quad \beta_m = \sqrt{1 - \alpha_m^2}. \quad (22)$$

The rate of change of the directions depends on the wave number because the weights are determined based on the eddy-turnover time of the respective mode $T_{E,m} = \sqrt{|\mathbf{k}_m|^3 E(|\mathbf{k}_m|)}$.¹⁰ The kinetic energy spectrum $E(|\mathbf{k}_m|)$ can be directly computed from the coefficients as

$$E(|\mathbf{k}_m|) = \frac{1}{4\Delta k_m} (|\mathbf{A}_m|^2 + |\mathbf{B}_m|^2), \quad (23)$$

where Δk_m is the distance between consecutive wave numbers for the wave number k_m . Similar to the forcing scheme of Mallouppas *et al.*,³⁸ the source term in the subgrid-scale equation is

$$f_{i,m} = \frac{1}{\Delta t} \frac{\sqrt{K_{desired}} - \sqrt{K_{actual}}}{\sqrt{K_{desired}}} v_{i,m}^{trigger}, \quad (24)$$

where the trigger velocity of the respective mode follows the slope of the inertial range and is given by

$$v_{i,m}^{trigger} = \sqrt{\frac{K_{desired}}{K_{source}}} V_{A,m} k_m^{-5/6}. \quad (25)$$

The forcing term is zero if the kinetic energy of the subgrid-scale velocity field K_{actual} is equal to the desired kinetic energy $K_{desired}$. The trigger velocity is scaled such that it has the same characteristic magnitude as the resulting subgrid-scale velocity. In order to do so, the energy of the source has to be determined as

$$K_{source} = \frac{1}{4} \sum_{m=0}^{N_m-1} (|\mathbf{V}_{A,m} k_m^{-5/6}|^2 + |\mathbf{V}_{B,m} k_m^{-5/6}|^2), \quad (26)$$

where $\mathbf{V}_{A,m}$ and $\mathbf{V}_{B,m}$ are the directions for the forcing of the respective equation of the coefficients \mathbf{A}_m and \mathbf{B}_m , which are determined from Eq. (21). The kinetic energy that is actually present in the subgrid scale is computed analogously

$$K_{actual} = \frac{1}{4} \sum_{m=0}^{N_m-1} (|\mathbf{A}_m|^2 + |\mathbf{B}_m|^2). \quad (27)$$

The forcing term $g_{i,m}$ has the same magnitude as $f_{i,m}$, but is based on a separate evolution of the direction $\mathbf{V}_{B,m}$. Since the expression for $g_{i,m}$ is almost identical to $f_{i,m}$, but with $\mathbf{V}_{B,m}$ instead of $\mathbf{V}_{A,m}$ in Eq. (25), the explicit formula is not shown here for conciseness. The desired kinetic energy of the subgrid-scale velocity is estimated with the approach of Yoshizawa³⁹

$$K_{desired} = C_I \Delta^2 2\tilde{S}_{ij} \tilde{S}_{ij} \quad (28)$$

with the constant $C_I = 0.0826$ and the filter width Δ . The constant can also be computed dynamically with the model of Moin *et al.*⁴⁰

D. Transition to a sub-domain-based discretization

Since the model described in Sec. II C is constructed in Fourier space [i.e., the coefficients $\mathbf{A}_m(t)$ and $\mathbf{B}_m(t)$ are spatially constant], it can only generate subgrid-scale velocities with spatially constant statistics. However, many types of flows are inhomogeneous, which is the motivation for modifying the above approach, so that inhomogeneous statistics across a domain can be achieved. Instead of assuming that the coefficients obtained from Eqs. (15)–(18) are constant globally, they are defined on a structured grid of sub-domains, coarser than the LES grid. This induces motion of the flow field whose scale is of the order of the sub-domain size. However, considering that the energy of the corresponding induced velocity is small compared to the energy of the large scales, its effect is minor compared to other modeling assumptions in LES. Every sub-domain possesses a distinct set of coefficients. In each sub-domain, the statistics are assumed homogeneous, but each sub-domain can have different statistics. Thus, the coefficients formally do not only depend on time, but also vary between the sub-domains. Therefore, the coefficients have an additional index for the respective sub-domain and are denoted as $\mathbf{A}_{d,m}$ and $\mathbf{B}_{d,m}$. This implies that the spatial variations of scales of the order of the domain size are represented by spatially varying coefficients and the high wave number fluctuations by the trigonometric functions in Eq. (12). The quantities from the LES that are required to solve Eqs. (15)–(18) are averaged within the respective sub-domain, as indicated by $\langle \cdot \rangle_{domain}$. In particular, this applies to the LES velocity $\langle \tilde{u}_i \rangle_{domain}$, the gradient of the LES velocity $\langle \partial \tilde{u}_i / \partial x_j \rangle_{domain}$, and theoretically also the estimation of the kinetic energy of the subgrid-scale velocity $\langle K_{desired} \rangle_{domain}$. The latter has severe consequences for the resulting subgrid-scale field, which are discussed in Sec. II F. A domain average of the subgrid-scale kinetic energy is thus not applied in the present model. Instead, the subgrid-scale kinetic energy is estimated at the center of the sub-domain.

Another consequence of this sub-domain discretization is that the spatial derivatives also possess contributions of the coefficients. This leads to a modified predictor step for the preliminary coefficients

$$\begin{aligned} & \frac{A_{m,i}^* - A_{m,i}^n}{\Delta t} + \langle \tilde{u}_j^n \rangle_{domain} \left(k_{m,j} B_{m,i}^n + \frac{\partial A_{m,i}^n}{\partial x_j} \right) + A_{m,j}^n \left\langle \frac{\partial \tilde{u}_i^n}{\partial x_j} \right\rangle_{domain} \\ &= (v_f + v'_i) \left(-|\mathbf{k}_m|^2 A_{m,i}^n + \frac{\partial^2 A_{m,i}^n}{\partial x_j \partial x_j} + 2k_{m,j} \frac{\partial B_{m,i}^n}{\partial x_j} \right) + f_{m,i}, \quad (29) \end{aligned}$$

$$\begin{aligned} & \frac{B_{m,i}^* - B_{m,i}^n}{\Delta t} + \langle \tilde{u}_j^n \rangle_{domain} \left(\frac{\partial B_{m,i}^n}{\partial x_j} - k_{m,j} A_{m,i}^n \right) + B_{m,j}^n \left\langle \frac{\partial \tilde{u}_i^n}{\partial x_j} \right\rangle_{domain} \\ &= (v_f + v'_i) \left(-|\mathbf{k}_m|^2 B_{m,i}^n + \frac{\partial^2 B_{m,i}^n}{\partial x_j \partial x_j} - 2k_{m,j} \frac{\partial A_{m,i}^n}{\partial x_j} \right) + g_{m,i}. \quad (30) \end{aligned}$$

The temporal and spatial dependencies of the coefficients are omitted for the sake of simplicity.

Figure 1 summarizes the proposed velocity enrichment strategy based on a LES. The first step is to perform a time step of the LES and average the required quantities in the sub-domains. Furthermore, the subgrid-scale kinetic energy is estimated and the direction and magnitude of the forcing terms are computed. The choice of the LES solving framework is arbitrary. Even a LES on an unstructured grid is possible, in which case solely the averaging has to be adapted. In the next step, Eqs. (29), (30), (17), and (18) are solved in every sub-domain to obtain

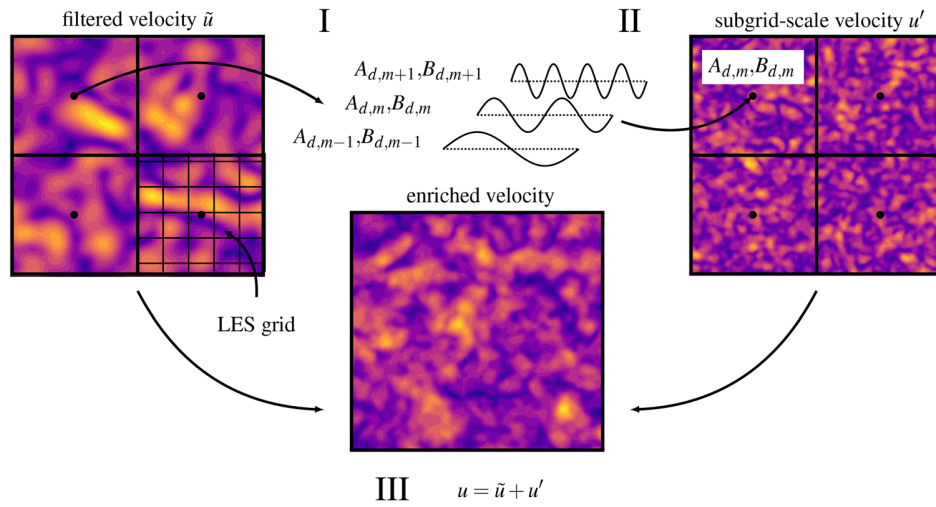


FIG. 1. General enrichment strategy consisting of three steps. (I) Information on the large-scale flow dynamics is obtained by averaging within sub-domains that are coarser than the LES grid. (II) The model equations (29), (30), (17), and (18) are solved in every sub-domain. (III) The enriched velocity is approximated as the sum of the resolved LES velocity and the modeled subgrid-scale velocity.

a distinct set of coefficients for every sub-domain. This step is rather inexpensive, since the equations are solved fully explicit and independent for every sub-domain. The parallelization is very simple and efficient if it is carried out in spectral space. If every processor solves a portion of the wave numbers of all sub-domains, no communication is necessary. The final step consists of adding up the LES velocity and the subgrid-scale velocity, which is obtained by computing Eq. (12) at the desired locations.

E. Treatment of the discontinuities

In some applications of the enrichment model, a spatially continuous reconstructed subgrid-scale velocity field may be required. Due to the proposed sub-domain discretization, this cannot be guaranteed at the boundaries of the sub-domains. A naive interpolation of the subgrid-scale velocity or the coefficients of the series expansion in Eq. (12) would not conserve the property of a divergence-free velocity field. However, since the divergence is only non-zero at sub-domain boundaries, the portion of the influenced regions is small compared to the entire simulation domain.

In this section, we present a modified interpolation between sub-domains that leads to a continuous and divergence-free velocity field. The modeled momentum equations are, in general, not satisfied within the interpolation regions. A compact interpolation kernel should be preferred in order to keep the regions with the subgrid-scale velocity that satisfies the model equations as large as possible.

The general idea is to add a correction velocity in a direction tangential to the boundary for every mode. We assume that the interpolated subgrid-scale velocity u'_{int} consists of a contribution of the lower sub-domain u'_{low} , the upper sub-domain u'_{up} , and a correction velocity u'_{corr} ,

$$u'_{int} = W(x)u'_{low} + (1 - W(x))u'_{up} + u'_{corr}, \tag{31}$$

where W is the interpolation kernel function. In the following, the interpolation in x direction is derived. The other directions can be

obtained analogously. For this case, the interpolation kernel function $W(x)$ is exclusively a function of x and the correction velocity has only contributions in y and z directions. The required criterion for the interpolated velocity is

$$\nabla \cdot u'_{int} = 0. \tag{32}$$

Furthermore, we assume that the velocity fields can be decomposed in the following way:

$$u' = \sum_{m=0}^{N_m-1} u'^{,m} = \sum_{m=0}^{N_m-1} (A_m(t) \cos(\mathbf{k}_m \cdot \mathbf{x}) + B_m(t) \sin(\mathbf{k}_m \cdot \mathbf{x})), \tag{33}$$

where $u'^{,m}$ is the velocity contribution corresponding to the wave number $|\mathbf{k}_m|$. Since the divergence is a linear operation, Eq. (32) is satisfied if the divergence of every velocity contribution $u'^{,m}$ is zero

$$\nabla \cdot u'^{,m} = 0. \tag{34}$$

In the x direction, the divergence-free requirement is expressed as

$$\frac{dW(x)}{dx} (u'_{low}{}^{,m} - u'_{up}{}^{,m}) + \frac{\partial v'_{corr}{}^{,m}}{\partial y} + \frac{\partial w'_{corr}{}^{,m}}{\partial z} = 0. \tag{35}$$

At this point, a choice has to be made for how the divergence of the velocity field is distributed over the boundary tangential velocities. One satisfactory way is to either set $w'_{corr}{}^{,m} = 0$, which leads to $v'_{corr}{}^{,m} = \Psi^m(\mathbf{x})/k_{m,2}$ or set $v'_{corr}{}^{,m} = 0$, which leads to $w'_{corr}{}^{,m} = \Psi^m(\mathbf{x})/k_{m,3}$. In order to keep the correction velocity magnitude small, $\min(|v'_{corr}{}^{,m}|, |w'_{corr}{}^{,m}|)$ decides which case is used. The correction velocity kernel is defined as

$$\Psi(\mathbf{x}) = \frac{\partial W(x)}{\partial x} [(A_{low,m,1} - A_{up,m,1}) \sin(\mathbf{k}_m \cdot \mathbf{x}) - (B_{low,m,1} - B_{up,m,1}) \cos(\mathbf{k}_m \cdot \mathbf{x})]. \tag{36}$$

The correction theoretically works with every interpolation kernel $W(x)$. However, we suggest to use a sigmoid function based on the signed distance to the sub-domain boundary r ,

$$W(r) = 1 - \frac{1}{1 + e^{-\alpha r}}, \quad (37)$$

where α is a parameter to control the sharpness of the interpolation kernel.

An extension to three dimensions is straightforward as long as the interpolation kernels of different directions are not overlapping. This leads to complicated integrations that have to be carried out analytically, which is not possible in some cases. If the overlapping of the interpolation kernels is ignored, the edges and corners of the sub-domains are not divergence free. With a sharp interpolation kernel, these regions are tiny and most likely unimportant for the majority of the applications. If the integrand is approximated with a Taylor series of the interpolation kernel, a nearly divergence-free field can also be obtained in the regions with overlapping interpolation kernels.

The divergence of the modeled subgrid-scale velocity with and without interpolation between sub-domains is depicted in Fig. 2. The detailed setup and the definition of the reference time T_{ref} which is used for normalization, are specified in Sec. III B 1. The divergence is computed with central differences for the spatial derivatives of the subgrid-scale velocity field that is sampled on a DNS-grid (i.e., a grid that can resolve the Kolmogorov length scale). In Fig. 2(a), where no interpolation between sub-domains is used, it can be observed that the divergence is significant between the sub-domains. With the proposed interpolation in Fig. 2(b), the divergence is approximately zero almost everywhere; solely at the edges between four sub-domains does non-zero divergence occur.

The divergence-free interpolation constitutes an option for applications where the discontinuity in the subgrid-scale velocity is not acceptable. The results of the present paper are obtained without the interpolation (i.e., with a discontinuous subgrid-scale velocity). However, it is shown in Sec. IV A that the influence of the interpolation on the presented statistics is negligible.

F. The role of the estimated subgrid-scale kinetic energy

As mentioned in Sec. II D, the subgrid-scale kinetic energy is evaluated in one grid cell within the sub-domain instead of averaged

over all grid cells in the sub-domain. This section justifies this choice.

The estimation of the kinetic energy of the subgrid-scale velocity strongly influences the predictions of the presented model, as it directly impacts the kinetic energy spectrum of the generated velocity field. For HIT, the estimation of the kinetic energy with Eq. (28) leads to average subgrid-scale kinetic energies that are close to the values obtained from a filtered DNS. More specifically, the estimated subgrid-scale kinetic energy lies within a ten percent margin of the subgrid-scale kinetic energy obtained from the DNS of the HIT case described in Sec. III B using a spectrally sharp filter.

Apart from the mean value of the kinetic energy of the subgrid-scale kinetic energy, its probability distribution is of importance. A characteristic aspect of turbulent flows is that the probability distribution function of the velocity gradients (and other quantities) exhibits a non-Gaussian behavior, which is widely known as “intermittency.”⁴¹ Typically, as the Reynolds number increases, the tails of the probability distribution functions (PDFs) get wider, and that is, high-intensity events become more likely. Since the effect of the subgrid-scale velocity on the filtered scales in a LES is commonly modeled using a turbulent viscosity, a spatially averaged LES may be interpreted as a DNS with smaller Reynolds number. Thus, the PDFs can be expected to tend to a Gaussian distribution. This is confirmed in Sec. IV A.

Due to the forcing of the subgrid-scale velocity, its distribution directly depends on the distribution of the subgrid-scale kinetic energy. Distributions of derived values, such as the subgrid-scale velocity gradients, thus also depend on the distribution of the subgrid-scale kinetic energy. This is why the PDF of the subgrid-scale kinetic energy is of great importance.

In Fig. 3, the probability distribution function of the estimated subgrid-scale kinetic energy is shown together with a squared Gaussian distribution. The simulation configuration again refers to the HIT case described in Sec. III B. The kinetic energy is centered with respect to the mean $\langle K_{est} \rangle$ and normalized with standard deviation σ_K . As expected, the two distributions do not coincide. More practically, relevant is how the PDF of the estimated subgrid-kinetic energy averaged in sub-domains consisting of 2^3 LES grid cells compares to this. It is not surprising that the averaging leads to a distribution that is

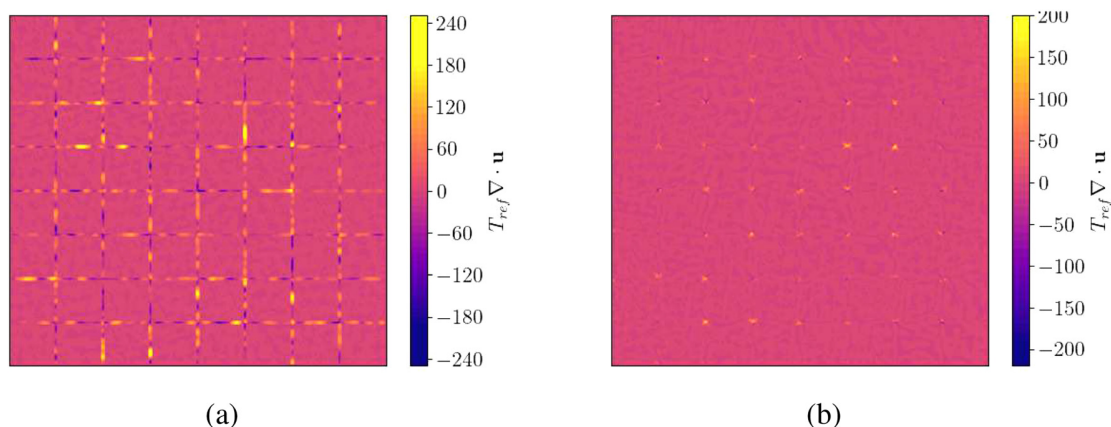


FIG. 2. Normalized divergence of the modeled subgrid-scale velocity computed using central differences. (a) is obtained without interpolation between the sub-domains and (b) is obtained using the proposed interpolation.

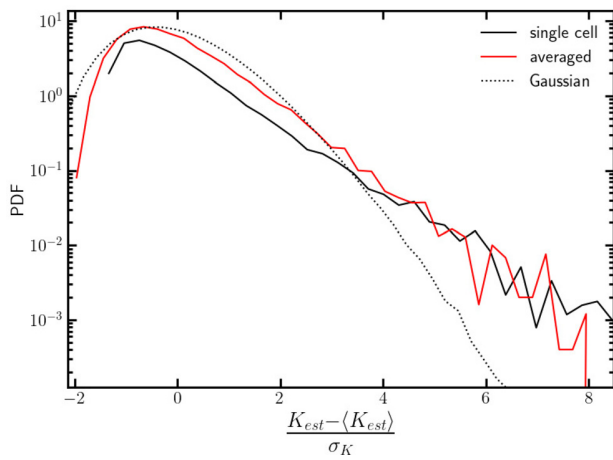


FIG. 3. PDF of the centered and normalized estimated subgrid-scale kinetic energy. We show the difference between averaging the kinetic energy in multiple LES grid cells (average) and evaluating it for every LES grid cells separately (single). In order to be able to assess the resulting distributions, a squared Gaussian distribution is plotted.

closer to a Gaussian distribution. As a consequence, derived quantities of the modeled subgrid-scale velocity field possess different PDFs, dependent on the averaging volume of the estimated subgrid-scale kinetic energy.

Since the averaging of the subgrid-scale kinetic energy within the sub-domains leads to artificial modification of its PDF, the averaging is avoided in the application of the model. Instead, the kinetic energy of the subgrid-scale velocity is chosen to be equal to the one computed for one arbitrary LES grid cell in the sub-domain (e.g., the cell in the sub-domain center).

Sections III–IV will show the features of the model and validate it for two flow configurations.

III. SIMULATIONS

The performance of the model proposed in this paper is evaluated on two test cases, HIT and a turbulent unbounded shear flow. The reference DNS is carried out on a very fine grid that captures all present length and time scales down to the Kolmogorov scales. LES that are enriched with the presented model are compared with the DNS results. Note that wall boundary conditions significantly increase the complexity of the flow and already constitute a problem for LES without modeling of the subgrid-scale velocity. This is why the scope of this paper is limited to unbounded flow configurations.

First, the numerical solution of the NSE and LES equations is briefly summarized in Sec. III A. Then, that the exact configurations of the two test cases are explained in Sec. III B.

A. Numerical solution of the Navier–Stokes equations and LES equations

For the two DNS (HIT and turbulent shear flow), the NSE are solved in their form as given in Eqs. (2) and (3). Since all time and length scales down to the Kolmogorov scales are resolved, no further modeling is applied to the set of governing physical equations. The LES is performed on a grid that is too coarse to resolve the full

turbulent spectrum and is based on the FNSE given by Eqs. (4) and (5). Due to the presence of the subgrid-scale stress tensor, these equations are not closed. That is why the following set of equations is solved in the case of a LES that are referred to as LES equations:

$$\begin{aligned} \frac{\partial \tilde{u}_i}{\partial x_i} &= 0, \\ \frac{\partial \tilde{u}_i}{\partial t} + \tilde{u}_j \frac{\partial \tilde{u}_i}{\partial x_j} &= -\frac{1}{\rho_f} \frac{\partial \mathcal{P}}{\partial x_i} + \frac{\partial}{\partial x_j} \left(\frac{\nu_f + \nu_t}{2} \left(\frac{\partial \tilde{u}_i}{\partial x_j} + \frac{\partial \tilde{u}_j}{\partial x_i} \right) \right) + F_i. \end{aligned} \quad (38)$$

The modified pressure \mathcal{P} accounts for the trace of the subgrid-scale stress tensor and the turbulent viscosity, ν_t , models the effect of additional dissipation by the omitted subgrid scales. For the HIT test case, the turbulent viscosity is determined by the Smagorinsky model³³

$$\nu_t = (C_S \Delta)^2 |\tilde{S}_{ij}|^2, \quad (40)$$

where C_S is the Smagorinsky constant, Δ is the filter width, and $|\tilde{S}_{ij}|$ is the following norm of the filtered strain rate tensor:

$$|\tilde{S}_{ij}| = \sqrt{2\tilde{S}_{ij}\tilde{S}_{ij}}. \quad (41)$$

In shear-dominated turbulent flows, it can be advantageous to replace the Smagorinsky model with the Vreman model,³⁶ which is known to produce more physical results in transitional shear flows. With this model, the turbulent viscosity is given by

$$\nu_t = C_V \sqrt{\frac{B_\beta}{\tilde{A}_{ij}\tilde{A}_{ij}}} \quad (42)$$

with the filtered velocity gradient tensor

$$\tilde{A}_{ij} = \frac{\partial \tilde{u}_i}{\partial x_j} \quad (43)$$

and

$$\beta_{ij} = \Delta^2 \tilde{A}_{ik}\tilde{A}_{jk}, \quad (44)$$

$$B_\beta = \beta_{11}\beta_{22} - \beta_{12}^2 + \beta_{11}\beta_{33} - \beta_{13}^2 + \beta_{22}\beta_{33} - \beta_{23}^2. \quad (45)$$

In the case of HIT, a statistically steady state is desired for the evaluation of the model. To achieve this, the same amount of kinetic energy that is dissipated has to be inserted into the flow. In addition to the constant kinetic energy, further requirements are that the flow is statistically homogeneous and isotropic. In the present work, the forcing scheme of Mallouppas *et al.*³⁸ is used. The applied procedure is very similar to the forcing of the small scales that is described in Sec. II C

$$F_i = \frac{1}{\Delta t} \frac{\sqrt{K_{desired}} - \sqrt{K_{actual}}}{\sqrt{K_{desired}}} v_i^{trigger}. \quad (46)$$

However, there are two differences. Instead of estimating the desired kinetic energy, $K_{desired}$, its value is given as a parameter and determines the kinetic energy in the flow. Furthermore, the trigger velocity $v_i^{trigger}$ is determined from the following series expansion:

$$v_i^{trigger} = \sum_m U_{m,i} \cos(k_{m,j}x_j + \psi_m). \quad (47)$$

The wave number vector $k_{m,j}$ has a magnitude corresponding to the triggered wave number and has random directions. The phase ψ_m is

chosen randomly from a uniform distribution in the range $0 \leq \psi \leq 2\pi$. The velocity coefficients $U_{m,i}$ are chosen to lead to a divergence-free trigger velocity and thus fulfills the condition $\mathbf{U}_m \cdot \mathbf{k}_m = 0$. Its magnitude corresponds to a von Kármán kinetic energy spectrum in the triggered wave number range and is given by

$$|\mathbf{U}_m| = 2\sqrt{E_{vk}(|k_m|)\Delta k}, \quad (48)$$

where E_{vk} is a von Kármán spectrum and Δk the difference between two consecutive discrete wave numbers. Similar to the directions in the forcing of the small scales, v_i^{trigger} is smoothly propagated in time by applying Eqs. (21) and (22). The trigger velocity consists only of modes within a predefined wave number range. This has the reason that isotropy of the generated velocity field cannot be achieved if the largest possible scales are triggered.⁴²

In this work, the NSE and the LES equations are discretized with a finite-volume approach that converges with second order in space and time. The numerical solution is similar to the one described in Denner *et al.*,⁴³ but is carried out on an equidistant structured Cartesian grid with the corresponding geometrical simplifications that result from constant cell volumes, cell face areas, and normal vectors that are aligned with the coordinate axes. The continuity equation and the three-momentum equations are solved in a single equation system for multiple iterations every time step. The continuity equation is coupled with the momentum equations using momentum-weighted interpolation, a concept that was originally introduced by Rhie and Chow.⁴⁴ As a result, two distinct velocity fields exist in the numerical framework, a cell centered velocity that satisfies the momentum balance with high accuracy and a face centered velocity that conserves the mass. With increasing spatial resolution, the velocities converge toward each other. The results that are presented in this paper are based on the cell-centered velocity.

B. Flow configurations

1. Homogeneous isotropic turbulence

The first of the two considered test cases is forced HIT. The simulation domain is a cube with the edge length L and periodic boundary conditions in all three directions. A statistically steady turbulence is obtained by applying the forcing procedure described in Sec. III A. In order to obtain a homogeneous, isotropic velocity field, the forcing is exclusively applied between the wave number k_{start} and k_{end} . Physical parameters of the resulting turbulent velocity field are the Taylor-Reynolds number $Re_\lambda = \lambda u_{\text{rms}}/\nu_f$, the turbulent Reynolds number $Re_l = l_{11} u_{\text{rms}}/\nu_f$, the Kolmogorov length scale η , the Taylor microscale λ , and the longitudinal (l_{11}) and transverse (l_{22}, l_{33}) integral length scales, and are summarized in Table I. Spatial quantities are presented normalized by the domain length and temporal quantities are normalized by a reference time $T_{\text{ref}} = L/u_{\text{rms}}$, with the root mean square velocity $u_{\text{rms}} = \sqrt{2/3K}$ and the total kinetic energy K .

The solution of the DNS is obtained on a numerical grid with 256^3 cells. This leads to a product of the largest resolved wave number k_{max} and the Kolmogorov length scale of $k_{\text{max}}\eta = 1.37$.

The LES of the same case is solved on a grid consisting of 32^3 cells. The influence of the omitted subgrid scales is accounted for by adding a turbulent viscosity that is obtained from the Smagorinsky model with a model constant $C_S = 0.1$ and a filter width Δ corresponding to the size of a computational cell.

TABLE I. Parameters of the HIT simulation configuration.

Parameter	Value
Re_λ	75
Re_l	205
η/L	0.0017
τ_η/T_{ref}	0.0075
λ/L	0.029
l_{11}/L	0.079
l_{22}/L	0.49
l_{33}/L	0.38
$k_{\text{start}}L/2\pi$	3
$k_{\text{end}}L/2\pi$	6

The resulting kinetic energy spectra $E(k)$ of the DNS and the LES are shown in Fig. 4. The DNS spectrum possesses a pronounced inertial range that is characterized by a slope of $|\mathbf{k}_m|^{-5/3}$. It can be observed that the kinetic energy spectrum of the LES resembles the one of the DNS well for the smaller wave numbers. The cutoff wave number of the LES lies within the inertial range.

For a homogeneous isotropic flow, the spatial autocorrelations $B_{xx}^{(1)}$ are defined as⁴⁵

$$B_{xx}^{(1)}(r) = \frac{\langle u_x(\mathbf{x}, t)u_x(\mathbf{x} + r\mathbf{e}_1, t) \rangle}{\langle u_x(\mathbf{x}, t)u_x(\mathbf{x}, t) \rangle}, \quad (49)$$

where r denotes the distance between the evaluated velocities and \mathbf{e}_1 the unit vector in the first coordinate direction. Thus, $B_{11}^{(1)}$ indicates the longitudinal and $B_{22}^{(1)}$ and $B_{33}^{(1)}$ the transverse spatial autocorrelation functions, respectively. As already mentioned, isotropy is not achieved if the smallest wave numbers are included in the forcing. Based on the spatial autocorrelations, the integral length scales l_{xx} are defined as

$$l_{xx} = \int_0^\infty B_{xx}^{(1)}(r) dr. \quad (50)$$

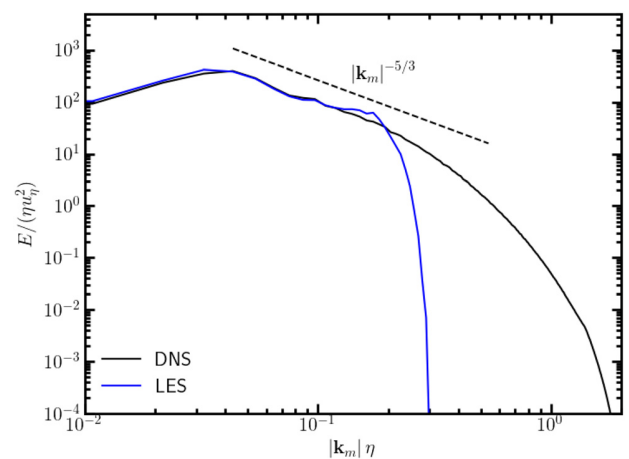


FIG. 4. Kinetic energy spectrum of forced HIT. We compare the spectra of the HIT case of a DNS with 256^3 grid cells and a LES with 32^3 grid cells.

Note that no implicit summation is carried over double occurring indices α . In isotropic turbulence, the transverse integral length scale is half the longitudinal integral length scale.³⁰ It can be seen in Table I that this relation approximately holds for the generated turbulent field.

2. Turbulent shear flow

The second case that is investigated is a turbulent shear flow that is driven by a source term in the momentum equation. Figure 5 sketches the simulation setup. The domain is a cube with edge length L and periodic boundary conditions in all the three directions. The momentum source acts in the x direction and varies with the shape of one period of a sine-profile in the y direction

$$s = s_{max} \sin(2\pi y/L) \mathbf{e}_1. \quad (51)$$

The amplitude is given by s_{max} and \mathbf{e}_1 indicates the unit vector in x direction. Assuming a shear velocity $u_{shear} = \sqrt{s_{max}L}$, the shear Reynolds number can be defined as $Re_{shear} = u_{shear}L/\nu_f$. The value of this and other physical parameters is summarized in Table II. Similar to the shear velocity, a characteristic shear time can be defined for normalization $T_{shear} = L/u_{shear}$.

A DNS with 128^3 grid cells fully resolves the length scales down to the Kolmogorov scale of the shear flow ($k_{max}\eta = 1.16$). In addition to the DNS, a LES with 16^3 grid cells is performed. Since it is well known that the Smagorinsky model is inaccurate in the prediction of shear-dominated flows (see, e.g., L ev eque *et al.*⁴⁶), the eddy viscosity is computed with the Vreman model using a model constant with the value $C_V = 0.025$.

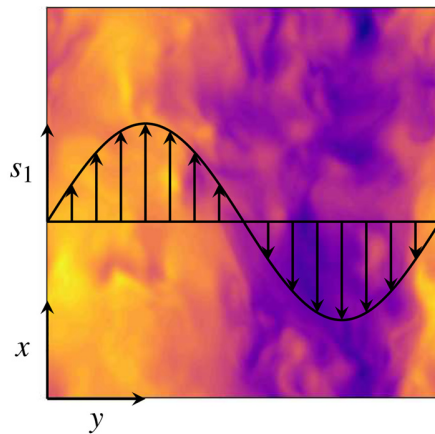


FIG. 5. Sketch of the shear flow configuration. The momentum source (black line) varies in the shape of a sin-profile in y direction and acts in the x direction. The cubic domain is periodic in all directions. The colors show the velocity in x direction.

TABLE II. Parameters of the turbulent shear flow simulation configuration.

Parameter	Value
Re_{shear}	3115
η/L	0.0029
τ_η/T_{shear}	0.026

Figure 6(a) shows the resulting mean velocity profiles of the DNS and the LES averaged in time. For both simulations, the mean velocity profiles in the y and z directions are very close to zero. According to the profile of the volumetric force that drives the flow, the mean velocity profiles in x direction have the shape of one period of a sine-function. However, the amplitudes of the mean velocity profiles differ significantly.

Figure 6(b) shows the kinetic energy of the DNS and the LES of the turbulent shear flow over time. The turbulent shear flow behaves aperiodic and contains strong fluctuations of flow quantities, for example, the kinetic energy. Periods of pronounced turbulence slow down the main velocity stream, which reduces the production of new turbulent structures. The flow becomes less turbulent and the main-stream accelerates because the resistance due to the turbulence decreases. This causes a chaotic change between periods of high and low kinetic energy. As already pointed out, the mean velocity profile of the LES possesses a higher amplitude than the one of the DNS. The consequence is that the average kinetic energy of the LES is also higher.

IV. RESULTS AND DISCUSSION

In Sec. IV A, predictions of the presented model are evaluated in HIT and the turbulent shear flow. We investigate the extent with which the actual intermittency and spatial structures can be reproduced by the proposed enrichment strategy as described in Sec. IV A. Furthermore, the ability of the model to generate the anisotropic and inhomogeneous subgrid-scale velocity of the turbulent shear flow is assessed in Sec. IV B.

A. Enriched velocity of the HIT case

In order to study the influence of different parameters on the resulting predictions of the subgrid-scale velocity, a standard model setup for the enrichment of the HIT case is defined. The standard model setup contains a grid with eight sub-domains per direction, which is of a factor four coarser per direction than the LES grid. The number of modes in the series expansion (12) is $N_m = 100$ and the constant in the turbulent viscosity in the enrichment model ν'_t is $C_\nu = 0.4$, which corresponds to the analytical value obtained from renormalization group theory.³⁷ The kinetic energy of the subgrid-scale velocity is estimated using the model of Yoshizawa³⁹ $K_{est} = C_I \Delta^2 \tilde{S}_{ij} \tilde{S}_{ij}$, with the originally proposed value of the model constant $C_I = 0.0826$.

In Fig. 7, slices of the instantaneous velocity magnitudes of the DNS, the LES, and the LES enriched with the proposed model are depicted. The LES does not contain small velocity structures, and the maximum velocity magnitude is still somewhat smaller than the one of the DNS. With enrichment, the velocity magnitude of the DNS is better recovered and smaller velocity structures than in the LES without enrichment are observed. However, the DNS field consists of thin elongated structures, whereas the enrichment yields a less structured velocity field. This missing structure in the subgrid-scale velocity can be traced back to the forcing of the subgrid scales that is applied in randomly chosen directions instead of the actual directions of the subgrid-scale stress tensor. Furthermore, the non-linear relaxation term, which is not part of the model equations, may contribute to the formation of the observed structures in the DNS velocity field.

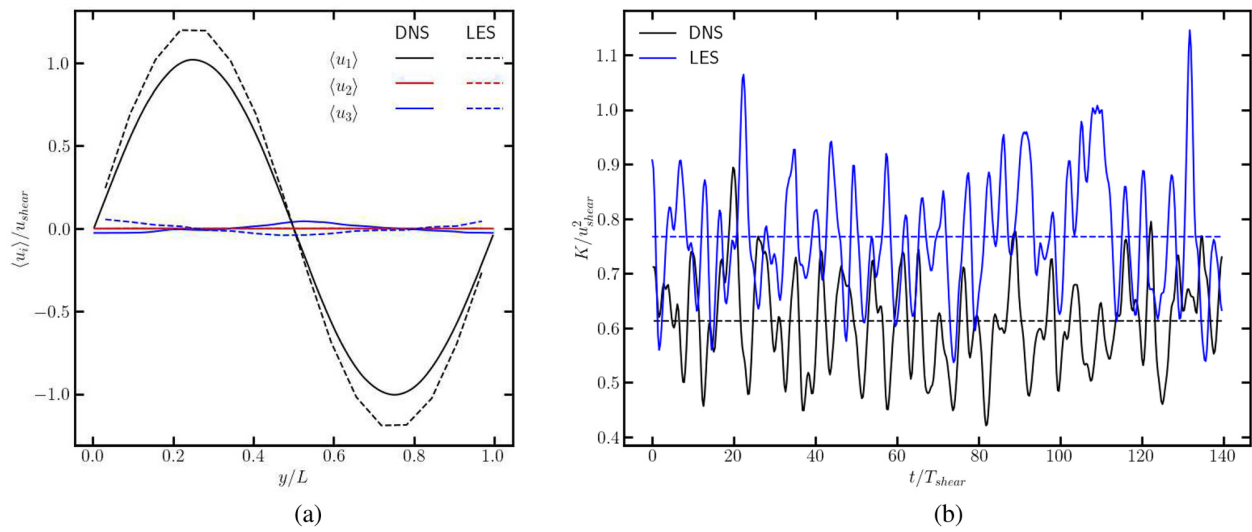


FIG. 6. (a) Comparison of the mean velocity profiles over the y -coordinate in the turbulent shear flow of the DNS (solid line) and the LES with the Vreman model (dashed line) and (b) dimensionless kinetic energy over dimensionless time for the DNS and the LES of the turbulent shear flow. The dashed lines are the average kinetic energies.

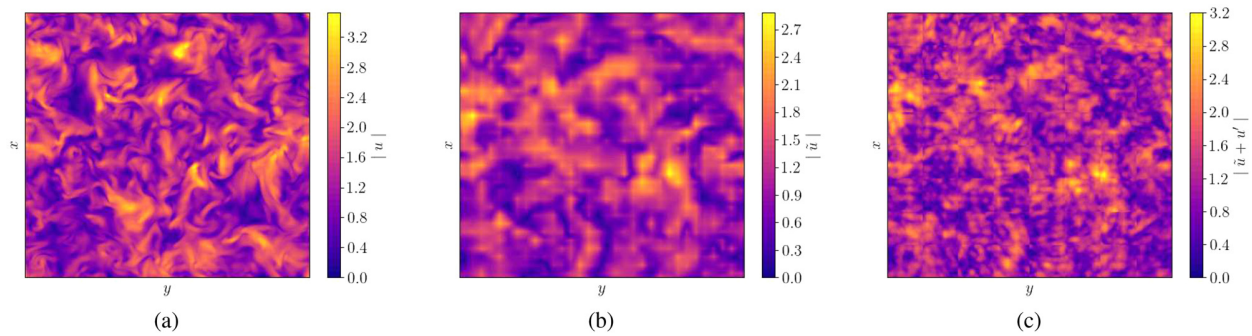


FIG. 7. Slices in the x - y plane of the velocity magnitudes of (a) the DNS velocity, (b) the LES velocity without enrichment, and (c) the LES velocity enriched with the proposed model for the HIT case.

Figure 8 shows the kinetic energy spectrum that results from the subgrid-scale velocity. The kinetic energy spectrum of the modeled subgrid-scale velocity coincides well with the DNS. The LES and the modeled subgrid-scale spectrum together recover the entire range of scales of the DNS. Note that the subgrid-scale spectrum is obtained directly from the coefficients of the series expansion Eq. (12). If the discrete Fourier transform of the sampled subgrid-scale velocity field, which is discontinuous across the sub-domains, were to be computed, additional spurious spectral content would occur. This is known as the Gibbs phenomenon and is avoided here by computing the kinetic energy spectrum directly from the coefficients in Eq. (23).

The kinetic energy spectrum provides insight into the average kinetic energy belonging to a certain wave number. However, it does not contain information on how likely events with a specific intensity are. A characteristic of turbulent flows is that the PDFs exhibit a higher incidence of high-intensity events, leading to a non-Gaussian (more widely shaped) distribution of the velocity gradients.⁴¹ Figure 9 shows

the PDFs of the longitudinal and transverse velocity gradients A_{11} and A_{12} normalized with their standard deviations $\sigma_{A_{11}}$ and $\sigma_{A_{12}}$. In both cases, the LES predicts the gradients with smaller magnitudes, and the PDF tends to be closer to a Gaussian distribution than the PDF of the DNS. With the LES including the newly proposed enrichment model with the standard model setup, a much wider distribution of the velocity gradients is achieved that increases the intermittency of the flow compared to the LES. Solely, the very rare events with the greatest magnitude (i.e., the ends of the tails of the PDF) cannot be fully reproduced. It may seem surprising, that despite the Gaussian forcing of the subgrid-scale velocity, a non-Gaussian PDF of the velocity gradients is accomplished. There are two main reasons for the observed non-Gaussian distribution of the velocity gradients of the enriched LES: first, the forcing is only Gaussian within a sub-domain. Since the estimated subgrid-scale kinetic energy shows a non-Gaussian distribution, the forcing is also non-Gaussian on a scale of the domain size, and second, there are other terms in the model equations (13) and (14) apart

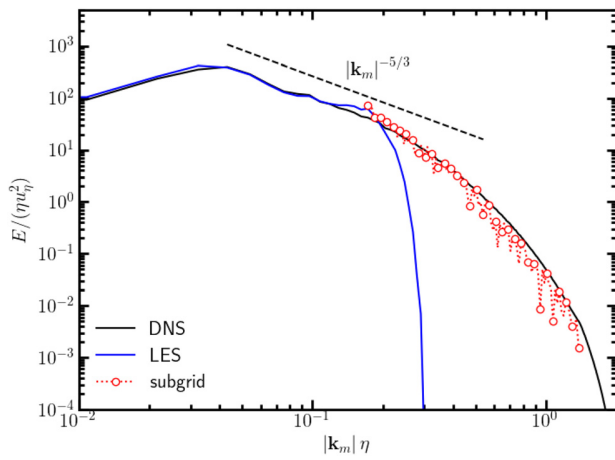


FIG. 8. Kinetic energy spectrum of forced HIT. We compare the results of the DNS with 256^3 grid cells, the LES with 32^3 grid cells, and the modeled subgrid-scale velocity field.

from the forcing term that verifiably cause intermittency, that is, the sweeping term and the straining term.²⁸ It is also worth noting that the PDF of the longitudinal velocity gradient possesses a non-zero skewness. The modeled subgrid-scale velocity obtained from the enrichment model has difficulties in reproducing this asymmetric behavior.

In addition to the distribution of single entries in the velocity gradient tensor, a characteristic feature of turbulence is the distribution of the second invariant Q of the velocity gradient tensor, which is defined as

$$Q = \frac{1}{2} (\Omega_{ij}\Omega_{ij} - S_{ij}S_{ij}), \quad (52)$$

where Ω_{ij} is the rotation-rate tensor and S_{ij} is the strain-rate tensor. The second invariant of the velocity gradient tensor can be interpreted as a measure of how strong rotation is compared to straining. The right prediction of Q is of practical importance, for instance in particle-laden flows, since the vorticity-strain relations of a turbulent

flow can be directly related to the clustering behavior of inertial particles of very small Stokes numbers that are immersed in the flow.^{47,48} The ability to predict this behavior is often viewed as important property for structural subgrid-scale models to predict the right amount of particle clustering.^{13,18,49,50} Note however that the right prediction of Q does not guarantee that the right particle clustering is obtained.

The PDFs of the second invariant of the velocity gradient tensor of the DNS, the LES, and multiple predictions of the enriched LES velocity are compared in Fig. 10. Four different parameters of the model are systematically varied with respect to the standard model setup in order to determine their impact: (i) the number of subdomains, (ii) the kinetic energy of the subgrid-scale velocity, (iii) the number of modes, and (iv) the model constant C_v in the turbulent viscosity ν'_t of the subgrid-scale momentum equation.

The most obvious observation in Fig. 10 is that the LES without an enrichment model severely underpredicts the width of the PDF compared to the DNS. The previously defined standard model setup, which is depicted for comparison in all of the figures, improves the width and also the shape of the PDF of the second invariant of the velocity gradient tensor. However, the skewness is somewhat less pronounced than for the DNS.

An indication for the observed bias in the PDF of the second invariant of the velocity gradient tensor may be obtained by decomposing Q as follows:

$$Q = \frac{1}{2} (\Omega_{ij}\Omega_{ij} - S_{ij}S_{ij}) = -\frac{1}{2} \frac{\partial u_i}{\partial x_j} \frac{\partial u_j}{\partial x_i} = -\frac{1}{2} \frac{\partial}{\partial x_i} \left(u_j \frac{\partial u_i}{\partial x_j} \right). \quad (53)$$

In fact, the divergence of the advective term is proportional to the second invariant of the velocity gradient tensor. Neither the non-linearity in the subgrid-scale momentum equation (8) nor the non-linearities in the subgrid-scale stress tensor are represented correctly in the model. The second invariant of the velocity gradient tensor can be further expanded

$$Q = \frac{\partial}{\partial x_i} \frac{\partial}{\partial x_j} \left(\underbrace{\tilde{u}_i \tilde{u}_j + u'_i \tilde{u}_j + \tilde{u}_i u'_j}_{\text{non-local contributions}} + u'_i u'_j \right). \quad (54)$$

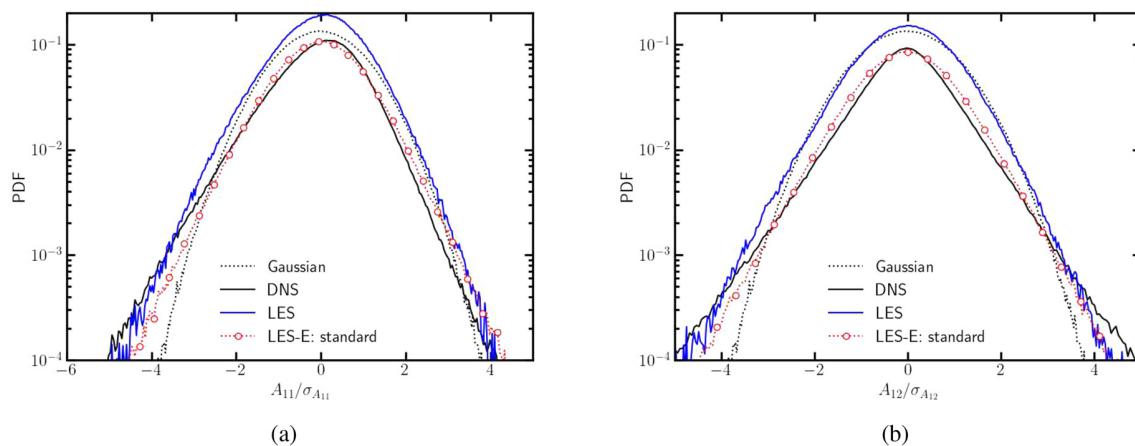


FIG. 9. PDF of longitudinal (a) and transverse (b) velocity gradient for DNS, LES without enrichment, and enriched LES (LES-E) velocity field normalized with their standard deviations together with a Gaussian distribution for comparison. The results of the enriched LES are obtained with the standard model setup.

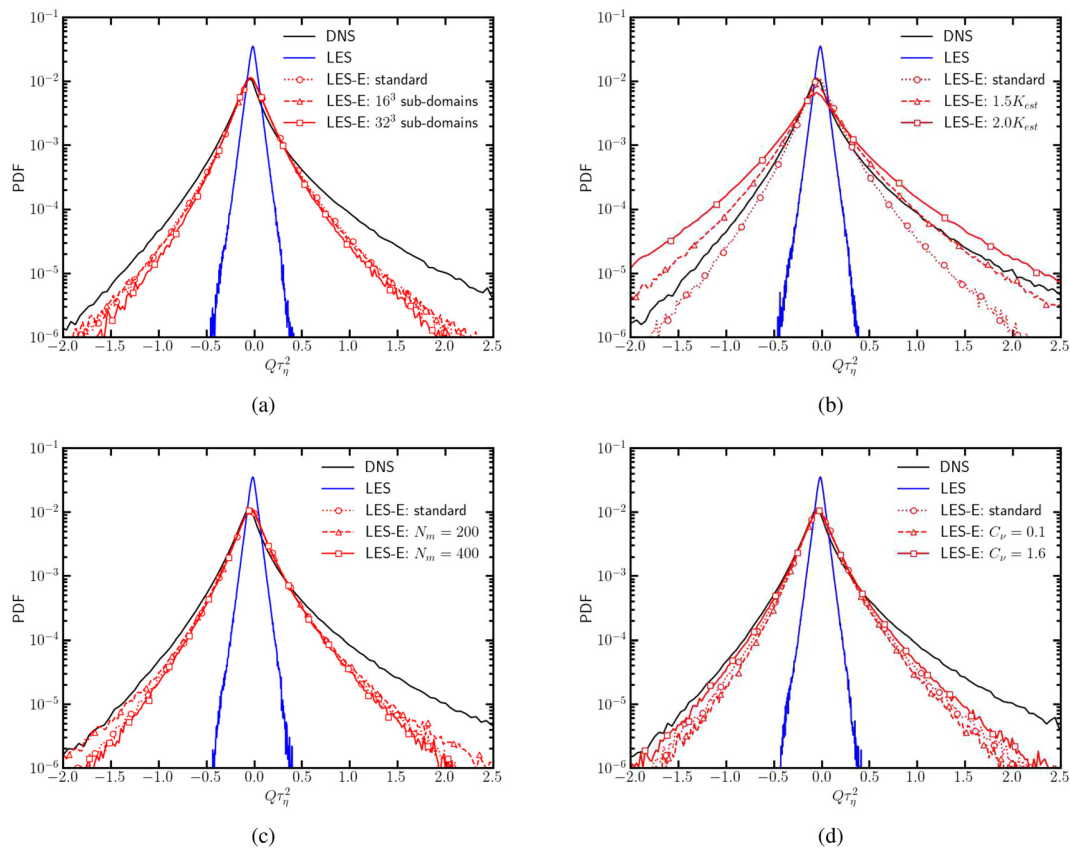


FIG. 10. PDF of the second invariant of the velocity gradient tensor for DNS, LES without enrichment, and the enriched LES (LES-E) for the HIT case. The influence of four parameters of the proposed enrichment model is compared to the previously defined standard model setup: (a) the number of sub-domains, (b) the estimated subgrid-scale kinetic energy, (c) the number of modes in the series expansion (12), and (d) the constant C_ν in the subgrid-scale turbulent viscosity.

In contrast to the local contributions $\tilde{u}_i \tilde{u}_j$ and $u'_i u'_j$, the non-local terms in Eq. (54) are represented in the model equations and contribute to the improved results of the PDF compared to the LES. This suggests that for further improvements of the predictions of the second invariant of the velocity gradient tensor, the non-linear relaxation term has to be included and the forcing has to be modified.

Next to the standard setup of the enrichment model, other configurations with variation of the four previously defined influence parameters are also shown. Figure 10(a) compares the obtained PDFs for the second invariant of the velocity gradient tensor with a varying number of sub-domains that are used for the solution of the model equations. Instead of the 8^3 sub-domains of the standard model setup, two further simulations are performed with 16^3 and 32^3 sub-domains, respectively. The PDFs of the three cases almost coincide, suggesting that neither the smaller averaging volume for the LES quantities nor the increased accuracy of the spatial derivatives of the coefficients in Eq. (12) yields improved strain–rotation relations in HIT. However, the number of sub-domains becomes important if an inhomogeneous flow is considered, since the sub-domains have to be small enough to resolve the spatial changes of the mean or larger structures.

The next investigated model parameter is the estimated subgrid-scale kinetic energy. The effect of multiplying the estimated kinetic

energy with a factor of 1.5 and 2.0 on the PDF of the second invariant of the velocity gradient tensor is shown in Fig. 10(b). A higher kinetic energy leads to wider tails of the PDF, because larger absolute velocity gradients become more likely. The shape of the PDF does not notably change with different kinetic energies. The lack of asymmetry as observed with the standard model setup still remains.

Another investigated parameter is the number of modes in the series expansion of the subgrid-scale velocity in Eq. (12). Its influence is shown in Fig. 10(c). For this parameter, no clear trend can be observed in the PDF. The second invariant of the velocity gradient tensor is relatively independent of the number of modes of the subgrid-scale velocity, for $N_m \geq 100$. Since the non-linear term is not present in the model equations for the subgrid-scale velocity, Eqs. (13) and (14), there is no information exchange between the coefficients of different wave numbers. This has an advantageous side effect for the implementation. The parallelization of the solution procedure for Eqs. (29), (30), (17), and (18) can be carried out straightforwardly in wave number space. However, it is expected that, in order to properly represent the kinetic energy spectrum and achieve a suitable complexity of the sampled subgrid-scale velocity field, a minimal amount of wave numbers is required.

The last model parameter, which is investigated with respect to the PDF of the second invariant of the velocity gradient tensor, is the

constant in the expression of the subgrid-scale turbulent viscosity given in Eq. (11), C_ν . The PDFs of the second invariant of the velocity gradient tensor are shown for different values of C_ν in Fig. 10(d). Higher values of this constant lead to slightly wider PDFs compared to smaller values. This can be explained by the fact that higher turbulent viscosities marginally increase the kinetic energy for the higher wave numbers relative to the small wave numbers, which typically yields larger velocity gradient magnitudes and hence wider tails of the PDF. The shape of the PDF is not affected. Even though the constant is varied by a factor of 16, the difference between the PDFs is very small. Thus, the results are not very sensitive to the choice of C_ν .

The specific choice of parameters in the model depends on the application of the enrichment with subgrid-scale velocity. General guidelines for the choice of parameter are thus not possible. However, it is shown that the subgrid-scale velocity statistics are rather insensitive to the change of parameters.

In order to verify that the interpolation proposed in Sec. III E does not significantly influence the results of this paper, the PDFs of Q with and without the proposed divergence-free interpolation between sub-domains is shown in Fig. 11. The PDFs almost coincide, suggesting that the interpolation does not affect the turbulence statistics on a global scale. The fact that the desirable properties are conserved and the resulting velocity field is divergence free makes the combination of the enrichment with the proposed interpolation between sub-domains advisable.

For the application of the model, it is also interesting to measure the increase in computational time due to the enrichment compared to the LES. In Table III, the computational times for the DNS, the LES, and the enriched LES with the standard model setup are compared with each other. The computational time is shown that it is needed to simulate a physical time of T_{ref} . The enrichment approximately doubles the required computational time of the LES. Compared to the computational time required for the DNS, this is an acceptable increase in computational time. The computational time of the DNS is approximately four orders of magnitude larger compared to the

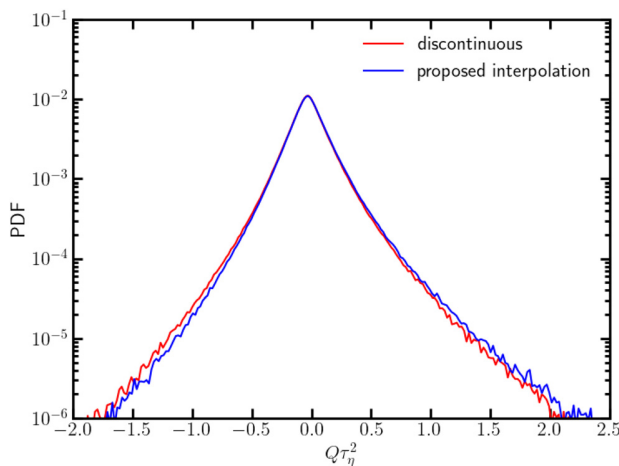


FIG. 11. PDF of the second invariant of the velocity gradient tensor of the enriched velocity of the HIT case. The velocity field of the enrichment with the standard model setup is used with discontinuities between the sub-domains and with the proposed divergence-free interpolation.

TABLE III. Comparison of the computational times for the DNS, the LES, and the enriched LES for the simulation time T_{ref} .

Type	Computational time per T_{ref}
LES	32×10^3 s
LES + model (standard setup)	69×10^3 s
DNS	340×10^6 s

enriched LES. The presented statistics of the enriched LES are much closer to the DNS compared to the LES by only increasing the computational costs by a factor of two.

B. Enriched velocity of the turbulent shear flow case

In order to verify the ability of the proposed enrichment model at simulating inhomogeneous and anisotropic flows, the enrichment is applied to the turbulent shear flow configuration that is described in Sec. III B 2. The fact that a distinct set of coefficients exists for every sub-domain makes the model capable of representing inhomogeneous subgrid-scale velocity fields. Furthermore, anisotropy of the subgrid-scale velocity [i.e., preferential alignment of the coefficients in the series expansion of Eq. (12)] may be induced by the sweeping and straining terms in the governing equations for the subgrid scales.

Due to the chaotic fluctuations of the kinetic energy of the shear flow, temporal averaging has to be performed over long times. The statistics are evaluated within a time span of $140T_{shear}$, starting from a flow field that converged toward a statistically steady state for at least the same time, in order to obtain meaningful statistics.

The generated subgrid-scale velocity is investigated in terms of its anisotropy and spatial variation. The results are assessed based on the averaged fluctuation velocity correlations

$$\mathcal{C}_{ij} = \langle (u_i - \langle u_i \rangle)(u_j - \langle u_j \rangle) \rangle, \quad (55)$$

where the ensemble average $\langle \cdot \rangle$ in this case stands for averaging in time and along the homogeneous directions (i.e., x and z directions). Similarly, the filtered velocity $\bar{\mathbf{u}}$ or the subgrid-scale velocity \mathbf{u}' can be used in Eq. (55) in order to obtain the velocity correlations for the filtered velocity and the subgrid-scale velocity, respectively.

In Fig. 12, the velocity correlations for the DNS and the LES [Fig. 12(a)] as well as for the subgrid-scale velocity obtained with the model [Fig. 12(b)] are depicted. Similar to the standard model setup of Sec. IV A, the model equations are solved for $N_m = 100$ modes, with the analytical value of the constant in the subgrid-scale turbulent viscosity $C_\nu = 0.4$ and a subgrid-scale kinetic energy estimation with the model of Yoshizawa and the analytical constant $C_I = 0.0826$. However, the number of sub-domains is 16^3 , which corresponds to the LES grid. Since the model equations are solved based on the domain-averaged filtered velocity, the average modeled subgrid-scale velocity is approximately constant in a domain, which is why a relatively high number of sub-domains is required to resolve the mean velocity profile.

The profiles of the correlations \mathcal{C}_{11} , \mathcal{C}_{22} , and \mathcal{C}_{33} in Fig. 12(a) exhibit the same qualitative behavior. Over one domain length two periods of the correlations can be observed, which is the double frequency of the mean velocity profile in x direction. The maximum values of the correlations are in the regions of the highest mean shear. The cross-correlation \mathcal{C}_{12} has the same frequency as the mean velocity

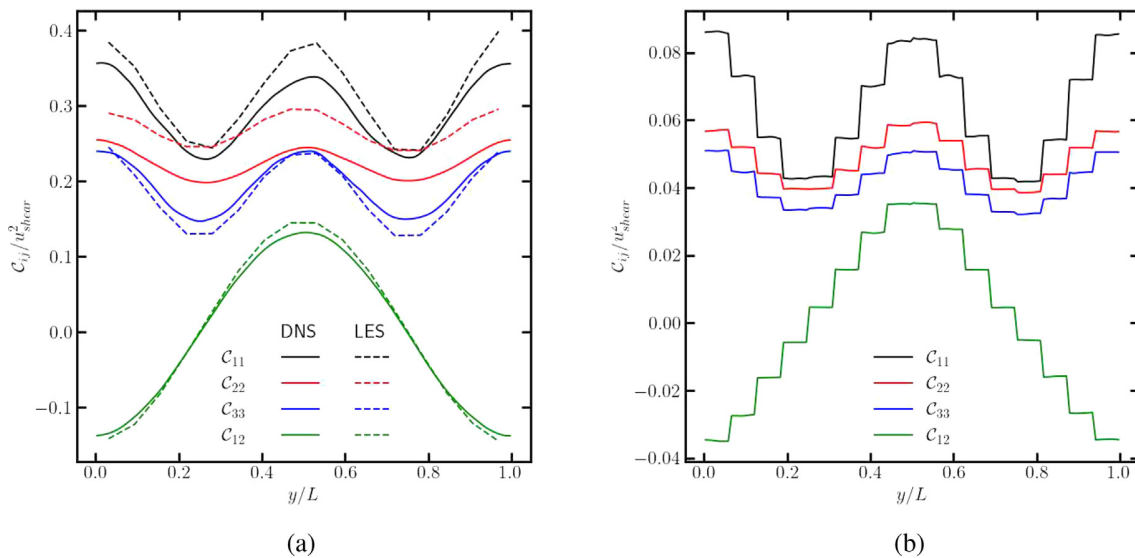


FIG. 12. Dimensionless velocity correlations of the turbulent shear flow in y direction. (a) Velocity correlations of the DNS (solid lines) and the LES (dashed lines). (b) Velocity correlations of the generated subgrid-scale velocity.

in x direction. It is negative for positive values of $\partial u_1/\partial y$ and positive for negative values of $\partial u_1/\partial y$. The other two cross-correlations are zero, which is not shown in Fig. 12(a).

The velocity correlations obtained with the LES clearly deviate from the velocity correlations of the DNS, especially for C_{11} and C_{22} . This can be explained with the too high amplitudes of the mean velocity profile. Adding the subgrid-scale velocity to the LES velocity does not correct the observed deviations. Compared to the total kinetic energy, the kinetic energy of the subgrid scales is very small in this configuration. However, note that the subgrid-scale velocity possesses properties that are important for some applications (e.g., increased turbulent mixing) and omitting them can lead to wrong results.

As it can be observed in Fig. 12(b), the generated subgrid-scale velocity field possesses a similar qualitative behavior as the velocity field of the DNS. Note that the magnitude of the velocity correlations of the subgrid-scale velocity is smaller, since the kinetic energy of the subgrid scale is only a small fraction of the total kinetic energy. Since the correlations vary in the y direction, an inhomogeneous field is generated. Furthermore, the regions of high and low values of the correlations coincide with those of the DNS. The reasons for the stepwise increase and decrease in the correlations are caused by the statistically homogeneous subgrid-scale velocity in the sub-domains. The ability of the model to generate an inhomogeneous subgrid-scale velocity field is a prerequisite to predict turbophoresis in a particle-laden flow.

In addition to the inhomogeneity of the subgrid-scale velocity, there is also evidence that the velocity field is anisotropic. In particular, the cross-correlation C_{12} demonstrates the capability of the model to produce an anisotropic velocity field. It has a similar trend as the cross-correlation of the DNS, whereas the other two cross-correlations C_{13} and C_{23} are zero (not shown in the figure).

It can be concluded that the concept of sub-domains indeed enables inhomogeneous subgrid-scale velocity fields. Moreover, the spatial change of the temporally averaged subgrid-scale velocity correlations

behaves qualitatively the right way. Furthermore, anisotropy of the subgrid-scale velocity is obtained, because the correlations differ in function of the used subgrid-scale velocity components.

V. CONCLUSIONS

A new model for enriching the velocity of a LES with a subgrid-scale velocity is introduced. The enrichment model enables closures for LES when these are required. It is shown that the generated subgrid-scale velocity possesses several important characteristic properties of real turbulent fields, such as the shape of the kinetic energy spectrum, non-Gaussian PDFs of velocity gradients, and similar strain-rotation relations. Compared to other models for the subgrid-scale velocity, common problems are mitigated with our proposed model: the influence of the small number of tuning parameters required in the model is shown to be insignificant, the computational cost of the enrichment model is of the order of the LES, and it is shown that inhomogeneous and anisotropic subgrid-scale velocities can also be generated. These properties make our enrichment model suitable for a variety of applications, in which a closure for the subgrid-scale velocity is required.

ACKNOWLEDGMENTS

This research was funded by the Deutsche Forschungsgemeinschaft (DFG, German Research Foundation)—Project-ID No. 457509672.

F. Evrard has received funding from the European Union's Horizon 2020 research and innovation program under the Marie Skłodowska-Curie Grant Agreement No. 101026017.

AUTHOR DECLARATIONS

Conflict of Interest

The authors have no conflicts to disclose.

Author Contributions

Max Hausmann: Conceptualization (equal); Methodology (lead); Writing – original draft (lead). **Fabien Evrard:** Conceptualization (equal); Funding acquisition (supporting); Supervision (equal); Writing – review & editing (equal). **Berend van Wachem:** Conceptualization (equal); Funding acquisition (lead); Project administration (lead); Resources (lead); Software (equal); Supervision (equal); Writing – review & editing (equal).

DATA AVAILABILITY

The data that support the findings of this study are available from the corresponding author upon reasonable request.

APPENDIX: PROJECTION OF THE MODEL EQUATIONS

Equation (14) can be written in a short form

$$\frac{\partial u_i'}{\partial t} + \mathcal{A}_i = -\frac{1}{\rho_f} \frac{\partial p'}{\partial x_i} + \mathcal{D}_i + \mathcal{F}_i \quad (\text{A1})$$

using \mathcal{A} , \mathcal{D} , and \mathcal{F} for the convective term, diffusive term, and source term, respectively. Neglecting the pressure term and approximating the time derivative with an explicit Euler scheme yields a preliminary subgrid-scale velocity $u_i'^*$

$$\frac{u_i'^* - u_i'^n}{\Delta t} + \mathcal{A}_i^n = \mathcal{D}_i^n + \mathcal{F}_i^n. \quad (\text{A2})$$

The same equation but with the pressure term leads to the physically right (up to discretization error of the time derivative) subgrid-scale velocity of the next time level $u_i'^{n+1}$

$$\frac{u_i'^{n+1} - u_i'^n}{\Delta t} + \mathcal{A}_i^n = -\frac{1}{\rho_f} \frac{\partial p'}{\partial x_i} + \mathcal{D}_i^n + \mathcal{F}_i^n. \quad (\text{A3})$$

The difference of $u_i'^{n+1}$ and $u_i'^*$ is obtained by subtracting Eq. (A2) from (A3)

$$\frac{u_i'^{n+1} - u_i'^*}{\Delta t} = -\frac{1}{\rho_f} \frac{\partial p'}{\partial x_i}. \quad (\text{A4})$$

Assuming the divergence of the subgrid-scale velocity of the next time level to vanish, the following Poisson equation can be derived:

$$\frac{\partial u_i'^*}{\partial x_i} = \frac{\Delta t}{\rho_f} \frac{\partial^2 p'}{\partial x_i \partial x_i}. \quad (\text{A5})$$

Similar to the subgrid-scale velocity, the pressure can be written as a truncated Fourier series

$$p' = \sum_{m=0}^{N_m-1} (P_m(t) \cos(\mathbf{k}_m \cdot \mathbf{x}) + Q_m(t) \sin(\mathbf{k}_m \cdot \mathbf{x})) \quad (\text{A6})$$

with the gradient

$$\nabla p' = \sum_{m=0}^{N_m-1} \mathbf{k}_m (-P_m(t) \sin(\mathbf{k}_m \cdot \mathbf{x}) + Q_m(t) \cos(\mathbf{k}_m \cdot \mathbf{x})) \quad (\text{A7})$$

and the Laplacian

$$\nabla^2 p' = \sum_{m=0}^{N_m-1} -|\mathbf{k}_m|^2 (P_m(t) \cos(\mathbf{k}_m \cdot \mathbf{x}) + Q_m(t) \sin(\mathbf{k}_m \cdot \mathbf{x})). \quad (\text{A8})$$

Plugging the Fourier series expansions into Eq. (A5) yields

$$\begin{aligned} & \sum_{m=0}^{N_m-1} \mathbf{k}_m (-A_m^*(t) \sin(\mathbf{k}_m \cdot \mathbf{x}) + B_m^*(t) \cos(\mathbf{k}_m \cdot \mathbf{x})) \\ &= \frac{\Delta t}{\rho_f} \sum_{m=0}^{N_m-1} -|\mathbf{k}_m|^2 (P_m(t) \cos(\mathbf{k}_m \cdot \mathbf{x}) + Q_m(t) \sin(\mathbf{k}_m \cdot \mathbf{x})). \quad (\text{A9}) \end{aligned}$$

After sorting by cos- and sin-terms and evaluating each mode separately, the following relations for the coefficients $P_m(t)$ and $Q_m(t)$ are obtained:

$$P_m(t) = -\frac{\rho_f}{\Delta t |\mathbf{k}_m|^2} \mathbf{k}_m \cdot \mathbf{B}_m^*(t), \quad (\text{A10})$$

$$Q_m(t) = \frac{\rho_f}{\Delta t |\mathbf{k}_m|^2} \mathbf{k}_m \cdot \mathbf{A}_m^*(t). \quad (\text{A11})$$

Finally, the divergence-free coefficients for the subgrid-scale velocity $\mathbf{A}_m^{n+1}(t)$ and $\mathbf{B}_m^{n+1}(t)$ can be computed using Eq. (A4)

$$\mathbf{A}_m^{n+1}(t) = \mathbf{A}_m^*(t) - \frac{\Delta t}{\rho_f} Q_m(t) \mathbf{k}_m = \mathbf{A}_m^*(t) - \mathbf{k}_m \frac{\mathbf{k}_m \cdot \mathbf{A}_m^*(t)}{|\mathbf{k}_m|^2}, \quad (\text{A12})$$

$$\mathbf{B}_m^{n+1}(t) = \mathbf{B}_m^*(t) + \frac{\Delta t}{\rho_f} P_m(t) \mathbf{k}_m = \mathbf{B}_m^*(t) - \mathbf{k}_m \frac{\mathbf{k}_m \cdot \mathbf{B}_m^*(t)}{|\mathbf{k}_m|^2}. \quad (\text{A13})$$

REFERENCES

- 1P. Fede and O. Simonin, "Numerical study of the subgrid fluid turbulence effects on the statistics of heavy colliding particles," *Phys. Fluids* **18**, 045103 (2006).
- 2B. Ray and L. R. Collins, "Preferential concentration and relative velocity statistics of inertial particles in Navier-Stokes turbulence with and without filtering," *J. Fluid Mech.* **680**, 488–510 (2011).
- 3C. Marchioli, "Large-eddy simulation of turbulent dispersed flows: A review of modelling approaches," *Acta Mech.* **228**, 741–771 (2017).
- 4P. L. Johnson and C. Meneveau, "Predicting viscous-range velocity gradient dynamics in large-eddy simulations of turbulence," *J. Fluid Mech.* **837**, 80–114 (2018).
- 5M. Herrmann, "A sub-grid surface dynamics model for sub-filter surface tension induced interface dynamics," *Comput. Fluids* **87**, 92–101 (2013).
- 6D. Kedelty, J. Uglietta, and M. Herrmann, "A volume-of-fluid dual-scale approach for simulating turbulent liquid/gas interactions," in *Turbulence and Interactions*, edited by M. Deville, C. Calvin, V. Couaillier, M. De La Llave Plata, J.-L. Estivalèzes, T. H. Lê, and S. Vincent (Springer International Publishing, Cham, 2021), Vol. 149, pp. 39–51, Series Title: Notes on Numerical Fluid Mechanics and Multidisciplinary Design.
- 7Z. Zhang, P. Huang, G. Bitsuamlak, and S. Cao, "Large-eddy simulation of wind-turbine wakes over two-dimensional hills," *Phys. Fluids* **34**, 065123 (2022).
- 8A. M. Garcia, S. L. Bras, J. Prager, M. Häring, and W. Polifke, "Large eddy simulation of the dynamics of lean premixed flames using global reaction mechanisms calibrated for CH₄-H₂ fuel blends," *Phys. Fluids* **34**, 095105 (2022).
- 9A. Scotti and C. Meneveau, "A fractal model for large eddy simulation of turbulent flow," *Physica D* **127**, 198–232 (1999).
- 10N. A. Malik and J. C. Vassilicos, "A Lagrangian model for turbulent dispersion with turbulent-like flow structure: Comparison with direct numerical simulation for two-particle statistics flow structure," *Phys. Fluids* **11**, 1572 (1999).

- ¹¹J. C. H. Fung, J. C. R. Hunt, N. A. Malik, and R. J. Perkins, "Kinematic simulation of homogeneous turbulence by unsteady random Fourier modes," *J. Fluid Mech.* **236**, 281–318 (1992).
- ¹²R. H. Kraichnan, "Diffusion by a random velocity field," *Phys. Fluids* **13**, 22 (1970).
- ¹³B. Ray and L. R. Collins, "A subgrid model for clustering of high-inertia particles in large-eddy simulations of turbulence," *J. Turbul.* **15**, 366–385 (2014).
- ¹⁴Z. Zhou, S. Wang, and G. Jin, "A structural subgrid-scale model for relative dispersion in large-eddy simulation of isotropic turbulent flows by coupling kinematic simulation with approximate deconvolution method," *Phys. Fluids* **30**, 105110 (2018).
- ¹⁵J. A. Domaradzki and K.-C. Loh, "The subgrid-scale estimation model in the physical space representation," *Phys. Fluids* **11**, 2330–2342 (1999).
- ¹⁶J. A. Domaradzki and E. M. Saiki, "A subgrid-scale model based on the estimation of unresolved scales of turbulence," *Phys. Fluids* **9**, 2148–2164 (1997).
- ¹⁷G. I. Park, M. Bassenne, J. Urzay, and P. Moin, "A simple dynamic subgrid-scale model for LES of particle-laden turbulence," *Phys. Rev. Fluids* **2**, 044301 (2017).
- ¹⁸M. Bassenne, M. Esmaily, D. Livescu, P. Moin, and J. Urzay, "A dynamic spectrally enriched subgrid-scale model for preferential concentration in particle-laden turbulence," *Int. J. Multiphase Flow* **116**, 270–280 (2019).
- ¹⁹T. J. Hughes, G. R. Feijóo, L. Mazzei, and J.-B. Quincy, "The variational multiscale method—A paradigm for computational mechanics," *Comput. Methods Appl. Mech. Eng.* **166**, 3–24 (1998).
- ²⁰T. J. Hughes, L. Mazzei, and K. E. Jansen, "Large eddy simulation and the variational multiscale method," *Comput. Visualization Sci.* **3**, 47–59 (2000).
- ²¹M. Terracol, P. Sagaut, and C. Basdevant, "A multilevel algorithm for large-eddy simulation of turbulent compressible flows," *J. Comput. Phys.* **167**, 439–474 (2001).
- ²²B. Dubrulle, J. P. Laval, S. Nazarenko, and N. K.-R. Kevlahan, "A dynamic subfilter-scale model for plane parallel flows," *Phys. Fluids* **13**, 2045–2064 (2001).
- ²³J.-P. Laval, B. Dubrulle, and S. Nazarenko, "Fast numerical simulations of 2D turbulence using a dynamic model for subfilter motions," *J. Comput. Phys.* **196**, 184–207 (2004).
- ²⁴A. S. Ghate and S. K. Lele, "Subfilter-scale enrichment of planetary boundary layer large eddy simulation using discrete Fourier-Gabor modes," *J. Fluid Mech.* **819**, 494–539 (2017).
- ²⁵A. S. Ghate and S. K. Lele, "Gabor mode enrichment in large eddy simulations of turbulent flow," *J. Fluid Mech.* **903**, A13 (2020).
- ²⁶A. Leonard, "Energy cascade in large-eddy simulations of turbulent fluid flows," in *Advances in Geophysics* (Elsevier, 1975), Vol. 18, pp. 237–248.
- ²⁷P. Sagaut, *Large Eddy Simulation for Incompressible Flows*, 3rd ed. (Springer, 2005).
- ²⁸J.-P. Laval, B. Dubrulle, and S. Nazarenko, "Nonlocality and intermittency in three-dimensional turbulence," *Phys. Fluids* **13**, 1995–2012 (2001).
- ²⁹J. C. R. Hunt and D. J. Carruthers, "Rapid distortion theory and the 'problems' of turbulence," *J. Fluid Mech.* **212**, 497 (1990).
- ³⁰S. B. Pope, *Turbulent Flows*, 6th ed. (Cambridge University Press, Cambridge, 2000).
- ³¹C. Cambon and J. F. Scott, "Linear and nonlinear models of anisotropic turbulence," *Annu. Rev. Fluid Mech.* **31**, 1–53 (1999).
- ³²K. Horiuti, "Roles of non-aligned eigenvectors of strain-rate and subgrid-scale stress tensors in turbulence generation," *J. Fluid Mech.* **491**, 65–100 (2003).
- ³³J. Smagorinsky, "General circulation experiments with the primitive equations. I. The basic experiment," *Mon. Weather Rev.* **91**, 99–165 (1963).
- ³⁴M. Germano, U. Piomelli, P. Moin, and W. H. Cabot, "A dynamic subgrid-scale eddy viscosity model," *Phys. Fluids A* **3**, 1760–1765 (1991).
- ³⁵F. Nicoud and F. Ducros, "Subgrid-scale stress modelling based on the square of the velocity gradient tensor," *Flow Turbul. Combust.* **62**, 183–200 (1999).
- ³⁶A. W. Vreman, "An eddy-viscosity subgrid-scale model for turbulent shear flow: Algebraic theory and applications," *Phys. Fluids* **16**, 3670–3681 (2004).
- ³⁷V. M. Canuto and M. S. Dubovikov, "A dynamical model for turbulence. I. General formalism," *Phys. Fluids* **8**, 571–586 (1996).
- ³⁸G. Mallouppas, W. K. George, and B. van Wachem, "New forcing scheme to sustain particle-laden homogeneous and isotropic turbulence," *Phys. Fluids* **25**, 083304 (2013).
- ³⁹A. Yoshizawa, "Statistical theory for compressible turbulent shear flows, with the application to subgrid modeling," *Phys. Fluids* **29**, 2152 (1986).
- ⁴⁰P. Moin, K. Squires, W. Cabot, and S. Lee, "A dynamic subgrid-scale model for compressible turbulence and scalar transport," *Phys. Fluids A* **3**, 2746 (1991).
- ⁴¹J. Jimenez, "Intermittency in turbulence," in Proceedings of the 15th "Aha Huliko" a Winter Workshop (2007).
- ⁴²G. Mallouppas, "Modelling of turbulent gas-solid flows from DNS to LES," Ph.D. thesis (Imperial College, London, 2013).
- ⁴³F. Denner, F. Evrard, and B. van Wachem, "Conservative finite-volume framework and pressure-based algorithm for flows of incompressible, ideal-gas and real-gas fluids at all speeds," *J. Comput. Phys.* **409**, 109348 (2020).
- ⁴⁴C. M. Rhie and W. L. Chow, "Numerical study of the turbulent flow past an airfoil with trailing edge separation," *AIAA J.* **21**, 1525–1532 (1983).
- ⁴⁵W. K. George, *Lectures in Turbulence for the 21st Century* (Chalmers University of Technology, Gothenburg, Sweden, 2013), Vol. 550, 353 pp.
- ⁴⁶E. Lévêque, F. Toschi, L. Shao, and J.-P. Bertoglio, "Shear-improved Smagorinsky model for large-eddy simulation of wall-bounded turbulent flows," *J. Fluid Mech.* **570**, 491–502 (2007).
- ⁴⁷S. Balachandar and J. K. Eaton, "Turbulent dispersed multiphase flow," *Annu. Rev. Fluid Mech.* **42**, 111–133 (2010).
- ⁴⁸M. R. Maxey, "The gravitational settling of aerosol particles in homogeneous turbulence and random flow fields," *J. Fluid Mech.* **174**, 441 (1987).
- ⁴⁹Z. Zhou, S. Wang, X. Yang, and G. Jin, "A structural subgrid-scale model for the collision-related statistics of inertial particles in large-eddy simulations of isotropic turbulent flows," *Phys. Fluids* **32**, 095103 (2020).
- ⁵⁰L. Brandt and F. Coletti, "Particle-laden turbulence: Progress and perspectives," *Annu. Rev. Fluid Mech.* **54**, 159–189 (2022).

A.2 Paper II

Large eddy simulation model for two-way coupled particle-laden turbulent flows

M. Hausmann, F. Evrard, B. van Wachem

Published in *Physical Review Fluids* 8, 084301 (2023)

Large eddy simulation model for two-way coupled particle-laden turbulent flows

M. Hausmann , F. Evrard ,* and B. van Wachem [†]

*Chair of Mechanical Process Engineering, Otto-von-Guericke-Universität Magdeburg,
Universitätsplatz 2, 39106 Magdeburg, Germany*



(Received 20 February 2023; accepted 24 July 2023; published 11 August 2023)

In this paper, we propose a modeling framework for large eddy simulations of particle-laden turbulent flows that captures the interaction between the particle and fluid phase on both the resolved and subgrid scales. Unlike the vast majority of existing subgrid-scale models, the proposed framework not only accounts for the influence of the subgrid-scale velocity on the particle acceleration but also considers the effect of the particles on the turbulent fluid flow. This includes the turbulence modulation of the subgrid scales by the particles, which is taken into account by the modeled subgrid-scale stress tensor and the effect of the unresolved particle motion on the resolved flow scales. Our modeling framework combines a recently proposed model for enriching the resolved fluid velocity with a subgrid-scale component, with the solution of a transport equation for the subgrid-scale kinetic energy. We observe very good agreement of the particle pair separation and particle clustering compared to the corresponding direct numerical simulation. Furthermore, we show that the change of subgrid-scale kinetic energy induced by the particles can be captured by the proposed modeling framework.

DOI: [10.1103/PhysRevFluids.8.084301](https://doi.org/10.1103/PhysRevFluids.8.084301)

I. INTRODUCTION

To capture particle-turbulence interactions within the whole turbulence spectrum down to the Kolmogorov length and timescale, a direct numerical simulation (DNS) has to be performed. For academic cases, DNSs of particle-laden turbulent flow is commonly used to gain insights into the underlying physical phenomena. As the flow configurations become more relevant for practical applications, however, resolving such a wide range of flow length and timescales becomes prohibitively expensive. An established surrogate in single phase flows is large eddy simulation (LES), which resolves only the large flow scales and models the mainly dissipative effect of the small scales. Even though many challenges still remain, LES is commonly applied to different single phase flow applications. Severe problems can arise, however, if particle-laden flows are considered, especially if the particles significantly affect the flow (two-way coupling).

The majority of the literature on particle-laden flows focuses on the one-way coupling, where the modification of the particle statistics by the flow is considered but not the effect of the particles on the flow. The effect of neglecting the subgrid-scale velocity contributions on the transport of the particles has been investigated and quantified in a variety of studies [1–4]. It has been observed that even though the kinetic energy of the subgrid-scale velocity is small, the consequence of neglecting

*Also at Sibley School of Mechanical and Aerospace Engineering, Cornell University, Ithaca, New York 14853, USA.

[†]berend.vanwachem@ovgu.de

the subgrid-scale fluid velocity on the motion of the particles can strongly affect the preferential concentration and other statistics of the particles.

There are several classes of models that attempt to produce realistic particle statistics in the scope of LES. Lagrangian models typically rely on the solution of a stochastic differential equation for every individual particle (see, e.g., Fede *et al.* [5], Bini and Jones [6], Berrouk *et al.* [7], Shotorban and Mashayek [8], Pozorski and Apte [9], and Knorps and Pozorski [10]). These models are typically simple to implement, computationally efficient, and can also be applied in complex domains. However, they usually contain empirical parameters and their Lagrangian nature prevents them from predicting accurate particle pair statistics. Other models rely on successive deconvolution of the LES velocity and use the resulting fluid velocity field to transport the particles [11,12]. Park *et al.* [13] extended the deconvolution of the filtered velocity by dynamically adjusting an elliptic differential filter such that the model is either kinetic energy or dissipation consistent with the subgrid-scale model. The main drawback of approximate deconvolution methods is that they do not introduce velocities with higher wave numbers than the LES, but only modify the LES velocity. That is why these models are not able to reproduce the particle statistics of a DNS to the full extent.

The most promising predictions of particle statistics using a LES framework are obtained with models that reconstruct the subgrid-scale velocity. Bassenne *et al.* [14] proposed such a model that alternately applies the dynamic approximate deconvolution of Park *et al.* and a spectral extrapolation based on the work of Domaradzki and Loh [15]. The proposed model improves the prediction of particle clustering for a wide range of Stokes numbers. However, the model requires a projection operation that has to be carried out with a resolution comparable to the DNS to obtain a divergence-free subgrid-scale velocity, which introduces prohibitively high computational costs. The kinematic simulation is a much cheaper approach and relies on the reconstruction of the subgrid-scale velocity using a truncated Fourier series [16–18]. The Fourier coefficients required for the kinematic simulation are chosen such that the resulting velocity field is divergence-free and matches a given kinetic energy spectrum. Even though kinematic simulations yield improved predictions of particle clustering for Stokes numbers $St > 1.5$, it only applies to spatially homogeneous problems. Considering the available models, there still does not exist a model that yields satisfying improvements in predicting particle clustering and the Lagrangian particle statistics, while maintaining important features for practical applicability, such as a reasonable computational cost and the absence of empirical model parameters of critical influence.

Extensive research has been carried out to better understand the modulation of turbulence by particles. Studies of forced and decaying homogeneous isotropic turbulence (HIT) have shown that the presence of particles can modify the total dissipation in two ways [19–23]: (i) The particles can remove or add kinetic energy to the turbulent flow. The sign of the particle kinetic energy transfer and the scales at which the kinetic energy transfer occurs have been shown to depend on at least three parameters: the Stokes number, the particle number density, and the mass fraction [21]. (ii) The fluid dissipation is influenced by the presence of particles [19]. Similarly, depending on the characteristic turbulence and particle parameters and on the considered length scales, the fluid dissipation can either be enhanced or diminished.

A LES only resolves part of the kinetic energy spectrum and can thus only account directly for a modified total dissipation at the resolved scales. While the particle dissipation at the subgrid scale is fully disregarded in a classical LES, the subgrid-scale fluid dissipation is assumed to be equal to the fluid dissipation of a single phase flow. Classical LES uses one of the many subgrid-scale models designed for single phase flows (see, e.g., Sagaut [24]) and a fluid-particle coupling force obtained without information of the subgrid-scale fluid velocity at the particle positions. The application of several single-phase subgrid-scale models to particle-laden flows has been investigated by Boivin *et al.* [25], displaying very different results between the models. Boivin *et al.* also argued that at high particle mass fractions, the modeling error in predicting the fluid dissipation becomes less important, since the particle dissipation is then dominant. In fact, we show in the present paper that the neglected portion of the particle dissipation and fluid dissipation partially compensate each other. Rohilla *et al.* [26] showed that the Smagorinsky or dynamic Smagorinsky model applied to

particle-laden flows is unable to predict the critical particle volume loading at which the turbulence in a channel flow collapses (i.e., the flow becomes laminar). They state that one of the main reasons for this issue is the error made in modeling subgrid-scale dissipation.

Due to the complexity of two-way coupled turbulent particle-laden flows, models that account for all the coupling effects between the particles and all fluid length and timescales are very rare. An attempt has been made by Yuu *et al.* [27], who derived an algebraic model for the subgrid-scale kinetic energy that serves as input for a turbulent viscosity. In the studies of Pannala and Menon [28] and Sankaran and Menon [29], a source term accounting for the presence of particles is added to an evolution equation for the subgrid-scale kinetic energy equation, in a manner somewhat similar to the method presented in this paper. However, their particle source term is not closed because it contains the subgrid-scale velocity, which requires additional modeling.

In this paper, we present a framework that accounts for particle turbulence interactions that are typically neglected in a LES. The framework contains two coupled models: (i) a subgrid-scale model based on the localized dynamic kinetic energy model (LDKM) of Menon and coworkers [30,31], with an additional source term accounting for the influence of the particles on the subgrid-scale kinetic energy, and (ii) a model for the subgrid velocity that is used to close the particle equations of motion and the particle source terms in the momentum and subgrid-scale kinetic energy equations [32]. In Sec. II, the general numerical framework for treating the particle-laden flows in this paper is introduced, including the transport equation for the subgrid-scale kinetic energy upon which the subgrid-scale model is built. Section III gives an overview of the closures that are required in a particle-laden LES and provides a derivation of the proposed modeling framework. Subsequently, simulation setups for one-way and two-way coupled HIT are introduced in Sec. IV, and results of the comparison between DNS, LES, and modeled LES are presented in Sec. V. Finally, Sec. VI concludes the present paper.

II. GENERAL NUMERICAL FRAMEWORK

In this paper, we consider an incompressible fluid with density ρ_f and kinematic viscosity ν_f in the absence of a gravitational field. The fluid is laden with particles of index p having a density ρ_p and volume V_p . By volume filtering the Navier-Stokes equations (NSEs), the effect of the particles on the fluid can be modeled without needing to solve for the detail of the flow around each individual particle. The following equations are commonly used to approximate the volume-filtered velocity \mathbf{u} and pressure p for small particle volume fractions (see, e.g., Maxey [33]):

$$\nabla \cdot \mathbf{u} = 0, \quad (1)$$

$$\frac{\partial \mathbf{u}}{\partial t} + \nabla \cdot (\mathbf{u} \otimes \mathbf{u}) = -\frac{1}{\rho_f} \nabla p + \nabla \cdot \boldsymbol{\sigma} - \frac{1}{\rho_f} \sum_p g(|\mathbf{x} - \mathbf{x}_p|) \mathbf{F}_p, \quad (2)$$

where $\boldsymbol{\sigma} = \nu_f (\nabla \mathbf{u} + (\nabla \mathbf{u})^T)$ is the Newtonian viscous stress tensor and \mathbf{F}_p is the sum of the fluid-particle interface forces of the particle with index p that can originate from drag, lift, added mass, or other effects. Gravity is neglected in the present paper. The kernel g of the volume filtering operation (see, e.g., Anderson and Jackson [34]) corresponds to filter size δ . Note that the filtering is only applied over volumes that are occupied by the fluid. Strictly speaking, the solution of Eqs. (1) and (2) is the approximation of volume-filtered quantities, which is not equivalent to the actual fluid velocity and pressure. In a simulation, the smallest resolvable flow structures are related to the smallest affordable cell size of the numerical grid. Similar to the LES approach, the volume-filtered approach solves for the large scales that can be resolved by the grid and models the effect of the small scales. It should be noted that in this paper, the influence of particle volume fraction α_p is not considered in the governing equations of the DNS and LES, even though it can be significant in dense particle regimes (i.e., $\alpha_p > 0.01$). The proposed modeling is also only valid for dilute regimes.

Particles are considered as Lagrangian rigid point-particles. The particle position \mathbf{x}_p is governed by the equation

$$\frac{d\mathbf{x}_p}{dt} = \mathbf{v}_p, \quad (3)$$

and the particle velocity by Newton's second law:

$$\frac{d\mathbf{v}_p}{dt} = \frac{1}{\rho_p V_p} \mathbf{F}_p. \quad (4)$$

There are a variety of mechanisms that lead to different forces acting on the particle, and additional source terms can arise in Eq. (4) if, e.g., gravity is considered, which is neglected in this paper. A summary of the possible force contributions and the regimes whereby their consideration is important has been provided by Kuerten [35].

We only consider cases in which the particles are significantly smaller than the Kolmogorov length scale (i.e., the smallest turbulent structures). The turbulence of the scales down to the Kolmogorov length scale are resolved with the DNS. Note that the DNS is based on the assumption of point particles. In cases, where not even the smallest flow structures can be resolved by the numerical grid, a LES can be performed. The governing equations for the LES are obtained by filtering Eqs. (1) and (2) once more with a filter G of width Δ , with $\Delta \gg \delta$:

$$\nabla \cdot \tilde{\mathbf{u}} = 0, \quad (5)$$

$$\frac{\partial \tilde{\mathbf{u}}}{\partial t} + \nabla \cdot (\widetilde{\mathbf{u} \otimes \mathbf{u}}) = -\frac{1}{\rho_f} \nabla \tilde{p} + \nabla \cdot \tilde{\boldsymbol{\sigma}} - \frac{1}{\rho_f} \sum_p \widetilde{g(|\mathbf{x} - \mathbf{x}_p|) \mathbf{F}_p}. \quad (6)$$

Note that the filter G is applied to already continuous quantities (due to the previous filtering with g) and $\tilde{\cdot}$ represents the filtering operator. No further assumptions are introduced with the second filter level.

Due to the fact that the particles are much smaller than the Kolmogorov length scale (and therefore of the grid spacing), the numerical discretization of the source terms is realized with the particle-source-in-cell (PSIC) method of Crowe *et al.* [36],

$$\sum_p g(|\mathbf{x} - \mathbf{x}_p|) \mathbf{F}_p \approx \frac{1}{V_{\text{cell}}(\mathbf{x})} \sum_{p \in \Omega_{\text{cell}}(\mathbf{x})} \mathbf{F}_p \quad (7)$$

and

$$\sum_p \widetilde{g(|\mathbf{x} - \mathbf{x}_p|) \mathbf{F}_p} \approx \frac{1}{\tilde{V}_{\text{cell}}(\mathbf{x})} \sum_{p \in \tilde{\Omega}_{\text{cell}}(\mathbf{x})} \mathbf{F}_p, \quad (8)$$

where Ω_{cell} and $\tilde{\Omega}_{\text{cell}}$ indicate computational cells of the DNS and the LES, respectively, and $V_{\text{cell}} < \tilde{V}_{\text{cell}}$ their volumes.

For the modeling of the flow scales that are filtered out by kernel G , a transport equation for the subgrid-scale kinetic energy $K_{\text{sgs}} = 1/2(\widetilde{\mathbf{u} \cdot \mathbf{u}} - \tilde{\mathbf{u}} \cdot \tilde{\mathbf{u}})$ is derived. This is done in two steps. First, Eq. (2) is dotted with the velocity \mathbf{u} and subsequently filtered with G , which yields

$$\begin{aligned} & \frac{1}{2} \frac{\partial \widetilde{\mathbf{u} \cdot \mathbf{u}}}{\partial t} + \frac{1}{2} \nabla \cdot (\widetilde{\mathbf{u} \otimes \mathbf{u} \cdot \mathbf{u}}) \\ &= -\frac{1}{\rho_f} \nabla \cdot (\widetilde{p\mathbf{u}}) + \nabla \cdot (\widetilde{\boldsymbol{\sigma} \cdot \mathbf{u}}) - \widetilde{\nabla \mathbf{u} : \boldsymbol{\sigma}} - \frac{1}{\rho_f \tilde{V}_{\text{cell}}} \sum_{p \in \tilde{\Omega}_{\text{cell}}} \mathbf{F}_p(\mathbf{u}(\mathbf{x}_p)) \cdot \mathbf{u}(\mathbf{x}_p). \end{aligned} \quad (9)$$

The last term on the right-hand side is realized by multiplying the fluid-particle interface forces \mathbf{F}_p with the fluid velocity at the particle position and taking the sum over all particles within a LES grid cell. In the following, we will emphasize that the forces \mathbf{F}_p require the unfiltered fluid velocity

at the particle position by explicitly writing its dependency on $\mathbf{u}(\mathbf{x}_p)$. The reader may be reminded, however, that the forces may also depend on additional parameters.

The sum over all particles within a LES grid cell replaces the filtering operation $\widetilde{\mathbf{F}_p \cdot \mathbf{u}}$. In fact, this resembles the approach of Schumann [37], who defines a set of LES equations based on averaging over the volume of the computational cell, which is arguably closer to the numerical realization of a LES than a spatially continuous filtering operation. Second, Eq. (6) is dotted with the filtered velocity $\tilde{\mathbf{u}}$, which leads to

$$\begin{aligned} & \frac{1}{2} \frac{\partial \tilde{\mathbf{u}} \cdot \tilde{\mathbf{u}}}{\partial t} + \frac{1}{2} \nabla \cdot (\widetilde{\mathbf{u} \otimes \mathbf{u}} \cdot \tilde{\mathbf{u}}) \\ &= -\frac{1}{\rho_f} \nabla \cdot (\tilde{\rho} \tilde{\mathbf{u}}) + \nabla \cdot (\tilde{\boldsymbol{\sigma}} \cdot \tilde{\mathbf{u}}) - \nabla \tilde{\mathbf{u}} : \tilde{\boldsymbol{\sigma}} - \frac{1}{\rho_f \tilde{V}_{\text{cell}}} \tilde{\mathbf{u}} \cdot \sum_{p \in \tilde{\Omega}_{\text{cell}}} \mathbf{F}_p(\mathbf{u}(\mathbf{x}_p)). \end{aligned} \quad (10)$$

The numerical realization of the last term on the right-hand side includes a sum of the forces \mathbf{F}_p within a LES grid cell and subsequent multiplication with the LES velocity of the present grid cell.

Subtracting Eq. (10) from Eq. (9) yields an equation for K_{sgs} :

$$\begin{aligned} & \frac{\partial K_{\text{sgs}}}{\partial t} + \frac{1}{2} \frac{\partial}{\partial x_j} (\widetilde{u_i u_j u_i} - \tilde{u}_i \tilde{u}_j \tilde{u}_i) \\ &= -\frac{1}{\rho_f} \frac{\partial}{\partial x_i} (\tilde{\rho} \tilde{u}_i - \tilde{\rho} \tilde{u}_i) + \nu_f \frac{\partial^2 K_{\text{sgs}}}{\partial x_j \partial x_j} - \nu_f \left(\frac{\partial \tilde{u}_i}{\partial x_j} \frac{\partial \tilde{u}_i}{\partial x_j} - \frac{\partial \tilde{u}_i}{\partial x_j} \frac{\partial \tilde{u}_i}{\partial x_j} \right) \\ & \quad - \frac{1}{\rho_f \tilde{V}_{\text{cell}}} \left(\sum_{p \in \tilde{\Omega}_{\text{cell}}} F_{i,p}(\mathbf{u}(\mathbf{x}_p)) u_i(\mathbf{x}_p) - \tilde{u}_i \sum_{p \in \tilde{\Omega}_{\text{cell}}} F_{i,p}(\mathbf{u}(\mathbf{x}_p)) \right). \end{aligned} \quad (11)$$

The last term on the right-hand side is the source term due to the subgrid-scale kinetic energy transfer by the particles. This equation is the foundation for the modeling of the turbulence modulation by particles of scales that are filtered out by G .

III. MODELING IN THE LES FRAMEWORK

The second filtering operation with G leads to equations governing the fluid behavior that cannot be solved explicitly without knowing the fluid velocity \mathbf{u} . We model these equations in the framework of a LES. In addition to the modeling of the subgrid-scale stress tensor, a particle-laden flow requires further closures, which are first explained and then modeled.

A. Required closures

The fluid equations with the assumption of a dilute particle-laden flow with sufficiently small particles and subsequent filtering with the kernel G can be written in the typical form of a LES [38] as

$$\frac{\partial \tilde{u}_i}{\partial x_i} = 0, \quad (12)$$

$$\frac{\partial \tilde{u}_i}{\partial t} + \tilde{u}_j \frac{\partial \tilde{u}_i}{\partial x_j} = -\frac{1}{\rho_f} \frac{\partial \tilde{p}}{\partial x_i} + \nu_f \frac{\partial^2 \tilde{u}_i}{\partial x_j \partial x_j} - \frac{\partial \tau_{ij}}{\partial x_j} - \frac{1}{\rho_f \tilde{V}_{\text{cell}}} \sum_{p \in \tilde{\Omega}_{\text{cell}}} F_{D,i,p}(\mathbf{u}(\mathbf{x}_p)), \quad (13)$$

where we assumed that only the drag force \mathbf{F}_D acts on the particles. The subgrid-scale stress tensor τ_{ij} is defined as

$$\tau_{ij} = \tilde{u}_i \tilde{u}_j - \tilde{u}_i \tilde{u}_j. \quad (14)$$

With the particle force reducing to the drag force, the particle velocity \mathbf{v}_p is governed by

$$\frac{d\mathbf{v}_p}{dt} = \frac{1}{\rho_p V_p} \mathbf{F}_{D,p}(\mathbf{u}(\mathbf{x}_p)). \quad (15)$$

To solve for the filtered fluid velocity $\tilde{\mathbf{u}}$ and the particle velocity \mathbf{v}_p , two further modeling steps are required: (i) The subgrid-scale stress tensor τ_{ij} has to be closed to model the effect of the unresolved subgrid scales on the resolved (filtered) quantities. It should be noted that the presence of the particles modifies the subgrid-scale velocity. As a consequence, models for the subgrid-scale stress tensor that are based on assumptions of the single-phase flow subgrid-scale velocity are, strictly speaking, not valid. (ii) To compute the drag force acting on the particle and vice versa, the force that is coupled back to the fluid with opposite sign, the unfiltered fluid velocity at the particle position is required, which is an unknown quantity in a LES. It is well understood that the particles behave differently when the drag force is obtained from the filtered fluid velocity at the particle position $\mathbf{F}_{D,p}(\tilde{\mathbf{u}}(\mathbf{x}_p))$ [2,3]. In the present paper, a modeling framework for both closures is provided.

B. Modeling the subgrid-scale stress tensor

The subgrid-scale stress tensor accounts for the effect of the subgrid-scale velocities on the velocity that is resolved in a LES. In a LES, this subgrid-scale stress tensor is modeled. Typically, the focus lies exclusively on modeling the energetic effects of the subgrid scales on the resolved scales, even though the mechanisms of turbulent energy transfer (vorticity stretching and strain self-amplification) possess characteristic directional dependencies [39]. In single phase turbulent flows, the construction of the subgrid-scale model can be based on the assumption that the energy transferred towards smaller scales is either dissipated by the viscosity or scattered back towards larger scales. In a particle-laden turbulent flow, however, additional energy sources and sinks occur due to the interactions with the particles that classical subgrid-scale models (designed for single phase flows) do not account for.

To take the interactions of the fluid with the particles into account, we modify the LDKM of Menon and coworkers [30,31]. The modeling of the subgrid-scale stress tensor is based on an eddy viscosity ν_k ,

$$\tau_{ij} = -2\nu_k \tilde{S}_{ij} + \frac{2}{3} K_{\text{sgs}} \delta_{ij}, \quad (16)$$

where \tilde{S}_{ij} is the filtered strain-rate tensor and δ_{ij} is the Kronecker tensor. The eddy viscosity is computed from the subgrid-scale kinetic energy,

$$\nu_k = C_k \sqrt{K_{\text{sgs}}} \Delta, \quad (17)$$

where C_k is a constant. The evolution of the subgrid-scale kinetic energy K_{sgs} is governed by the transport Eq. (11). However, several terms of the transport equation for K_{sgs} require the unfiltered fluid velocity. Lilly [40] introduced a model for the transport Eq. (11) (without particle source term), such that it can be solved by knowing filtered quantities only, which is the basis of the LDKM,

$$\frac{\partial K_{\text{sgs}}}{\partial t} + \tilde{u}_i \frac{\partial K_{\text{sgs}}}{\partial x_i} = -\tau_{ij} \frac{\partial \tilde{u}_i}{\partial x_j} - C_\epsilon \frac{K_{\text{sgs}}^{3/2}}{\Delta} + \frac{\partial}{\partial x_i} \left(\nu_k \frac{\partial K_{\text{sgs}}}{\partial x_i} \right) + \Phi_P, \quad (18)$$

where C_ϵ is a constant. The particle source term Φ_P is not part of the original LDKM but introduced in the present model based on the derivations in Sec II:

$$\Phi_P = -\frac{1}{\rho_f \tilde{V}_{\text{cell}}} \left(\sum_{p \in \tilde{\Omega}_{\text{cell}}} F_{D,i,p}(\mathbf{u}(\mathbf{x}_p)) u_i(\mathbf{x}_p) - \tilde{u}_i \sum_{p \in \tilde{\Omega}_{\text{cell}}} F_{D,i,p}(\mathbf{u}(\mathbf{x}_p)) \right). \quad (19)$$

The particle source term represents the kinetic energy added to or removed from the subgrid-scale velocity by the particles. Although the source term is written as a function of the drag force, the

derivation in Sec. II shows that the source term can be computed from all the fluid-particle interface forces used in the fluid momentum equation, such as lift force or added mass force.

Note that Pannala and Menon [28] and Sankaran and Menon [29] already applied the concept of a particle source term in the transport equation of the subgrid-scale kinetic energy, but with a different realization and without providing a rigorous derivation. To distinguish the present model including the particle source term Eq. (19) from the original LDKM, we refer to it as modified LDKM (mLDKM). The constants C_ϵ and C_k are computed dynamically based on the assumption of scale similarity. The Leonard stress tensor is defined as

$$L_{ij} = \widehat{\tilde{u}_i \tilde{u}_j} - \hat{u}_i \hat{u}_j, \quad (20)$$

where $\hat{\cdot}$ indicates a filtering operation with the filter width $\hat{\Delta} = 2\Delta$. Assuming that the Leonard stress tensor is analogously computed to the subgrid-scale stress tensor,

$$L_{ij} = -2C_k \hat{\Delta} K_{\text{test}}^{1/2} \hat{S}_{ij} + \frac{1}{3} \delta_{ij} L_{kk}, \quad (21)$$

the constant C_k can be dynamically computed from

$$C_k = \frac{1}{2} \frac{L_{ij} \sigma_{ij}}{\sigma_{lm} \sigma_{lm}}, \quad (22)$$

with

$$\sigma_{ij} = -\hat{\Delta} K_{\text{test}}^{1/2} \hat{S}_{ij} \quad (23)$$

and

$$K_{\text{test}} = \frac{1}{2} (\widehat{\tilde{u}_i \tilde{u}_i} - \hat{u}_i \hat{u}_i) = \frac{1}{2} L_{ii}. \quad (24)$$

Note that $\delta_{ij} \hat{S}_{ij} = 0$ for incompressible flows.

Assuming the scale similarity to also be valid for the dissipation gives

$$C_\epsilon \frac{K_{\text{test}}^{3/2}}{\hat{\Delta}} = (\nu_f + \nu_k) \left(\frac{\partial \widehat{\tilde{u}_i}}{\partial x_j} \frac{\partial \tilde{u}_i}{\partial x_j} - \frac{\partial \hat{u}_i}{\partial x_j} \frac{\partial \hat{u}_i}{\partial x_j} \right). \quad (25)$$

With this, the dynamic value of C_ϵ can be obtained from

$$C_\epsilon = \frac{\hat{\Delta} (\nu_f + \nu_k)}{K_{\text{test}}^{3/2}} \left(\frac{\partial \widehat{\tilde{u}_i}}{\partial x_j} \frac{\partial \tilde{u}_i}{\partial x_j} - \frac{\partial \hat{u}_i}{\partial x_j} \frac{\partial \hat{u}_i}{\partial x_j} \right). \quad (26)$$

The original LDKM for single phase flows (without the particle source term) has some advantageous properties. The dynamical constant C_k can become negative and, thus, theoretically enables emulating the backward energy cascade. However, similar to Kim *et al.* [41], the eddy viscosity is numerically limited to $\nu_k > -\nu_f$ to ensure a stable numerical solution of the flow equations. In contrast to the dynamic model of Germano *et al.* [42], no averaging along statistically homogeneous directions is required with the LDKM, which requires the existence of statistically homogeneous directions. With the dynamic computation of the constants, the model does not contain any adjustable constants.

Besides the theoretical advantages of the LDKM in a single phase flow, the main advantage is that it provides a framework for incorporating the particle source term in a deterministic way. If the particles remove kinetic energy from the subgrid scales, K_{sgs} decreases and the fluid dissipation (i.e., the eddy viscosity) is reduced. However, the model is not capable of considering at which scales the enhancement or attenuation of turbulence takes place. In reality, the spectral distribution of the subgrid-scale kinetic energy can play an important role.

The particle source term Φ_p is not closed in the scope of LES because the unfiltered velocity at the particle position is required, whereas only the filtered velocity is available. Thus, the mLDKM

including the particle source term is only applicable if a suitable model for the subgrid-scale velocity at the particle position is provided.

C. Approximate reconstruction of the subgrid-scale velocity

The computation of the drag force acting on the particle requires knowledge of the fluid velocity at the particle positions, which is used in the equations of motion of the particles and as the feedback force on the fluid. In addition to the LES velocity, the subgrid-scale velocity has to be provided. We approximate the subgrid-scale velocity as a truncated Fourier-series expansion,

$$\mathbf{u}' = \sum_{m=0}^{N_m-1} (\mathbf{A}_m(t) \cos(\mathbf{k}_m \cdot \mathbf{x}) + \mathbf{B}_m(t) \sin(\mathbf{k}_m \cdot \mathbf{x})), \quad (27)$$

where $\mathbf{A}_m(t)$ and $\mathbf{B}_m(t)$ are time-dependent coefficients, N_m the number of modes, and \mathbf{k}_m the wave vectors. With similar coefficients for the entire domain, the subgrid-scale velocity is statistically homogeneous. To overcome the limitation of global statistical homogeneity, statistically homogeneous subdomains $\Omega_{\text{domain}} \in \Omega$ are defined that own a distinct set of coefficients $\mathbf{A}_m(t)$ and $\mathbf{B}_m(t)$, respectively. Quantities that are known in the LES may be averaged over the subdomain,

$$\langle \phi \rangle_{\text{domain}} = \frac{1}{V_{\text{domain}}} \int_{\Omega_{\text{domain}}} \phi dV, \quad (28)$$

where V_{domain} indicates the volume of a subdomain. We exploit the findings of Laval *et al.* [43] that suggest that the effects of the nonlinear term in the governing equations for the subgrid-scale velocity on the kinetic energy spectrum and intermittency may be replaced by an additional viscosity that can be obtained from renormalization groups [44],

$$\nu'_t(k) = \left(\nu_f^2 + C_v \int_k^\infty q^{-2} E(q) dq \right)^{1/2} - \nu_f, \quad (29)$$

with the fluid kinetic energy spectrum E and an analytical constant $C_v = 2/5$. An equation to obtain a preliminary set of coefficients $A_{m,i}^*$ and $B_{m,i}^*$ can be derived [32]:

$$\begin{aligned} & \frac{A_{m,i}^* - A_{m,i}^n}{\Delta t} + \langle \tilde{u}_j^n \rangle_{\text{domain}} \left(k_{m,j} B_{m,i}^n + \frac{\partial A_{m,i}^n}{\partial x_j} \right) + A_{m,j}^n \left\langle \frac{\partial \tilde{u}_i^n}{\partial x_j} \right\rangle_{\text{domain}} \\ & = (\nu_f + \nu'_t) \left(-|\mathbf{k}_m|^2 A_{m,i}^n + \frac{\partial^2 A_{m,i}^n}{\partial x_j \partial x_j} + 2k_{m,j} \frac{\partial B_{m,i}^n}{\partial x_j} \right) + f_{m,i}, \end{aligned} \quad (30)$$

$$\begin{aligned} & \frac{B_{m,i}^* - B_{m,i}^n}{\Delta t} + \langle \tilde{u}_j^n \rangle_{\text{domain}} \left(\frac{\partial B_{m,i}^n}{\partial x_j} - k_{m,j} A_{m,i}^n \right) + B_{m,j}^n \left\langle \frac{\partial \tilde{u}_i^n}{\partial x_j} \right\rangle_{\text{domain}} \\ & = (\nu_f + \nu'_t) \left(-|\mathbf{k}_m|^2 B_{m,i}^n + \frac{\partial^2 B_{m,i}^n}{\partial x_j \partial x_j} - 2k_{m,j} \frac{\partial A_{m,i}^n}{\partial x_j} \right) + g_{m,i}. \end{aligned} \quad (31)$$

Note that no summation over the index m is carried out. The index n indicates the time level and $f_{m,i}$ and $g_{m,i}$ are forcing terms to maintain a desired kinetic energy of the subgrid scales. The coefficients are made divergence-free by applying a subsequent projection operation to the preliminary coefficients

$$\mathbf{A}_m^{n+1}(t) = \mathbf{A}_m^*(t) - \mathbf{k}_m \frac{\mathbf{k}_m \cdot \mathbf{A}_m^*(t)}{|\mathbf{k}_m|^2}, \quad (32)$$

$$\mathbf{B}_m^{n+1}(t) = \mathbf{B}_m^*(t) - \mathbf{k}_m \frac{\mathbf{k}_m \cdot \mathbf{B}_m^*(t)}{|\mathbf{k}_m|^2}. \quad (33)$$

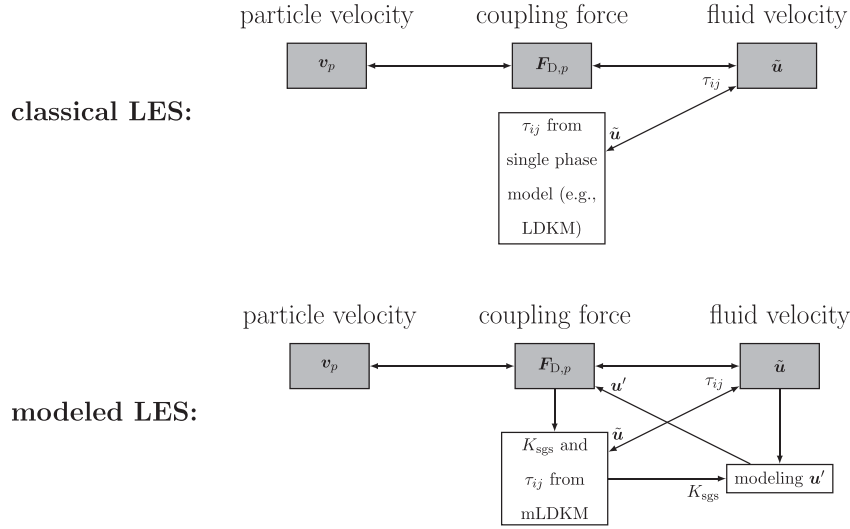


FIG. 1. Visualization of the modeled interactions in a classical LES (top) compared to the modeled interactions in the modeled LES (bottom).

Since with discretized spatial derivatives the solution for the coefficients essentially consists of explicit algebraic operations, the numerical solution is rather inexpensive. Numerical experiments show that the solution for the coefficients $A_{m,i}$ and $B_{m,i}$ requires a computing time of the same order as the LES [32].

The fact that every subdomain possesses a distinct set of coefficients requires the interpolation of the coefficients between the subdomains. In Hausmann *et al.* [32], an interpolation of the coefficients is presented that leads to a divergence-free subgrid-scale velocity field between subdomains. Homogeneous Dirichlet boundary conditions for the subgrid-scale velocity, as they occur in wall-bounded flows, may be realized by using the divergence free interpolation between the subdomains and the fluid velocity at the wall.

D. Coupling between the fluid phase and the particle phase

In a particle-laden LES, at least three effects are not or insufficiently considered: (i) The particles are accelerated by a drag force which requires the fluid velocity at the particle position. Using the filtered fluid velocity instead leads to different clustering and Lagrangian statistics of the particles [2,3]. (ii) The effect of the particles on the scales that are resolved in a LES is incomplete, since the feedback force is only computed from the filtered velocity instead of the unfiltered velocity. (iii) The effect of the particles on the subgrid scales is not considered in a classical LES. The modified subgrid-scale velocity changes the subgrid-scale stress tensor compared to a single phase flow (i.e., the dissipation by the subgrid-scale fluid velocity).

In Fig. 1, the procedure of a classical LES is compared to our proposed modeling framework that combines the mLDKM and the model for the subgrid-scale velocity. We refer to the latter as modeled LES. In the classical LES, the filtered fluid velocity \tilde{u} is obtained by solving the filtered NSE with a subgrid-scale stress tensor that is predicted by one of the subgrid-scale models commonly used for single phase flows. Note that subgrid-scale models for single phase flows do not incorporate information of the fluid-particle coupling force. The coupling force is computed from the filtered velocity at the particle position and is used to obtain the particle acceleration and the source terms in the fluid momentum equation.

The modeled LES exhibits a stronger coupling between the fluid phase and the particle phase. Using the filtered fluid velocity and the coupling force as input, the mLDKM returns a prediction of the subgrid-scale stress tensor, which is used for solving the filtered NSE and the subgrid-scale kinetic energy, which serves as the target kinetic energy for the generated subgrid-scale velocity.

With the modeled subgrid-scale velocity, the coupling force is computed considering all turbulent length and timescales down to the Kolmogorov scales. This enables a more realistic prediction of the particle velocity, the momentum source term in the filtered NSE, and the kinetic energy source term in the mLDKM. As a consequence, the subgrid-scale stress tensor and the modeled subgrid-scale velocity contain information about the turbulence modification by the particles at the unresolved scales. In theory, the modeled LES covers all occurring interactions between the fluid and the particles.

In Sec. V A, we also study one-way coupling simulations with the modeled LES, in which case all arrows of Fig. 1 that point from the coupling force to anything else than the particle velocity vanish. The mLDKM then reduces to the original LDKM or can be replaced by any subgrid-scale model that is developed for single phase flows. The subgrid-scale kinetic energy that is required as input for the modeling of the subgrid-scale velocity can be alternatively estimated with the model of Yoshizawa [45] or the dynamic model of Moin *et al.* [46].

IV. SIMULATIONS

Our proposed modeling is verified and validated by means of DNS and LES of particle-laden turbulent flows. For all the simulation cases, HIT is considered. First, the model for the subgrid-scale velocity at the particle position is assessed by comparing the particle statistics in the modeled LES with the particle statistics in a DNS of the same one-way coupled case of statistically stationary turbulence. In a second case, the feedback force of the particles on the fluid is investigated. This requires the full modeling framework as described in Sec. III D, which is evaluated by comparing the modeled LES and DNS of two-way coupled particle laden decaying turbulence. The subsequent sections provide details of the realizations and configurations of the simulations.

A. Solving the governing equations

The NSE are solved with a finite volume approach that is second order in space and time [47]. The continuity equation and the momentum equations are coupled using momentum weighted interpolation [48]. Therefore, two distinct velocity fields exist numerically, a cell-centered velocity accurately satisfying the momentum balance and a face centered velocity conserving mass.

Statistically steady turbulence is maintained by supplying the flow with energy through source terms in the momentum equations [49]. An important property of the forcing is that the artificial source terms can be introduced in a limited range of wave numbers, $k \in [k_{\text{start}}, k_{\text{end}}]$. For particle-laden flows, this is essential to avoid directly impacting the particle behavior by the forcing.

The particle equations of motion Eqs. (3) and (4) are solved with the Verlet scheme [50]. The drag force acting on the Lagrangian particle p is computed from

$$\mathbf{F}_{D,p} = C_D \frac{\rho_f}{8} \pi d_p^2 |\mathbf{u}_{\text{rel}}| \mathbf{u}_{\text{rel}}, \quad (34)$$

with the drag coefficient from the Schiller-Naumann correlation [51]

$$C_D = \frac{24}{\text{Re}_p} (1 + 0.15 \text{Re}_p^{0.687}), \quad (35)$$

and the particle Reynolds number $\text{Re}_p = |\mathbf{u}_{\text{rel}}| d_p / \nu_f$. The relative velocity \mathbf{u}_{rel} is defined as the difference between the fluid velocity at the particle position and the particle velocity $\mathbf{u}_{\text{rel}} = \mathbf{u}(\mathbf{x}_p) - \mathbf{v}$.

To obtain the fluid velocity at the particle position, an interpolation from the Cartesian grid is required. An essential property of the interpolation scheme is that the interpolated velocity needs to be divergence-free. In the present paper, a second-order divergence-free interpolation from the face-centered velocity (that fulfills the continuity equation with high accuracy) to the particle position is applied [52].

TABLE I. Single phase flow parameters of the HIT simulation configuration.

Parameters	Values
Re_λ	75
Re_l	205
η/L	0.0017
τ_η/T_{ref}	0.0075
λ/L	0.029
l_{11}/L	0.079
$k_{\text{start}}L/2\pi$	3
$k_{\text{end}}L/2\pi$	6

In the case of the two-way coupling simulations, the PSIC method of Crowe *et al.* [36] is utilized.

B. Simulation setups

1. Single phase flow setups

The studies in this paper consist of two different flow types: (i) one-way coupling simulations of forced HIT and (ii) two-way coupling simulations of decaying HIT. The computational domain of both simulation types is a cube with periodic boundary conditions in all directions and an edge length of L . Time quantities are given with respect to a reference time $T_{\text{ref}} = L/\sqrt{2/3\langle K \rangle}$, where $\langle K \rangle$ is the average kinetic energy of the fluid.

The setup of the single-phase flow simulations is summarized in Table I. The given values correspond to the statistically steady state of the flow (before the decay) without the particles. The two-way coupled simulations also undergo a two-way coupled forcing period to obtain a statistically steady state before the forcing is turned off. The symbols in the table correspond to the Taylor-Reynolds number Re_λ , the turbulent Reynolds number based on the integral length scale Re_l , the Kolmogorov timescale τ_η , the Taylor microscale λ , and the longitudinal integral length scale l_{11} .

The DNS are carried out on a grid consisting of $N^3 = 256^3$ grid cells, which leads to a product of the maximum resolvable wave number k_{max} and the Kolmogorov length scale of $k_{\text{max}}\eta = 1.37$. The LES are solved on a grid with $N^3 = 32^3$ cells.

2. Particle setups of the one-way coupled case

In the one-way coupled case, particles of five different Stokes numbers, $St = \tau_p/\tau_\eta$, are introduced in the previously defined flow setup. The Stokes numbers are based on the Kolmogorov timescale of the statistically steady single phase flow. Since in the one-way coupling simulations the flow does not experience any feedback by the particles, the previously defined parameters of the flow do not change.

The particle relaxation time, $\tau_p = \rho_p d_p^2 / (18 \rho_f \nu_f)$, the number of particles of the respective simulation N_p , and the particle diameter to mesh spacing ratio $d_p/\Delta h$ are summarized in Table II. In

TABLE II. Particle configurations of the one-way coupling case.

Parameter	St = 0.5	St = 1	St = 2	St = 4	St = 8
τ_p/T_{ref}	0.0037	0.0075	0.015	0.03	0.06
N_p	480115	480115	480115	480115	480115
$d_p/\Delta h$	0.2	0.2	0.2	0.2	0.2

TABLE III. Particle configurations of the two-way coupling case.

Parameter	St = 1	St = 2	St = 8
τ_p/T_{ref}	0.0075	0.015	0.060
N_p	91377408	45830011	12057066
$d_p/\Delta h$	0.1	0.1	0.1
ϕ	1.0	1.0	1.0

the one-way coupled simulation cases, the ratio of the particle diameter to the Kolmogorov length scale is $d_p/\eta = 0.047$ for all Stokes numbers.

The simulations run more than $150\tau_\eta$ before the statistics are evaluated to obtain converged statistics that are independent of the initial conditions.

3. Particle setups of the two-way coupled case

Two simulation configurations are performed, including two-way coupled particles of two different Stokes numbers. Both configurations are started with a period of forced turbulence until the particle-laden turbulence reaches a statistically steady state (at least $150\tau_\eta$). The decay of the turbulence and the tracking of the statistics starts after this forcing period. Note that the Kolmogorov timescale and thus also the Stokes numbers are based on the statistically steady single phase flow turbulence. In the one-way coupled simulation cases, the ratio of the particle diameter to the Kolmogorov length scale is $d_p/\eta = 0.023$, and the particle mass fraction is $\phi = 1.0$, for all Stokes numbers. The particle related parameters of the two two-way coupled simulations are summarized in Table III.

4. Parameters of the modeling framework

Besides the DNS and the classical LES, we also conduct simulations using the proposed LES modeling framework. For the mLDKM part of the modeling framework, there are no tunable model parameters that have to be specified. The model for the subgrid-scale velocity however, requires us to choose some parameters. It was shown by Hausmann *et al.* [32] that the statistics of the subgrid-scale velocity are relatively insensitive to the values of these parameters.

The number of statistically homogeneous subdomains, N_{domain} , depends on the characteristic length scales at which the statistics of the subgrid-scale velocity vary. Based on experience, we suggest choosing the size of a subdomain approximately four times the size of a LES grid cell per direction. Note that in previous studies, the number of subdomains did not critically influence the velocity statistics.

Another parameter is related to the interpolation between the subdomains to obtain a divergence-free velocity field. The interpolation kernel is [32]

$$W(r) = 1 - \frac{1}{1 + e^{-\alpha r}}, \quad (36)$$

where r is the distance to the respective subdomain boundary, and α a parameter that determines the thickness of the region that is influenced by the interpolation. In general, the influence region of the interpolation should be as small as possible to keep the region that is not affected by the interpolation as large as possible. However, the influence region should not be so small that the particles experience the subdomain boundary as discontinuity of the subgrid-scale velocity. We empirically found that $\alpha = 40/\Delta h_{\text{domain}}$ works well for the considered cases, where Δh_{domain} is the width of a subdomain. It is shown in Appendix A that the clustering of the particles is not significantly influenced even if the parameter α is varied over a wide range.

The remaining parameter that has to be set is the number of modes N_m in the series expansion Eq. (27). Similar to the number of subdomains, it has been shown previously that the influence of

TABLE IV. Parameters of the model for the subgrid-scale velocity.

Parameter	Value
N_{domain}	8
α	$40/\Delta h_{\text{domain}}$
N_{m}	108

N_{m} on the velocity statistics is negligible as long as $N_{\text{m}} = O(10^2)$. The particular choice for N_{m} in the present paper is mainly based on load balancing considerations. Although we did not observe the results to sensitively depend on the choice of the number of modes in our previous study [32], we cannot exclude that as the range of modeled scales increases significantly, e.g., by a significantly larger Re_λ , the number of modes needs to increase accordingly. The values of the parameters in the present paper are summarized in Table IV.

V. RESULTS AND DISCUSSIONS

A. One-way coupled configurations

In this section, the configurations described in Sec. IV B 2 are investigated. In the following, it is referred to as enriched LES if the particles are propagated with a drag force based on the sum of the LES velocity and the modeled subgrid-scale velocity at the particle positions.

The particle pair dispersion is evaluated in the enriched LES, the classical LES, and the DNS. The particle pair dispersion is defined as the ensemble-averaged and time-dependent distance between particle pairs, whereas a particle pair is considered as two particles with an initial separation of the Kolmogorov length scale,

$$\langle \delta \rangle(t) = \langle |\mathbf{x}_{p0}(t) - \mathbf{x}_{p1}(t)| \rangle, \quad (37)$$

where $\mathbf{x}_{p0}(t)$ and $\mathbf{x}_{p1}(t)$ are the positions of the particles belonging to a particle pair and $\langle \delta \rangle(t = 0) = \eta$.

The particle pair dispersion in the DNS, the classical LES, and the enriched LES for the five different Stokes numbers of the one-way coupling case is depicted in Fig. 2. It can be observed that for all the considered Stokes numbers, the particle pairs stay together for a short time before they disperse rapidly. Eventually, the average separation reaches a steady state, which corresponds approximately to the half domain size, indicating that the maximum separation that is possible in a fully periodic cubic domain is reached. For higher Stokes numbers, the particle pairs stay close to each other for a shorter time, as particles with a large Stokes numbers are more likely to have different velocities caused by their high inertia. The classical LES predicts the particle pairs to disperse much slower than in the DNS due to the missing effect of the subgrid-scale velocity sweeping the particles into regions of different large scale velocities. This effect is observed for all investigated Stokes numbers, but is slightly more dominant for the larger Stokes numbers.

In the enriched LES, the predicted particle pair dispersion almost overlaps with those of the DNS. An important reason why the enriched LES performs so well is that the subgrid-scale velocity at the particle position is computed from a spatially continuous velocity field. As a consequence, two particles that are very close also experience a similar subgrid-scale velocity. This is not the case for Lagrangian models (see, e.g., Fede *et al.* [5], Bini and Jones [6], Pozorski and Apte [9]), which typically solve an evolution equation for each particle individually. Lagrangian models typically perform poorly in particle pair dispersion [53].

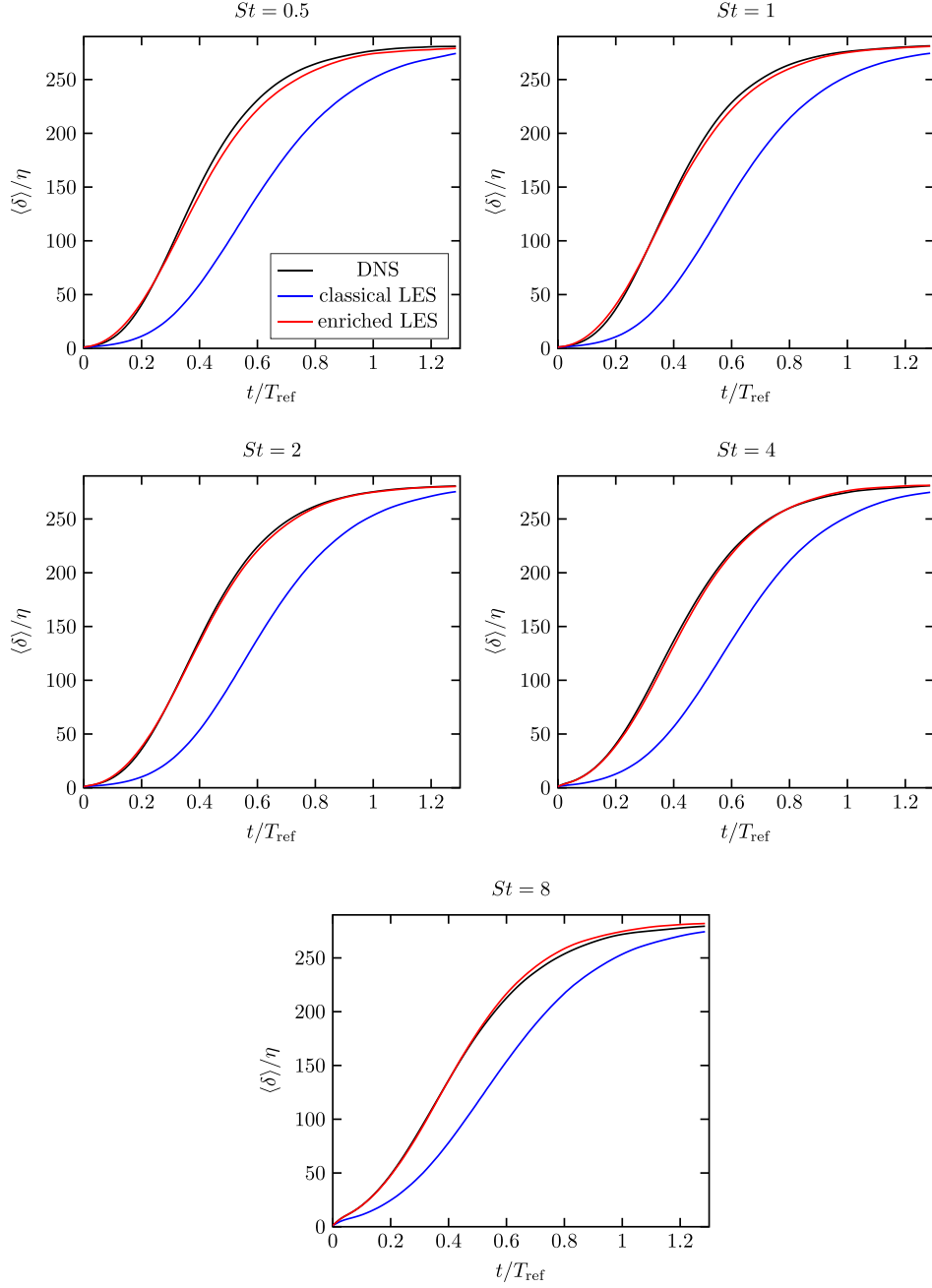


FIG. 2. Particle pair dispersion of the one-way coupled simulations for different Stokes numbers in forced HIT with the flow parameters given in Table I. The results are shown for the DNS, the classical LES, and the enriched LES.

A property that is of high practical importance is the extent with which particles form clusters. Particle clustering can be quantified by the radial distribution function, defined as

$$g(r) = \left\langle \frac{N_{p,i}(r) / \Delta V_i(r)}{N_p / V} \right\rangle, \quad (38)$$

where $N_{p,i}(r)$ is the number of particles in a spherical shell with radius r centered at the location of the original particle and $V_i(r)$ is the volume of this spherical shell. The radial distribution function is normalized by the total number of particles N_p and the total volume of the domain V . Values of $g > 1$ indicate particle clustering and $g = 1$ uniformly distributed particles.

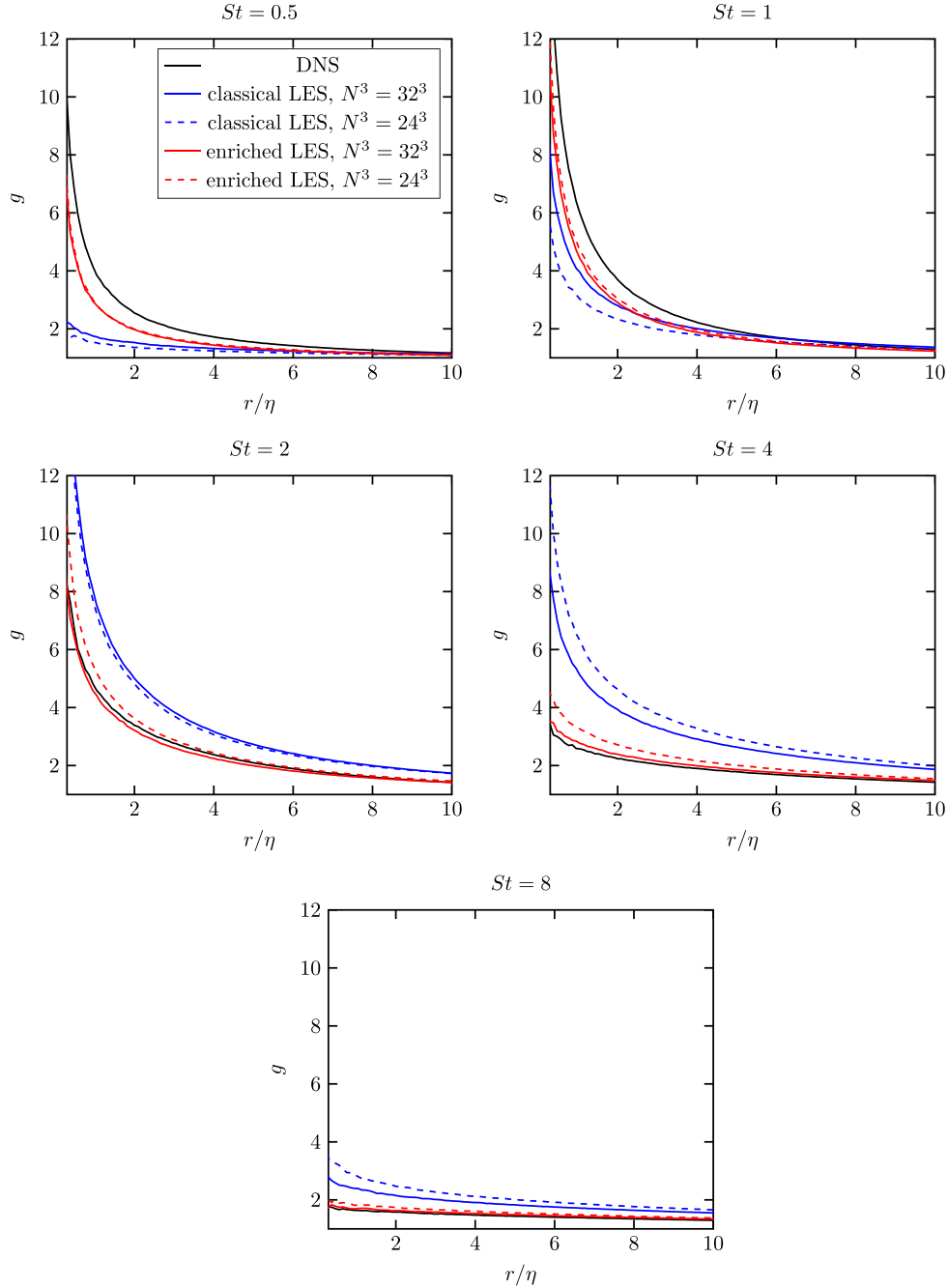


FIG. 3. Radial distribution function of the one-way coupled simulations for different Stokes numbers in forced HIT with the flow parameters given in Table I. The results are shown for the DNS, the classical LES, and the enriched LES. The results of the classical LES and the enriched LES are additionally shown with a coarser resolution of $N^3 = 24^3$ cells.

In Fig. 3, the radial distribution functions are shown. In addition to the LES simulations using $N^3 = 32^3$ cells, we also investigate particle clustering as a key statistic for assessing the influence of turbulence on particles in an even coarser LES, using $N^3 = 24^3$ cells. The setup for the enriched LES is similar to that of the LES with $N^3 = 32^3$ cells, with the exception of the number of subdomains. According to the presented guidelines, $N^3 = 24^3$ cells require $N_{\text{domain}} = 6$ subdomains, with each subdomain size corresponding to four times the size of a LES cell per direction. We have shown that other parameters have little influence on the observed fluid statistics [32].

The clustering reaches its maximum at $St \approx 1$. For smaller and larger Stokes numbers, clustering is reduced. The classical LES yields an underestimation of the clustering for $St = 0.5$ and $St = 1$ and to an overestimation of the clustering for the Stokes numbers $St = 2$, $St = 4$, and $St = 8$. This phenomenon has also been observed in previous studies [2,14,17]. This means that the modeled subgrid-scale velocity has to increase the clustering for the small St and increase the dispersion for the larger St . Note that increasing the particle dispersion is much simpler to achieve than increasing the particle clustering. In fact, the relations between strain and rotation of the velocity field are crucial for the correct prediction of particle clustering [54,55].

The enriched LES using $N^3 = 32^3$ cells shows that for Stokes numbers $St = 2$, $St = 4$, and $St = 8$, particle clustering almost matches the clustering predicted by the DNS. When using a coarser resolution, clustering slightly increases, and the radial distribution function obtained from the enriched LES shows a small deviation from the DNS radial distribution function. For the Stokes numbers $St = 4$ and $St = 8$, a similar increase in clustering is observed in classical LES using $N^3 = 24^3$ cells. Therefore, the more accurate prediction of clustering behavior observed in the enriched LES is relatively independent of the LES resolution for these Stokes numbers.

For Stokes numbers $St = 0.5$ and $St = 1$, particle clustering is increased by the enriched LES compared to classical LES. However, the agreement with the DNS is not as good as for higher Stokes numbers, and the improvement in the radial distribution function for $St = 1$ is minor. With a coarser grid of $N^3 = 24^3$ cells, the radial distribution function of the enriched LES remains almost unchanged, while the clustering intensity of the classical LES is further reduced due to the coarser resolution.

Our previous study [32] has shown that the probability distribution function (PDF) of the second invariant of the velocity gradient tensor is significantly improved with the enriched LES compared to the classical LES, which explains the ability of the model to increase the clustering of particles with small Stokes numbers.

The kinetic energy of the classical LES relative to the kinetic energy of the DNS is $K_{LES}/K_{DNS} \approx 0.83$. Together with the estimated subgrid-scale kinetic energy, this gives $(K_{LES} + K_{sgs})/K_{DNS} \approx 1.07$. The fact that the total kinetic energy of the enriched LES overpredicts the kinetic energy of the DNS is important for the interpretation of the following results.

Figure 4 shows the PDF of the cosine of the angles between the particle velocity and the fluid velocity at the particle position, together with the mean values. The most likely event for all the considered Stokes numbers is the case where the fluid velocity is aligned with the particle velocity. However, for increasing Stokes numbers the probability of larger angles between the fluid velocity and the particle velocity also increases. Except for $St = 0.5$, the classical LES always predicts too strong an alignment of fluid and particle velocities. For higher Stokes numbers, in particular, the particles are too heavy to follow the subgrid-scale velocity fluctuations, which typically change with high frequency and small magnitude. In the classical LES, these fluctuations are missing. The enriched LES provides the subgrid-scale fluctuations, which explains the improved PDF and means of velocity alignment for larger Stokes numbers. However, for Stokes numbers $St = 0.5$, $St = 1$, and $St = 2$, the enriched LES does not improve the results of the classical LES. It is worth noting, however, that when considering all Stokes numbers, the prediction of the mean angle between the fluid velocity and the particle velocity is better for the enriched LES, as the absolute deviations from the mean angle of the DNS increase with the Stokes number. One possible reason for the deviation for $St = 0.5$ and $St = 1$ is that it is caused by the too-high kinetic energy of the enriched LES. Therefore, the particles with the small Stokes numbers cannot follow the velocity fluctuations as well as in the case of the DNS and the classical LES. For higher Stokes numbers, the deviation between the velocities is more significant and the higher subgrid-scale kinetic energy has a smaller influence.

From the results of the one-way coupled simulations, it can be concluded that the enrichment with subgrid-scale velocity can significantly improve the particle statistics in HIT for Stokes numbers $St \geq 2$. Particularly worth highlighting is that the clustering can be improved for both qualitatively different cases of $St \leq 1$ and $St > 1$ with the modeled subgrid-scale velocity although the improvements for the smaller Stokes numbers are less pronounced.

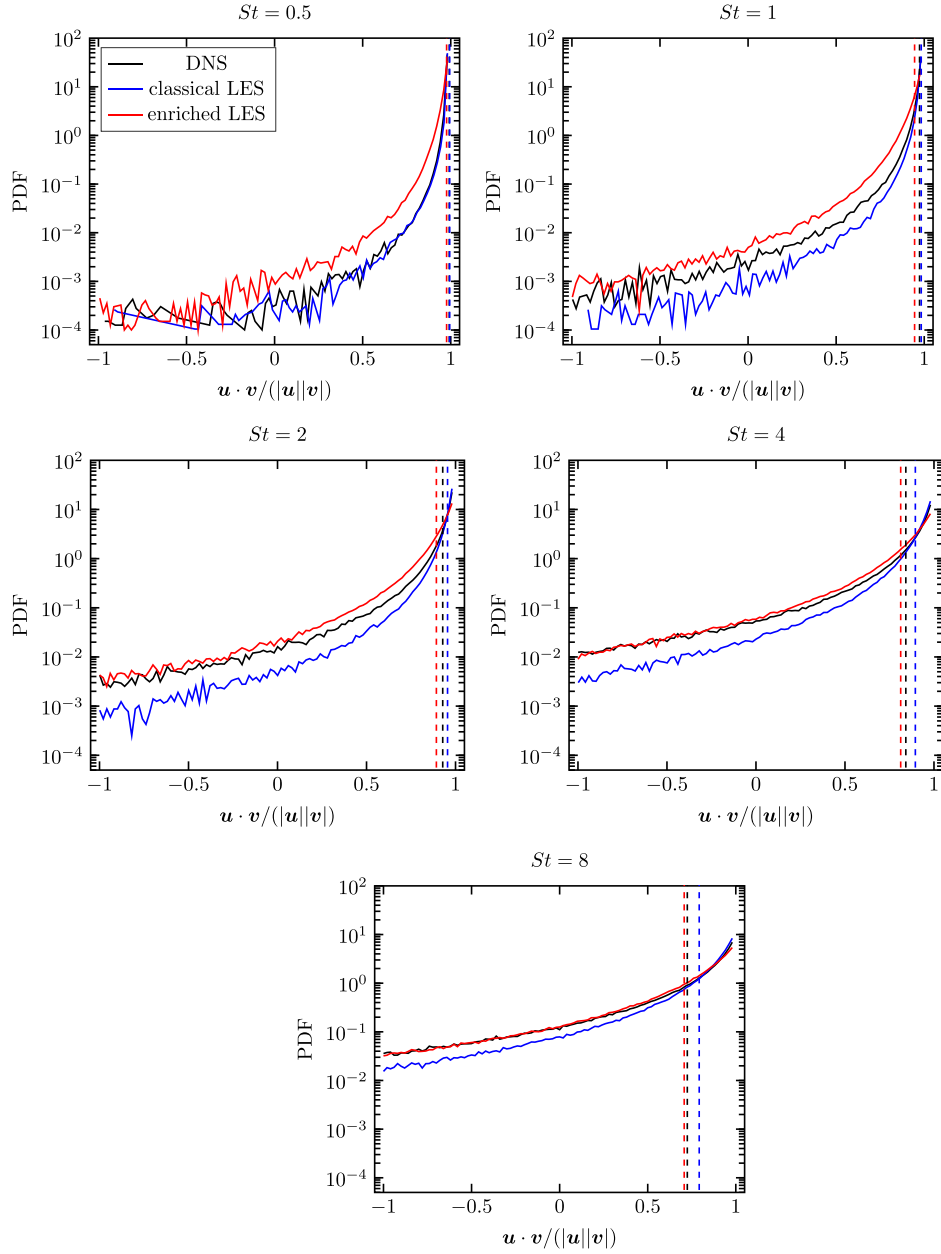


FIG. 4. PDF of cosine of angle between the fluid velocity at the particle position and the particle velocity of the one-way coupled simulations for different Stokes numbers in forced HIT with the flow parameters given in Table I. The results are shown for the DNS, the classical LES, and the enriched LES. The vertical lines indicate the respective mean value.

The computational cost of the proposed model is of high practical relevance, but it strongly depends on the specific configuration being considered. Solving for the enriched LES velocity approximately doubles the computational cost compared to the classical LES. However, there is an additional computational cost if particles are transported, namely, the subgrid-scale velocity interpolation to each particle position. For example, in the present one-way coupled simulations, the enriched LES with 2.4 million particles is six to seven times more expensive than the classical LES without enrichment. However, the total enriched framework is still orders of magnitude cheaper than the DNS.

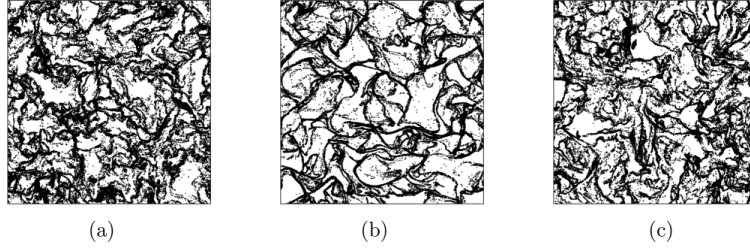


FIG. 5. Particle positions of the two-way coupled simulations with $St = 2$ of HIT with the flow parameters given in Table I. The results are evaluated at the last forced time step. The particle positions are projected from a slice of thickness equal to the Kolmogorov length scale η . (a) shows the particles of the DNS, (b) the particles of the classical LES, and (c) the particles of the modeled LES.

B. Two-way coupled configurations

In the present section, the modification of the turbulent flow by the particles is considered, which enables the assessment of the full modeling framework including the modeling of the subgrid-scale velocity combined with the mLDKM (previously introduced as modeled LES).

In Fig. 5, the projected particles in a slice of the thickness η are plotted for the case of $St = 2$ for the DNS, the classical LES, and the modeled LES. The positions are evaluated at the end of the forcing period. The particles reached steady statistics at this point in time.

The shapes of the clusters that are formed by the DNS and the classical LES differ significantly. The clusters of the classical LES are much coarser and more pronounced than the clusters of the DNS. The additional subgrid-scale velocity of the modeled LES breaks up the large clusters of the classical LES into clusters of smaller size, which are also less dense.

Figure 6 shows the kinetic energy spectra of the two-way coupled simulations for $St = 1$, $St = 2$, and $St = 8$, respectively. Due to the interaction with the particles, the results obtained with the DNS deviate significantly from the inertial range slope of single phase turbulence. In addition to the DNS, the results of the classical LES and the modeled LES are depicted. The kinetic energy spectrum that is resolved by the LES grid is shown separately from the kinetic energy spectrum of the modeled subgrid-scale velocity.

The filter imposed by the spatially varying turbulent viscosity is unknown. To achieve realistic particle transport, it is advantageous if the kinetic energy spectrum of the LES is similar to that of the DNS. In other words, it is desirable that the turbulent viscosity imposes a filter that closely resembles a spectrally sharp filter.

The classical LES overestimates the subgrid-scale fluid dissipation, resulting in a deviation from the slope of the DNS spectrum. The modeled LES takes into account the reduced subgrid-scale fluid dissipation caused by particle dissipation. As a result, the modeled LES leads to a spectrum that is in better agreement with the DNS spectrum for all three Stokes numbers.

The kinetic energy spectrum of the modeled subgrid-scale velocity is in good agreement with the DNS spectrum but its shape deviates in all three cases. The shape of the modeled subgrid-scale kinetic energy spectrum is very similar for $St = 1$, $St = 2$, and $St = 8$ even though the shapes of the two DNS spectra are very different. The model for the subgrid-scale velocity does not receive any information on the presence of the particle, except for the kinetic energy. Therefore, the modeled subgrid-scale kinetic energy spectrum is a shifted spectrum that matches very well with a single phase flow spectrum [32].

A classical LES does not fully consider the interphase kinetic energy transfer, since the interactions of the subgrid-scale velocity with the particles and the unresolved particle motion with the resolved flow scales are neglected. For small-particle Reynolds numbers, the kinetic energy transfer is proportional to the fluid velocity times the Stokes drag, $\mathbf{u} \cdot (\mathbf{v} - \mathbf{u})/\tau_p$, which is plotted in Fig. 7 for the present cases. Negative values indicate that kinetic energy is removed from the fluid and positive values correspond to kinetic energy that is added to the fluid by the particles. Note that, as

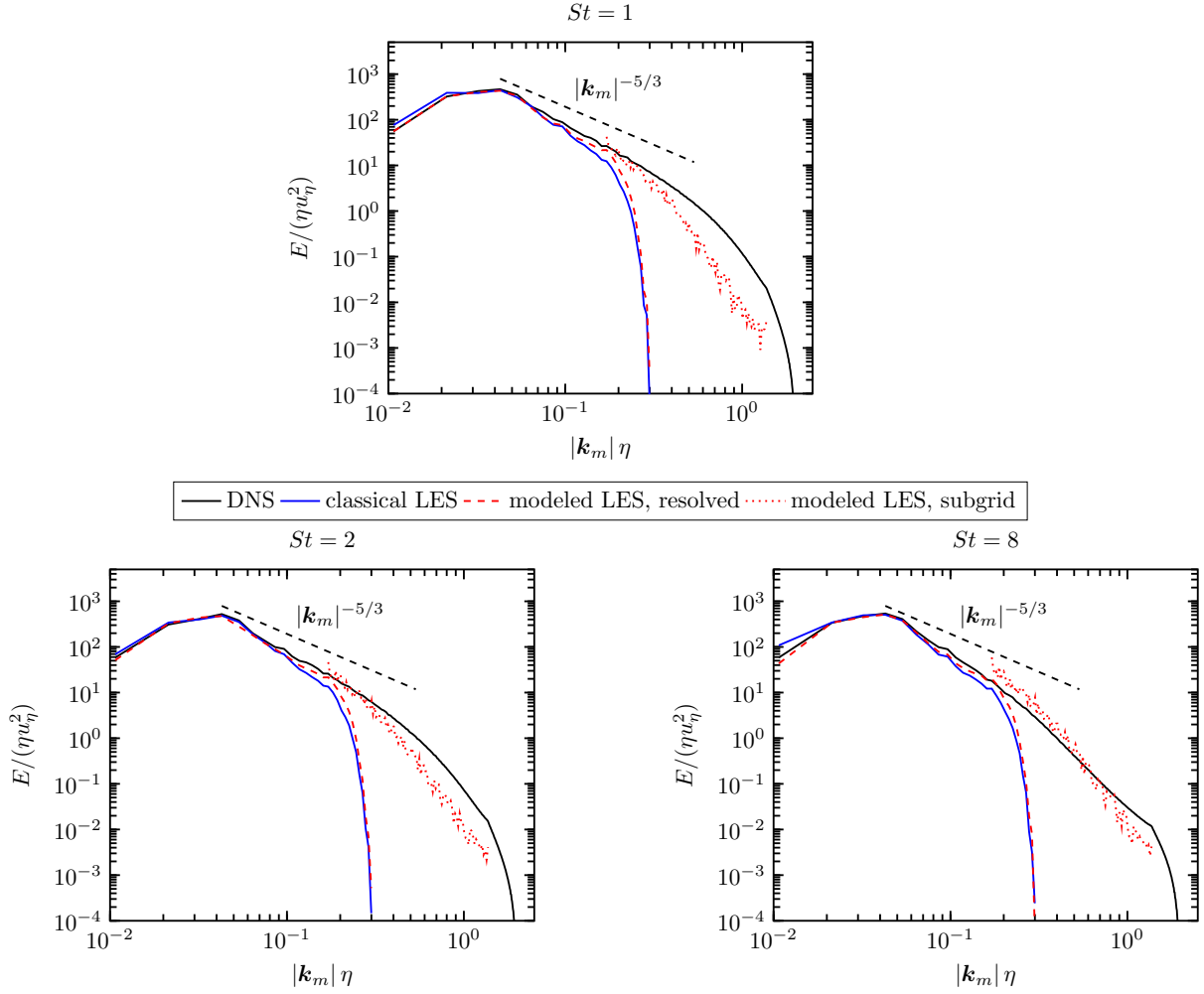


FIG. 6. Kinetic energy spectrum of the two-way coupled simulations with $St = 1$, $St = 2$, and $St = 8$ of HIT with the flow parameters given in Table I. The results are evaluated at the last forced time step. Compared are the DNS, the classical LES, and the modeled LES. The spectrum of the modeled LES is split into a part that is resolved by the LES grid and a subgrid-scale contribution that is modeled.

shown by Xu and Subramaniam [56], the energy that is removed from the fluid does not necessarily equal the kinetic energy that is added to the particles in a point-particle simulation.

The PDF in Fig. 7 shows a negative mean value for all Stokes numbers, indicating that, on average, the particles remove energy from the fluid. The PDF becomes wider and possesses larger absolute mean values as the Stokes number increases. The classical LES underpredicts the absolute of the mean values of the DNS for all Stokes numbers. With the proposed modeled LES, the kinetic energy that is removed by the particles is increased, which is qualitatively similar to the behavior of the DNS relative to the classical LES. In the classical LES, the particle velocities tend to align more with the local fluid velocity compared to the DNS because of the absence of small vortices that the particles cannot follow. With the proposed modeling, small velocity structures are provided, which increases the absolute energy transfer. However, for all Stokes numbers the width of the PDFs is overpredicted by the modeled LES.

The second effect that is neglected in a classical LES is the reduced subgrid-scale kinetic energy due to the turbulence modification by the particles. The subgrid-scale kinetic energies over time are depicted in Fig. 8. The subgrid-scale kinetic energy of the DNS is computed by subtracting the kinetic energy of the spectrally sharp filtered DNS from the kinetic energy of the DNS. Since the actual filter of a LES imposed by the turbulent viscosity is unknown, the DNS is also

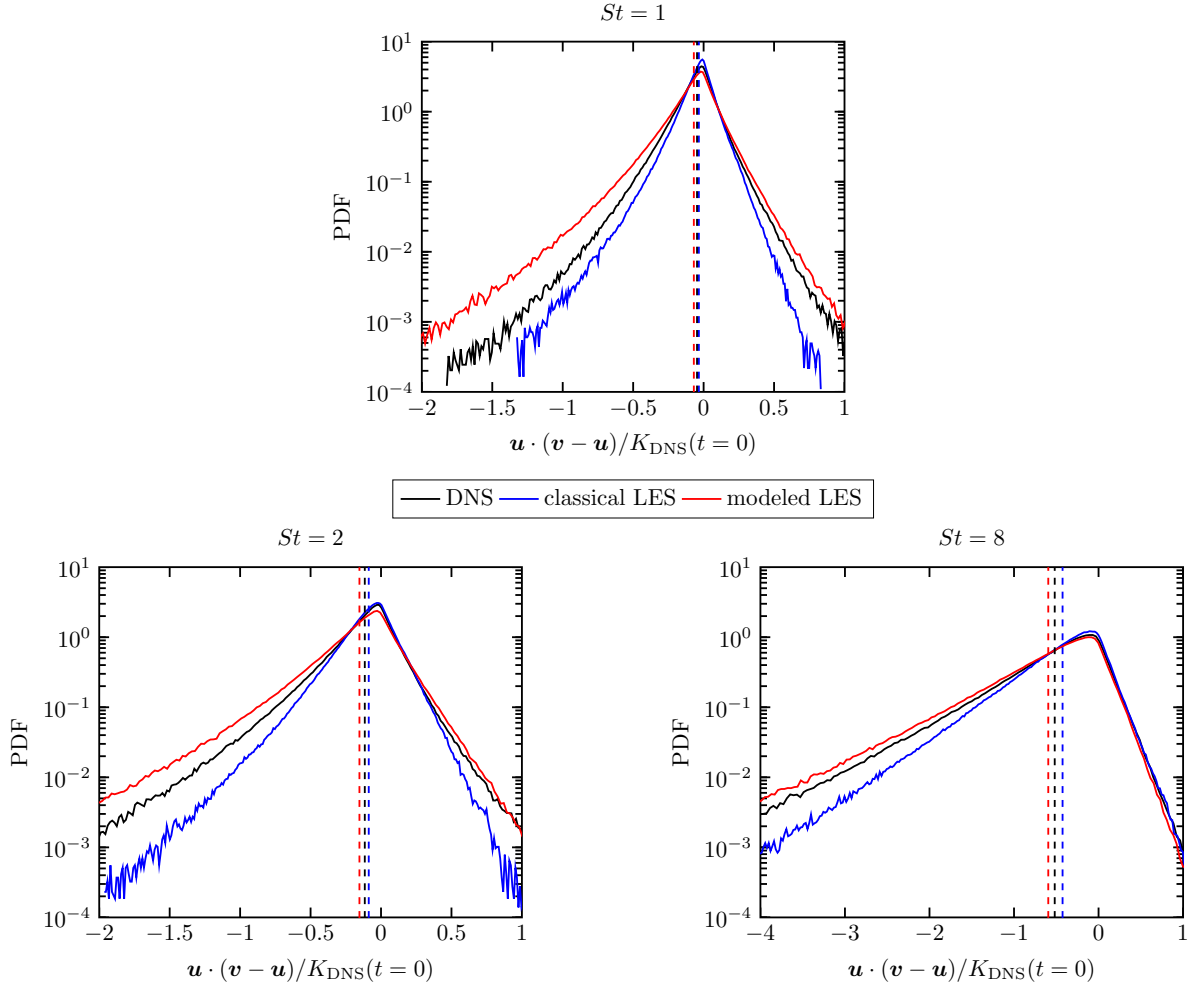


FIG. 7. PDF of the kinetic energy transfer between fluid and particles of the two-way coupled simulations with $St = 1$, $St = 2$, and $St = 8$ of HIT with the flow parameters given in Table I. The results are evaluated at the last forced time step. The vertical lines indicate the respective mean values.

volume averaged for comparison. The kinetic energies of the LES are obtained from the transport equation in the LDKM and mLKDM, respectively. It is observed that for all Stokes numbers, the classical LES predicts a much higher subgrid-scale kinetic energy than the DNS. The subgrid-scale kinetic energy of the modeled LES is significantly smaller because of the source term Φ_P in the transport equation for the subgrid-scale kinetic energy. A higher subgrid-scale kinetic energy yields a higher eddy viscosity and thus more subgrid-scale dissipation. The classical LES overpredicts the kinetic energy of the subgrid-scale velocity because the particle dissipation at high wave numbers is not accounted for. The additional source term in the subgrid-scale kinetic energy equation of the mLKDM considers the effect of the particles on the subgrid-scale quantities. The choice of the explicit filter introduces uncertainties that complicate the quantitative comparison of the LES predictions with the DNS. Nonetheless, the reduction of subgrid-scale kinetic energy is qualitatively consistent with the results obtained from explicitly filtering the DNS.

It is observed that the effects that are neglected in a classical LES act in opposite directions for the considered configurations. While the classical LES underpredicts the dissipation by the particles, it over-predicts the dissipation of the subgrid-scale velocity. Thus, these two errors at least partially compensate each other, which in total may lead to fair agreement with the total kinetic energy of the DNS. However, the proposed modeled LES considers each effect (i.e., the increased particle dissipation and the reduced fluid dissipation) separately and does not rely on compensation of errors.

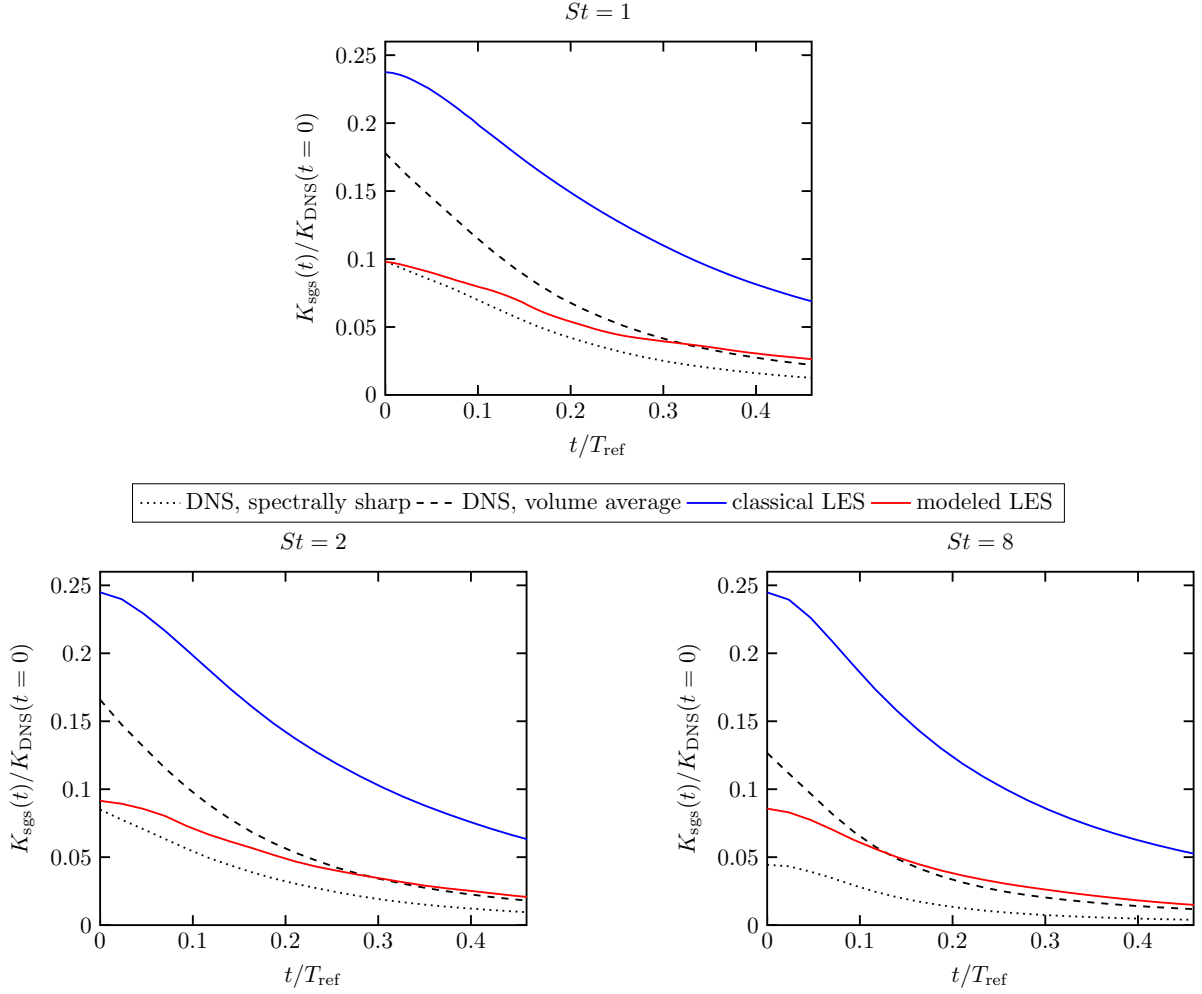


FIG. 8. Normalized subgrid-scale kinetic energy over time of the two-way coupled simulations with $St = 1$, $St = 2$, and $St = 8$ of decaying HIT with the flow parameters given in Table I. Compared are the results of the DNS (with a spectrally sharp filter and volume averaged), the classical LES, and the modeled LES with particle source term.

Figure 9 shows the normalized kinetic energy over time for the two-way coupled simulations with $St = 1$, $St = 2$, and $St = 8$, respectively. Besides the spectrally sharp filtered and volume averaged DNS (FDNS) and the classical LES, the results of the modeled LES are plotted. To investigate the influence of the particle source term Φ_P in the transport Eq. (18) of the subgrid-scale kinetic energy, the modeled LES is shown with the source term (modeled LES-mLDKM) and without the source term (modeled LES-LDKM). For $St = 1$ and $St = 2$, the LES, the modeled LES-mLDKM, and the modeled LES-LDKM predict a slower decay of the fluid kinetic energy than the DNS. The deviation of the three LES cases from the DNS is much smaller for $St = 8$. All Stokes numbers show only relatively small deviations between the LES cases. For $St = 1$, the kinetic energy predicted by the classical LES and the modeled LES-mLDKM are nearly identical. This is remarkable considering that the particle dissipation and fluid dissipation are significantly different between the two methods. The kinetic energy of the modeled LES-LDKM is always smaller than the kinetic energy of the modeled LES-mLDKM.

It is known from the literature that for Stokes numbers that are not significantly smaller than one, the total dissipation in a particle-laden flow is increased [19–21,23], which also applies to the Stokes numbers investigated in the present paper. The total dissipation has contributions from the particles and the fluid, as occurs in a single-phase flow. In a LES, the particle and the fluid dissipation have to

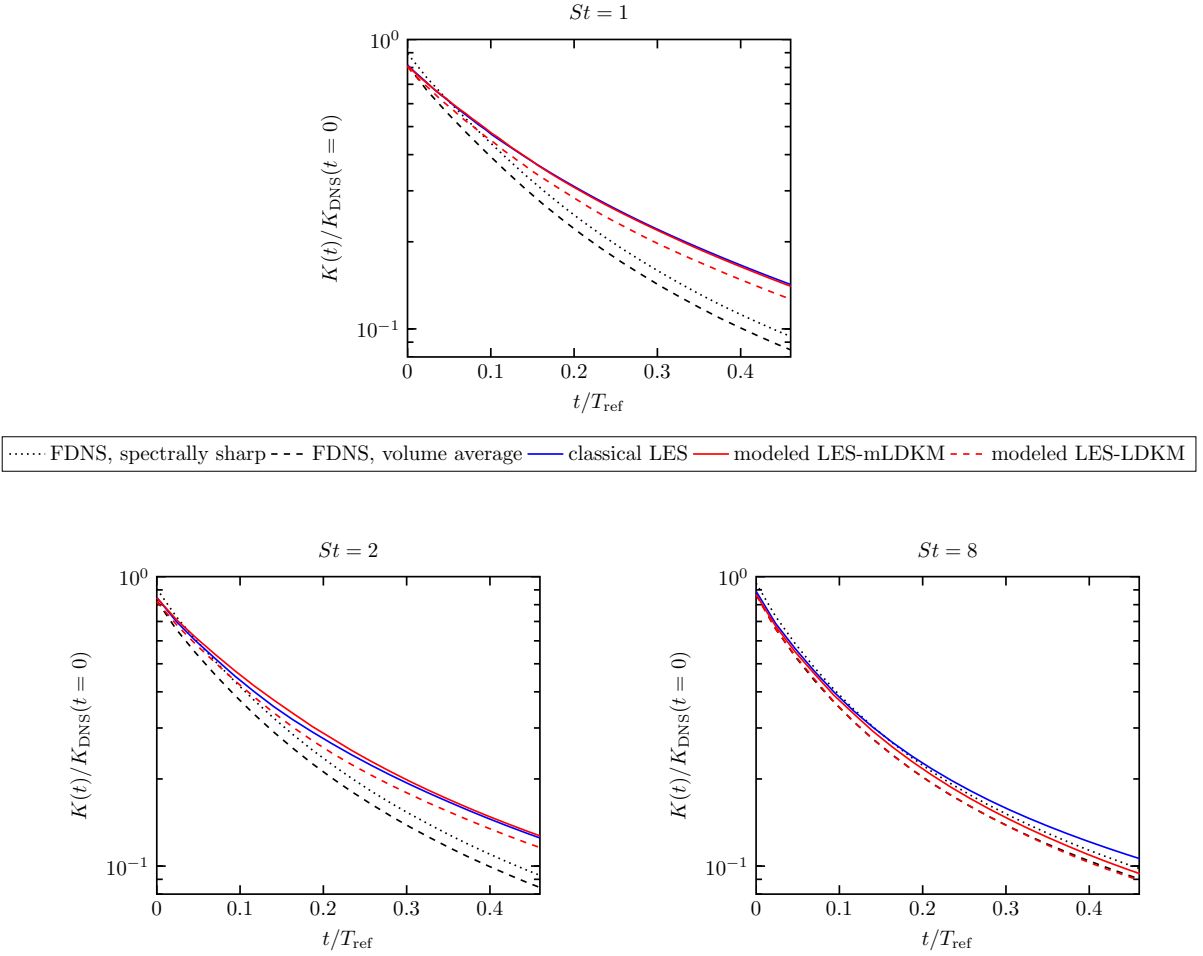


FIG. 9. Normalized kinetic energy over time of the two-way coupled simulations with $St = 1$, $St = 2$, and $St = 8$ of decaying HIT with the flow parameters given in Table I. Compared are the FDNS (with a spectrally sharp filter and volume averaged), the classical LES (LES-LDKM), the modeled LES with particle source term (modeled LES-mLDKM), and the modeled LES without particle source term (modeled LES-LDKM).

be modeled. As already pointed out, both contributions have opposite signs in the present cases. This becomes evident by the fact that the modeled LES without the particle source term Φ_P increases the total dissipation. The difference to the classical LES in this case is that the two-way coupling force is computed using the total fluid velocity consisting of the LES velocity and the modeled subgrid-scale velocity, which leads to increased dissipation relative to the classical LES. The dissipation by the particles yields a negative source term Φ_P , which reduces the subgrid-scale kinetic energy. This is why the total dissipation of the modeled LES-mLDKM is smaller than the total dissipation of the modeled LES-LDKM.

Note that both effects, the increased dissipation due to the particles and the reduced fluid dissipation, are at least qualitatively in agreement with the literature and desired. Since both effects act in opposite directions, the classical LES is still in acceptable agreement with the DNS even though it accounts for neither of the two effects.

We investigate the effect of LES resolution on two-way coupling statistics by conducting a coarser LES with $N^3 = 24^3$ cells of the two-way coupled simulation configuration with particles with a Stokes number $St = 2$. Figure 10 displays the results, which exhibit similar overall trends to those observed in the LES with $N^3 = 32^3$ cells. Notably, the shape of the kinetic energy spectrum of the modeled LES in Fig. 10(a) is closer to the DNS spectrum than the classical LES spectrum.

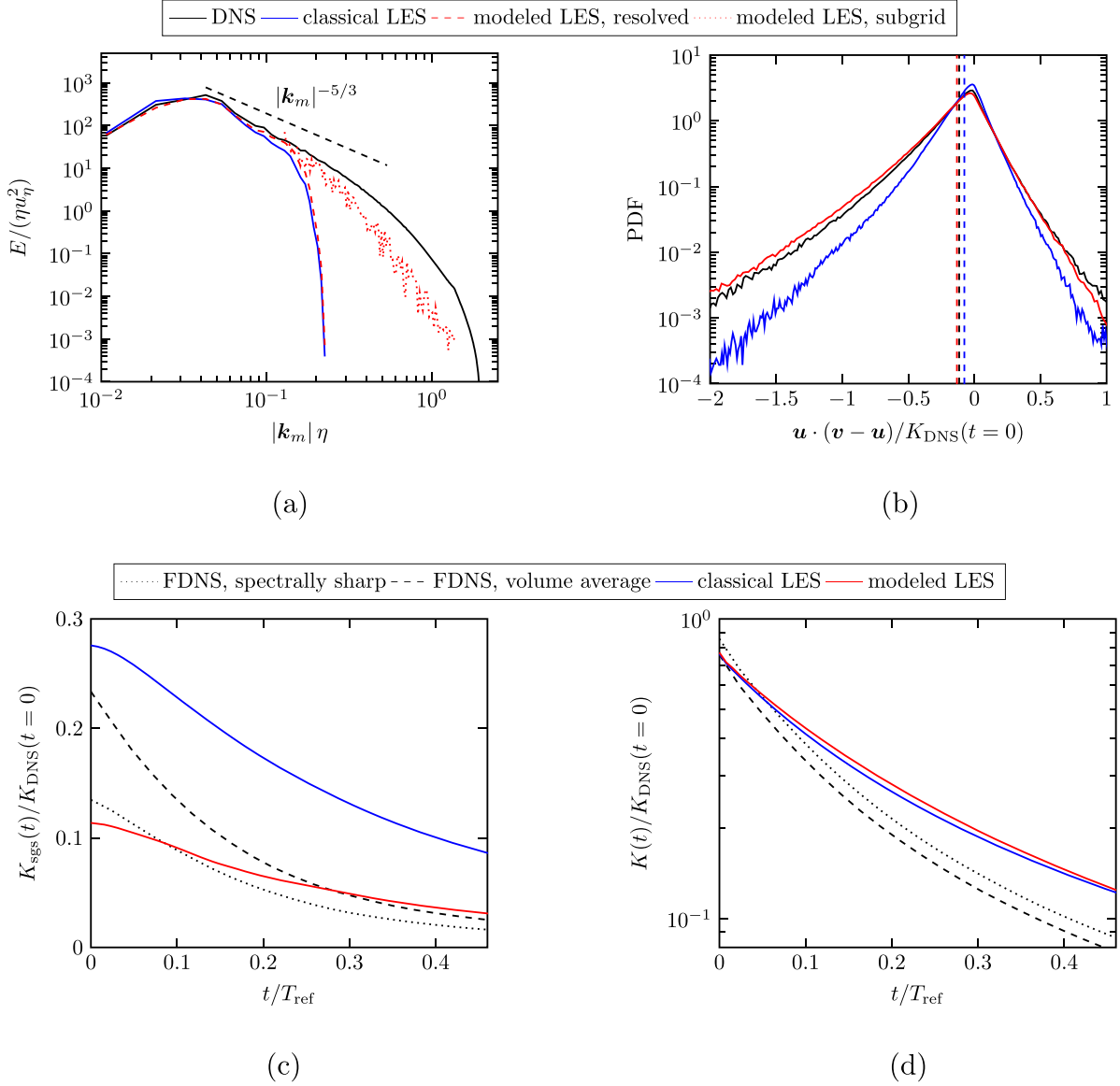


FIG. 10. Kinetic energy spectrum (a), PDF of the kinetic energy transfer between fluid and particles (b), subgrid-scale kinetic energy over time (c), and resolved kinetic energy over time (d) of decaying HIT with particles of Stokes number $St = 2$ and the flow parameters given in Table I. Compared are the results of the DNS (with a spectrally sharp filter and volume averaged), the classical LES and the modeled LES with particle source term. The LES are performed on a grid of $N^3 = 24^3$ cells.

However, the subgrid-scale kinetic energy spectrum from the modeled LES underpredicts the DNS spectrum. In Fig. 10(b), it is noticeable that the classical LES predicts a PDF of the kinetic energy transfer that is too narrow, and this discrepancy is even more pronounced than in the higher resolution case. The modeled LES yields an improved shape of the PDF and the mean when compared to the classical LES. The subgrid-scale kinetic energy of the modeled LES is smaller, which leads to better agreement with the DNS results than the modeled LES with $N^3 = 24^3$ cells. The subgrid-scale kinetic energy is shown in Fig. 10(c). As expected, the predicted subgrid-scale kinetic energies are higher than with the finer resolution. The modeled LES reduces the too high subgrid-scale kinetic energy of the classical LES but predicts too small values during the beginning of the decay. The trends of the resolved kinetic energy in Fig. 10(d) are similar to the higher resolution. Both classical LES and modeled LES predict a too-slow decay of kinetic energy. The

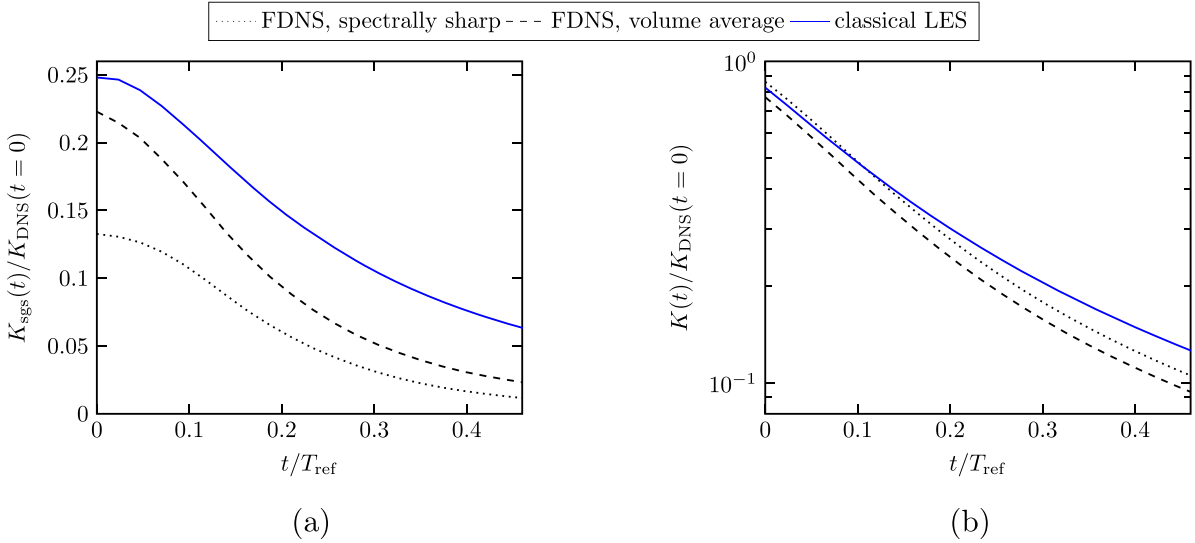


FIG. 11. Subgrid-scale kinetic energy over time (a) and resolved kinetic energy (b) of decaying HIT without particles and the flow parameters given in Table I. Compared are the results of the DNS (with a spectrally sharp filter and volume averaged) and the classical LES.

results of LES with $N^3 = 24^3$ cells suggest that the conclusions drawn for the proposed modeling framework qualitatively also apply to coarser LES.

To determine the source of the deviation of the resolved kinetic energy of the LES from the FDNS, it is instructive to investigate decaying single phase flow turbulence of the DNS and the classical LES with the LKDM. In Fig. 11, the subgrid-scale kinetic energy and the resolved kinetic energy of the classical LES are compared with DNS values that are obtained by explicit filtering. Owing to the uncertainties of the choice of the explicit filter, the spectrally sharp filtered and volume averaged DNS are both plotted. The subgrid-scale kinetic energy predicted by the LES is larger than the both estimations from the FDNS. The resolved kinetic energy of the LES shows the same discrepancy from the FDNS as the LES of the two-way coupled simulation, namely, a too-slow decay. If the subgrid-scale kinetic energy is too large and the decay of kinetic energy is too slow, it may be inferred that the primary source of error causing the inaccuracies lies in the computation of the viscosity constant C_k . On average, this constant seems to be too small, which results in the deviations of the modeled LES from the filtered DNS. It can be concluded that the introduced particle source term in the transport equation for the subgrid-scale kinetic energy plays a minor role in these inaccuracies, since the reduction of the predicted subgrid-scale kinetic energy and the increased particle dissipation are qualitatively captured by the model. The dynamical computation of C_k leaves space for future improvements of the model.

VI. CONCLUSIONS

In the present paper, we propose a model for predicting the behavior of two-way coupled particle-laden flow in the framework of LES. The model accounts for the interactions that are not captured by a classical LES of a particle-laden flow, which are (i) the prediction of the particle motion due to the missing subgrid-scale fluid velocity, (ii) the effect of the particles on the resolved flow scales, and (iii) the effect of the particles on the subgrid scales.

The proposed modeling framework consists of two components, a modeled transport equation for the subgrid-scale kinetic energy that includes a source term which accounts for the modification of the subgrid-scale kinetic energy by the particles and a model for the subgrid-scale velocity, which is used to close the particle equations of motion and the source-term in the transport equation for the subgrid-scale kinetic energy. The two model components are further coupled by directly using

the resulting subgrid-scale kinetic energy of the transport equation as input for the model for the subgrid-scale velocity that thus also accounts for the turbulence modulation of the subgrid-scales by the particles.

One-way coupled simulations are performed that are used to assess the isolated effect of missing subgrid-scale velocity in the computation of the forces acting on the particles and its modeling using the enriched LES. The proposed model accurately predicts particle pair-dispersion over a wide range of Stokes numbers using the modeled subgrid-scale velocity. Additionally, for Stokes numbers $St \geq 2$, the model accurately recovers the particle clustering observed in the corresponding DNS simulations. For the challenging case of a small Stokes number ($St = 0.5$), the model significantly improves particle clustering, while the improvement is less pronounced for $St = 1$. The improvements achieved in the enriched LES come with computational costs that are reasonable within the scope of a LES. Furthermore, two-way coupled simulations of decaying HIT are carried out that require modeling of the turbulence modulation by the particles. The coupled framework yields an increased particle dissipation compared to the classical LES by considering the modeled subgrid-scale velocity in the feedback force. The subgrid-scale fluid dissipation is decreased relative to the classical LES because the mLDKM predicts a subgrid-scale kinetic energy that considers the turbulence modulation by the particles. Both effects are in agreement with the observed physics in a DNS. As a consequence, we observe a kinetic energy spectrum with the proposed modeling that is in good agreement with the spectrum observed in the DNS. We demonstrate that the predictions of the model are only weakly affected by changes in resolution of the LES while keeping Re_λ constant. However, investigating the ability of the model to accurately predict particle-turbulence interactions as the ratio between grid spacing and the Kolmogorov length scale, Δ/η , significantly increases, is an area that requires further investigation in future studies.

Finally, it is important to mention that the proposed modeling strategy possesses the prerequisites for simulating inhomogeneous and anisotropic flows since the subgrid-scale enrichment is formulated on a grid of statistically homogeneous subdomains, which allows for spatially varying statistics. Considering this, the present modeling framework has the potential to improve the capabilities of LES of particle-laden turbulent flows for a wide range of applications.

ACKNOWLEDGMENTS

This research was funded by the Deutsche Forschungsgemeinschaft (DFG, German Research Foundation)—Project-ID No. 457509672.

APPENDIX

Figure 12 shows the radial distribution function of the one-way coupled simulations for different Stokes numbers and varying parameter α in the interpolation of the modeled subgrid-scale velocity between the subdomains. The parameter α is reduced and increased by a factor of 2 relative to the value $\alpha = 40$ that is used in the present paper, respectively. It can be observed that even for this relatively wide parameter range the radial distribution functions almost coincide. The particle clustering is thus essentially independent of α for the considered range of values.

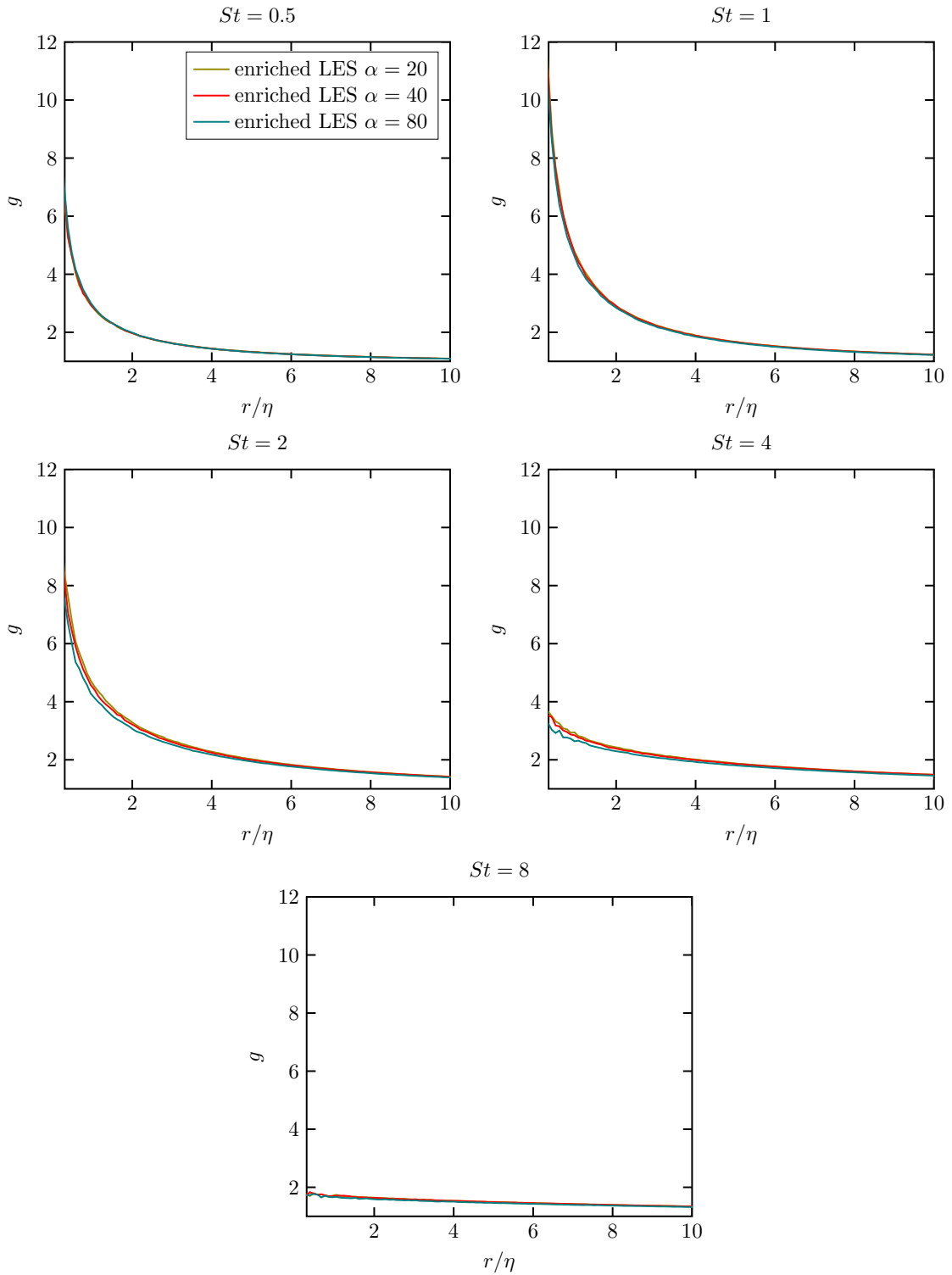


FIG. 12. Radial distribution function of the one-way coupling simulations for different Stokes numbers and different thickness constants α of the interpolation of the subgrid-scale velocity between the subdomains in forced HIT with the flow parameters given in Table I.

[1] V. Armenio, U. Piomelli, and V. Fiorotto, Effect of the subgrid scales on particle motion, *Phys. Fluids* **11**, 3030 (1999).

- [2] B. Ray and L. R. Collins, Preferential concentration and relative velocity statistics of inertial particles in Navier–Stokes turbulence with and without filtering, *J. Fluid Mech.* **680**, 488 (2011).
- [3] P. Fede and O. Simonin, Numerical study of the subgrid fluid turbulence effects on the statistics of heavy colliding particles, *Phys. Fluids* **18**, 045103 (2006).
- [4] B. Rosa and J. Pozorski, Impact of subgrid fluid turbulence on inertial particles subject to gravity, *J. Turbul.* **18**, 634 (2017).
- [5] P. Fede, O. Simonin, P. Villedieu, and K. D. Squires, Stochastic modeling of the turbulent subgrid fluid velocity along inertial particle trajectories, in *Proceedings of the Summer Program, Center for Turbulence Research, Stanford* (Citeseer, 2006), pp. 247–258.
- [6] M. Bini and W. P. Jones, Particle acceleration in turbulent flows: A class of nonlinear stochastic models for intermittency, *Phys. Fluids* **19**, 035104 (2007).
- [7] A. S. Berrouk, D. Laurence, J. J. Riley, and D. E. Stock, Stochastic modelling of inertial particle dispersion by subgrid motion for LES of high Reynolds number pipe flow, *J. Turbul.* **8**, N50 (2007).
- [8] B. Shotorban and F. Mashayek, A stochastic model for particle motion in large-eddy simulation, *J. Turbul.* **7**, N18 (2006).
- [9] J. Pozorski and S. Apte, Filtered particle tracking in isotropic turbulence and stochastic modeling of subgrid-scale dispersion, *Int. J. Multiphase Flow* **35**, 118 (2009).
- [10] M. Knorps and J. Pozorski, Stochastic modeling for subgrid-scale particle dispersion in large-eddy simulation of inhomogeneous turbulence, *Phys. Fluids* **33**, 043323 (2021).
- [11] J. G. M. Kuerten, Subgrid modeling in particle-laden channel flow, *Phys. Fluids* **18**, 025108 (2006).
- [12] B. Shotorban and F. Mashayek, Modeling subgrid-scale effects on particles by approximate deconvolution, *Phys. Fluids* **17**, 081701 (2005).
- [13] G. I. Park, M. Bassenne, J. Urzay, and P. Moin, A simple dynamic subgrid-scale model for LES of particle-laden turbulence, *Phys. Rev. Fluids* **2**, 044301 (2017).
- [14] M. Bassenne, M. Esmaily, D. Livescu, P. Moin, and J. Urzay, A dynamic spectrally enriched subgrid-scale model for preferential concentration in particle-laden turbulence, *Int. J. Multiphase Flow* **116**, 270 (2019).
- [15] J. A. Domaradzki and K.-C. Loh, The subgrid-scale estimation model in the physical space representation, *Phys. Fluids* **11**, 2330 (1999).
- [16] B. Ray and L. R. Collins, A subgrid model for clustering of high-inertia particles in large-eddy simulations of turbulence, *J. Turbul.* **15**, 366 (2014).
- [17] Z. Zhou, S. Wang, X. Yang, and G. Jin, A structural subgrid-scale model for the collision-related statistics of inertial particles in large-eddy simulations of isotropic turbulent flows, *Phys. Fluids* **32**, 095103 (2020).
- [18] S. Murray, M. F. Lightstone, and S. Tullis, Single-particle Lagrangian and structure statistics in kinematically simulated particle-laden turbulent flows, *Phys. Fluids* **28**, 033302 (2016).
- [19] G. Mallouppas, W. George, and B. van Wachem, Dissipation and inter-scale transfer in fully coupled particle and fluid motions in homogeneous isotropic forced turbulence, *Int. J. Heat Fluid Flow* **67**, 74 (2017).
- [20] A. Ferrante and S. Elghobashi, On the physical mechanisms of two-way coupling in particle-laden isotropic turbulence, *Phys. Fluids* **15**, 315 (2003).
- [21] R. Letournel, F. Laurent, M. Massot, and A. Vié, Modulation of homogeneous and isotropic turbulence by sub-Kolmogorov particles: Impact of particle field heterogeneity, *Int. J. Multiphase Flow* **125**, 103233 (2020).
- [22] M. Boivin, O. Simonin, and K. D. Squires, Direct numerical simulation of turbulence modulation by particles in isotropic turbulence, *J. Fluid Mech.* **375**, 235 (1998).
- [23] M. Nabavi, M. Di Renzo, and J. Kim, Modulation of interphase, cross-scale momentum transfer of turbulent flows by preferentially concentrated inertial particles, *Phys. Rev. Fluids* **7**, 044305 (2022).
- [24] P. Sagaut, *Large Eddy Simulation for Incompressible Flows*, 3rd ed. (Springer, Berlin, 2005).
- [25] M. Boivin, O. Simonin, and K. D. Squires, On the prediction of gas–solid flows with two-way coupling using large eddy simulation, *Phys. Fluids* **12**, 2080 (2000).
- [26] N. Rohilla, P. Muramulla, and P. S. Goswami, Applicability of large eddy simulations to capture turbulence attenuation in particle-laden channel flows, *Phys. Rev. Fluids* **7**, 024302 (2022).

- [27] S. Yuu, T. Ueno, and T. Umekage, Numerical simulation of the high Reynolds number slit nozzle gas-particle jet using subgrid-scale coupling large eddy simulation, *Chem. Eng. Sci.* **56**, 4293 (2001).
- [28] S. Pannala and S. Menon, On LEM/LES methodology for two-phase flows, in *35th Joint Propulsion Conference and Exhibit* (American Institute of Aeronautics and Astronautics, Los Angeles, CA, 1999).
- [29] V. Sankaran and S. Menon, LES of spray combustion in swirling flows, *J. Turbul.* **3**, N11 (2002).
- [30] W.-W. Kim and S. Menon, An unsteady incompressible Navier-Stokes solver for large eddy simulation of turbulent flows, *Int. J. Numer. Methods Fluids* **31**, 983 (1999).
- [31] S. Menon, P.-K. Yeung, and W.-W. Kim, Effect of subgrid models on the computed interscale energy transfer in isotropic turbulence, *Computers & Fluids* **25**, 165 (1996).
- [32] M. Hausmann, F. Evrard, and B. van Wachem, An efficient model for subgrid-scale velocity enrichment for large-eddy simulations of turbulent flows, *Phys. Fluids* **34**, 115135 (2022).
- [33] M. Maxey, Simulation methods for particulate flows and concentrated suspensions, *Annu. Rev. Fluid Mech.* **49**, 171 (2017).
- [34] T. B. Anderson and R. Jackson, A fluid mechanical description of fluidized beds, *I and EC Fundamentals* **6**, 527 (1967).
- [35] J. G. M. Kuerten, Point-particle DNS and LES of particle-laden turbulent flow—a state-of-the-art review, *Flow, Turbul. Combust.* **97**, 689 (2016).
- [36] C. T. Crowe, M. P. Sharma, and D. E. Stock, The particle-source-in cell/PSI-CELL/model for gas-droplet flows, *J. Fluids Eng.* **99**, 325 (1977).
- [37] U. Schumann, Subgrid scale model for finite difference simulations of turbulent flows in plane channels and annuli, *J. Comput. Phys.* **18**, 376 (1975).
- [38] G. Mallouppas and B. van Wachem, Large eddy simulations of turbulent particle-laden channel flow, *Int. J. Multiphase Flow* **54**, 65 (2013).
- [39] P. L. Johnson, On the role of vorticity stretching and strain self-amplification in the turbulence energy cascade, *J. Fluid Mech.* **922**, A3 (2021).
- [40] D. K. Lilly, The representation of small scale turbulence in numerical simulation experiments, in *Proceedings of the IBM Scientific Computing Symposium on Environmental Sciences, Yorktown, NY, USA*, National Center for Atmospheric Research (USA), NCAR Manuscript No. 281 (1966), pp. 195–210.
- [41] W.-W. Kim, S. Menon, W.-W. Kim, and S. Menon, Application of the localized dynamic subgrid-scale model to turbulent wall-bounded flows, in *35th Aerospace Sciences Meeting and Exhibit* (American Institute of Aeronautics and Astronautics, Reno, NV, 1997).
- [42] M. Germano, U. Piomelli, P. Moin, and W. H. Cabot, A dynamic subgrid-scale eddy viscosity model, *Phys. Fluids A* **3**, 1760 (1991).
- [43] J.-P. Laval, B. Dubrulle, and S. Nazarenko, Nonlocality and intermittency in three-dimensional turbulence, *Phys. Fluids* **13**, 1995 (2001).
- [44] V. M. Canuto and M. S. Dubovikov, A dynamical model for turbulence. I. General formalism, *Phys. Fluids* **8**, 571 (1996).
- [45] A. Yoshizawa, Statistical theory for compressible turbulent shear flows, with the application to subgrid modeling, *Phys. Fluids* **29**, 2152 (1986).
- [46] P. Moin, K. Squires, W. Cabot, and S. Lee, A dynamic subgrid-scale model for compressible turbulence and scalar transport, *Phys. Fluids* **3**, 2746 (1991).
- [47] F. Denner, F. Evrard, and B. van Wachem, Conservative finite-volume framework and pressure-based algorithm for flows of incompressible, ideal-gas and real-gas fluids at all speeds, *J. Comput. Phys.* **409**, 109348 (2020).
- [48] P. Bartholomew, F. Denner, M. Abdol-Azis, A. Marquis, and B. van Wachem, Unified formulation of the momentum-weighted interpolation for collocated variable arrangements, *J. Comput. Phys.* **375**, 177 (2018).
- [49] G. Mallouppas, W. K. George, and B. van Wachem, New forcing scheme to sustain particle-laden homogeneous and isotropic turbulence, *Phys. Fluids* **25**, 083304 (2013).
- [50] L. Verlet, Computer “e” on classical fluids. I. Thermodynamical properties of Lennard-Jones molecules, *Phys. Rev.* **159**, 98 (1967).

- [51] L. Schiller and A. Naumann, über die grundlegenden Berechnungen bei der Schwerkraftaufbereitung, *Z. Ver. Dtsch. Ing.* **77**, 318 (1933).
- [52] G. Tóth and P. Roe, Divergence- and curl-preserving prolongation and restriction formulas, *J. Comput. Phys.* **180**, 736 (2002).
- [53] C. Marchioli, Large-eddy simulation of turbulent dispersed flows: A review of modelling approaches, *Acta Mech.* **228**, 741 (2017).
- [54] M. R. Maxey, The gravitational settling of aerosol particles in homogeneous turbulence and random flow fields, *J. Fluid Mech.* **174**, 441 (1987).
- [55] L. Brandt and F. Coletti, Particle-laden turbulence: Progress and perspectives, *Annu. Rev. Fluid Mech.* **54**, 159 (2022).
- [56] Y. Xu and S. Subramaniam, Consistent modeling of interphase turbulent kinetic energy transfer in particle-laden turbulent flows, *Phys. Fluids* **19**, 085101 (2007).

A.3 Paper III

Wavelet-based modeling of subgrid scales in large-eddy simulation of particle-laden turbulent flows

M. Hausmann, F. Evrard, B. van Wachem

Published in *Physical Review Fluids* 8, 104604 (2023)

Wavelet-based modeling of subgrid scales in large-eddy simulation of particle-laden turbulent flows

M. Hausmann , F. Evrard *, and B. van Wachem †

*Chair of Mechanical Process Engineering, Otto-von-Guericke-Universität Magdeburg,
Universitätsplatz 2, 39106 Magdeburg, Germany*



(Received 17 May 2023; accepted 5 October 2023; published 24 October 2023)

We propose a model to obtain the subgrid-scale velocity in the context of large-eddy simulation (LES) of particle-laden turbulent flows, to recover accurate particle statistics. In our wavelet enrichment model, the subgrid-scale velocity is discretized with a divergence-free wavelet vector basis, and the coefficients of the expansion are obtained by minimizing the squared error of the linearized subfilter Navier-Stokes equations (SFNSE). The compact support of the wavelet basis is exploited to achieve continuously varying subgrid-scale velocity statistics across the domain. The performance of our wavelet enrichment model is evaluated in single-phase and particle-laden flow simulations, comparing the results with the results of direct numerical simulations (DNS). The simulations show that the model can generate inhomogeneous and anisotropic velocity statistics, accurate strain-rotation relations, and a good approximation of the kinetic energy spectrum of the corresponding DNS. Furthermore, the model significantly improves the prediction of the particle-pair dispersion, the clustering of the particles, and the turbulence modulation by particles in two-way coupled simulations. The proposed model recovers the most important interactions between fluid turbulence and the behavior of the particles, while maintaining the computational cost on the order of an LES.

DOI: [10.1103/PhysRevFluids.8.104604](https://doi.org/10.1103/PhysRevFluids.8.104604)

I. INTRODUCTION

The understanding of the underlying physics of the interactions between turbulence and particles has attracted a lot of research interest for many decades, because of its ubiquity in natural and industrial processes. The only way to capture the most important complex phenomena of these multiphase flows numerically is to perform direct numerical simulation (DNS), which resolves the turbulent length- and timescales down to the Kolmogorov scales. In single-phase turbulence, extensive research and model development have enabled good predictions of turbulence statistics with computational costs significantly smaller than the costs of a DNS. One of the methods that achieves this is large-eddy simulation (LES), which resolves the large flow structures with the numerical grid while modeling the effect of the smaller, unresolved scales. The success of LES in single-phase turbulence does not apply to particle-laden flows, since various interactions between the phases are not captured by existing LES models.

The dispersion and preferential concentration of particles in the turbulent flow can be very different if they are transported with the filtered fluid velocity field instead of the fluid velocity

*Also at Sibley School of Mechanical and Aerospace Engineering, Cornell University, Ithaca, New York 14853, USA.

†berend.vanwachem@ovgu.de

field that contains the full turbulent spectrum [1–4]. A solution to this is to model the unresolved fluid velocity at each particle position.

The reconstruction of the subgrid-scale fluid velocity field, even in the absence of particles, has been a topic of interest for decades, which explains the large variety of existing models. The majority of these models, however, suffers from drawbacks that make them unsuitable for the application to particle-laden turbulent flows.

A well-known method to generate a fictitious subgrid-scale fluid velocity field is the kinematic simulation that approximates the fluid velocity field as a truncated Fourier series with coefficients that are chosen from a Gaussian distribution, such that a given kinetic energy spectrum is achieved, and the resulting velocity field is divergence-free [5–7]. Since real turbulence is typically not Gaussian and potentially statistically inhomogeneous and anisotropic, the kinematic simulation does not provide a realistic turbulent field. The subgrid-scale velocity field can also be reconstructed by fractal interpolation as proposed by Scotti and Meneveau [8]. Even though the model is computationally cheap, no physical knowledge of turbulence is incorporated. Domaradzki and Loh [9] proposed a velocity field extrapolation method for the velocity field on a refined grid using explicit filtering of the nonlinear advective term in the Navier-Stokes equations. Without further modification, however, the resulting velocity field is not divergence-free. Another family of models either solves the subfilter Navier-Stokes equations (SFNSE) with a simplifying numerical method such as, e.g., partially freezing the velocity field [10], or model the SFNSE itself [11–15]. Even though accurate predictions are reported, the models can be computationally expensive or may introduce assumptions that cannot be justified in some contexts [16].

Approaches that approximate turbulent velocity fields inspired the development of models for LES of particle-laden flows. A class of models emerged that solve a stochastic differential equation for every particle independently (see, e.g., Refs. [17–22]), which turns out to be versatile and computationally efficient. By construction, however, these models predict poor particle pair statistics, and their results strongly depend on the choice of model parameters [23]. Improved particle statistics are observed with models that apply a deconvolution operator on the LES velocity field [24–26], but these models merely modify the velocity field on the LES grid and do not augment the range of modeled scales. Bassenne *et al.* [27] combine the dynamical deconvolution of Park *et al.* [26] with the subgrid extrapolation of Domaradzki and Loh [9] and obtain realistic particle clustering with LES of homogeneous isotropic turbulence (HIT) and for a wide range of Stokes numbers. The high computational cost, originating from a divergence-free projection on a very fine grid, make this model unsuitable for LES. Recently, Hausmann *et al.* [28] proposed a model that solves the linearized SFNSE with Fourier basis functions in statistically homogeneous subdomains and apply it to particle-laden turbulent flows. In LES of HIT, the model mainly recovers particle pair dispersion and clustering of the corresponding DNS for particles of many Stokes numbers. Because of the statistically homogeneous subdomains, however, the subgrid-scale velocity field is partially discontinuous and requires interpolation.

In the present work, we derive a model for predicting the subgrid-scale fluid velocity field that recovers characteristic properties of turbulence, while maintaining computational costs that are acceptable in the scope of an LES. To obtain the right particle statistics and clustering, the modeled subgrid-scale velocity field is expected to have realistic spatial and temporal correlations, strain-rotation relations, and non-Gaussian distributions of, e.g., the fluid velocity gradients. A model for the subgrid-scale velocity must also be able to generate statistically inhomogeneous and anisotropic velocity fields.

In our model, the SFNSE are linearized by means of the rapid distortion theory and approximately solved by minimizing their squared error. The discrete solution spaces are spanned by divergence-free wavelet vector functions. The narrow support of the wavelet basis in physical and spectral space allows for spatially varying fluid velocity statistics and localization in spectral space, that is required to control the kinetic energy spectrum. Conceptually, the wavelet enrichment is superior to Fourier enrichment, which requires special treatment, such as statistically homogeneous subdomains, to generate an inhomogeneous subgrid-scale velocity field [15]. Divergence-free

wavelet vector bases are also used by Letournel [29] to generate a turbulent velocity field by transporting the wavelet coefficients by a stochastic Langevin model. In the proposed model, however, a transport equation for the wavelet coefficients is derived that minimizes the error in the momentum balance. Other application of wavelets in reduced order turbulence modeling include the modeling of the subgrid-scale stress tensor in the scope of LES, by applying a wavelet transform to the resolved fluid velocity (see, e.g., Denev *et al.* [30]), which models the effect of the subgrid-scale velocity on the resolved scales but not the subgrid-scale velocity itself. A different approach involves performing LES with adaptive mesh refinement based on a wavelet decomposition of the resolved velocity. This approach employs thresholding to preserve only the most energetic scales, in contrast to the standard LES, which preserves only the largest scales (see, e.g., De Stefano and Vasilyev [31]). In contrast to the present work, however, the unresolved scales are not reconstructed. In a related study, Xiong *et al.* [32] study the particle statistics of particles transported with the fluid velocity field of an LES with wavelet-based adaptive mesh refinement (corresponding to the energetically optimal wavelet filtered DNS) and compare it to the statistics of particles transported with the fluid velocity field of a standard LES. It is concluded that the right particle statistics can be better recovered if the most energetic fluid velocity structures are used to transport the particles instead of the largest structures, which are resolved in a standard LES. In a subsequent study, they apply the dynamical deconvolution method of Park *et al.* [26] to the wavelet filtered DNS [33]. However, no model is proposed that can be applied to a standard LES to account for the unresolved fluid velocity field on the particle motion.

Even though the literature on LES of particle-turbulence interaction is dominated by studies and models for the subgrid-scale velocity at the particle positions, to enable one-way coupled simulations, more modeling is required in the case of two-way coupled simulations (i.e., where the turbulence modification by the particles is taken into account). Recently, Hausmann *et al.* [28] proposed a modeling framework that models the two-way coupling effects in an LES, caused by the unresolved fluid velocity field.

The paper is outlined as follows. The wavelet enrichment is derived in Sec. II, and the background of the governing equations and the wavelet basis is provided. In Sec. III, we introduce the simulation configuration that we use to evaluate the performance of the wavelet enrichment. The results and validation for single-phase and particle-laden flows are given in Sec. IV before the paper is concluded in Sec. V.

II. WAVELET MODEL FOR THE SUBGRID-SCALE VELOCITY

In this section, we describe the wavelet enrichment for the subgrid-scale velocity. The subgrid-scale fluid velocity field is projected onto a wavelet basis, and the coefficients of the expansion are determined by locally minimizing the mean-squared error of the linearized SFNSE.

A. Scale decomposition

LES is based on separating the flow into large-scale contributions and small-scale contributions. This is realized mathematically by filtering a quantity φ [34]:

$$\tilde{\varphi}(x) = \int_{-\infty}^{\infty} G(x - \xi)\varphi(\xi)d\xi, \quad (1)$$

where $\tilde{\cdot}$ indicates a filtered quantity and G is the filter kernel. Subfilter quantities are given by $\varphi' = \varphi - \tilde{\varphi}$, which we also refer to as subgrid-scale quantities in the scope of LES. Filtering the Navier-Stokes equations (NSE) of an incompressible fluid with constant density ρ_f and kinematic viscosity ν_f yields the filtered Navier-Stokes equations (FNSE):

$$\frac{\partial \tilde{u}_i}{\partial x_i} = 0, \quad (2)$$

$$\frac{\partial \tilde{u}_i}{\partial t} + \tilde{u}_j \frac{\partial \tilde{u}_i}{\partial x_j} = -\frac{1}{\rho_f} \frac{\partial \tilde{p}}{\partial x_i} + \nu_f \frac{\partial^2 \tilde{u}_i}{\partial x_j \partial x_j} - \frac{\partial \tau_{ij}}{\partial x_j} + \tilde{s}_i, \quad (3)$$

where u_i is the velocity and p is the pressure. The source term s_i represents, for instance, the momentum coupling of a second phase or a forcing to maintain statistically stationary turbulence. The subgrid-scale stress tensor accounts for the influence of the subgrid scales on the filtered scales and is given by

$$\tau_{ij} = \widetilde{u_i u_j} - \tilde{u}_i \tilde{u}_j. \quad (4)$$

By subtracting the FNSE from the NSE, the governing equations for the subgrid-scale fluid velocity are obtained. In models for the subgrid-scale velocity, the nonlinear term in the SFNSE is often omitted, or replaced by, a turbulent viscosity [11,12,14,15,35]. The resulting linearized SFNSE can be written as

$$\frac{\partial u'_i}{\partial x_i} = 0, \quad (5)$$

$$\frac{\partial u'_i}{\partial t} + \tilde{u}_j \frac{\partial u'_i}{\partial x_j} + u'_j \frac{\partial \tilde{u}_i}{\partial x_j} = -\frac{1}{\rho_f} \frac{\partial p'}{\partial x_i} + (\nu_f + \nu'_t) \frac{\partial^2 u'_i}{\partial x_j \partial x_j} + \frac{\partial \tau_{ij}}{\partial x_j} + s'_i. \quad (6)$$

The turbulent viscosity can be derived from renormalization groups [36]:

$$\nu'_t(k) = \left(\nu_f^2 + \frac{2}{5} \int_k^\infty q^{-2} E(q) dq \right)^{1/2} - \nu_f, \quad (7)$$

where $E(k)$ is the kinetic energy spectrum of the wave number k . The replacement of the nonlinear term with a turbulent viscosity can be justified energetically and by means of their contribution to intermittency [35]. Similar to subgrid-scale models relying on the Boussinesq hypotheses, however, the linearization mistakenly assumes an alignment of the eigenvectors of the subgrid-scale stress tensor with those of the fluid velocity gradient tensor (see, e.g., Horiuti [37]). Therefore, the use of an eddy viscosity, may it be in the SFNSE or LES subgrid-scale models, are only justified energetically. Furthermore, the derivation of Eq. (7) relies on the assumption homogeneous isotropic turbulence [36]. We justify its use in inhomogeneous and anisotropic configurations by the fact that the small velocity scales, which are reconstructed in the proposed model, are typically much more homogeneous and isotropic than the large scales. This is a typical assumption for modeling the subgrid-scale stress tensor [16].

Similar to our recently proposed model, we aim to efficiently solve the linearized SFNSE to approximate the subgrid-scale fluid velocity field. Instead of expanding the subgrid-scale fluid velocity field in Fourier space [15], we approximate it as a finite series of wavelet basis functions. The rapidly decaying support of a wavelet basis in spectral and physical space enables a model that incorporates spectral space information and spatial inhomogeneities.

B. Multiresolution analysis

A Fourier series consists of basis functions (i.e., sines and cosines) that are perfectly localized in spectral space (they can be associated to exactly one wave number), but it has no localization in physical space (it is unknown where a frequency occurs). Convoluting the trigonometric basis functions of a Fourier series with a Gaussian window function enables localization of the spectral information in physical space. This is known as the discrete Gabor transform (see, e.g., Ref. [38]). Because of the constant window size, the low wave numbers tend to be spectrally underresolved and high wave numbers spatially underresolved. In fact, it is more appropriate to provide a wide physical support for small wave numbers and a narrow physical support for large wave numbers. A multiresolution analysis (MRA) applies this idea [38,39]. A MRA uses scaling functions ϕ and wavelets ψ as basis functions, that have compact support (or at least decay rapidly) in physical and spectral space. The scaling functions and the wavelets are elements of function spaces, which

have specific properties. We consider subspaces of the Lebesgue space $(V_j)_{j \in \mathbb{Z}} \subset L^2(\mathbb{R})$, where the index j can be understood as an indicator of the range of wave numbers the functions possess that are deduced from the respective subspace. Functions that belong to subspaces of a large index j contain higher wave numbers than functions belonging to subspaces of a smaller index j . In the context of turbulence, that means that functions deduced from a subspace approximate eddies of a particular range of size, whereas a larger index corresponds to smaller eddies. The subspaces V_j have the following properties [39]:

- (i) the subspaces are nested $V_j \subset V_{j+1}$,
- (ii) their intersection is zero $\bigcap_{j \in \mathbb{Z}} V_j = \{0\}$,
- (iii) $\bigcup_{j \in \mathbb{Z}} V_j$ is dense in $L^2(\mathbb{R})$,
- (iv) they are invariant with respect to scaling $f \in V_j \iff f(2 \cdot) \in V_{j+1}$, and
- (v) they are invariant with respect to translation $f \in V_j \implies f(\cdot - k) \in V_j, \forall k \in \mathbb{Z}$.

One can imagine the functions of a subspace to represent a prototype eddy that is scaled in size, shifted in space, and superposed. Complementary spaces to V_j can be defined such that

$$V_{j+1} = V_j \oplus W_j. \quad (8)$$

Every function $f \in V_{j+1}$ is either $f \in V_j$ or $f \in W_j$, but not both. Consequently, we can decompose the $L^2(\mathbb{R})$ as

$$L^2(\mathbb{R}) = V_0 \bigoplus_{j=0}^{\infty} W_j. \quad (9)$$

From the so-called scaling function, or father wavelet, $\phi \in V_0$ and mother wavelet $\psi \in W_0$ functions are deduced such that V_j is spanned by $\{\phi_{j,k}; j, k \in \mathbb{Z}\}$ and W_j is spanned by $\{\psi_{j,k}; j, k \in \mathbb{Z}\}$:

$$\phi_{j,k}(\xi) = \phi(2^j \xi - k), \quad (10)$$

$$\psi_{j,k}(\xi) = \psi(2^j \xi - k). \quad (11)$$

Thus, a function $f \in L^2(\mathbb{R})$ may be expressed with a basis of scaling functions and wavelet functions

$$f(\xi) = \sum_{k \in \mathbb{Z}} c_{0,k} \phi_{0,k}(\xi) + \sum_{j \geq 0} \sum_{k \in \mathbb{Z}} d_{j,k} \psi_{j,k}(\xi). \quad (12)$$

Note that it is common to scale $\phi_{j,k}$ and $\psi_{j,k}$ with a factor of $2^{j/2}$. For simplicity, we absorb this factor in the coefficients $c_{0,k}$ and $d_{j,k}$.

The mother scaling function is defined by the low pass filter

$$\phi\left(\frac{\xi}{2}\right) = \sum_{k \in \mathbb{Z}} h_k \phi(\xi - k), \quad (13)$$

and the mother wavelet function is defined by the high pass filter

$$\psi\left(\frac{\xi}{2}\right) = \sum_{k \in \mathbb{Z}} g_k \phi(\xi - k). \quad (14)$$

The coefficients h_k, g_k characterize the different scaling functions and wavelets with different properties. We express the subgrid-scale velocity as a finite sum of divergence-free wavelet vector basis function as derived by Lemarié-Rieusset [40]

$$\mathbf{u}'(\mathbf{x}) = \sum_{j=j_{\min}}^{j_{\max}} \sum_{\mathbf{k}} \sum_{\epsilon} d_{\text{div},j,\mathbf{k}}^{\epsilon} \boldsymbol{\Psi}_{\text{div},j,\mathbf{k}}^{\epsilon}[\boldsymbol{\xi}(\mathbf{x})], \quad (15)$$

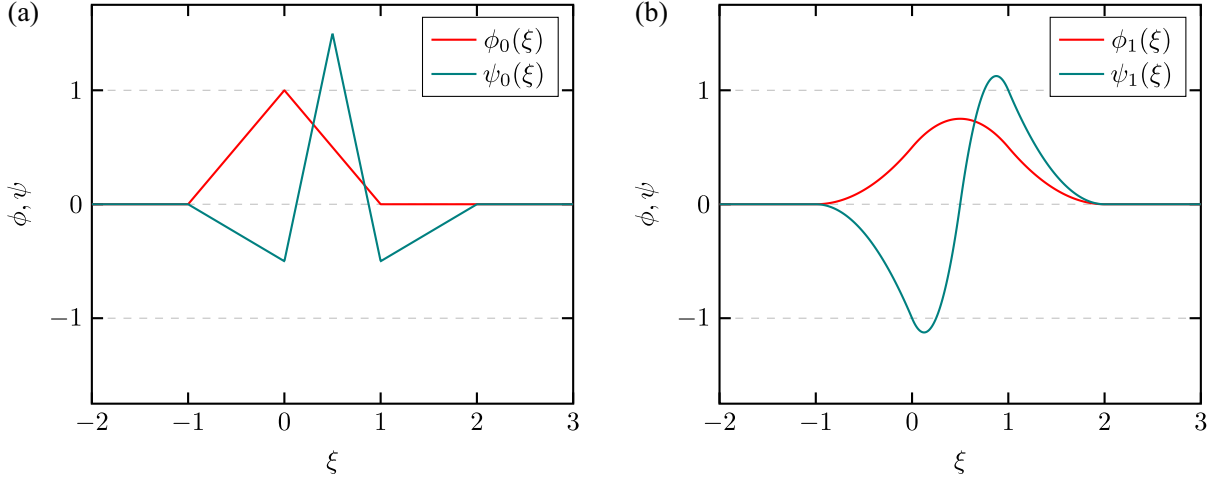


FIG. 1. Plot of the piecewise linear (a) and piecewise quadratic (b) spline scaling and wavelet functions.

where $d_{\text{div},j,k}^\epsilon$ are the wavelet coefficients, $\Psi_{\text{div},j,k}^\epsilon$ are divergence-free wavelet vector basis functions, j_{min} and j_{max} the limits of the considered levels, and $\xi(\mathbf{x})$ is a mapping from physical space coordinates \mathbf{x} to the reference coordinates ξ . The index ϵ specifies one of the 14 basis vector functions such that $\Psi_{\text{div},j,k}^\epsilon$ form a Riesz basis of the space of divergence-free vector functions in \mathbb{R}^3 [41]. Note that 21 basis vector functions are required to span the whole \mathbb{R}^3 , and the projection onto the divergence free subspace reduces the number of basis vector functions to 14. The derivation of the basis functions and their exact expressions is relatively lengthy and can be found in Deriaz and Perrier [41]. Therefore, we do not repeat the derivation in the present work. The divergence-free vector functions are composed of four one-dimensional compactly supported spline functions that are depicted in Fig. 1 and defined by the coefficients h_k, g_k (in the proposed model similar to coefficients given by Deriaz and Perrier [41] but multiplied with a factor $\sqrt{2}$).

The mapping from physical coordinates to reference coordinates is given as

$$\xi_i(x_i) = (x_i - x_{i,\text{min}})/(x_{i,\text{max}} - x_{i,\text{min}}), \quad (16)$$

where $x_{i,\text{min}}$ and $x_{i,\text{max}}$ are the limits of the cuboid domain. With the given mapping a periodic basis can be realized for $j \geq 3$, which is the first level with a support smaller than one.

C. Local least-squares approximation of the model equations

The subgrid-scale fluid velocity field lies within the space of divergence free vector functions in \mathbb{R}^3 . Hence, it can be expressed as an infinite series of wavelet vector functions $\Psi_{\text{div},j,k}^\epsilon$ and coefficients $d_{\text{div},j,k}^\epsilon$. We are searching coefficients of the finite series expansion Eq. (15), such that the subgrid-scale fluid velocity field is approximated well, which is divergence-free and conserves momentum at least by fulfilling the linearized momentum equation (6). With the expansion of the subgrid-scale velocity with the divergence-free vector functions, the former is satisfied immediately. The latter is achieved by a least-squares approximation, which is explained in the following.

The advective term in the linearized SFNSE can be Helmholtz decomposed in a divergence-free and a curl-free contribution. Since we seek a solution in the divergence-free wavelet vector space, the curl-free contribution can be dropped together with the pressure term, which gives

$$\frac{\partial u_i'}{\partial t} + \mathcal{A}_i^\perp = \mathcal{D}_i + \mathcal{F}_i^\perp, \quad (17)$$

where $\mathcal{A}_i^\perp = (\tilde{u}_j \frac{\partial u_i'}{\partial x_j} + u_j' \frac{\partial \tilde{u}_i}{\partial x_j})^\perp$ is an abbreviation for the projected advective term, $\mathcal{D}_i = (v_f + v_i') \frac{\partial^2 u_i'}{\partial x_j \partial x_j}$ for the diffusive term, and $\mathcal{F}_i^\perp = (\frac{\partial \tau_{ij}}{\partial x_j})^\perp$ for the projected forcing term, which originates

from the subgrid-scale stress tensor and mainly supplies the subgrid-scale velocity field with kinetic energy (further details in Appendix B).

Minimizing the squared error of Eq. (17) over the whole domain results in the well known Galerkin method, which we refer to as globally optimal solution.

If the vector valued error of a differential equation at time t and point \mathbf{x} is given as $\mathcal{E}_i(t, \mathbf{x})$, the optimal solution is achieved if

$$\int \mathcal{E}_i(t, \mathbf{x}) \mathcal{E}_i(t, \mathbf{x}) dV_x$$

is minimal. This can be achieved by adjusting the coefficients $d_{\text{div},j,k}^\epsilon$ of the discretized solution such that a stationary point is found, which corresponds to a minimum.

To make the solution for the coefficients affordable in the scope of an LES, we seek locally optimal solutions for every j and k independently:

$$\frac{\partial}{\partial d_{\text{div},j,k}^{\zeta,n+1}} \int \left[\frac{\mathbf{u}'_{j,k}{}^{n+1} - \mathbf{u}'_{j,k}{}^n}{\Delta t} + \mathcal{A}_{j,k}^\perp - \mathcal{D}_{j,k} - \mathcal{F}_{j,k}^\perp \right]^2 dV_x = 0, \quad (18)$$

which yields the condition

$$\int \left[\frac{\mathbf{u}'_{j,k}{}^{n+1} - \mathbf{u}'_{j,k}{}^n}{\Delta t} + \mathcal{A}_{j,k}^\perp - \mathcal{D}_{j,k} - \mathcal{F}_{j,k}^\perp \right] \cdot \Psi_{\text{div},j,k}^\zeta[\xi(\mathbf{x})] dV_x = 0. \quad (19)$$

The fluid velocity field local in j and k , which we also refer to as local wave packets, is given as

$$\mathbf{u}'_{j,k}(\mathbf{x}) = \sum_{\epsilon} d_{\text{div},j,k}^\epsilon \Psi_{\text{div},j,k}^\epsilon[\xi(\mathbf{x})], \quad (20)$$

and $\mathcal{A}_{j,k}^\perp$, $\mathcal{D}_{j,k}$, and $\mathcal{F}_{j,k}^\perp$ are the projected advective, diffusive, and projected forcing term, as a function of the local velocity wave packets, respectively. The time derivative is discretized with an explicit Euler-scheme, where n indicates the time level.

Relaxing the global optimality condition to local j, k avoids the solution of a large equation system of size $14N_k \times 14N_k$. Instead, we invert N_k systems of size 14×14 . Note that the matrix is always identical, and in practice only one inversion of the 14×14 matrix is required. The linear nature of the projected linearized SFNSE (17) allows for superposition of solutions, such as the approximated solutions for the local wave packets $\mathbf{u}'_{j,k}(\mathbf{x})$. If the local wave packets would perfectly satisfy Eq. (17), then their superposition would also satisfy Eq. (17). Since $\mathbf{u}'_{j,k}(\mathbf{x})$ is a numerical approximation, the discretization errors add up by superposing the solutions and, in total, lead to an error that is larger than the solutions of the global optimization using the Galerkin method. However, only with the localization of the optimization, and the associated increase of the numerical error compared to the Galerkin method, the solution for the subgrid-scale velocity field becomes computational feasible in the scope of LES. Together with the linearization of the SFNSE, the localization of the optimization constitutes the main assumption of our wavelet model.

Since the wavelet basis possesses no degrees of freedom in the space that is orthogonal to the divergence-free $[L^2(\mathbb{R}^3)]^3$, no explicit projection of the advective term is required to obtain a divergence-free subgrid-scale velocity. The projected advective term is obtained by expanding it in a series of wavelet basis functions (similar to the subgrid-scale velocity field) and solving the following problem:

$$\langle \mathcal{A}_{j,k}^\perp | \Psi_{\text{div},j,k}^\epsilon \rangle = \langle \mathcal{A}_{j,k} | \Psi_{\text{div},j,k}^\epsilon \rangle, \quad (21)$$

where $\langle \cdot | \cdot \rangle$ indicates the inner product. Equation (19) is solved with the resulting coefficients, which leads to the same discrete equations as using $\mathcal{A}_{j,k}$ without prior projection in Eq. (19).

Note the solution of Eq. (19) is guaranteed to produce the energetically optimal coefficients, because the Hessian

$$\begin{aligned} \mathcal{H}_{j,k} &= \mathcal{H}_{j,k}^{\epsilon,\zeta} = \frac{\partial^2}{\partial d_{\text{div},j,k}^{\epsilon,n+1} \partial d_{\text{div},j,k}^{\zeta,n+1}} \int \left[\frac{\mathbf{u}'_{j,k}{}^{n+1} - \mathbf{u}'_{j,k}{}^n}{\Delta t} + \mathcal{A}_{j,k}^\perp - \mathcal{D}_{j,k} - \mathcal{F}_{j,k}^\perp \right]^2 dV_x \\ &= \frac{2}{\Delta t^2} \int \Psi_{\text{div},j,k}^\epsilon[\boldsymbol{\xi}(\mathbf{x})] \cdot \Psi_{\text{div},j,k}^\zeta[\boldsymbol{\xi}(\mathbf{x})] dV_x, \end{aligned} \quad (22)$$

is positive-definite, i.e., $\mathbf{v}^T \mathcal{H}_{j,k} \mathbf{v} > 0$, $\forall \mathbf{v} \in \mathbb{R}^{14} \setminus \{\mathbf{0}\}$. It follows that Eq. (18) constitutes a convex optimization problem and the solution has always a minimal error.

For a solution of Eq. (19) to exist, all terms of Eq. (19) must be integratable and finite, which means that the following expression have to be satisfied:

- (i) $\int \Psi_{\text{div},j,k}^\epsilon(\mathbf{x}) \cdot \Psi_{\text{div},j,k}^\zeta(\mathbf{x}) dV_x < \infty$,
- (ii) $\int \frac{\partial(\Psi_{\text{div},j,k}^\epsilon(\mathbf{x}) \cdot \Psi_{\text{div},j,k}^\zeta(\mathbf{x}))}{\partial x_j} dV_x < \infty$,
- (iii) $\int \Psi_{\text{div},j,k}^\epsilon(\mathbf{x}) \cdot \nabla^2 \Psi_{\text{div},j,k}^\zeta(\mathbf{x}) dV_x < \infty$,

where $\Psi_{\text{div},j,k}^\epsilon$ must possess second-order weak derivatives. The divergence-free basis introduced in Sec. II B satisfies these requirements.

D. Realization of the model in practice

The forcing term \mathcal{F}_i represents the energy transfer from the resolved scales to the subgrid scales and is modeled in the proposed framework. A direct evaluation of $\mathcal{F}_i = \frac{\partial \tau_{ij}}{\partial x_j}$ requires explicit filtering with an a priori unknown filter. Kinetic energy can be added to the subgrid-scale velocity by the advective terms and the subgrid-scale stress tensor, that both underlie modeling assumptions (e.g., the linearization and the explicit filtering) and discretization errors. Consequently, undesired high or low kinetic energies can occur and even destabilize the numerical solution.

Since it is essential for the subgrid-scale velocity to have a realistic kinetic energy, we seek a model forcing term that can easily adjust the kinetic energy in both directions. The advective term \mathcal{A}_i can add and remove kinetic energy across the scales. The diffusive term \mathcal{D}_i , however, always removes kinetic energy if the viscosity is positive. The advective term and the diffusive term are scaled to remove kinetic energy from or add kinetic energy to the subgrid-scale velocity field. The total viscosity is replaced by an effective viscosity:

$$\nu_{\text{eff}}(k) = \sqrt{\frac{K_{j,k}}{K_{j,\text{desired}}}} [\nu_f + \nu'_t(k)]. \quad (23)$$

The kinetic energy of each wavelet is obtained with

$$K_{j,k} = \frac{C_{d \rightarrow K}}{N_\epsilon} \sum_\epsilon (d_{\text{div},j,k}^\epsilon)^2, \quad (24)$$

where $C_{d \rightarrow K}$ is a constant that depends on the distribution of $d_{\text{div},j,k}^\epsilon$ and is frequently adjusted by rearranging Eq. (24) and sampling $K_{j,k} = (\mathbf{u}'_{j,k} \cdot \mathbf{u}'_{j,k})/2$ at random positions. The desired kinetic energy follows the scaling of the spectrum of the inertial range

$$K_{j,\text{desired}} = \frac{K_{\text{desired}}}{\mathcal{N}} k_j^{-5/3} \Delta k_j, \quad (25)$$

with the norm

$$\mathcal{N} = \sum_j k_j^{-5/3} \Delta k_j, \quad (26)$$

and the wave number $k_j = 2^j 2\pi/L$. The wave number step is given by

$$\Delta k_j = \frac{k_{j+1} - k_{j-1}}{2}, \quad (27)$$

and L indicates the size of the domain. Since the basis functions are associated with a range of wave numbers, k_j must be interpreted as a characteristic wave number of the respective level j .

The advective term is also scaled with a factor of $\sqrt{K_{j,\text{desired}}/K_{j,k}}$, which accelerates the adaption to the desired kinetic energy. This procedure for maintaining the kinetic energy is stable and insensitive to external disturbances, such as momentum sources originating from two-way coupled particles. Note that no forcing is introduced that prescribes a specific (typically Gaussian) probability distribution function (PDF).

As described in Sec. II B, the wavelet basis functions are shifted by discrete integer values in space. This leads to points in space that coincide with peaks of the basis functions and, consequently, to statistically higher kinetic energy at these points. To avoid such a spatial bias, the basis functions are not fixed in space but move with a velocity much smaller than the eddy-turnover time of the respective level and within a small region near their original position. There are many ways of realizing a random movement of the wavelets. The method we applied is described in Appendix A. Note that the movement of the wavelets solely requires modification of the sampling of the subgrid-scale velocity because the coefficients $d_{\text{div},j,k}^\epsilon$ are determined independently for every j and \mathbf{k} .

In practice, the solution for the wavelet coefficients requires the evaluation of integrals, such as

$$\int \Psi_{\text{div},j,k}^\epsilon[\boldsymbol{\xi}(\mathbf{x})] \cdot \Psi_{\text{div},j,k}^\zeta[\boldsymbol{\xi}(\mathbf{x})] dV_x.$$

Other integrals also contain spatial derivatives of the wavelet basis functions. Since the basis functions do not change, the integrals can be computed only once and can be reused. The advective term requires the filtered fluid velocity and the filtered fluid velocity gradient. The interpolation of the filtered quantities to the position of the respective wavelet is the only interaction of the wavelet enrichment with the LES flow solver. This simple interpolation step can be realized across different types of flow solvers. Solving for the wavelet coefficients results in the solution of the following linear equation system for every j and \mathbf{k} :

$$\sum_{\zeta} A_{j,k}^{\epsilon,\zeta} d_{\text{div},j,k}^\zeta = b_{j,k}^\epsilon, \quad (28)$$

where the coefficient matrix $A_{j,k}^{\epsilon,\zeta}$ is of size 14×14 and identical for all j and \mathbf{k} . The right-hand side vector $b_{j,k}^\epsilon$ contains the wavelet coefficients of the previous time step and interpolated LES quantities. Therefore, its values change every time step.

III. SIMULATION SETUPS

The predictions of the proposed wavelet enrichment model are evaluated by means of different single-phase and particle-laden flow configurations. In this section the numerical solution of the flow and the particle transport is briefly introduced, and the parameters of the simulations are provided.

A. Numerical solution

The NSE and FNSE are solved numerically for different configurations in cubic domains of size L and periodic boundary conditions in every direction. The subgrid-scale stress tensor in the LES is modeled with the localized dynamic kinetic energy model (LDKM) as proposed by Menon and coworkers [42,43] and extended to two-way coupled particle-laden flows by Hausmann *et al.* [28] (referred to as mLDKM). Note that the mLDKM requires a model for the subgrid-scale velocity at the positions of the particles to be closed. Besides the subgrid-scale stress tensor, the mLDKM also provides an estimation of the subgrid-scale kinetic energy considering the turbulence modulation

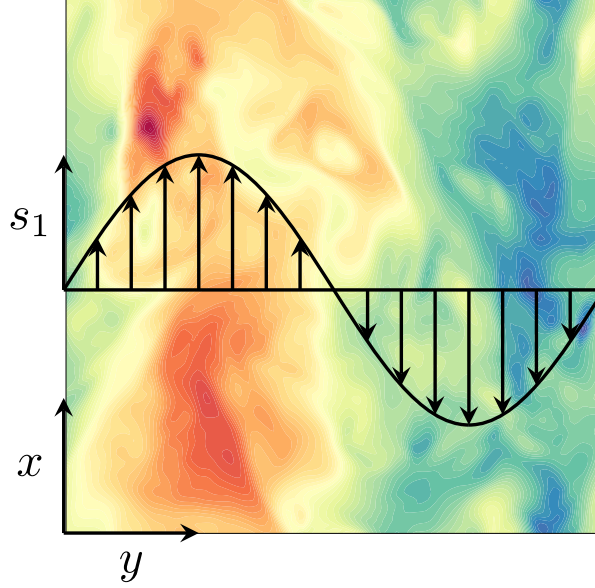


FIG. 2. Sketch of the turbulent shear flow configuration. A source term in x direction is added that varies with one period of a sin-profile across the y direction and drives a turbulent shear flow. The black arrows indicate the profile of the momentum source and the color represents a slice of the velocity in x direction.

by the particles. This subgrid-scale kinetic energy serves as K_{desired} for the wavelet enrichment in Eq. (25). Therefore, the generated subgrid-scale velocity considers, at least energetically, the turbulence modulation by the particles. Note that the effect of a changing slope of the kinetic energy spectrum is not accounted for. Altogether, the two-way coupling framework accounts for the influence of the subgrid-scale velocity on the particle transport, the influence of the particles on the resolved flow scales, and the effect of the particles on the subgrid scales. Details on how the two-way coupling interactions are modeled, can be found in Hausmann *et al.* [28]. A second-order finite volume solver is used to numerically solve the flow equations. More details on the flow solver may be found in Denner *et al.* [44] and Bartholomew *et al.* [45].

The investigated configurations differ in the source terms that appear in the momentum equations. We consider simulations of HIT, where a statistically steady state is obtained by continuously supplying kinetic energy through turbulence forcing. The forcing procedure is described in Mallouppas *et al.* [46].

A second type of flow investigated in this paper is a turbulent shear flow. This flow is simulated by a constant momentum source that varies as a sin-function across the domain:

$$\mathbf{s} = s_{\text{max}} \sin(2\pi y/L) \mathbf{e}_1, \quad (29)$$

where s_{max} is the amplitude of the momentum source, and \mathbf{e}_1 is the basis vector in the x direction. For this turbulent shear flow configuration a shear Reynolds number is defined $\text{Re}_{\text{shear}} = L\sqrt{s_{\text{max}}L}/\nu_f$. A sketch of this configuration is provided in Fig. 2.

We also assess the wavelet enrichment model using a simulation configuration with two-way coupled point-particles, where the particle-induced momentum source is taken into account with the particle-source-in-cell (PSIC) method [47]

$$\mathbf{s} = -\frac{1}{\rho_f V_{\text{cell}}} \sum_{p \in \Omega_{\text{cell}}} \mathbf{F}_p, \quad (30)$$

where Ω_{cell} represents a computational grid cell used in the finite volume solver that has a volume of V_{cell} . The particles are treated in a Lagrangian framework, and their motion is governed by the fluid-particle interface force, \mathbf{F}_p . We consider small, heavy, and spherical particles that we assumed to be only influenced by the drag force $\mathbf{F}_p = \mathbf{F}_{D,p}$, which we compute using Stokes' law augmented

TABLE I. Summary of the parameters that define the four simulations configurations.

Name	HIT-f-s	TS-s	HIT-f-1wc	HIT-d-2wc
Flow type	Forced HIT	turb. shear flow	Forced HIT	Decaying HIT
Energy supply	Turb. forcing	Sinusoidal force	Turb. forcing	–
Particles	–	–	One-way coupled	Two-way coupled
Taylor Reynolds number Re_λ	75	–	75	75
Turbulent Reynolds number Re_1	205	–	205	205
Shear Reynolds number Re_{shear}	–	3115	–	–
Reference time T_{ref}	$L/\sqrt{2/3\langle K \rangle}$	$\sqrt{L/s_{\text{max}}}$	$L/\sqrt{2/3\langle K \rangle}$	$L/\sqrt{2/3\langle K \rangle}$
Kolmogorov length scale η/L	0.0017	0.0029	0.0017	0.0017
Kolmogorov timescale τ_η/T_{ref}	0.0075	0.026	0.0075	0.0075
Computational cells DNS N_{DNS}^3	256^3	128^3	256^3	256^3
Computational cells LES N_{LES}^3	32^3	16^3	32^3	32^3
Number of particles N_p	–	–	$5 \times 480\,115$	$12\,057\,066$
Stokes number St	–	–	0.5, 1, 2, 4, 8	8

with the Schiller-Naumann correlation [48]

$$\mathbf{F}_{D,p} = C_D \frac{\rho_f}{8} \pi d_p^2 |\mathbf{u}_{\text{rel}}| \mathbf{u}_{\text{rel}}, \quad (31)$$

with the drag coefficient

$$C_D = \frac{24}{\text{Re}_p} (1 + 0.15 \text{Re}_p^{0.687}), \quad (32)$$

where d_p is the diameter of the particle with the index p and $\text{Re}_p = \mathbf{u}_{\text{rel}} d_p / \nu_f$ is its Reynolds number. The relative velocity is the difference between the velocity of the particle \mathbf{v}_p and the fluid velocity $\mathbf{u}(\mathbf{x}_p)$ at the position of the particle \mathbf{x}_p :

$$\mathbf{u}_{\text{rel}} = \mathbf{u}(\mathbf{x}_p) - \mathbf{v}_p. \quad (33)$$

The particle position changes according to

$$\frac{d\mathbf{x}_p}{dt} = \mathbf{v}_p, \quad (34)$$

and the particle velocity according to Newton's second law

$$\frac{d\mathbf{v}_p}{dt} = \frac{1}{\rho_p V_p} \mathbf{F}_p, \quad (35)$$

where ρ_p is the density of the particle. The motion of the particles is obtained using the Verlet-scheme [49]. The fluid velocity is interpolated to the particle position by divergence-free interpolation [50].

B. Parameters of the simulations

We consider four different simulation configurations to assess the predictions of the proposed model: forced HIT of a single-phase flow (HIT-f-s), a single-phase turbulent shear flow (TS-s), forced HIT with one-way coupled particles of five different Stokes numbers (HIT-f-1wc), and decaying HIT with two-way coupled particles of Stokes number $\text{St} = 8$ and a particle mass fraction of $\phi_m = 1$ (HIT-d-2wc). In Table I, important parameters of the four simulations are summarized. The flow quantities of the simulation HIT-d-2wc are given for the corresponding single-phase flow and before the onset of the decay of the turbulence.

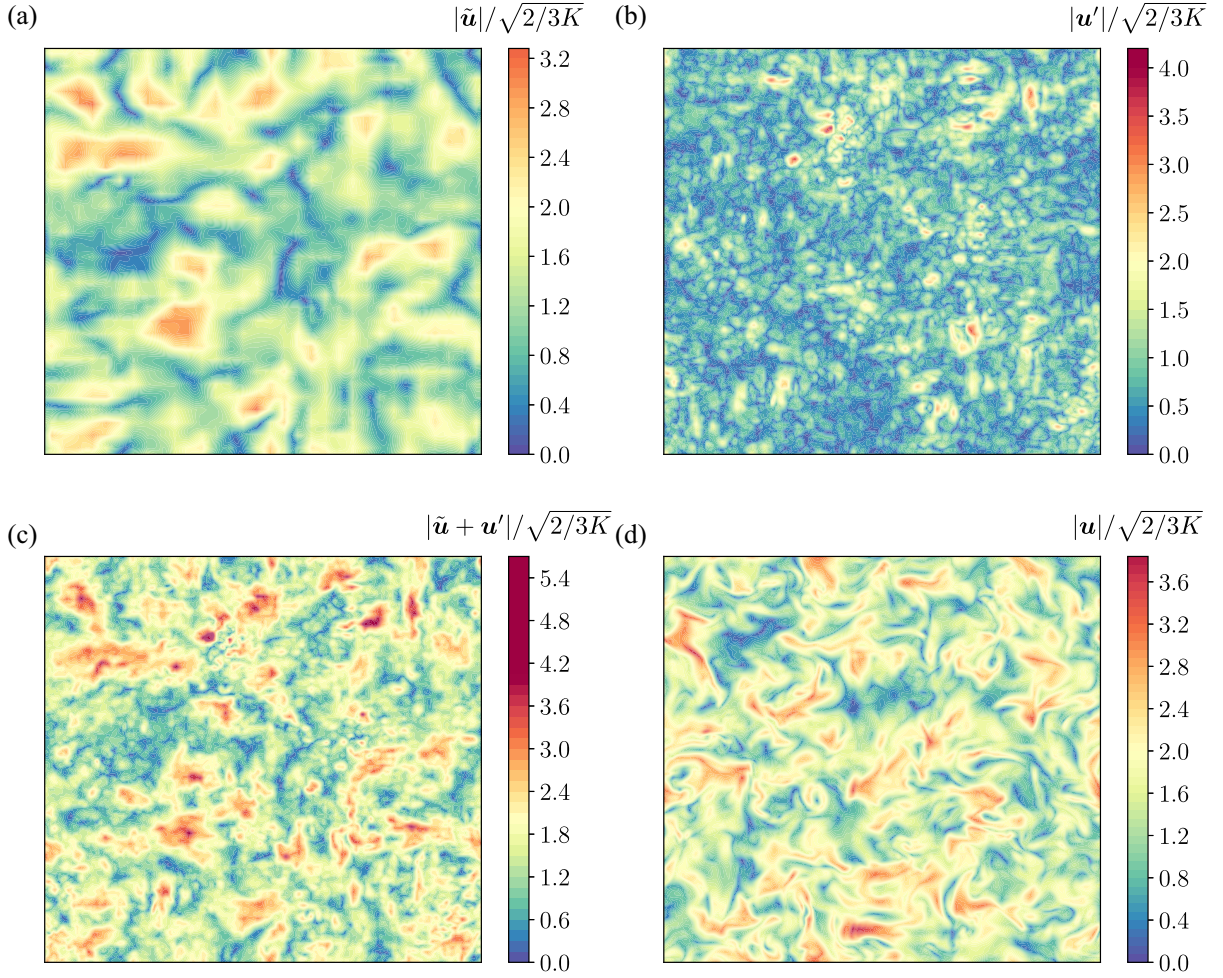


FIG. 3. Slice of the velocity magnitude for the simulation configuration HIT-f-s. The results are shown for the LES (a), the subgrid-scale velocity obtained from the wavelet enrichment (b), the superposition of the LES velocity and the modeled subgrid-scale velocity (c), and the DNS (d). The color scaling of all subfigures is the same even though the maximum velocities are different.

The forcing is only applied in the wave number range $kL/2\pi \in [3, 6]$ for the forced HIT simulations. For the HIT simulations, the resolution is $k_{\max}\eta = 1.37$, and for the turbulent shear flow it is $k_{\max}\eta = 1.16$. The maximum resolved wave number is defined as $k_{\max} = \pi N_{\text{DNS}}/L$.

In the LES of the HIT with the wavelet enrichment the range of considered levels is $j \in [4, 6]$ and in the LES of the turbulent shear flow $j \in [3, 5]$. The lowest levels are chosen such that their characteristic wave numbers correspond to the respective cutoff wave numbers of the LES. The upper level limits are chosen such that the significant amount of kinetic energy is captured with the modeled wave numbers.

IV. RESULTS AND DISCUSSIONS

In the present section we evaluate the predictions of the wavelet-enriched LES (LES-WL) and compare it to an LES without enrichment and the corresponding DNS. We separately discuss the single-phase flow statistics and the statistics of particle-laden flows.

A. Single-phase flow statistics

We first consider the flow statistics of the forced HIT configuration (HIT-f-s). Figure 3 compares the normalized fluid velocity magnitudes of the LES, the modeled subgrid-scale velocity obtained

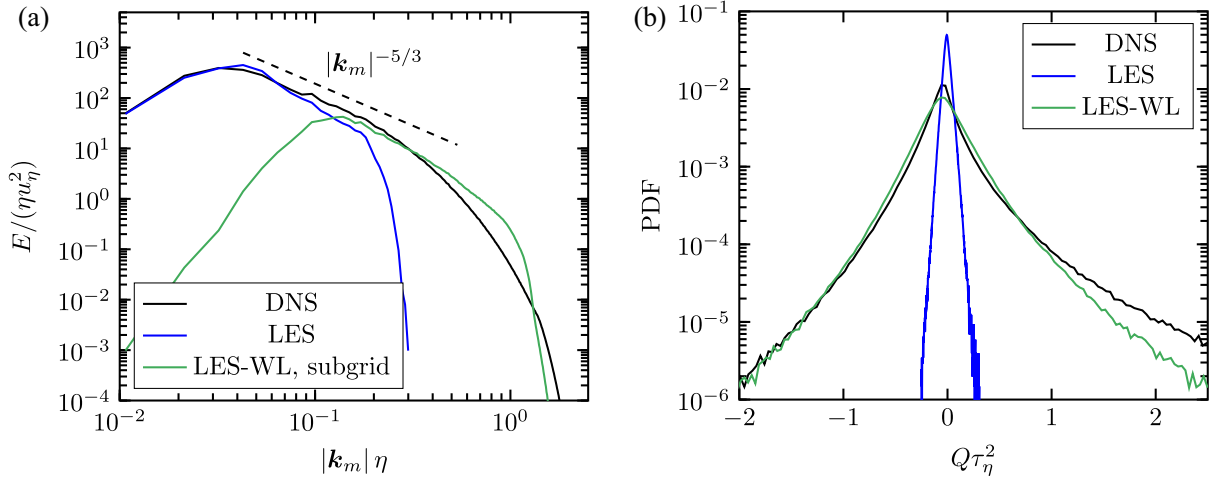


FIG. 4. Kinetic energy spectrum (a) and PDF of the second invariant of the velocity gradient tensor (b) for the simulation configuration HIT-f-s. The results are shown for the DNS, the LES, and the wavelet-enriched LES (LES-WL). The inertial range slope is plotted for comparison.

from the wavelet enrichment, and their sum with the DNS. The small flow structures, which are absent in the LES and provided by the wavelet enrichment, possess regions with different kinetic energies. This is possible because the compact support of the wavelet basis enables varying statistics across the domain. Some small regions with very high kinetic energy are observed. Such rare high intensity events are characteristic for turbulence and an indicator for intermittency. The superposition of the LES velocity and the modeled subgrid-scale velocity approximates the DNS velocity, which is widely similar in magnitude and range of length scales, but shows differences in the shape of the flow structures. The wavelet enrichment minimizes the local errors and, hence, prevents the systematical formation of flow structures with the neighbor wave packets.

The similarities of the velocity fields of the DNS and the wavelet-enriched LES can be quantified by comparing the kinetic energy spectra E normalized by the Kolmogorov length scale η and velocity u_η as shown in Fig. 4. The kinetic energy of the small wave numbers is recovered well by the LES. For the unresolved fluid velocity field the LES, the kinetic energy spectrum of the modeled subgrid-scale fluid velocity field approximates the kinetic energy spectrum of the DNS. Except for an overprediction of the spectrum of relatively small energy at high wave numbers, the general trend is captured. The observed deviation originates from the inertial range power law scaling prescribed by the forcing and may be improved if knowledge of the dissipation range is incorporated in the model.

As shown analytically by Maxey [51], the clustering of inertial particles of very small Stokes number is proportional to the second invariant of the fluid velocity gradient tensor

$$Q = \frac{1}{2}(\Omega_{ij}\Omega_{ij} - S_{ij}S_{ij}), \quad (36)$$

with the rotation-rate tensor Ω_{ij} and the strain-rate tensor S_{ij} . Therefore, to be able to correctly predict clustering, an accurate prediction of this tensor is crucial. Figure 4 shows the PDF of the second invariant of the velocity gradient tensor for the LES, the wavelet-enriched LES and the DNS. It can be observed that the LES by itself does not predict very high strain and low vorticity, or high vorticity and low strain events as is predicted by the DNS. With the wavelet-enriched LES, such events occur, even with a very similar probability as in the DNS; only the degree of asymmetry of the PDF (i.e., the higher probability of high rotation low strain events) is slightly underestimated as compared to the DNS. With the linearization of the SFNSE, the nonlinear term, as a contribution to the second invariant of the velocity gradient tensor, is modeled by a turbulent viscosity, that does not affect the second invariant of the velocity gradient tensor the same way as the nonlinear term.

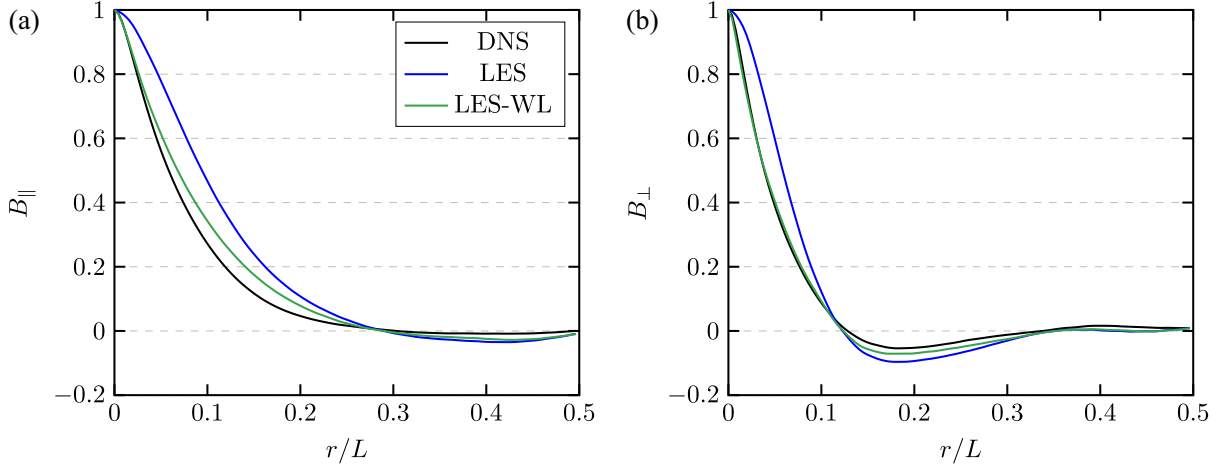


FIG. 5. Longitudinal (a) and transverse (b) fluid velocity autocorrelations over the distance r for the simulation configuration HIT-f-s. The results are shown for the DNS, the LES, and the wavelet-enriched LES (LES-WL).

This linearization can be an explanation for the observed deviation between the wavelet-enriched LES and the DNS.

Figure 5 shows the longitudinal and transverse fluid velocity autocorrelation functions, B_{\parallel} and B_{\perp} , for the DNS, the LES without wavelet enrichment and the wavelet-enriched LES. For homogeneous isotropic flows, they are defined as [52]

$$B_{\parallel}(r) = \frac{\langle u_{\alpha}(\mathbf{x}, t) u_{\alpha}(\mathbf{x} + r\mathbf{e}_{\parallel}, t) \rangle}{\langle u_{\alpha}(\mathbf{x}, t) u_{\alpha}(\mathbf{x}, t) \rangle}, \quad (37)$$

$$B_{\perp}(r) = \frac{\langle u_{\alpha}(\mathbf{x}, t) u_{\alpha}(\mathbf{x} + r\mathbf{e}_{\perp}, t) \rangle}{\langle u_{\alpha}(\mathbf{x}, t) u_{\alpha}(\mathbf{x}, t) \rangle}, \quad (38)$$

where r denotes the distance between the evaluated fluid velocities and \mathbf{e}_{\parallel} and \mathbf{e}_{\perp} the unit vector in the longitudinal and transverse direction, respectively. Note that no summation is carried out over the index α .

It can be seen in Fig. 5, that the fluid velocity decorrelates faster in the transverse direction than in the longitudinal direction, which is qualitatively also captured by the two LES. The LES without wavelet enrichment, however, predicts too slow decorrelation of the velocity in the longitudinal and transverse direction. The decorrelation can be accelerated by the wavelet-enriched LES, as it provides the unresolved subgrid-scale velocity field. As a result, the autocorrelations of the wavelet-enriched LES are in very good agreement with the autocorrelations of the DNS for small distances r . As the distance increases, the energetic resolved eddies dominate the autocorrelation and the autocorrelations of the wavelet-enriched LES converge toward the autocorrelations of the LES without wavelet enrichment.

Figure 6 shows the PDF of the longitudinal and transverse velocity gradients, $A_{11} = \partial u_1 / \partial x_1$ and $A_{12} = \partial u_1 / \partial x_2$, normalized by their respective standard deviations, σ_{11} and σ_{12} . Similar to the DNS, the wavelet-enriched LES increases the probability of events of high magnitude of the gradients compared to the LES. The tails of the PDFs of the wavelet-enriched LES are wider than in a Gaussian distribution, which is also observed in the DNS. In the PDF of the transverse velocity gradients, the wavelet-enriched LES shows a good agreement with the shape of the DNS. For the longitudinal gradients, the PDF of the wavelet-enriched LES lacks asymmetry, but the overall agreement with the PDF of the DNS is significantly improved compared to the LES without wavelet enrichment.

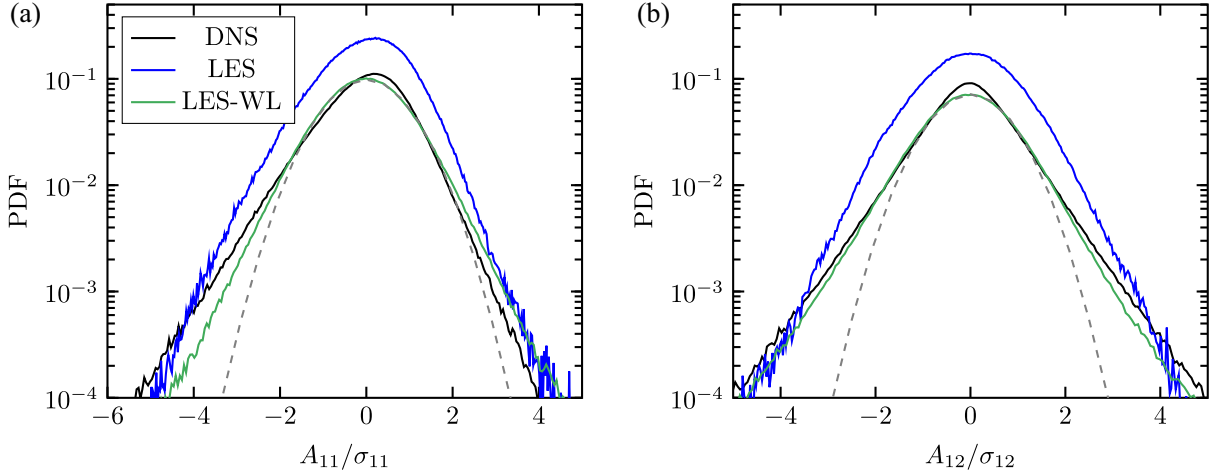


FIG. 6. PDF of longitudinal (a) and transverse (b) velocity gradients normalized by their standard deviations for the simulation configuration HIT-f-s. The results are shown for the DNS, the LES, and the wavelet-enriched LES (LES-WL). The dashed lines represent a Gaussian.

The analysis of the forced HIT proves that characteristic properties of turbulence can be reproduced by the wavelet enrichment, which cannot be achieved by, for instance, sampling random coefficient of Fourier-modes as done by a kinematic simulation (see, e.g., Zhou *et al.* [53]).

The computational cost of the wavelet-enriched LES for the simulation configuration HIT-f-s are approximately a factor 3–4 of the computational cost of the LES without enrichment. The computational cost of the corresponding DNS is four orders of magnitude higher.

Even though the wavelet enrichment proves to be capable of predicting realistic single-phase flow statistics in HIT, the vast majority of relevant flows in industry and nature is inhomogeneous and anisotropic. A simple inhomogeneous and anisotropic flow configuration is the turbulent shear flow (TS-s) introduced in Sec. III. In Fig. 7, we compare the spatial correlations of the subgrid-scale velocity, which are defined as

$$C_{ij} = \langle (u'_i - \langle u'_i \rangle)(u'_j - \langle u'_j \rangle) \rangle, \quad (39)$$

where $\langle \cdot \rangle$ indicates temporal averaging and averaging along the spatially homogeneous directions (i.e., x and z directions). The reference subgrid-scale fluid velocity field is obtained by subtracting

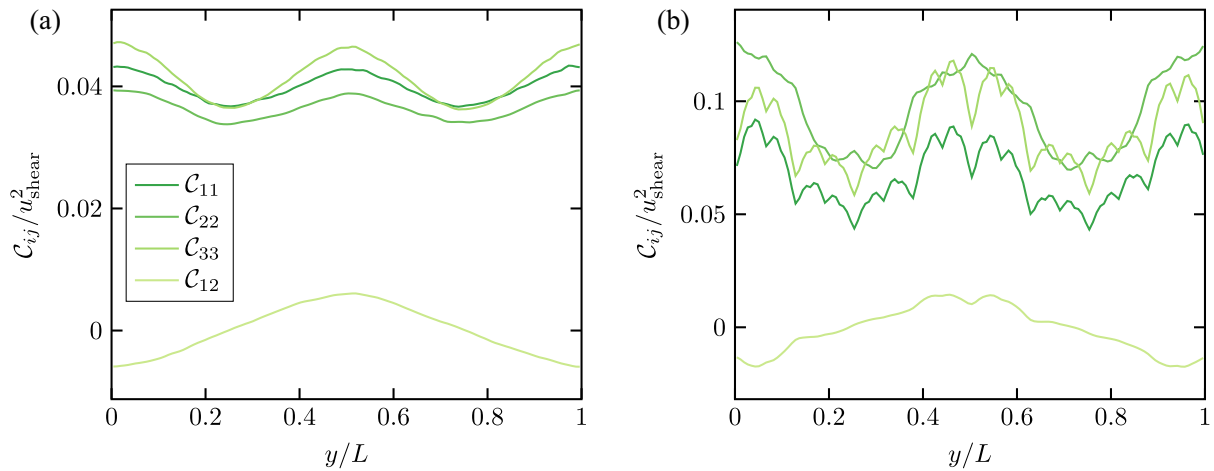


FIG. 7. Normalized spatial correlations in the y direction for the simulation configuration TS-s. (a) The correlations of the DNS explicitly filtered with a spectrally sharp filter and (b) the correlations of the subgrid-scale velocity that is modeled with the wavelet enrichment.

the explicitly filtered fluid velocity field of the DNS from the unfiltered fluid velocity field of the DNS, where a spectrally sharp filter is used. Because of the arbitrary choice of the filter, we compare the results only qualitatively.

It can be seen from Fig. 7 that the correlations of the wavelet enrichment are not as smooth as the correlations of the DNS. Because of the shape of the wavelet basis functions, regions occur that have statistically higher kinetic energy than other regions. Owing to the temporarily changing positions of the wavelet basis functions, which is explained in Sec. II D, the fluctuations are significantly reduced, but fluctuations remain in the ensemble averaged correlations that, however, are much smaller than the instantaneous velocity fluctuations.

The velocity correlations C_{11} , C_{22} , and C_{33} vary with two periods of a sine-shape across the y direction. With the wavelet enrichment this shape can be reproduced, albeit with different magnitudes, which can be traced back to the filter choice of the DNS and the estimation of the subgrid-scale kinetic energy. The cross-correlation C_{12} varies with one period of a sine-shape. At the domain center the velocities in the x and y directions are positively correlated and at the domain boundary negatively correlated. The wavelet enrichment reproduces this trend, which proves that the right anisotropic behavior can be generated from information that the wavelet enrichment receives from the LES.

B. Particle-laden flow statistics

We evaluate the particle statistics by comparing the results of forced HIT laden with one-way coupled particles (HIT-f-1wc). Figure 8 shows the particle pair dispersion, which is defined as the ensemble averaged temporal evolution of the distance between particle pairs with the position $\mathbf{x}_{p0}(t)$ and $\mathbf{x}_{p1}(t)$:

$$\langle \delta \rangle(t) = \langle |\mathbf{x}_{p0}(t) - \mathbf{x}_{p1}(t)| \rangle. \quad (40)$$

A particle pair is defined as two particles that have an initial separation of approximately the Kolmogorov length scale.

For all the considered Stokes numbers, three phases of the dispersion are observed in Fig. 8: (i) Particle pairs are located in the same eddy and stay close together, before (ii) they rapidly disperse by experiencing widely uncorrelated fluid velocities, and (iii) their maximum separation is reached, which is determined by the domain size. Since the LES only contains the largest eddies, that even the particles with the largest considered Stokes number can follow well, the dispersion is much slower than for the particles transported with the DNS velocity field. The wavelet-enriched LES leads to a particle pair dispersion that almost coincides with the DNS, for all considered Stokes numbers.

Most important for many applications is a correct prediction of particle clustering, i.e., that the particles preferentially concentrate in specific regions. A quantitative measure of particle clustering is provided by the radial distribution function, defined as

$$g(r) = \left\langle \frac{N_{p,i}(r)/\Delta V_i(r)}{N_p/V} \right\rangle, \quad (41)$$

where $\Delta V_i(r)$ is the volume of spherical shells in a distance r , and $N_{p,i}(r)$ is the number of particle in the respective spherical shell. The radial distribution function is normalized with the total number of particles N_p and the total volume of the simulation domain V .

The radial distribution function in Fig. 9 predicted by the LES without wavelet enrichment significantly deviates from the radial distribution function predicted by the DNS, whereas the LES predicts too little clustering for $St \in \{0.5, 1\}$ and too strong clustering for $St \in \{2, 4, 8\}$. For the small Stokes numbers, the small eddies, that are absent in the LES without wavelet enrichment, move the particles toward regions of small vorticity and large strain. The particles with the larger Stokes numbers cannot follow the small eddies well. Consequently, the small fluid velocity structures increase the dispersion of the particles with large Stokes numbers. The correct prediction of clustering of the particles with small Stokes numbers is far more challenging, because

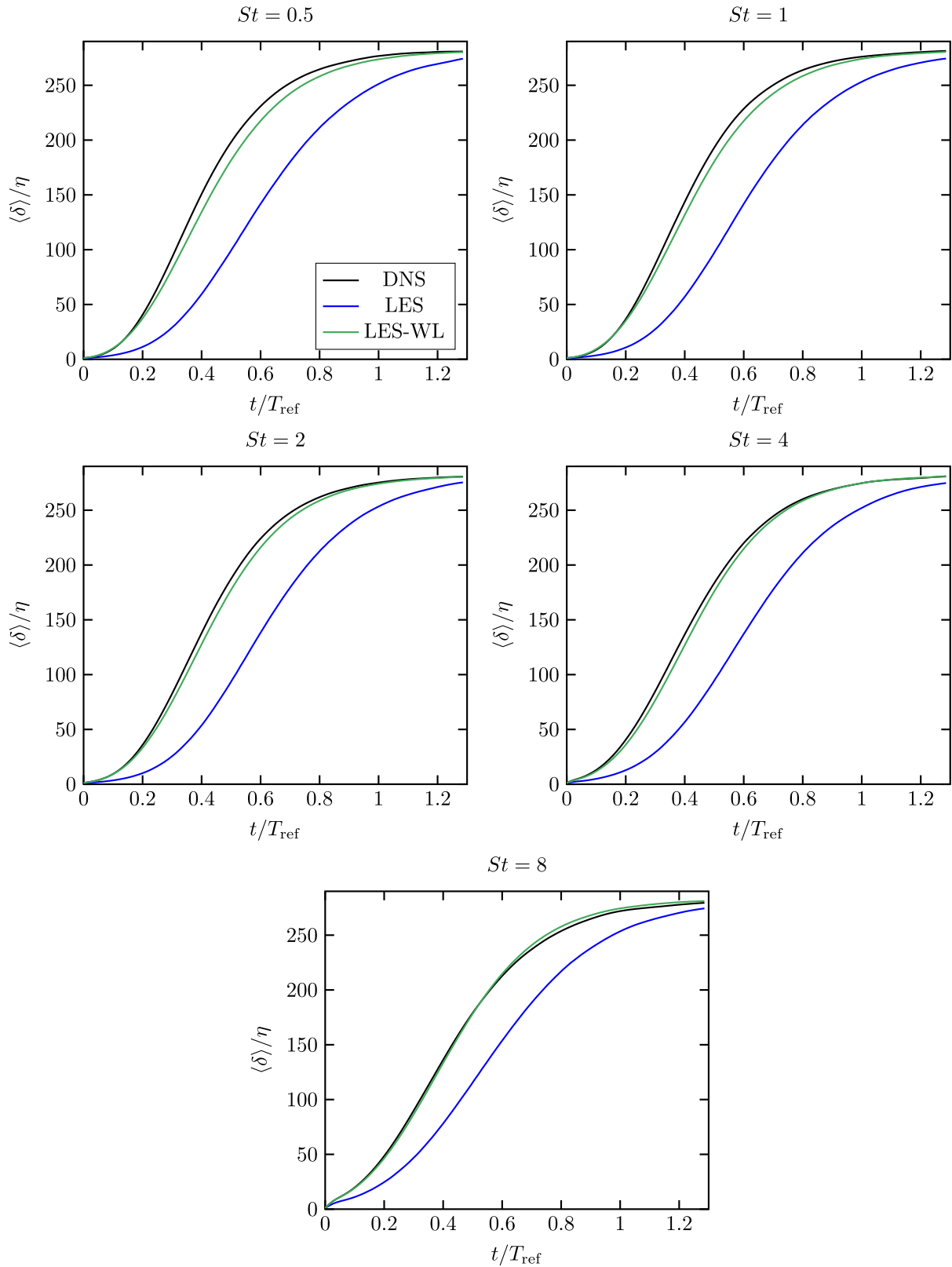


FIG. 8. Particle pair dispersion of particles with Stokes numbers in the range $St \in \{0.5, 1, 2, 4, 8\}$ for the simulation configuration HIT-f-1wc. The considered particles pairs have an initial separation of the size of the Kolmogorov length scale η . The results are shown for the DNS, the LES, and the wavelet-enriched LES (LES-WL).

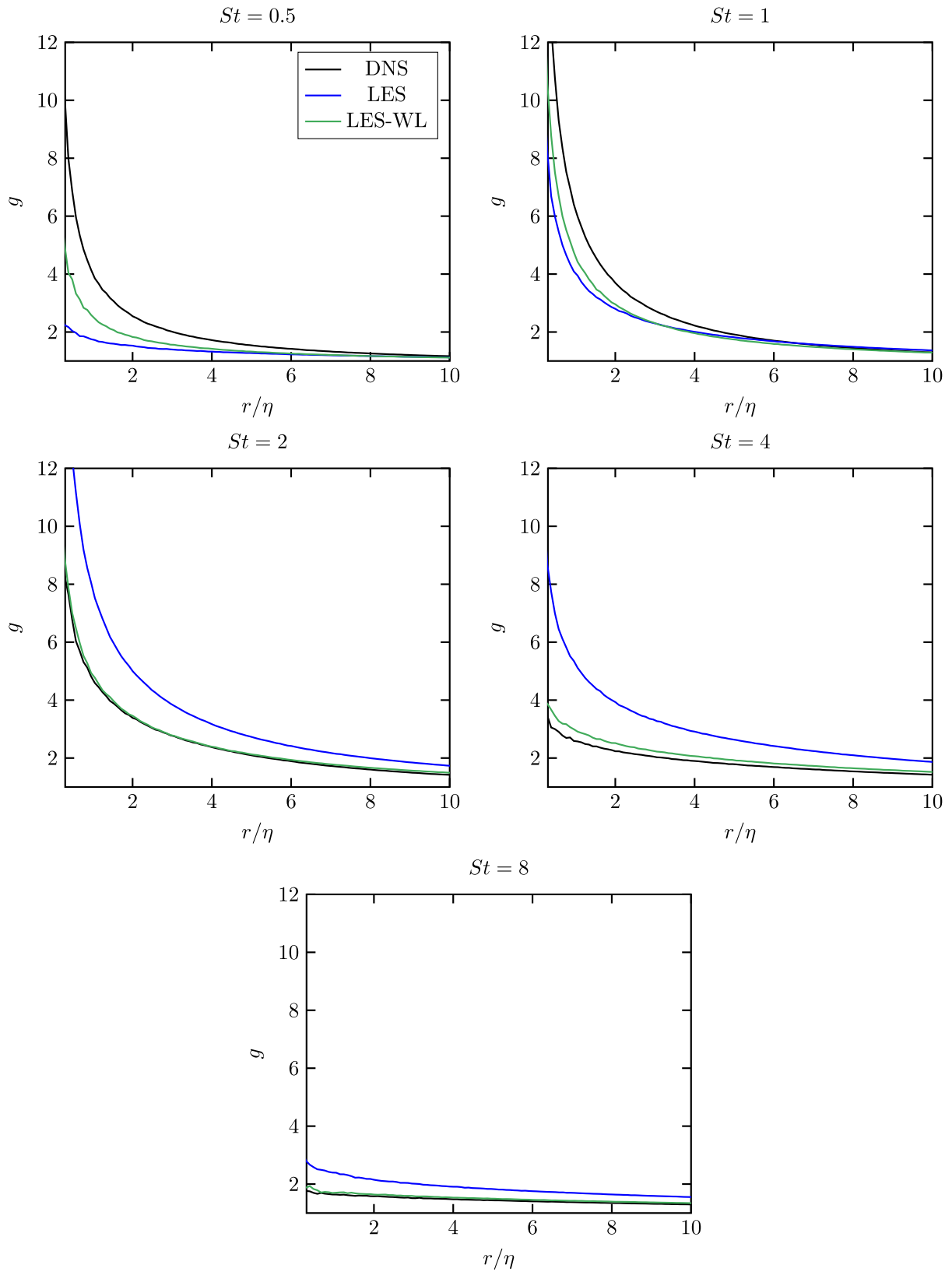


FIG. 9. Radial distribution function of particles with Stokes numbers in the range $St \in \{0.5, 1, 2, 4, 8\}$ for the simulation configuration HIT-f-1wc. The results are shown for the DNS, the LES, and the wavelet-enriched LES (LES-WL).

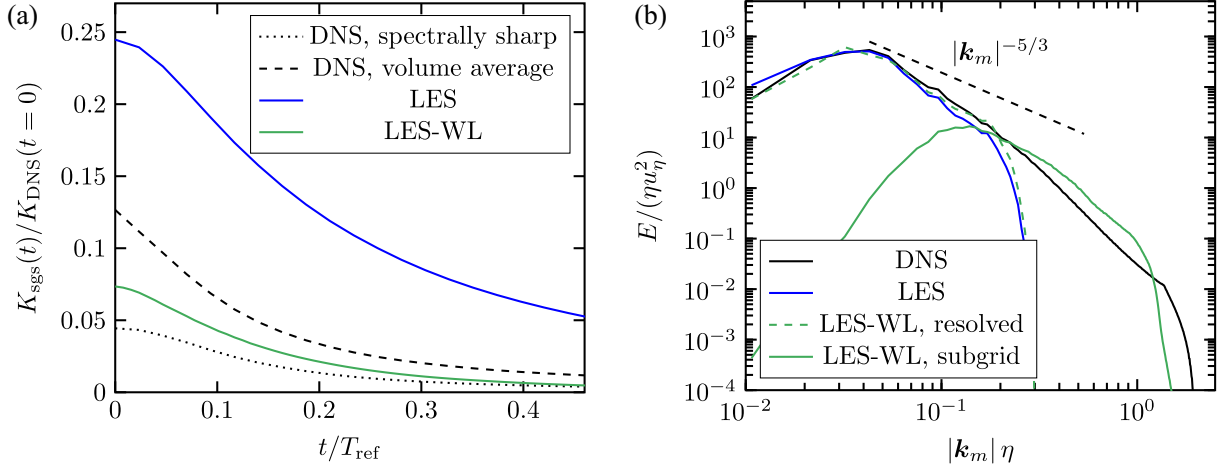


FIG. 10. Subgrid-scale kinetic energy over time (a) and kinetic energy spectrum before the onset of the decay (b) in decaying HIT laden with particles of Stokes number $St = 8$ for the simulation configuration HIT-d-2wc. The results are shown for the DNS, the LES, and the wavelet-enriched LES (LES-WL). The inertial range slope is plotted for comparison.

the strain-rotation relations of the small fluid velocity structures have a larger impact. It is observed in Fig. 9 that the wavelet-enriched LES significantly improves the radial distribution function for the Stokes numbers $St \geq 2$. The increased dispersion by the modeled subgrid-scale fluid velocity field yields an excellent agreement of the radial distribution function of the wavelet-enriched LES with the radial distribution function of the DNS. For the intricate case of Stokes numbers $St = 0.5$ and $St = 1$, only a relatively minor increase in particle clustering is observed.

The computational costs of the wavelet-enriched LES mainly depend on the levels, i.e., functions of the subspaces V_j that are considered and the number of particles that require sampling of the subgrid-scale velocity. The sampling of the subgrid-scale velocity at the positions of the particles is much more computationally expensive than computing the wavelet coefficients. The wavelet-enriched LES requires approximately twice the CPU-time for the HIT-f-1wc configuration than the Fourier enrichment [28]. This corresponds to approximately 10–15 times the CPU-time of the corresponding LES, which is significant, but still orders of magnitudes cheaper than a DNS.

The final test case considered in this paper considers two-way coupling. The abilities of the wavelet enrichment to predict the unresolved effects of two-way coupled particle-laden flows is assessed with the simulation configuration HIT-d-2wc, representing decaying HIT with two-way coupled particles with Stokes number $St = 8$. Figure 10(a) shows the temporal evolution of the subgrid-scale kinetic energy predicted by the LES without the wavelet enrichment and the LDKM, the wavelet-enriched LES with the mLDKM including the effect of the particles, and the DNS.

The reference subgrid-scale kinetic energy is obtained by explicit filtering the DNS. In an LES, the spatially varying turbulent viscosity imposes the filtering. This unknown filter leads to an uncertainty of the actual subgrid-scale kinetic energy. Therefore, the DNS is explicitly filtered with two different filters, a spectrally sharp filter and by volume averaging. During the whole decay the LES without wavelet enrichment and with the single-phase flow subgrid-scale model predicts a much too large subgrid-scale kinetic energy. The subgrid-scale model, i.e., the LDKM, assumes single-phase turbulence for the unresolved velocity scales, which contains more kinetic energy than the same flow laden with particles of Stokes number $St = 8$. Since the wavelet-enriched LES enables the use of the mLDKM that takes the turbulence modification by the particles into account, the predicted subgrid-scale kinetic energy is much smaller and lies between the subgrid-scale kinetic energy obtained from the DNS using the two different explicit filters. Note that the subgrid-scale kinetic energy obtained from the DNS is sensitive to the specific filter that is used.

The kinetic energy spectra before the onset of the decay are shown in Fig. 10(b). The turbulence modulation by the particles leads to a clear deviation of the DNS spectrum from the well known power-law of the inertial range that is observed in single-phase turbulence. Close to the cutoff wave number, the spectrum of the LES without wavelet enrichment using the LDKM deviates from the DNS spectrum because of the overestimated subgrid-scale kinetic energy and, thus, the too large turbulent viscosity. This is improved by the wavelet-enriched LES using the mLDKM that predicts a smaller turbulent viscosity and a better agreement with the kinetic energy spectrum of the DNS. The kinetic energy of the subgrid-scale velocity generated by the wavelet enrichment is slightly larger than the kinetic energy of the DNS. The shape of the kinetic energy spectrum, however, is very similar to the kinetic energy spectrum of the DNS.

V. CONCLUSIONS

We propose a model to predict the unresolved subgrid-scale fluid velocity field in the scope of an LES. In LES of particle-laden turbulent flows, the subgrid-scale velocity at the particle positions is required to predict correct particle behavior, such as their dispersion and clustering. Our wavelet enrichment model discretizes the subgrid-scale velocity by means of a divergence-free wavelet vector basis. The coefficients of this basis are obtained by minimizing the squared error of the linearized SFNSE. In contrast to structural models using a Fourier basis, the wavelet enrichment enables a continuous change of velocity statistics across the domain and, hence, the generation of an inhomogeneous subgrid-scale velocity field. Furthermore, the wavelet enrichment does not require to specify parameters that critically affect the results.

The model is validated with four distinct test cases that separately assesses the predictions of the wavelet enrichment in single-phase and particle-laden flows. Simulations of forced HIT show that the wavelet enrichment produces strain-rotation relations that are similar to the DNS. The PDFs of the longitudinal and transverse velocity gradients possess the expected non-Gaussian behavior. The wavelet enrichment is shown to be capable of predicting inhomogeneous and anisotropic velocity fields in a turbulent shear flow, where the spatial velocity correlations match those of DNS.

One-way coupled simulations of forced HIT of particles with different Stokes numbers revealed excellent agreement with the particle pair dispersion of the DNS. The predictions of particle clustering are improved, whereas the wavelet-enriched LES recovers the radial distribution function of the DNS very well for Stokes numbers $St \geq 2$. By combining the wavelet enrichment with the recently proposed modification of the LDKM [28] to particle-laden flows, we report improved predictions of the subgrid-scale kinetic energy and the kinetic energy spectrum in two-way coupled decaying HIT.

The proposed wavelet enrichment is able to recover the most important interactions between turbulence and particles while maintaining computational costs of the order of the costs of an LES.

ACKNOWLEDGMENT

This research was funded by Deutsche Forschungsgemeinschaft (DFG, German Research Foundation) Project ID No. 457509672.

APPENDIX A: MOVEMENT OF THE WAVELETS

Let $\mathbf{x}_{j,k,c}(t)$ be the coordinates of the center positions of the wavelets with the indices j and k that are initially given as

$$x_{i,j,k,c}(t=0) = \frac{x_{i,\max} - x_{i,\min}}{2^j} (k_i + 1/2) + x_{i,\min}. \quad (\text{A1})$$

A wavelet center is allowed to move within a region

$$\mathbf{x}_{j,k,c}(t=0) - \delta_j \leq \mathbf{x}_{j,k,c}(t) \leq \mathbf{x}_{j,k,c}(t=0) + \delta_j, \quad (\text{A2})$$

where

$$\delta_{i,j} = \frac{x_{i,\max} - x_{i,\min}}{2^{j+1}}. \quad (\text{A3})$$

Within this region target coordinates $\mathbf{x}_{j,k,t}$ are generated from a uniform distribution. The wavelet center moves toward the target coordinates with a constant velocity that is equal to 10% of the local eddy turnover time. As soon as the center coordinates are close to the target coordinates, new random target coordinates are generated

APPENDIX B: PROJECTION OF THE LINEARIZED SFNSE

This Appendix describes how the pressure term in the linearized SFNSE can be dropped if we solve it in the divergence-free subspace. We start from the linearized SFNSE

$$\frac{\partial u'_i}{\partial t} + \mathcal{A}_i = -\mathcal{P}_i + \mathcal{D}_i + \mathcal{F}_i, \quad (\text{B1})$$

with the abbreviations

$$\begin{aligned} \mathcal{A}_i &= \tilde{u}_j \frac{\partial u'_i}{\partial x_j} + u'_j \frac{\partial \tilde{u}_i}{\partial x_j}, \\ \mathcal{P}_i &= \frac{1}{\rho_f} \frac{\partial p'}{\partial x_i}, \\ \mathcal{D}_i &= (v_f + v'_t) \frac{\partial^2 u'_i}{\partial x_j \partial x_j}, \quad \text{and} \quad \mathcal{F}_i = \frac{\partial \tau_{ij}}{\partial x_j}. \end{aligned}$$

Taking the divergence gives

$$\frac{\partial}{\partial x_i} \mathcal{P}_i = -\frac{\partial}{\partial x_i} \mathcal{A}_i + \frac{\partial}{\partial x_i} \mathcal{F}_i, \quad (\text{B2})$$

because the divergence of the time derivative of the velocity and the diffusive term are zero, as it can be easily verified. Similarly, by taking the curl of Eq. (B1), we get

$$\text{Curl} \left(\frac{\partial u'_i}{\partial t} \right) + \text{Curl}(\mathcal{A}_i) = \text{Curl}(\mathcal{D}_i) + \text{Curl}(\mathcal{F}_i). \quad (\text{B3})$$

Because the curl of a gradient is zero, the curl of the pressure term vanishes. According to the Helmholtz decomposition, the advective term and the forcing term can be decomposed into a divergence-free contribution, indicated with a \perp , and a curl-free contribution, indicated with the superscript curl, as follows:

$$\mathcal{A}_i = \mathcal{A}_i^\perp + \mathcal{A}_i^{\text{curl}}, \quad (\text{B4})$$

$$\mathcal{F}_i = \mathcal{F}_i^\perp + \mathcal{F}_i^{\text{curl}}. \quad (\text{B5})$$

Equation (B2) is satisfied if

$$\mathcal{P}_i = -\mathcal{A}_i^{\text{curl}} + \mathcal{F}_i^{\text{curl}}, \quad (\text{B6})$$

and Eq. (B3) is satisfied if

$$\frac{\partial u'_i}{\partial t} + \mathcal{A}_i^\perp = \mathcal{D}_i + \mathcal{F}_i^\perp. \quad (\text{B7})$$

Adding Eq. (B6) and Eq. (B7), gives the linearized SFNSE (B1). Equations (B6) and (B7) can be solved instead of solving the continuity equation together with Eq. (B1).

-
- [1] V. Armenio, U. Piomelli, and V. Fiorotto, Effect of the subgrid scales on particle motion, *Phys. Fluids* **11**, 3030 (1999).
- [2] B. Ray and L. R. Collins, Preferential concentration and relative velocity statistics of inertial particles in Navier–Stokes turbulence with and without filtering, *J. Fluid Mech.* **680**, 488 (2011).
- [3] P. Fede and O. Simonin, Numerical study of the subgrid fluid turbulence effects on the statistics of heavy colliding particles, *Phys. Fluids* **18**, 045103 (2006).
- [4] B. Rosa and J. Pozorski, Impact of subgrid fluid turbulence on inertial particles subject to gravity, *J. Turbul.* **18**, 634 (2017).
- [5] R. H. Kraichnan, Diffusion by a random velocity field, *Phys. Fluids* **13**, 22 (1970).
- [6] J. C. H. Fung, J. C. R. Hunt, N. A. Malik, and R. J. Perkins, Kinematic simulation of homogeneous turbulence by unsteady random Fourier modes, *J. Fluid Mech.* **236**, 281 (1992).
- [7] N. A. Malik and J. C. Vassilicos, A Lagrangian model for turbulent dispersion with turbulent-like flow structure: Comparison with direct numerical simulation for two-particle statistics flow structure, *Phys. Fluids* **11**, 1572 (1999).
- [8] A. Scotti and C. Meneveau, A fractal model for large-eddy simulation of turbulent flow, *Physica D* **127**, 198 (1999).
- [9] J. A. Domaradzki and K.-C. Loh, The subgrid-scale estimation model in the physical space representation, *Phys. Fluids* **11**, 2330 (1999).
- [10] M. Terracol, P. Sagaut, and C. Basdevant, A multilevel algorithm for large-eddy simulation of turbulent compressible flows, *J. Comput. Phys.* **167**, 439 (2001).
- [11] B. Dubrulle, J. P. Laval, S. Nazarenko, and N. K.-R. Kevlahan, A dynamic subfilter-scale model for plane parallel flows, *Phys. Fluids* **13**, 2045 (2001).
- [12] A. S. Ghate and S. K. Lele, Subfilter-scale enrichment of planetary boundary layer large-eddy simulation using discrete Fourier–Gabor modes, *J. Fluid Mech.* **819**, 494 (2017).
- [13] T. J. Hughes, G. R. Feijóo, L. Mazzei, and J.-B. Quincy, The variational multiscale method—A paradigm for computational mechanics, *Comput. Methods Appl. Mech. Eng.* **166**, 3 (1998).
- [14] T. J. Hughes, L. Mazzei, and K. E. Jansen, Large-eddy simulation and the variational multiscale method, *Comput. Visual. Sci.* **3**, 47 (2000).
- [15] M. Hausmann, F. Evrard, and B. van Wachem, An efficient model for subgrid-scale velocity enrichment for large-eddy simulations of turbulent flows, *Phys. Fluids* **34**, 115135 (2022).
- [16] P. Sagaut, *Large Eddy Simulation for Incompressible Flows*, 3rd ed. (Springer, Berlin, 2005).
- [17] P. Fede, O. Simonin, P. Villedieu, and K. D. Squires, Stochastic modeling of the turbulent subgrid fluid velocity along inertial particle trajectories, in *Proceedings of the Summer Program* (2006), p. 247.
- [18] M. Bini and W. P. Jones, Particle acceleration in turbulent flows: A class of nonlinear stochastic models for intermittency, *Phys. Fluids* **19**, 035104 (2007).
- [19] A. S. Berrouk, D. Laurence, J. J. Riley, and D. E. Stock, Stochastic modelling of inertial particle dispersion by subgrid motion for LES of high Reynolds number pipe flow, *J. Turbul.* **8**, N50 (2007).
- [20] B. Shotorban and F. Mashayek, A stochastic model for particle motion in large-eddy simulation, *J. Turbul.* **7**, N18 (2006).
- [21] J. Pozorski and S. Apte, Filtered particle tracking in isotropic turbulence and stochastic modeling of subgrid-scale dispersion, *Int. J. Multiphase Flow* **35**, 118 (2009).
- [22] M. Knorps and J. Pozorski, Stochastic modeling for subgrid-scale particle dispersion in large-eddy simulation of inhomogeneous turbulence, *Phys. Fluids* **33**, 043323 (2021).
- [23] C. Marchioli, Large-eddy simulation of turbulent dispersed flows: A review of modelling approaches, *Acta Mech.* **228**, 741 (2017).
- [24] J. G. M. Kuerten, Subgrid modeling in particle-laden channel flow, *Phys. Fluids* **18**, 025108 (2006).
- [25] B. Shotorban and F. Mashayek, Modeling subgrid-scale effects on particles by approximate deconvolution, *Phys. Fluids* **17**, 081701 (2005).
- [26] G. I. Park, M. Bassenne, J. Urzay, and P. Moin, A simple dynamic subgrid-scale model for LES of particle-laden turbulence, *Phys. Rev. Fluids* **2**, 044301 (2017).
- [27] M. Bassenne, M. Esmaily, D. Livescu, P. Moin, and J. Urzay, A dynamic spectrally enriched subgrid-scale model for preferential concentration in particle-laden turbulence, *Int. J. Multiphase Flow* **116**, 270 (2019).

- [28] M. Hausmann, F. Evrard, and B. van Wachem, Large-eddy simulation model for two-way coupled particle-laden turbulent flows, *Phys. Rev. Fluids* **8**, 084301 (2023).
- [29] R. Letournel, Reduced-Order Modeling and Simulation of Turbulent Disperse Two-Phase Flows: New Theoretical and Modeling Approaches for Reproducing Intermittency, Segregation and Two-Way Coupling, Ph.D. thesis, Université Paris-Saclay, Paris, France, 2022.
- [30] J. A. Denev, C. J. Falconi, J. Fröhlich, and H. Bockhorn, Wavelet-adapted subgrid-scale models for LES, in *Turbulence and Interactions*, Vol. 110, edited by E. H. Hirschel, W. Schröder, K. Fujii, W. Haase, B. Leer, M. A. Leschziner, M. Pandolfi, J. Periaux, A. Rizzi, B. Roux, Y. I. Shokin, M. Deville, T.-H. Lê, and P. Sagaut (Springer, Berlin, 2010), pp. 111–117.
- [31] G. De Stefano and O. V. Vasilyev, Wavelet-based adaptive large-eddy simulation with explicit filtering, *J. Comput. Phys.* **238**, 240 (2013).
- [32] Y. Xiong, J. Li, F. Fei, Z. Liu, and W. Luo, Influence of coherent vortex structures in subgrid-scale motions on particle statistics in homogeneous isotropic turbulence, *Int. J. Multiphase Flow* **113**, 358 (2019).
- [33] Y. Xiong, R. Cai, J. Li, F. Fei, Z. Liu, and W. Luo, Structural subgrid-scale model based on wavelet filter for large-eddy simulation of particle-laden turbulence, *Int. J. Multiphase Flow* **143**, 103730 (2021).
- [34] A. Leonard, Energy Cascade in Large-eddy simulations of turbulent fluid flows, in *Advances in Geophysics*, Vol. 18 (Elsevier, Amsterdam, 1975), pp. 237–248.
- [35] J.-P. Laval, B. Dubrulle, and S. Nazarenko, Nonlocality and intermittency in three-dimensional turbulence, *Phys. Fluids* **13**, 1995 (2001).
- [36] V. M. Canuto and M. S. Dubovikov, A dynamical model for turbulence. I. General formalism, *Phys. Fluids* **8**, 571 (1996).
- [37] K. Horiuti, Roles of non-aligned eigenvectors of strain-rate and subgrid-scale stress tensors in turbulence generation, *J. Fluid Mech.* **491**, 65 (2003).
- [38] S. L. Brunton and J. N. Kutz, *Data-Driven Science and Engineering: Machine Learning, Dynamical Systems, and Control*, 1st ed. (Cambridge University Press, Cambridge, UK, 2019).
- [39] I. Daubechies, *Ten Lectures on Wavelets*, CBMS-NSF Regional Conference Series in Applied Mathematics No. 61 (Society for Industrial and Applied Mathematics, Philadelphia, PA, 1992).
- [40] P. G. Lemarié-Rieusset, Analyses multi-résolutions non orthogonales, commutation entre projecteurs et dérivation et ondelettes vecteurs à divergence nulle, *Rev. Mat. Iberoam.* **8**, 221 (1992).
- [41] E. Deriaz and V. Perrier, Divergence-free and curl-free wavelets in two dimensions and three dimensions: Application to turbulent flows, *J. Turbul.* **7**, N3 (2006).
- [42] W.-W. Kim and S. Menon, An unsteady incompressible Navier-Stokes solver for large-eddy simulation of turbulent flows, *Int. J. Numer. Methods Fluids* **31**, 983 (1999).
- [43] S. Menon, P.-K. Yeung, and W.-W. Kim, Effect of subgrid models on the computed interscale energy transfer in isotropic turbulence, *Comput. Fluids* **25**, 165 (1996).
- [44] F. Denner, F. Evrard, and B. van Wachem, Conservative finite-volume framework and pressure-based algorithm for flows of incompressible, ideal-gas and real-gas fluids at all speeds, *J. Comput. Phys.* **409**, 109348 (2020).
- [45] P. Bartholomew, F. Denner, M. Abdol-Azis, A. Marquis, and B. van Wachem, Unified formulation of the momentum-weighted interpolation for collocated variable arrangements, *J. Comput. Phys.* **375**, 177 (2018).
- [46] G. Mallouppas, W. K. George, and B. van Wachem, New forcing scheme to sustain particle-laden homogeneous and isotropic turbulence, *Phys. Fluids* **25**, 083304 (2013).
- [47] C. T. Crowe, M. P. Sharma, and D. E. Stock, The particle-pource-in cell (PSI-CELL) model for gas-droplet flows, *J. Fluids Eng.* **99**, 325 (1977).
- [48] L. Schiller and A. Naumann, über die grundlegenden Berechnungen bei der Schwerkraftaufbereitung, *Z. Ver. Dtsch. Ing.* **77**, 318 (1933).
- [49] L. Verlet, Computer “experiments” on classical fluids. I. Thermodynamical properties of Lennard-Jones molecules, *Phys. Rev.* **159**, 98 (1967).
- [50] G. Tóth and P. Roe, Divergence- and curl-preserving prolongation and restriction formulas, *J. Comput. Phys.* **180**, 736 (2002).

- [51] M. R. Maxey, The gravitational settling of aerosol particles in homogeneous turbulence and random flow fields, *J. Fluid Mech.* **174**, 441 (1987).
- [52] W. K. George, Lectures in Turbulence for the 21st Century, Tech. Rep. (Department of Applied Mechanics, Chalmers University of Technology, Gothenburg, Sweden, 2010).
- [53] Z. Zhou, S. Wang, X. Yang, and G. Jin, A structural subgrid-scale model for the collision-related statistics of inertial particles in large-eddy simulations of isotropic turbulent flows, *Phys. Fluids* **32**, 095103 (2020).